Development of Road Haulage Trailer Design

Anthony Bukowski

A thesis submitted in partial fulfillment of the requirements

of the Manchester Metropolitan University

for the degree of Doctor of Philosophy

Department of Science and Engineering

2014

THIS PAGE IS INTENTIONALLY LEFT BLANK

Abstract

Heavy goods vehicles (HGVs) are synonymous with high fuel consumption due to their weight and bluff nature. At a time when fuel prices are high and haulage operators have an environmental responsibility to reduce CO^2 emissions, there is great interest in the possible methods of curbing fuel consumption. With up to 50 percent of HGV fuel consumption attributed to aerodynamic drag, there are improvements which can be made to the design and manufacture of haulage trailers in order to reduce fuel consumption and reduce CO^2 emissions.

Various design modifications, both those able to be retrofitted and only possible at the point of manufacture, are tested using computational fluid dynamics (CFD), to establish the potential drag reduction when compared to a baseline case. These are evaluated in both normal and side-wind conditions. The baseline case is modelled to represent a HGV combination that is representative of the average trailer in operation in the UK industry. It is found that in combination, the trailer modifications analysed can reduce the aerodynamic drag of the overall vehicle geometry by up to 26%.

Additional geometry is also tested that is specific to the UK industry due to the lack of a limitation on overall vehicle height. These tests highlight the consequences of unchecked vehicle geometry and the effects that inappropriate truck and trailer matching can have on the overall drag contribution of the vehicle. These cases along with the comparative and baseline cases show that the flow characteristics of the vehicle geometry differs greatly between normal and conditions of side-wind. This in turn dictates the effectiveness of the geometry modifications dependent on their intended area of drag improvement, and can inform design decisions when incorporating these at the point of manufacture.

Acknowledgements

This work would not have been possible without the assistance of my supervisor, to whom I owe great thanks. Not just for his assistance in the study, but for all the time and effort given up beyond the scope of this work.

Also, without the involvement of The Cartwright Group this work would not have been possible, the opinions from the point of manufacture and that of operators is invaluable, for whom work such as this is intended to benefit.

Finally I would like to thank my wife, for forever tolerating my own particular brand of insanity.

Contents

List of Figures

List of Tables

Nomenclature

$\boldsymbol{\rho}$	Fluid Density
$\boldsymbol{v}$	Fluid Velocity
$\boldsymbol{\mu}$	Fluid Viscosity
$\boldsymbol{\mu_t}$	Fluid Turbulent Viscosity
$\boldsymbol{t}$	Time
$\boldsymbol{k}$	Turbulence Energy
$\boldsymbol{\varepsilon}$	Dissipation Rate of Turbulence Energy
$\boldsymbol{T}$	Temperature
$\boldsymbol{A}$	Frontal Area
$\boldsymbol{Re}$	Reynolds Number
$\boldsymbol{Cd}$	Drag Coefficient
$\boldsymbol{Fd}$	Drag Force
$\boldsymbol{F(xyz)}$	Force in direction
$\boldsymbol{Fxrear}$	Force on Trailer Rear Face
$\boldsymbol{BulkFx}$	Force on Trailer Bulkhead
$\boldsymbol{CdBase}$	Baseline Drag Coefficient
$\boldsymbol{CdDD}$	Standard Double Deck Drag Coefficient
$\boldsymbol{Cp}$	Pressure Coefficient
$\boldsymbol{\tau_w}$	Wall Shear Stress
$\boldsymbol{\tau_{ij}}$	ij-th Component of the Laminar Stress Tensor
$\boldsymbol{\tau_{ij}^R}$	ij-th Component of the Reynolds Stress Tensor
$\boldsymbol{Q_H}$	Heat Source
$\boldsymbol{q_i}$	Diffusive Heat Flux
$\boldsymbol{S_i}$	An External Force
$\boldsymbol{\imath, j, k = x, y, z}$	Directional coordinates
$\boldsymbol{x_i}$	i-th Component of the Cartesian Coordinate System

Chapter 1

An Introduction to Trailer Development

There are many papers available discussing the context of improving heavy goods vehicle (HGV) design with specific intention to improve the aerodynamic performance of such vehicles. Through papers that span a number of decades, and the current resurgence in the perceived importance of aerodynamics due to the increasing costs of fuel, the research available varies across the subject of heavy vehicle aerodynamics as a whole, including papers that discuss many different devices and designs. These vary across different classifications of heavy vehicles, with some methodology developed for integration in trailer development, others regarding buses, and some for locomotive design improvement. What all of these have in common, particularly that of trucks, trailers and buses is that these are traditionally bluff geometry due to their intended use for the transportation of goods. Not aided in this respect by legislation intended to provide greater safety measures, these vehicles have classically been developed with maximum operability for transport in mind, rendering aspects such as fuel efficiency as a secondary or lower concern. With increasing operational costs however there is incentive to improve design methodology and integrate solutions that reduce the aerodynamic penalty of their bluff nature, while maintaining the operability that is of utmost importance to the business function of these vehicles.

Research into the efficiency improvement of heavy vehicles is somewhat sporadic and peaks at points where the incentive to reduce fuel consumption is great due to high fuel costs, meaning for example that there is little published research related to this during the 1990's. What research that does exist can be found in learned journals, thesis', research papers, and commissioned reports via industry or government organisations, as well as independent investigations into improving performance by companies attempting to improve their design options. Research in this subject area often focusses on a particular area of aerodynamic performance and improvement

via a singular method, with little in the way of combination analysis or varied option analysis, despite this hoewever, there is a wide range of studies of varied scope which attempt to theorise, design and test different aspects of HGV aerodynamics. Within this much of the work uses baseline measurements and characteristics that are typical of North American configurations, which do not conform to regional legislation within the EU, and are therefore not as applicable to research and developments in the EU. Despite this, there are many areas of interest to researchers that apply generally to bluff-body aerodynamics research and can be extrapolated, examined and developed with the specific regional legislation requirements in mind.

1.1 Trailer Aerodynamics

Early work investigating the aerodynamics of truck-trailer combinations by Flynn and Kyropoulos (1962) and Sherwood (1974) took place due to the potential for reducing the drag coefficient of haulage vehicles. This remains the driving force behind research in the area today because of the consequential reduction in fuel consumption, with additional relevance due to the present increases in fuel cost, and the large number of truck-trailer combinations operating on a daily basis across the globe. In 2009 HGV transport in the UK consumed $718,000,000$ litres of fuel (DECC, 2009), and with a diesel price of £1.44 per litre (The-Automobile-Association, 2012) in 2012 there are currently great economic benefits to be gained through the reduction of fuel consumption, in addition to the environmental benefits of reduced greenhouse gas (GHG) emissions. For every litre of diesel used $2.6008 KgCO_2e$ (kilograms carbon dioxide equivalent) is emitted (The Carbon Trust, 2013). If only 1% were saved of the total consumption recorded in 2009, it would equate to a GHG emission reduction of $18,673,744 KgCO_2e$, a huge reduction and one that will likely only become more relevant over time.

Numerous methods have been hypothesised and focussed on to improve the aerodynamics of HGV trailers, with many involving design alterations or devices that

can be attached to the trailer in order to modify the form and reduce the drag imparted on the vehicle while in motion. The reason for a focus on additive designs as opposed to the classical reduction and sculpting methodology to improve aerodynamics is the operational function of HGVs. The function is to transport goods, typically stacked and secured in cubed configurations (figure 1.1.1) meaning that the internal structure of the HGV trailer must remain cuboidal also.

Figure 1.1.1: Standard Pallet Stowed on a Trailer

1.1.1 Trailer Geometry

There are many variations of HGV trailer configuration that are manufactured and operated within the UK. These can be subdivided into the categories of rigid vehicles and articulated vehicles. Rigid vehicles are determined as such because the cab and storage trailer are mounted onto a singular chassis. These can range from 4.5 tonne to 18 tonne vehicles. Articulated trailers are those that are a standalone structure and are connected to a cab which pulls the structure behind it. These can typically weigh up to 44 tonnes when loaded and can measure up to 5 metres tall and 15.65 metres long. The potentially very large form of trailers means that in some circumstances, while travelling at the UK motorway limit of 56mph they can incur large amounts of aerodynamic drag as the cab attempts to move through the air.

The overall structure of the articulated trailer is dependent on its intended op-

erational requirements, the most basic differentiation is that of whether it is a curtain-sided trailer or a box-van. A curtain-sided trailer is characterised by the sides having a slide-able soft structure that can removed to expose the internal capacity of the trailer, as previously shown in figure 1.1.1. This structure is used when there is a need for the trailer to be able to be loaded/unloaded from the side. A box-van trailer by comparison has no side access, and as such access to the internal area is only available from the rear. This simple differentiation presents impacts to the trailer structure beyond the simple nature of the side face of the trailer. It defines the cant rail that must be used along the roof line, it defines the structure of the bulkhead frame, the side-rave used and the overall unladen weight of the trailer which in turn affects the total load that can be transported, due to these differences.

Figure 1.1.2: Refrigerated Box Van Trailer

Beyond the initial simple differentiation of curtain-sided trailer or box-van, the operational requirements then determine the number of axles, as a typical axle is rated to support 9 tonnes of load, this determines whether 2 or 3 axles are required, altering the number of wheel structures and tyres that are incorporated, which in turn alters the positioning of the tyres overall. The individualities of each trailer structure do not end at these differentiators, as every dimension of the trailer can be customised by the operator in question to fit their operation. This level of customisation exists because large investments are made by business into their logistics networks. This includes building their own distribution centres, the dimensional aspects of this such as the height of loading bays determine the requirements of

the trailers that they have manufactured. As a result, trailers manufactured in the UK are highly customised on a per-operator basis rather than being a standardised design. While the features of a trailer may be standard options across the industry, their implementation and the specifics of their design are anything but standardised.

This element of customisation in the UK market means that the potential implementation of design alterations to improve aerodynamic performance has both advantages and disadvantages. There is an advantage in that experience of creating every trailer in a bespoke manner means UK manufacturers are better able to implement deviations from standard design practises, in a more capable manner. However, there is a disadvantage present in that much of the literature that details geometry modifications and their effects on aerodynamic performance cannot be easily implemented because of the specific requirements of individual operations and their unique requirements.

Research into improving aerodynamic performance focusses on individual areas of potential improvement. Each of these focus areas has been the subject of independent research, with the goal of reducing vehicle drag of bluff-bodied HGVs. Typically the methods proposed for improvement are defined as devices that can be applied post-manufacture, rather than investigating the advantage that can be gained through implementation during manufacture. Some such devices and methods that have emerged for further testing and analysis under numerous circumstances through literature are that of base drag at the trailer rear, flow deflection, under body modification and cab-trailer gap treatment. These represent the core areas of research into the reduction of aerodynamic drag on HGVs, as they can all be implemented without needing to significantly alter the usable internal capacity of the trailer geometry.

1.1.2 Aerodynamic Trailer Development

As stated, the primary purpose of the HGV trailer is to transport goods, and its ability to do this is the most important factor to the end-user operator. Optimisation of its form and design for fuel efficiency are a secondary concern, but one that has been growing in the mindset of environmentally responsible operators and those that simply wish to reduce fuel consumption and lessen operational costs. This is not just a recent concern, in 1991 in the UK, a project to develop an improved cab-trailer combination for improved aerodynamic performance was undertaken between freight operator TNT and manufacturer Cartwright Freight Systems (Energy Efficiency Office, 1992). The results of this combination of cab deflector and modified trailer geometry yielded a 16% reduction in fuel consumption. This is the first instance of a trailer being specifically designed at the point of manufacture for the purpose of improving aerodynamic performance and reducing fuel consumption through the use of skirts and an angled rear roof section.

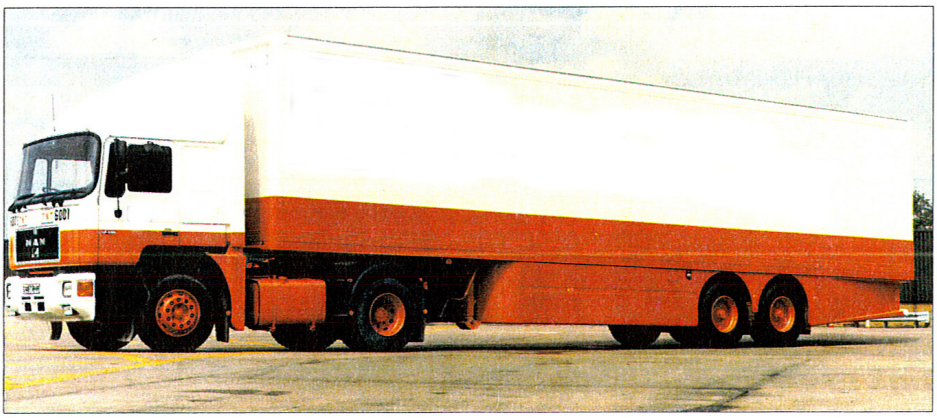

Figure 1.1.3: 1991 Prototype Trailer

Prior to this, there have been many investigations into the potential to improve the aerodynamic performance of trailers, much of these obtained their conclusions from on-road testing or coast-down analysis and comparison of fuel consumption, and were in conjunction with testing on the truck geometry. Investigations such as that of Saunders et al. (1985) which implemented both wind-tunnel and on-road

testing questioned the ability of wind-tunnel testing and recommended on-the road testing only due to experimental tests out performing the on-road equivalent. Other testing such as that of Allan (1981) used highly simplified geometry, in this case multiple cuboids, to represent theoretical testing on that of the truck-trailer combination, specifically focussing on the impact of the gap distance between the truck and the trailer. In the cases of Steers and Saltzman (1977), Muirhead (1981) and Cooper and Campbell (1981) a more general approach to studying flow around the combination vehicles was taken, while others focussed on the truck alone, such as Drollinger (1987) that aimed to analyse and improve the truck geometry of Kenworth Trucks alone without studying the trailer's effects.

These are all classical studies that show even three decades ago there was relatively significant studies on the bluff bodies of HGV combinations. Through the course of studies such as these and more focussed studies since, particular areas of investigation were identified and examined.

1.1.3 Areas of Investigation

Studies such as that in Wong et al. (1981) highlighted typical areas that were the source of drag on truck-trailer combinations. Due to the maintenance of the operational condition to transport cuboidal goods, these areas have remained the same sources of drag for many years, and have directed work on specific areas of drag improvement. This has lead to a standard list of areas and devices that are consistent among the majority of trailer geometry as either having the potential for improvement or consistently being improved with particular geometry modifications.

1.1.4 Trailer Base-Drag Reduction

Base drag created by the detachment region at the rear of the trailer was identified and reduced through the inclusion of angled plating around the rear face, such as those in (Muirhead, 1978) and (Muirhead, 1981). This aims to reduce the size of

the partial vacuum created at the rear of the trailer by reducing the area at the point of airflow detachment at the rear, and thus reducing the size of the wake region. In the case of Muirhead, this method reduced fuel consumption by 7-8%. The boat-tail design has since been tested in various configurations such as differences in size, positioning, surface orientation, and in more recent investigations have resulted in reduced drag improvement estimations of 10-12% (Leuschen and Cooper, 2009)(Browand et al., 2005).

The study in Hsu et al. (2004) showed that the plate length impacted the effectiveness of the device, and also investigated methods of optimising the use in this area by testing oscillating of the plates, finding that it was possible to improve performance further with this method. However, testing such as this is neglecting to consider the plausibility of use during operation. Even now, there is a reluctance in industry to incorporate boat-tail designs onto trailers in operation, because of the potential damage and inherent cost that could be involved with such a device, other methodologies such as that of inflatable boat-tails (Elankumaran, 1997) are less plausible still for real-world operation.

Trailers in operation can travel over 80,000 miles per year, and their general operation means that they will incur damage and must be hard-wearing. It is this circumstance that makes operators reluctant to risk incorporating such a device on a large scale, and implementing methods such as oscillation is simply not plausible for use in general operation in a fleet environment. Despite this, with between 50 and 60 percent of total trailer-drag attributed to the under body and rear interactions(Raemdonck, 2006) there is great potential for reduction in these areas.

Figure 1.1.4: North-American Trailer with Boat-Tail

Other investigations into the reduction of turbulence in the wake of a trailer refined the boat-tail through the introduction of active flow control (AFC) methods (El-alti et al., 2011), this involves the injection of air into the low-pressure wake at the rear of the trailer through blowers, either directly or with the integration of a boat-tail attempting to take advantage of the the Coanda effect(Coanda, 1938) to maintain flow attachment and reduce the rear wake. AFC methods have the potential to reduce drag by 3 percent over an equivalent boat-tail without AFC according to El-alti et al, however in other studies a drag reduction of up to 20 percent is reported as possible(Seifert et al., 2009) although no allowance is accounted for regarding the potential weight increase and power requirements that could negate potential savings in real-world conditions.

1.1.5 Side-Skirts and Under Body

Side-skirts are positioned low along the sides of the trailer, level with the trailer walls and outside tyres. Their purpose is to increase the flow-surface along the sides of the trailer and limit the turbulent airflow allowed to enter the undercarriage, which then incurs drag through interactions with complex structures on the underside of the trailer such as the tyres, axles, braking structures and the chassis itself. Cowperthwaite (1986) found that using a full side-skirt design on a trailer model could reduce drag by 8 percent while studying the scale effects of skirting in order to reduce water spray dispersion while on the road in wet conditions. Studies such

as this and that of Olson and Fry (1988) show the beneficial correlation between improved aerodynamics and safety aspects such as visibility for road-users and vehicle stability also.

There have been numerous other studies investigating the benefits of skirts including Hakansson and Lenngren (2010) which tested sideskirts alongside other devices offering an optimum combination including sideskirts capable of achieving 7 percent fuel savings over a standard base-trailer. Leuschen and Cooper (2009) tested skirt designs in an investigation into commercial aerodyamic products, finding that characteristics such as the clearance between the skirt and road surface influence their effectiveness, as seen with the differences in drag reduction from previous studies (Leuschen and Cooper, 2006). Studies on similar geometry as seen in Miralbes (2012), Martini et al. (2012) and in a more rudimentary manner by NASA in Saltzman and Meyer Jr (1999) all agree that on truck-trailer articulated bodies and indeed on any blunt body with an exposed under body region, that placing blocking/skirt geometry along the side faces improves the overall flow structure and aerodynamic performance of the geometry.

Figure 1.1.5: North-American Trailer with Skirts

While the geometry modification required to implement skirting is relatively simple in theory, implementing this on a vehicle that is in constant operation presents issues regarding reliability and longevity due to the degree of exposure the structure will undergo, especially given the required proximity to the road and wheel

structures. These issues raise questions regarding the usefulness of such geometry because of the potential additional maintenance costs that may delay the payback period while the geometry reduces fuel consumption. This has lead to studies such as that of Kiel (2009) where more suitable materials with higher resistance to impact and general wear and tear are identified for inclusion in the manufacturing process, though methods such as this are typically implemented in devices for retrofitting in North-America. In the UK structures such as these are still typically manufactured using glass re-enforced plastic (GRP) due to its low-cost and relative damage resistance. While GRP is still somewhat brittle and does not have the flexibility of thermoplastic compounds, operation in the UK is less prone to damaging the under body region due to a smaller area between that of the kingpin and the leading trailer axle, and also the legal inclusion of guard-rails as a safety measure to prevent trappage under the trailer body. As a result of this, European and UK trailers are less likely to encounter collisions involving the under body, resulting in trailer skirt damage being less of an issue. In the UK trailer manufacturers believe that collisions with the rear section of the skirting body, behind that of the rear axle is more of a problem area and typically occurs during manoeuvres or while reversing onto a distribution centre loading bay. Figure 1.1.6 shows impact damage occurring due to an incline, in this case the thermoplastic used warps under pressure.

Figure 1.1.6: North-American Trailer with Skirt Impact Damage

Figure 1.1.3 shown earlier displays the form of guards manufactured using GRP in the UK. As they are implemented at the point of manufacture, the appearance

is such that they are a part of the overall geometry rather than additional plates applied post-manufacture.

1.1.6 Truck-Trailer Gap Modification

Gap sealing devices aim to limit the airflow allowed to enter the gap between the truck cab and trailer bulkhead, an area that occurs as a result of the modular geometry, which is not exhibited on rigid bodywork, an early iteration of work investigating this area is found in Buckley and Waltson (1976). The overall dimensions of this area can vary depending on the configuration of the truck and trailer used. In North-America it is not uncommon for this area to be very large as the restrictions on overall length are not as stringent, and the fifth-wheel-plate of the truck may be manufactured in may cases is manufactured to allow articulation to occur correctly on the smallest to the largest trailers, meaning that the gap distance may be small on one pairing, and large on another.

Research into this area suggests that the larger the gap is, the higher the effect of the gap area on the overall drag of the geometry. Mason Jr and Beebe (1978) suggests that at the time, the gap region of a North-American combination contributed up to 40% of the overall drag on the geometry. Methodology to rectify this varies from plating the entire area to prevent flow from entering the gap as shown at various gap distances in experimental testing done by Wacker (1985), to other, smaller modifications that aim to affect flow through the region with less intrusive geometry that aims to maintain the articulation capabilities.

Figure 1.1.7: Trailer with Minimised Gap

Designs such as a single vertical strip protruding from the trailer bulkhead (Laydon-Composites-Ltd, 2012), a full seal with similar design to a rear-boat-tail attached to the bulkhead (Freight-Wing-Inc, 2012) and horizontally spaced vertical strips entitled vortex traps (Wood and Bauer, 2003) are examples of attempts to improve this. A more modern experimental study done on full-scale goemetry corroborated with the potential reductions in this area (Ortega et al., 2013). The usefulness of these measures is largely dependent once more of the plausibility of applying this to an operational vehicle. Furthermore, there is little work that has been conducted into this from a European or UK configuration perspective. There are already precedents for the gap to be somewhat reduced by geometry such as that of refrigeration trailers, that implement the powered refrigeration unit in this gap on the bulkhead without introducing issues regarding articulation. Figure 1.1.7 shows that the cab-trailer gap can be minimised very effectively without harming the articulation of the vehicle, however for fleet operation, it is typically prudent to incorporate as degree of tolerance, so that the cabs within the fleet can operate many different trailer configurations without raising an issue. Furthermore, typical control mechanisms for connecting the cab to the trailer reside in this gap region, closing this gap would mean implementing more costly methods of coupling the truck and trailer together. While this is more costly than the traditional method, it does provide a higher degree of safety for the operator as they no longer have to enter the gap region during operational set up, and would employ a ground-level

coupling system for operation without needing to board the structure.

1.1.7 Other Areas

Vortex generators are one area that has recently been added to the lexicon of truck-trailer drag reduction. Primarily used on wing structures to prevent flow separation, the principles behind vortex generators have been applied to trailers in an attempt to prevent or limit flow separation in key areas and smooth detachment in key areas such as the trailer rear. There is little published research specifically applied to their use on tractor-trailer combinations, however their uses in principle have been extensively investigated for aviation and automotive use. General investigations into their principles lend credence to their potential use on areas of probable separation on trailers; Lin et al. (1990) shows the potential for simple vortices to delay flow separation and increase reattachment, applicable to areas of surface flow directional change such as roof sloping on trailers to reduce separation and positively affect the rear-trailer wake.

A commercial product, aimed at the automotive and the haulage industry, has been investigated in use to establish if it can decrease drag on a tractor-trailer in operation (Motor-Industry-Research-Association, 2010*a*). The test focused on using vortex generators to reduce drag created in the gap between the cab and trailer and showed an average fuel saving between 3 and 4 percent. Their structure can be seen in figure 1.1.8.

Figure 1.1.8: Vortex Generator Marketed for use on Trailer Structures

These device-based drag reduction methods are primarily researched in and are applicable to the US market, whereas the European market is difficult to apply devices to, due once again to stringent legislation, and trailers being manufactured to the limits of their allowed dimensions in order to maximise transport capability. Due to this, any device that lengthens or widens the trailer in any way is difficult to implement on a European trailer, instead, in the UK aerodynamic trailers are produced with aerodynamic efficiencies introduced at the point of manufacture. In 2004 Cooper wrote

> "The issue is not how to lower the drag coefficient by a further 0.002, but rather to work with fleets, manufacturers, researchers and legislators to apply what we already know."(Cooper, 2004)

This is the approach European trailer manufacturers are attempting to take with trailer designs that include non-standard modifications such as curved roof structures and claim to reduce drag by doing so (The Cartwright Group, 2010) (Don Bur Bodies and Trailers Ltd, 2010). Because of legislation requirements limiting the potential for elongating the trailer in order to improve aerodynamic efficiency, trailers can be designed to incorporate streamlining techniques while maintaining operational efficiency and meeting legislation requirements. Manufacturers of the Teardrop claim fuel savings of 11 percent in use by operators and the Cheetah Fastback claims 12 percent fuel savings based on operational case studies. Both incorporate streamlined designs to achieve their claimed fuel savings, and maintain

the typical operational capacity of 26 pallets (Knight, 2010). This is a prime example of the development to which Cooper refers, and exists as a result of the stringent legislation that governs manufacture and operation within the EU. This legislation however still dampens the developmental possibilities somewhat, as there is no more direct method than incorporating devices such as boat-tails into trailer designs, yet these cannot be implemented in Europe as they are in North-America, where further research is being conducted on improvement methods through government funding. In 2010 the United States department of energy granted over $115 million in funds for the development of improved fuel efficiency of heavy duty trucks, among engine efficiency improvements, this also included funds for the further research on trailer aerodynamics (United States Department of Energy, 2010). Individual fleet operators are showing increasing interest in the area also, with commissioned reports being produced such as that of Kassim Mohamed-kassim (2009) and that of a report commissioned by the Department for Transport in the UK (Baker et al., 2009), which provides a comprehensive summary of much of the design methodologies that could be implemented in order to improve fuel efficiencies in the heavy goods sector.

Much of the original research that has been undertaken on the subject, as seen, has done so based on scale wind-tunnel testing or coast-down analysis. Full-scale testing is rare due to the scale of the vehicles overall, and facilities that have the capacity for such scale are small in number. Even now, full scale testing is limited to only a small number of cases, such as that of Ortega et al. (2013) and Leuschen and Cooper (2006). However, in recent times computational capability has increased sufficiently that simulations can be calculated using computational fluid dynamics (CFD). This is the case in more modern studies on trailer aerodynamics such as that of Pointer et al. (2009), Malviya et al. (2009), Östh and Krajnović (2012) and Consano et al. (2007). In this way, studying the effects of modifications to standard trailer design can be analysed and drag reductions predicted.

1.2 Computational Prediction of Flow

It is possible to predict flow in any circumstance through the creation of artificial environments that are designed to emulate flow conditions around or inside a geometric configuration that is of interest. This is conducted through the modelling and combination of a variety of methods that have been developed both independently and in tandem over time in order to better be able to simulate the flow of a fluid. Simply put, the primary components that are now classically required for computational fluid dynamics (CFD) are that of the equations governing the flow to be calculated and the method of constructing the geometry in and around the simulation environment for the flow to be calculated within.

The equations for fluid flow have developed alongside computational power over time due to their complexity, even now it is not feasible under normal conditions for fluid flow to be solved with direct numerical simulation due to the computational resources required to achieve this. Instead, partial differential equations are typically used to approximate fluid flow in an iterative fashion, with the involved variables dependent on one another for each iterative calculation. Despite the fundamental set of equations for fluid flow being defined during the 19th century, due to the iterative requirements of the calculations required and their complexity, it would take many years before they were able to be properly utilised through computational assistance.

In order to create an environment in which the equations can be solved computationally, there needs to be a method of defining the geometry and structure within the environment. In order to do this, the computational domain is populated with cells that are used to define the environment and store variables for use in the solver equations. The oldest of these methods is known as the finite difference method of discretisation and uses a series of points linked together by a series of lines to approximate the equations being solved. One of the earliest implementations of a method such as this is seen in Richardson (1911) where this method was imple-

mented in an attempt to predict stresses on a dam structure. As computational power came to fruition and opportunities for complex calculations became possible, further discretisation methods were developed as improvements to the basic finite difference method, namely the finite volume and finite element methods which are standards used today.

The finite volume method differs in light of its namesake, as the flow environment is defined by volumes rather than simply by points, similarly, each volume cell houses the variables to be used in the partial differential equations and is used to approximate evolutions in the flow from cell to cell. This is the basic definition of the environment that populates a typical CFD domain. The first stage of the computation involved in simulating a case however is known as meshing, and this process defines the overall structure of the finite volume grid. Simply put, while the computational domain is populated by cells, the regions of solid and fluid must first be defined, in order for the solver to establish the regions of flow interaction, rather than laminar flow from cell to cell in an empty domain. During the meshing process a number of different forms of volume can be implemented for the cells, and each can impact the effectiveness of the solution dependent on their implementation. Cells can be tetrahedral, hexahedral or cuboidal, and other variations of these structural elements. Whatever the geometric shape used, their intention is to capture the form of the geometry within the environment accurately. This presents the crux of CFD efficiency and accuracy, in order to more accurately capture the form of the flow domain, the higher the number of cells that must be used in order to do so, as the cells are only approximating the geometry because the volumes have sharp edges. The higher the density of cells are around the geometry, typically determines a better approximation of the form. Consequently, the larger the number of cells in the volume, the more expensive the computation is as there are more elements to incorporate into the equations per iteration. Largely this process is handled by software, with the user given tools to define the attributes that the meshing system takes into account when generating the structure in the domain. A popular method

employed for meshing tetrahedral elements originates from Delaunay (1911) which approximates the surface with a mesh of triangles, in a similar way that STL format does for 3D geometry (Roscoe et al., 1988).

Typically the mesh will require assessment to determine if it is fit for the purpose, depending on the mesh generation method used, this can result in erroneous representation of the geometry to varying degrees. In order to test the mesh, comparative establishment can be used if the mesh generation methodology allows this, whereby a geometry with a known value is tested to establish the margin of error. Additionally mesh independence is a method whereby a number of tests on varying mesh densities are conducted while comparing a set of variables. Once the difference between variables is sufficiently small despite the change in mesh density, then the mesh is considered to be independent, and further refinement can take place to make the mesh more efficient, aiming to achieve the same values with as few total cell volumes as possible so as to reduce the time taken to solve the simulation. Beyond this, the intention of the intended study is used to dynamically determine the appropriateness of the mesh for its given purpose.

The other crucial component to the simulation is that of the solver itself. As explained, this is the implementation of the partial differential equations over the entire computational domain. The main set of equations used for this process are the Navier-Stokes equations, consisting of the three conservation equations of mass, momentum and energy, these provide a complete mathematical description of the flow of incompressible Newtonian fluids (Munson et al., 1990). These equations were originally formulated by Stokes (1846) and their name is determined from his expansion of memoirs noted by Navier (1823) and Poisson (1831).

The Navier-Stokes equations for incompressible flow, as written in differential Eulerian (vector) notation are:

$$\Delta.\vec{u} = 0 \tag{1.1}$$

$$\rho\Delta.\vec{u} = -\Delta\rho + \mu\Delta^2\vec{u} + \rho g \tag{1.2}$$

Where ρ is density, $\vec{u}$ is the velocity vector and μ is dynamic viscosity.

The conservation equations for mass, momentum and energy equations implemented in a cartesian coordinate system can be written as (Dassault Systemes SolidWorks Corp, 2013):

$$\frac{\partial\rho}{\partial t} + \frac{\partial(\rho u_i)}{\partial x_i} = 0 \tag{1.3}$$

$$\frac{\partial\rho v_i}{\partial t} + \frac{\partial}{\partial x_j}(\rho v_i v_j) + \frac{\partial p}{\partial x_i} = \frac{\partial}{\partial x_j}(\tau_{ij} + \tau_{ij}^R) + S_i \tag{1.4a}$$

$$i = 1, 2, 3 \tag{1.4b}$$

$$\frac{\partial\rho H}{\partial t} + \frac{\partial\rho v_i H}{\partial x_i} = \frac{\partial}{\partial x_i}(v_j(\tau_{ij} + \tau_{ij}^R) + q_i) + \frac{\partial p}{\partial t} - \tau_{ij}^R\frac{\partial v_i}{\partial x_j} + \rho\varepsilon + S_i v_i + Q_H \tag{1.5a}$$

$$H = h + \frac{v^2}{2} \tag{1.5b}$$

Where v is fluid velocity, ρ is density, τ_{ij} is the viscous shear-stress tensor, S_i is an external force due to porus media, bouyancy or gravitational acceleration where g_i is the acceleration component along the i-th coordinate direction as well as any degree of rotation in the coordinate system. Q_H is a heat source per unit volume and q_i is the diffusive heat flux. This is the implementation within a specific solver from CFD software FloEFD (Mentor Graphics, 2011).

A more generalised expression of the Navier Stokes equations for a cartesian grid

can be written as (Munson et al., 2012):

X-Axis

$$\rho\left(\frac{\partial u}{\partial t}+u\frac{\partial u}{\partial x}+v\frac{\partial u}{\partial y}+w\frac{\partial u}{\partial z}\right)=-\frac{\partial \rho}{\partial x}+\rho g_x+\mu\left(\frac{\partial^2 u}{\partial x^2}+\frac{\partial^2 u}{\partial y^2}+\frac{\partial^2 u}{\partial z^2}\right) \quad (1.6a)$$

Y-Axis

$$\rho\left(\frac{\partial v}{\partial t}+u\frac{\partial v}{\partial x}+v\frac{\partial v}{\partial y}+w\frac{\partial v}{\partial z}\right)=-\frac{\partial \rho}{\partial y}+\rho g_y+\mu\left(\frac{\partial^2 v}{\partial x^2}+\frac{\partial^2 v}{\partial y^2}+\frac{\partial^2 v}{\partial z^2}\right) \quad (1.6b)$$

Z-Axis

$$\rho\left(\frac{\partial w}{\partial t}+u\frac{\partial w}{\partial x}+v\frac{\partial w}{\partial y}+w\frac{\partial w}{\partial z}\right)=-\frac{\partial \rho}{\partial z}+\rho g_z+\mu\left(\frac{\partial^2 w}{\partial x^2}+\frac{\partial^2 w}{\partial y^2}+\frac{\partial^2 w}{\partial z^2}\right) \quad (1.6c)$$

On the left are acceleration terms, and the right houses force, where u,v and w are the corresponding velocity components for their given dimensional axis.
Typically, the equations will be solved iteratively in an averaging manner so as to gauge the average flow phenomena independent of the flow variations that occur, especially in turbulent cases. While this method does not display the exact effects of flow in any given area, it gives an approximation of what occurs over the total number of iterations, leaving an impression of turbulent regions and their locations, while not defining the variations of this over time. An early example of this is as seen in Williams (1969) and given grater explanation in Taylor and Hood (1973)

This averaging is evident in the momentum equations used in the FloEFD solver. It uses averaging to incorporate turbulent fluctuations into the flow approximations and averages the fluctuations as they appear so as to provide a snapshot of flow as its effects over time, despite not being a transient solution. The typical method used for this is known as the Reynolds-Averaged Navier-Stokes (RANS). The equations in 1.3, 1.4a, 1.5a use Favre-Averaged Navier-Stokes originating from Favre (1969). Unlike standard Reynolds-Averaging, Favre-Averaging is density-weighted, it is also known as the compressible RANS equations. So while they serve the same purpose,

Favre-Averaging provides a greater usefulness when calculating compressible flows above $100m/s$, below this, flows are considered to be incompressible (Davidson, 2011).

Due to their nature, exact solutions for complex geometries are impossible as the flow field will be constantly changing dependent on the turbulent or laminar nature of the flow. For most flows, and particularly for flows over complex geometry such as that of a HGV truck-trailer combination, the flow sill be highly turbulent. A turbulent or laminar flow regime can be determined by the Reynolds number of the flow environment. This was originally defined by Reynolds (1883) as a ratio of inertial and viscous or friction forces, specifically to flow within a confined environment such as a pipe. The general Reynolds number is defined as

$$Re = \frac{(\rho v^2)}{(\mu v/L)} \tag{1.7}$$

Where ρ is density, v is flow velocity μ is dynamic viscosity and L is the characteristic length. This can be used to determine whether a flow regime is laminar or turbulent for any given flow environment using a blockage dimension as the characteristic length.

The Reynolds number defines whether a flow is laminar, transitional or turbulent. His work studying streamlines in a pipe showed that below a threshold the lines would not distort and above a threshold they would deform significantly, and the in between areas are transitional. While there are clearly defined definitions for these three states for flow in a pipe, there is no clearly defined range that encompasses all flows as the variation in flows can be infinite and the characteristic length does not take into account the overall size of the domain. Despite this, an understanding of the flow environment and the Reynolds number can provide a good insight as to whether the regime around a geometry will be laminar or turbulent. For example, flow around a cab-trailer truck combination that is 16500mm long and 4200mm high

is approximately 6,350,000, and the flow is turbulent.

Turbulent flow raises issues with computational approximation, as the Navier-Stokes equations do not account for the effects of turbulence directly. Areas of turbulence form primarily when there is separation from the blockage geometry and eddies form. The interactions that occur within the flow region because of turbulence are highly complex and difficult to approximate. The most accurate way to simulate turbulence is with direct numerical simulation, however as discussed, this method is not practical given the intense computational requirements of attempting to directly solve the flow, what's more it is required for this that the simulation be transient, adding further computational expense (Le et al., 1997).

In order to mitigate the problem of not being able to solve turbulence directly, turbulence models are integrated into the application of the RANS equations as briefly described previously. There are numerous turbulence models that have been proposed, the most classically used is that of the two-equation $k - \varepsilon$ model due to its wide applicability to a variety of engineering situations, it is the general function turbulence model. k determines the kinetic energy involved in turbulence while ε determines the scales of turbulence. The standard model has been modified numerous times in order to either improve particular elements of its performance or focus it in order to better model a particular scenario. One such modification is that of Lam and Bremhorst (1981) which modifies the two-equation model so as to better profile the boundary layer during turbulent flow and can be seen in equation 2.1a.

This is the general process behind the operation of CFD. Other work has focussed on developing CFD for non-engineering analysis such as for visualisation and animation, where numerical analysis is of less importance than visual accuracy of the physical representation of fluids.

1.3 Simplification of Fluid Flow

One of the first uses of a computer program to analyse three dimensional flow was published in 1967 (Hess and Smith, 1967), and this formed the basis for implementation of more simplified fluid flow simulation. The purpose of visualisation rather than physical properties analysis means that the complexities involved in computing the flow need not be as great, however to create a visually authentic simulation the same conservation laws of fluid must be adhered to (Stam, 1999). Some of the earliest uses of Navier-Stokes based simulations purely for visualisation purposes are found in Yaeger et al. (1986), where a 2D system was used to create a realistic planetary atmosphere for inclusion in a motion picture. Gamito (1995) and Chen et al. (1997) also used two-dimensional flow solvers based on Navier-Stokes equations for visualisation purposes, however their over-simplification meant that they did not accurately represent fluid flow to the point of being visually accurate, as a result of not using full three-dimension equations. One of the first implementations to do this is Foster and Metaxas (1997) where three dimensional Navier-Stokes equations are used to simulate the evolution of turbulent gas in a low resolution environment for animation purposes.

One of the main issues with these implementations for visualisation is that they were unstable and may not evolve as expected. The first instance of a stable, three dimensional flow solver that used the full Navier-Stokes equations for visualisation was Stam (1999). In this work Stam describes the creation of a stable fluid solver that is capable of producing high-accuracy fluid-flow simulations at high speed, through sacrificing unnecessary complexity such as the energy conservation equation, which is not needed as the temperature remains static and is rendered irrelevant. This method has remained the basis for fluid simulation with Navier-Stokes equations in products created by Autodesk Inc, such as Autodesk Maya (Autodesk-Inc, 2012). While it uses the same grid-based method for calculating the fluid evolution as typical CFD, one of the key differences in the implementation for visualisation is that

the simplified solver defined by Stam does not incorporate any method to accurately capture turbulence characteristics or allow for unstructured grids, which allow for key areas of flow interaction to be computed to a higher degree of accuracy without mitigating methods that are required to increase the accuracy of a structured grid, while reducing the resources assigned to areas of less importance within the computational domain, as reviewed with various other grid methods by Baker (1989).

Despite developments in simplification such as these and their achieving excellent visual results, the underlying complexity required for appropriate approximation still remains, and the discretisation and solving methods described previously must be adhered to in various forms in order to properly analyse flow phenomena.

Chapter 2

Computational Procedure

This chapter outlines the environment settings and geometry methodology that is used to conduct the test cases and assess the results. The rational behind the simulation structuring is explained with simulations on pre-determined geometry at both small and large-scale to establish the capability of the FloEFD CFD solver. It covers the specifics of the simulation environment and the different geometries that form the case library for testing.

2.1 The Solver

FloEFD integrated into the GUI of SolidWorks is used as the numerical solver for these simulations. The Navier-Stokes governing equations are solved using the finite volume method in a cartesian coordinate gridding system. The solver works implicitly to second order accuracy, and uses the Favre-averaged Navier-Stokes equations to model turbulent flows. Favre-averaging is used over the more typical Reynolds-averaging to better enable the solver to simulate compressible flows at high velocities and therefore broaden the solver's applicability to a larger range of potential simulation cases. Reynolds-averaging is usually preferred due to lesser complexity when studying incompressible flow phenomena, however all cases in this study are considered to be incompressible due to the velocity being below Mach 0.3.

In order to predict turbulent flow, the $k-\varepsilon$ turbulence model is incorporated (Launder and Spalding, 1972). This 'standard' model has been further modified to include dampening functions as described in Lam and Bremhorst (1981) so as to improve the profiling of the boundary layer. Typically, this would be handled by the $k-\varepsilon$ model directly with the wall function approach (Launder and Spalding, 1974) and requires a high density of mesh cells close to the geometry walls in order to do so correctly. As the method used here uses a structured cartesian mesh with immersed testing geometry, the distance between the wall and cell centre can vary greatly,

often it will be exceptionally small and sometimes undesirably large. To account for this, the solver integrates wall functions to fit the geometry boundary layer profile to that of the flow properties relative to its positioning. Taken from Van Driest (1956) these are known as the two-scale wall functions.

The $k-\varepsilon$ turbulence model used from Lam and Bremhorst (1981) consists of:

$$\frac{\partial \rho k}{\partial t}+\frac{\partial \rho k u_i}{\partial x_i}=\frac{\partial}{\partial x_i}\left(\left(\mu+\frac{\mu_t}{\sigma_k}\right)\frac{\partial k}{\partial x_i}\right)+\tau_{ij}^R\frac{\partial u_i}{\partial x_j}-\rho\varepsilon+\mu_t P_B \tag{2.1a}$$

$$\frac{\partial \rho \varepsilon}{\partial t}+\frac{\partial \rho \varepsilon u_i}{\partial x_i}=\frac{\partial}{\partial x_i}\left(\left(\mu+\frac{\mu_t}{\sigma_\varepsilon}\right)\frac{\partial \varepsilon}{\partial x_i}\right)+C_{\varepsilon l}\frac{\varepsilon}{k}\left(f_l\tau_{ij}^R\frac{\partial u_i}{\partial x_j}+C_B\mu P_B\right)-f_2C_{\varepsilon 2}\frac{\rho\varepsilon^2}{k} \tag{2.1b}$$

$$\tau_{ij}=\mu S_{ij}, \tau_{ij}^R=\mu_t S_{ij}-\frac{2}{3}\rho k\delta_{ij}, S_{ij}=\frac{\partial u_i}{\partial x_j}+\frac{\partial u_j}{\partial x_i}-\frac{2}{3}\delta_{ij}\frac{\partial u_k}{\partial x_k} \tag{2.1c}$$

$$P_B=-\frac{g_i}{\sigma_B}\frac{1}{\rho}\frac{\partial \rho}{\partial x_i} \tag{2.1d}$$

Where $C_\mu=0.09, C_{\varepsilon l}=1.44, C_{\varepsilon 2}=1.92, \sigma_k=1, \sigma_\varepsilon=1.3, \sigma_B=0.9$ and $C_B=1$ (Mentor Graphics, 2011).

The two-scale wall functions determine the coupling of the boundary layer calculation for the non-body-fitted cartesian mesh. If the near-wall mesh is deemed to be sufficiently capturing the boundary layer by means of the central point of the nearest cell normal to the geometry wall being greater than the boundary layer thickness, then it is handled as a thin boundary layer. If the thickness lies beyond the normal distance from the wall to the nearest cell centre then it is deemed to be thick and a variation of the momentum boundary condition is used for the Navier-Stokes equations. The turbulence boundary conditions for both thick and thin determinations are the same. Use of these methods ensures that the solver remains stable in all but the most extreme of circumstances, and will represent flow to a reasonable degree

of accuracy even with coarse grids of large near-wall cells that are not sufficiently fine, and due for refinement.

2.2 Performance: Ahmed Body

The Ahmed Body (Ahmed et al., 1984) is a simplified geometry that is intended to represent that of a bluff automobile. Over many years it has become a source of validation due to its geometric simplicity, known dimensions and relatively complex flow. As a result of this, drag values for it are well known and it serves as a good performance benchmark for CFD. The dimensions for the geometry can be seen in 2.2.1.

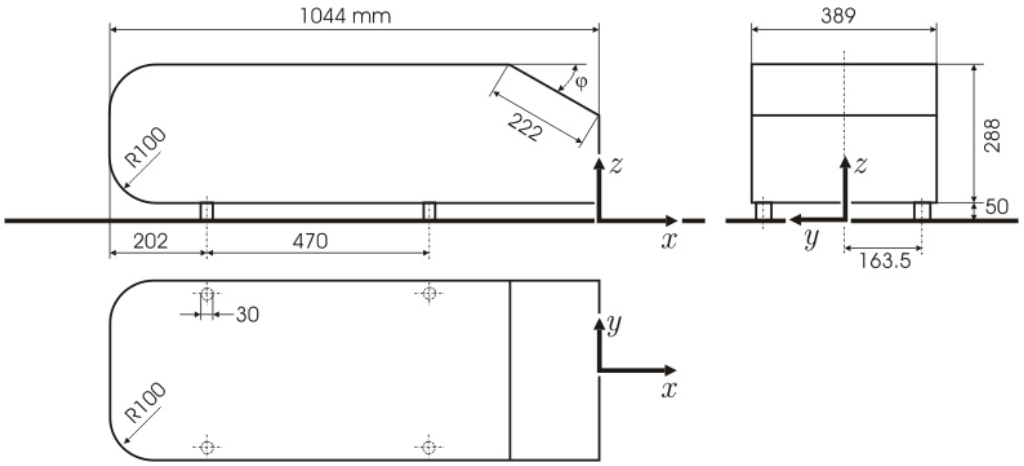

Figure 2.2.1: The Ahmed Body

Variants of the case include two angles of the rear slope, at 25° and 35°, and two velocities, 40m/s and 60m/s. The case studied here is the 25° slope at 40m/s. This is compared to the known experimental drag coefficient (Cd) of the original study and numerical results conducted by Rajsinh and Raj (2012).

The computational domain can be seen in figure 2.2.2.

Figure 2.2.2: Ahmed Computational Domain

The overall dimensions of the Ahmed body can be seen in table 2.1 and the dimensions of the computational domain can be seen in table 2.2.

Table 2.1: Ahmed Body Dimensions

Length (L)	**Height (H)**	**Width (W)**
1044mm	288mm	389mm

Table 2.2: Computational Domain Dimensions

Length (L)	**Height (H)**	**Width (W)**
8352mm	1400mm	1870mm

The domain matches that of the comparison case. The flow velocity is established as $40m/s$ and the density set to $1.2kg/m^3$. A mesh consisting of 2.5 million cells is used to give a reasonable mesh around the geometry, and another mesh of 12 million cells provides a finer mesh for further comparison. The initial mesh ratios are tweaked to centre the cell density around the geometry, giving a higher density of cells around the model. The meshed domain for the 2.5 million cell case can be seen in figure 2.2.3 and a closer image of the mesh around the Ahmed body can be seen in 2.2.4.

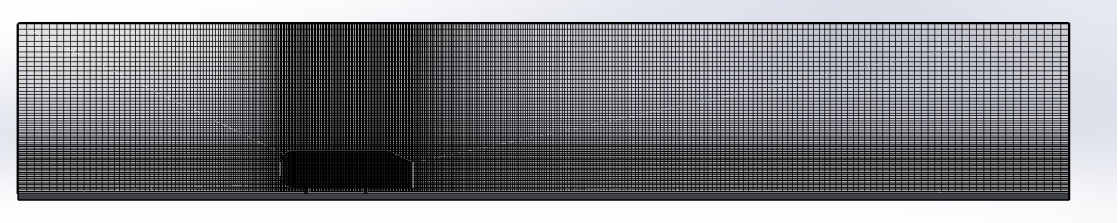

Figure 2.2.3: Ahmed Computational Mesh

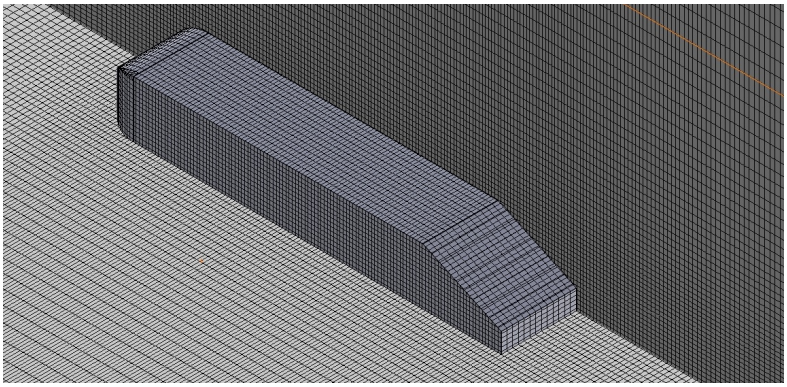

Figure 2.2.4: Ahmed Computational Mesh

Each simulation is run until full convergence over a complete travel, surface values for Fx, Fy and Fz are tracked for convergence and the final results averaged over the iterations of the previous travel through the domain so as to provide a clear representation of the values that are reported. Figure 2.2.5 shows a central plot of velocity in the domain of the 2.5M cell case. Expected flow characteristics are exhibited, including gradual thickening of the boundary layer.

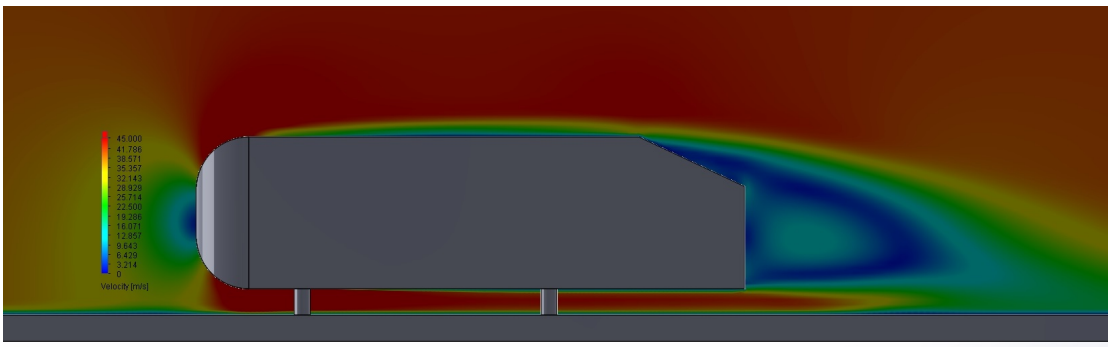

Figure 2.2.5: Ahmed Body Velocity Plot

Of most importance for the purposes of this simulation however is the degree to which it predicts the drag value of the geometry. The drag coefficient is defined as:

$$Cd = \frac{Fd}{\frac{1}{2}\rho\nu^2 A} \tag{2.2}$$

Where Fd is the force in the flow axis, ρ is the fluid density, ν is the fluid velocity and A is the frontal area normal to the flow direction.

Table 2.3 shows the drag coefficient of the four cases compared.

Table 2.3: Ahmed Body Cd Comparison

Experimental case	**Numerical case**	**Test Case 2.5M**	**Test Case 12M**
0.298	0.266	0.312	0.302

Both the 12M cell and 2.5M cell case predict the drag to be slightly higher than that of the experimental value. However, the 2.5M cell case predicts within 4.7% of the experimental value and the 12M cell case predicts within 1.35% of the experimental value. Both of these results show good agreement with the experimental case, especially the 12M cell case, and while the 2.5M case did not perform as well, it is still exceptional given the relatively coarse mesh, and remains close to that of the finer mesh.

This performance shows that the solver used performs well over a range of mesh densities, and can predict turbulent flow around a bluff body with good agreement to established experimental data, and indeed outperform other published cases of CFD analysis of the Ahmed body geometry.

2.3 Testing environment

The computational domain used for testing must be suitable to allow correct capturing of the flow characteristics before and after the test geometry. A view of the computational domain dimensions can be seen in figure 2.3.1.

Figure 2.3.1: Computational Domain

The geometry length used throughout the cases is 16.5 metres. In order to ade-

quately capture flow around a structure this size, the computational domain extends for five times the geometry length at the rear and three times the length at the fore, as well as extending three times the width of the model at each of the sides. In accordance with SAE J1252 (1981) in order to accurately capture flow the total domain blockage by the test geometry is below 5%.

Flow in the domain is established as $25m/s$ to match the maximum UK trunking speed of $56mph$. Fluid density is set to $1.2kg/m^3$ which corresponds to a Reynolds number of $6,354,000$ using the geometry height of $4.2m$ as the characteristic length, the flow is turbulent. To test optimum mesh density, a number of tests of varying cell counts are conducted at $0°$ yaw on a baseline geometry, with a further test using regions of mesh refinement to optimise the cell count. Tests of the domain with cell counts of 3 million, 5 million, 10 million, 20 million and 25 million are conducted and compared to establish mesh independence and can be seen in figure 2.3.2 below.

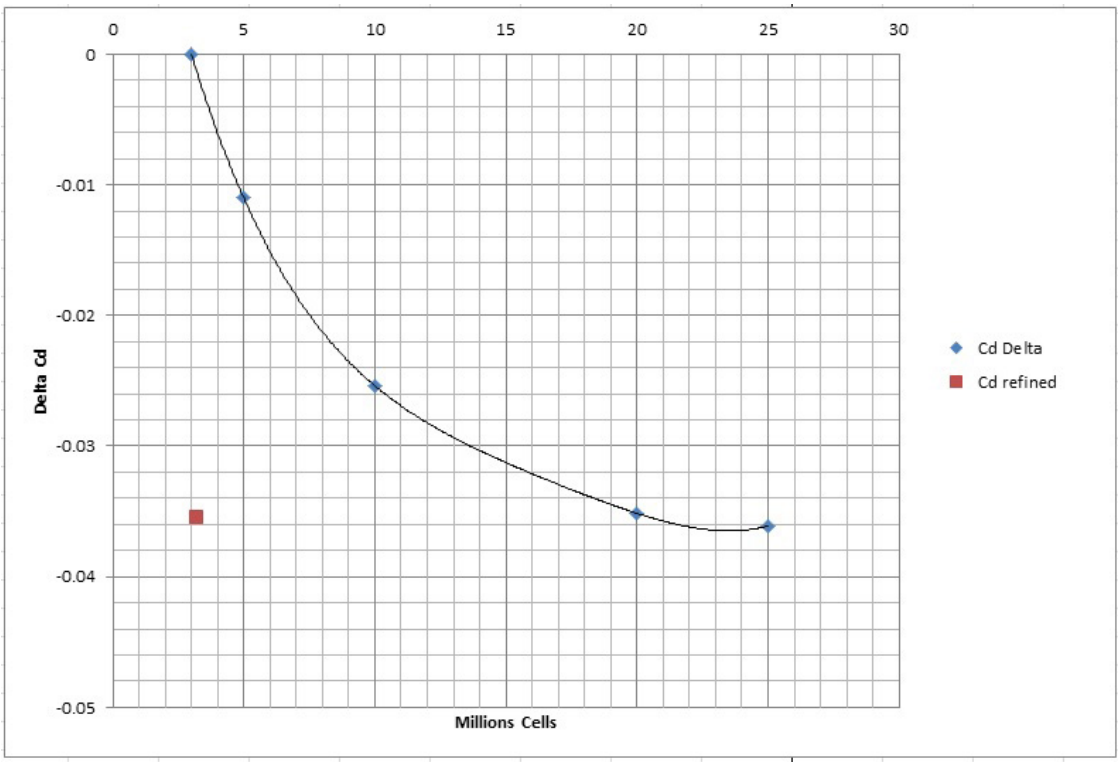

Figure 2.3.2: Mesh Size Cd Comparison

It shows that between 20 and 25 million cells there is very little between the averaged drag coefficient values; only 0.21% difference between the reported values. A further test was conducted incorporating refinement regions to reduce the overall cell count. It is possible to achieve comparative values as the 20 and 25 million cell cases with an overall grid of just over 3 million cells. The mesh and outer refinement region for this domain can be seen in figure 2.3.3. Further refinement takes place by an order of 2 for each cell that is split within this region, meaning that each cell that is defined as partial during the establishment of cell-centre distance is divided by a factor of 8, and the partial cells this creates are further divided by a factor of 8. While this overall cell count is relatively coarse by traditional standards, the methods discussed in the previous section that the solver employs to enable the use of a cartesian grid aid in the ability to reduce overall cell counts. A further performance case is conducted however to further assess the suitability of this domain.

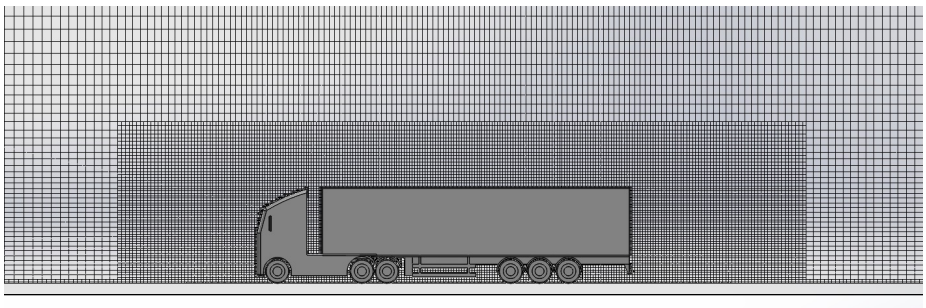

Figure 2.3.3: Refined Domain

2.4 Performance: GETS

The Generic European Transport System (GETS) (Van Leeuwen, 2009) is an example geometry intended to represent a simplified version of a European truck-trailer combination. It is a modification of a North-American equivalent model to represent a simplified truck-trailer combination (Croll et al., 1996).

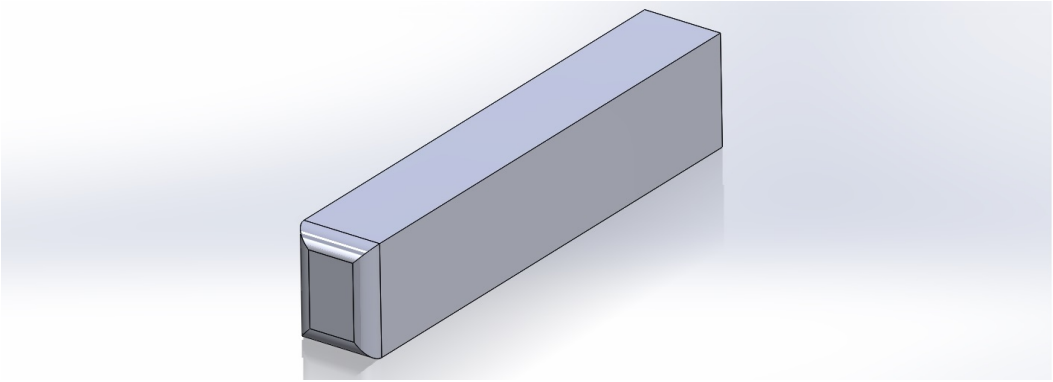

Figure 2.4.1: GETS Geometry

The geometry can be seen above, its dimensions are similar to that of the cases used in this study, as seen in table 2.4.

Table 2.4: GETS Dimensions

Length (L)	**Height (H)**	**Width (W)**
16500mm	2595mm	3510mm

The boundary condition of the ground in the comparison case is that of a moving floor, matching the speed of the free-stream flow of $25m/s$, and the model has a ground clearance of 495mm, this is also replicated in the test case.

The computational domain used is that of the refined mesh set up that was previously created to optimise the 20 and 25 million cell meshes. As the grid is un-fitted cartesian, the mesh settings can be pre-defined and are applied during the process of mesh creation. The same domain is used here as was used for the optimised refinement case, with the GETS geometry correctly positioned in the same position as the baseline model.

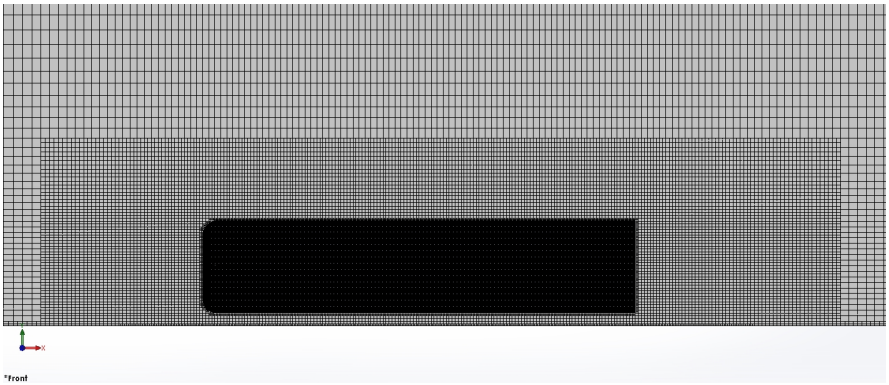

Figure 2.4.2: GETS Mesh

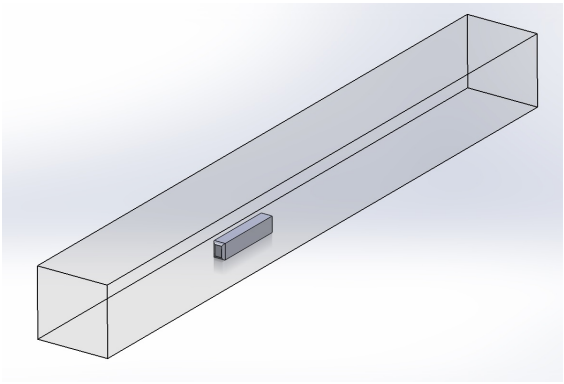

Figure 2.4.3: GETS Domain

Once again the simulation is run until convergence is seen and averaged over the previous travel through the domain to give the averaged drag value. The reported drag coefficient for the comparison case and the test conducted using the domain defined here is seen in table 2.5.

Table 2.5: GETS Cd

Cd (Van Leeuwen, 2009)	**Cd Test Case**
0.320	0.308

This shows that the compared domain produces a value with a 3.75% discrepancy. While not perfect, this value is reasonably close and the difference can be associated with the difference in meshes used for the two cases, and shows that the proposed domain can provide a good prediction of drag values.

This provides reasonable satisfaction that the refined domain will be able to provide sufficient information to be able to compare the drag values of variable geometry features, as is the intention of this study.

2.5 Case Definition

Having established an efficient domain and meshing regime, this is the domain that will be used for the main cases due to its combination of accuracy and computational efficiency. In order to assess each tested geometry more thoroughly, each case consists of two different flow configurations. The first is a zero-headwind case of perfect conditions which tests the geometry at 0° yaw and at $25m/s$ the equivalent of UK motorway speed, $56mph$. A second test is conducted at an angle of 10°. This is to simulate a side-wind condition, and 10° has been chosen because it corresponds with the average UK wind-speed from a westerly direction. In the 10° configuration, a flow in the Z-direction is introduced at a velocity of $4.47m/s$, this velocity is chosen as it is $10mph$, and the average wind-speed over 10 years from 2002 to 2011 in the UK varied from $12.08mph$ to $8.86mph$ depending on the season (Department of Energy and Climate Change, 2013). $10mph$ was chosen as a point in this range to base the side-wind condition on.

Analysing the side-wind condition allows the study to incorporate a more realistic interpretation of the performance of the geometry being tested. Operational conditions vary greatly, and in these conditions there is likely to always be a degree of side-wind influence. Testing at the average UK wind-speed from a 90° angle simulates a vehicle travelling North-South in the UK under influence from a westerly wind. This is a relatively extreme yaw angle, and it should serve to help identify the differences between test geometry further.

The solver and domain settings are identified below.

Table 2.6: Solver and Domain Settings

0° yaw	**Attribute**	**10° yaw**
$1.2kg/m^3$	**Density**	$1.2kg/m^3$
$25m/s$	**Velocity in X**	$25m/s$
$0m/s$	**Velocity in Z**	$4.47m/s$
0.1%	**Turbulence Intensity**	0.1%
$0.0451m$	**Turbulence Length**	$0.0451m$
$No-Slip 25m/s$	**Ground Boundary Condition**	$No-Slip 25m/s$
$No-Slip$	**Blockage Geometry**	$No-Slip$
$RotatingWall 46.9rad/s$	**Wheels**	$RotatingWall 46.9rad/s$
$Slip$	**Domain Walls**	$Slip$

As seen, the ground plane is a moving wall matching the geometry of the flow, and the wheel geometry is also simulated as a no-slip wall with a rotating boundary condition to better replicate real-world conditions. The rotating geometry positions can be seen in figure 2.5.1. The computational domain and geometry positioning is as in figure 2.3.1.

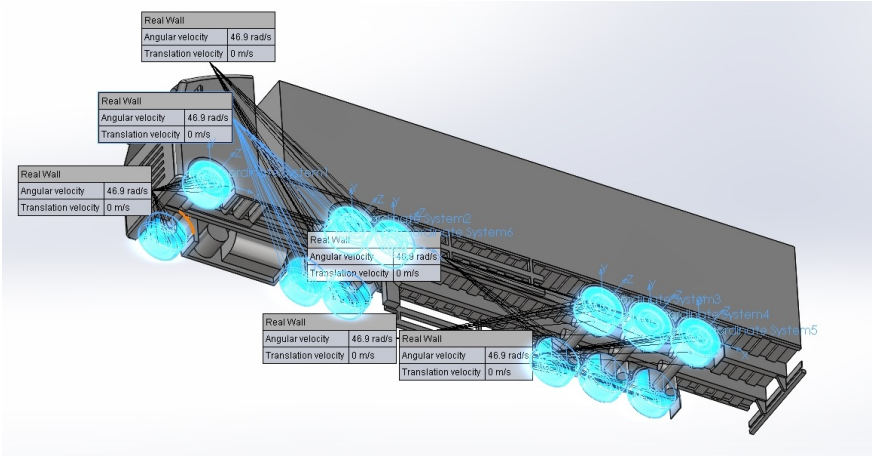

Figure 2.5.1: Rotating Wheel Regions

2.6 Test Geometry

A number of geometries have been selected for testing. Beginning with a baseline case, various other designs will be compared against the benchmark drag value obtained from the baseline. These geometries focus on differing areas of design development on the trailer geometry, as well as some which establish particular flow scenarios based on potential design configuration conditions. Dimension detail for all geometries can be seen in appendix .1.

All geometry cases use the same cab geometry, with the exception of cases that specify any modification to the cab geometry and states the reasons for this. In this way, the drag values compared are known to originate only from the changes to trailer geometry that are present. The choice has been made to match the cab deflector correctly to the height of the trailer at 4.2 metres for the baseline case. While European height limitations mean that overall height of the vehicle is not permitted to be over 4 metres, in the UK there is no such height limit, and trailer heights are very often over 4 metres and can be as high as 4.9 metres. Because of this, there is often the issue of misaligned cab deflector geometry as deflectors over 4 metres are typically specifically made for use in the UK. Due to this issue, there has often been confusion and a lack of standardisation when discussing or analysing trailer aerodynamics, as solutions were often compared with cab options that did not match. By using a correctly matched cab, the results variation source is easily identified and can be attributed to the trailer geometry modification.

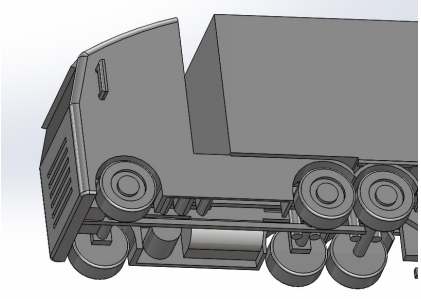

Figure 2.6.1: Cab Geometry

2.6.1 Baseline Case

The baseline geometry, against which the modifications will be tested, has been determined based on a typical UK trailer configuration, matched with the cab it represents a standardised articulated truck-trailer combination. To this end, the baseline trailer overall dimensions can be seen in table 2.7. with an overall drawing of the combination seen in figure 2.6.2.

Table 2.7: Baseline Trailer Dimensions

Length (L)	**Height (H)**	**Width (W)**
13600mm	4200mm	2500mm

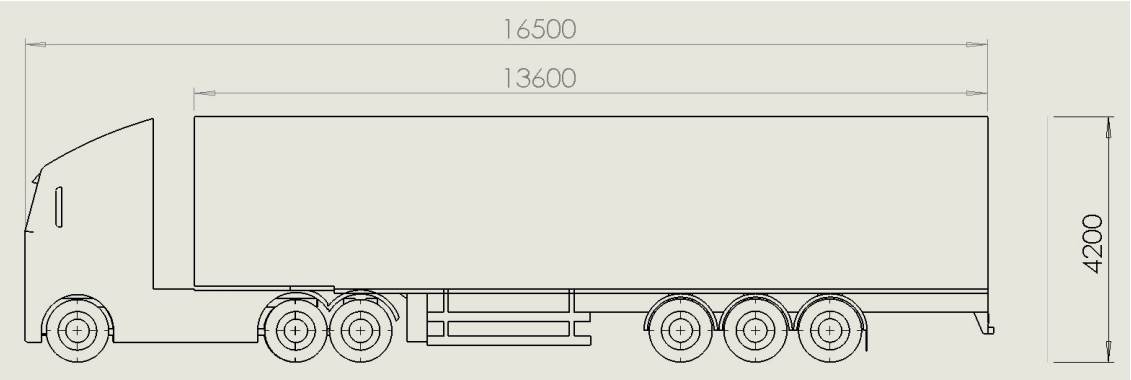

Figure 2.6.2: Baseline Geometry

This is a tri-axle box-van configuration, one which is very common in the UK. A lack of intricate detail means that it represents a tri-axle curtain-sided trailer also, these are the most commonly used specification of trailer in the UK. While operators specify intricate details about particular areas of the geometry at the point of manufacture, in terms of general form, this is the most commonly used baseline design and configuration. Because of this, it is an ideal baseline to compare areas of modified geometry against as it will represent a good approximation of the effects of implementing the particular modifications will have on the average configuration. Each geometry modification builds on this baseline case in some way to identify variances in flow characteristics.

2.6.2 Roof Line Modification

One of the most contended and typical modifications possible at the point of manufacture in the UK is roof line modification. In this section, two geometry modifications are to be tested.

2.6.2.1 Full-Curve Roof Line

In this geometry modification the entire roof line of the trailer is curved, from the bulkhead to the rear frame. This includes increasing the overall height 300mm so that at the peak of te curve the overall height is 4500mm. For the purposes of relative comparison, during the drag coefficient calculation the frontal area will remain the same as the baseline case so as not to skew the results.

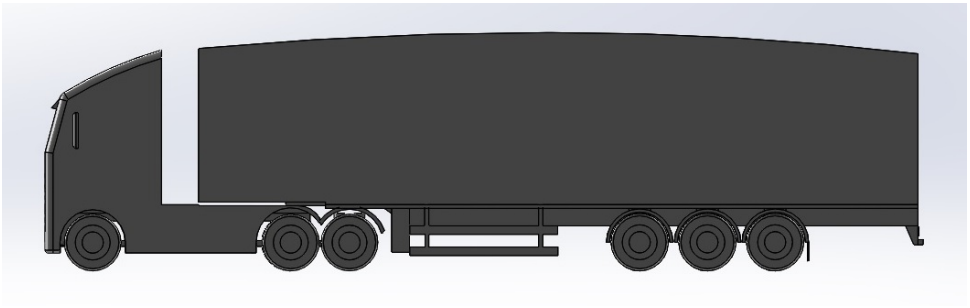

Figure 2.6.3: Full Curve Geometry

2.6.2.2 Rear-Curve Roof Line

This modified roof line is altered without any increase of height, and only the rear portion of the roof line is curved down to the rear frame.

Figure 2.6.4: Rear Curve Geometry

2.6.3 Boat-Tail Geometry

A range of boat-tails are to be studied. As seen in the literature, there is great potential for drag reduction using angles plates at the rear such as this. This study takes note of these despite their current inapplicability to the UK market because of current developments with legislation. Currently under review, the legislation that limits overall length and width of vehicles in the EU, while it currently prohibits the use of geometry such as this, is to undergo modification to allow special allowances for geometry that reduces vehicle drag to be exempted from the overall vehicle dimensions.

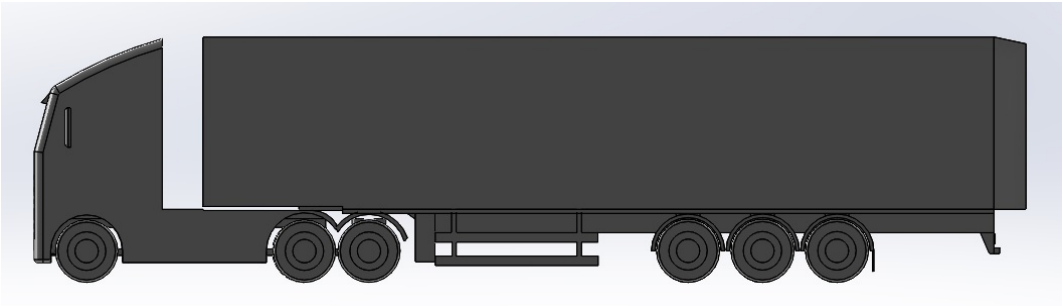

Figure 2.6.5: Boat-Tail Geometry

Four variants of the boat-tail are tested to establish the best performing plate angle, and a further two test geometries include only the top plate and the side plates, to allow identification of their performance in isolation. The geometries for testing are:

- 10° angled plates
- 12° angled plates
- 14° angled plates
- 16° angled plates
- 14° angled top plate
- 14° angled side plates

2.6.4 Side Skirts and Under Body Treatment

Protection bars are required by EU legislation to be in place at the exposed sides of a trailer in order to prevent or limit the degree to which a person or vehicle could get caught underneath the trailer. Replacing the metal guards in this section with smooth surfaces flush with the sides offers an aerodynamic benefit. Three different geometries of skirt are tested to establish flow characteristics and the potential of this method.

2.6.4.1 Basic Skirts

This geometry represents the most basic method of skirt implementation, with two separate flat sheets placed flush with the trailer sides.

Figure 2.6.6: Basic Skirts

2.6.4.2 Basic Skirts with Wheels Covered

Trailer wheels are a somewhat obvious area of drag, due to their complex geometry inside the wheel housing and axles, and rotating surfaces. This geometry adds a further section to the basic skirts that covers the wheel sections on both sides.

Figure 2.6.7: Basic Skirts with Wheels Covered

2.6.4.3 Full Skirts with Under-Plating

A final skirt geometry extends the skirts forward to fully cover the trailer side area as much as possible, flush with the landing legs, with a connecting series of plates on the trailer under side that covers the complex geometry of the trailer under body completely. The wheel covers are removed from this geometry so as to be able to compare the under-plating against that of the covers.

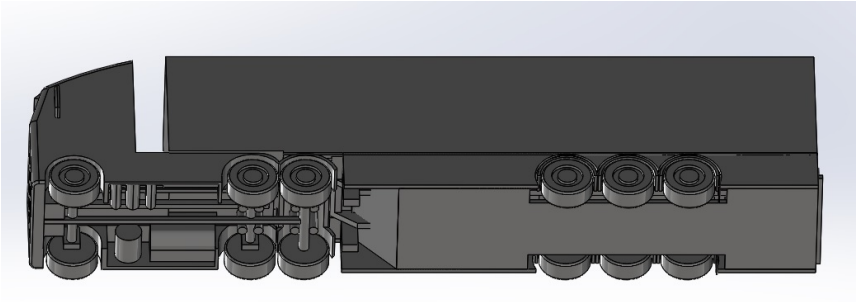

Figure 2.6.8: Full Skirts with Under-Plating

2.6.5 Standalone Cases

Three cases are defined that do not easily fit within a particular section of geometry modification. These cases are used because the modifications made are of interest because they either provide a good opportunity for drag reduction, or they represent a typical situation and are investigated in order to identify the consequences of this.

2.6.5.1 Cab-Trailer Gap Treatment

After studying flow in the baseline case as described in Chapter 3, flow characteristics within the cab trailer gap suggested that modification of this area might provide a positive alteration to the drag of the geometry. To this end, a standalone case that fills the cab-trailer gap is created.

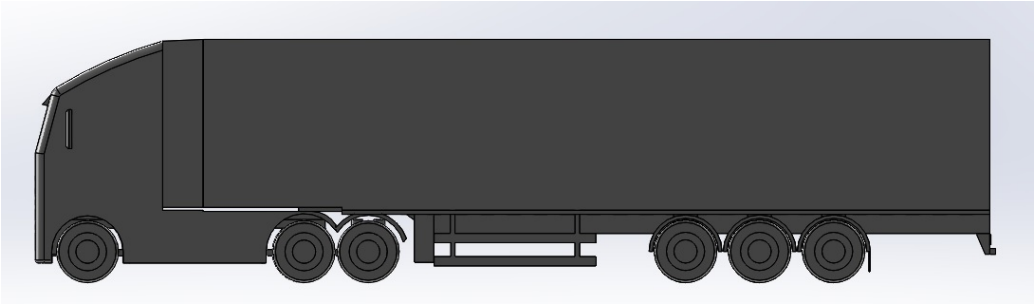

Figure 2.6.9: Cab-Trailer Gap Treatment

2.6.5.2 Misaligned Cab Deflector

As described previously, the baseline case studied here has an overall height of 4200mm, while European trailers will not be above 4000mm. Because of this, it is often possible that a cab deflector will be misaligned to some degree. Investigating the consequences of this, the baseline case is modified so that the cab deflector is set too low by 100mm.

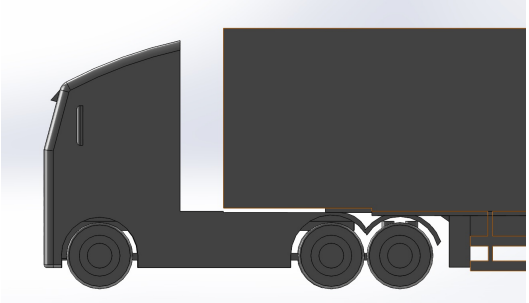

Figure 2.6.10: Misaligned Cab Deflector

2.6.5.3 Rounded Edges

The baseline case represents a standard UK box-van and curtain-sided trailer. To this end, the edges of the geometry are also bluff. While this can be the case for both box-vans and curtain-sided trailers in operation, it is easily rectifiable in the case of a box-van at the point of manufacture, whereas curtain-sided trailers are likely to remain bluff-edged because of the requirements to incorporate the curtain rolling mechanism into the cant rail along the trailer roof line. This geometry aims to test the potential benefits of rounding the trailer geometry edges.

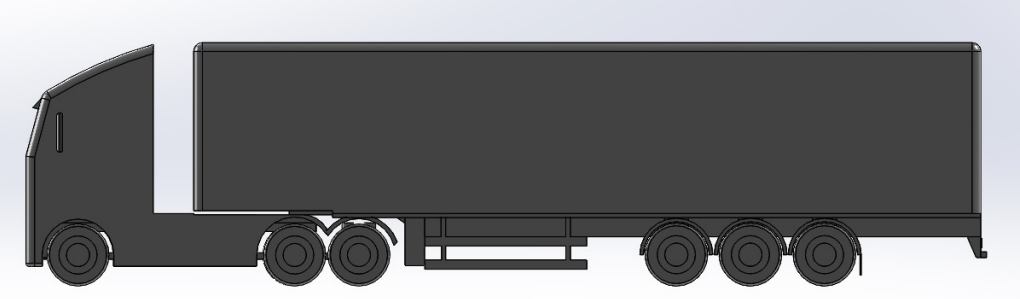

Figure 2.6.11: Rounded Edges

2.6.6 Double Deck Trailers

An extension of the reasoning behind the standalone test of the misaligned cab, three double deck configurations are tested. These are modifications to the baseline geometry that increase the overall height of the trailer up to 4880mm, one of the standard heights for double deck trailers in the UK. Once more, it is often the case that a cab will be misaligned with a double deck due to the enlarged height and the UK being the only market that operates vehicles of such a height. These geometries are intended to study the consequences of the increased height and two methods of mitigating those consequences.

2.6.6.1 Standard Double Deck

This is the baseline case with additional height up to 4880mm and the cab remaining matched to 4200mm. This geometry is intended to indicate the effect on overall drag that operating a double deck with a misaligned cab to this extent will incur.

Figure 2.6.12: Standard Double Deck

2.6.6.2 Double Deck with Deflector

This geometry adds a deflector geometry to the bulkhead intended to round the front face of the trailer. It is a standard method of mitigating the drag incurred, and the method's effectiveness will be investigated.

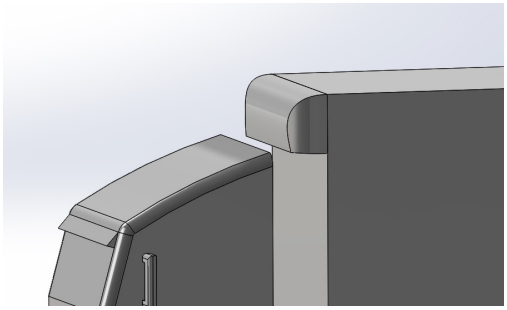

Figure 2.6.13: Standard Double Deck with Deflector

2.6.6.3 Double Deck with Sloping Front

This geometry brings the bulkhead down to a matching height of 4200mm with the cab deflector, while the majority of the trailer body remains at 4880mm. It is possible to implement geometry such as this, but it must be undertaken at the point of manufacture, unlike the bulkhead deflector geometry which can be retrofitted.

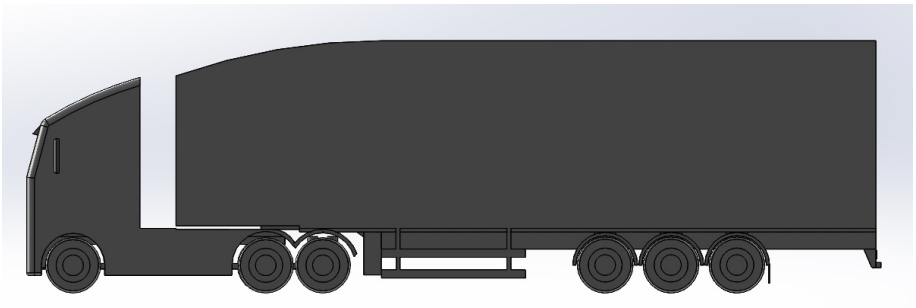

Figure 2.6.14: Double Deck with Sloping Front

Chapter 3

Test Cases Studied

A total of twenty cases have been studied, each at both 0° yaw and 10° yaw flow scenarios. These cases study particular elements in isolation compared to the baseline case geometry, which is intended to represent an average, standardised trailer.

Beginning with an analysis of the baseline case, areas of drag that are potentials for improvement are highlighted. These various areas have numerous solutions that are proposed before being tested to quantify the potential improvements possible.

Beyond direct comparison to the baseline case, several tests are conducted on larger trailer geometries, intended to represent typical double deck trailers. This is to identify the particular areas of drag increase that are incurred as a result of the overall enlargement, but also to identify mitigating geometry for these particular problem areas.

The cases display varying levels of drag reduction performance, with as much as 10% being saved by an individual geometry modification tested in isolation. The highest performing modifications are then combined into a singular geometry representing the optimum combination of methods that have been evaluated.

Table 3.1 overleaf displays a summary of all cases studied and the drag reduction over that of the baseline case in both 0° and 10° yaw. This is followed by analysis of the baseline case and the individual areas of geometry modification represented as a comparison to the baseline case and other companion cases in the same area of study.

Table 3.1: All Cases

Test Case	**ΔCdBase(%) 0°**	**ΔCdBase(%) 10°**
Baseline Case		
Baseline Case	$CdBase0°$	$CdBase10°$
Roofline Modifications		
Full-curve roof line	-6.00	-2.13
Rear-curve roof line	-6.44	-2.91
Boat-Tail Geometry		
10° Boat-tail (550mm)	-9.23	-5.82
12° Boat-tail (550mm)	-9.65	-6.39
14° Boat-tail (550mm)	-9.23	-6.61
16° Boat-tail (550mm)	-8.80	-6.50
14° Side-plates (550mm)	-5.58	-3.92
14° Top-plate (550mm)	-3.86	-2.13
Side-Guards and Skirts		
Basic Skirts	-1.72	-4.26
Basic Skirts with Wheels Covered	-1.93	-5.94
Fuller Skirts with Under-plating	-1.93	-7.62
Standalone Cases		
Cab-trailer gap treatment	-3.65	-10.31
Rounded Edges	-6.86	-4.71
Under-aligned cab	+3.65	-2.13
Double Deck Trailers		
4880mm Trailer	+49.79	+16.59
4880mm Trailer with Deflector	+19.96	+7.29
4880mm Trailer with Sloping Front	+7.73	+2.91
Optimised Combinations		
Optimised Trailer Complete	-16.52	-26.12
Optimised Trailer Limited	-12.66	-16.48

3.1 Baseline model results

3.1.1 0°yaw

Firstly, a detailed analysis of the baseline case is conducted before serving as the baseline of comparison for the other cases. The basic form of the 4.2m baseline model is as in figure 3.1.1. This represents a standard, tri-axle trailer with a height and width-matched cab deflector.

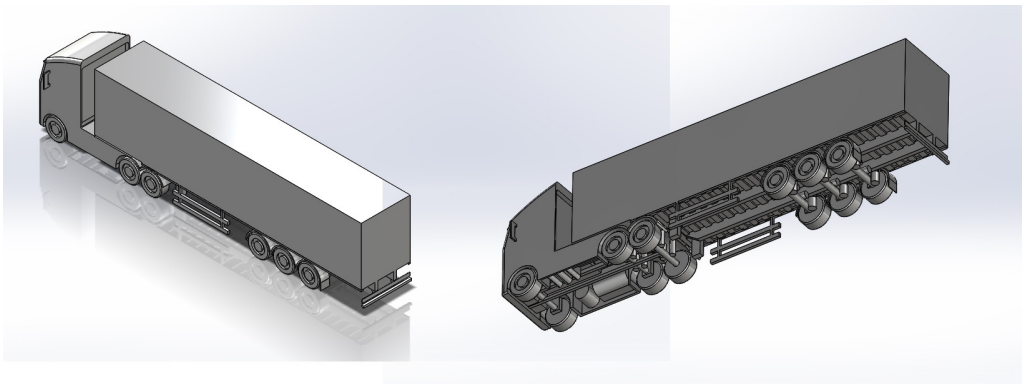

Figure 3.1.1: Baseline 4.2m model

Figure 3.1.2 shows a plot of the velocity in the X direction through the centre of the computational domain. It can be seen that there is a high velocity gradient as flow passes over the cab and transitions onto the trailer roof line. Also in this area it can be seen that there is a drastic separation aft of the the cab deflector. This leaves an undesirable and large area of recirculation at the forward area of the trailer roof line. In addition it can be seen that there is a high degree of acceleration as the flow enters the under-body cavity of the cab, the velocity of this reduces as it reaches the cab's powered wheel section. Flow velocity then remains reduced throughout its travel underneath the trailer before reaching the large wake generated aft of the trailer's rear face, implying a large area of negative pressure on the rear face of the trailer.

Figure 3.1.2: Centre plane velocity in the X direction

Figure 3.1.3 identifies these areas by pressure, showing the pressure coefficient (Cp) through the centre plane. It can be see that the largest area of high pressure is the cab front, due to its large and mostly flat profile. Immediately following this, as shown with the high velocity gradient in figure 3.1.2 there is a separation as flow transitions from the cab to the trailer, resulting in a large pressure drop. At the mid-point in the trailer under-body there is a restoration of ambient pressure briefly before further low pressure is evident as flow reaches the trailer wake. The end-point of the immediate wake is also evident from the Cp plot as a central point where the unsteady wake re-converges.

The pressure coefficient is a dimensionless number that describes relative pressures between the range of 1 and -1, It is defined below.

$$Cp = \frac{p - p\infty}{\frac{1}{2}\rho\infty\nu\infty^2} \tag{3.1}$$

Where p is the pressure at a point in the fluid, $p\infty$ is the pressure in freestream flow, $\rho\infty$ is the freestream density and $\nu\infty$ is the freestream fluid velocity.

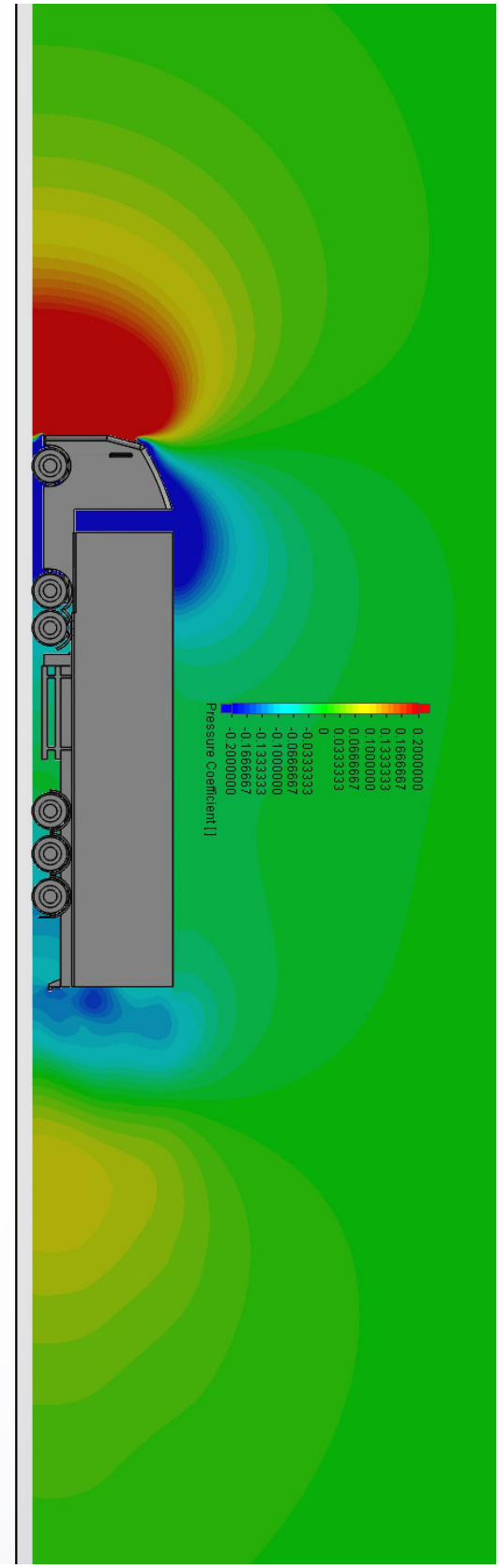

Figure 3.1.3: Centre plane pressure coefficient

Investigating the flow in the under-body region of the model shows that the majority of flow underneath the cab and trailer is low velocity, due to the large degree of separation aft of the cab. Figure 3.1.4 shows the velocity in the X direction while figure 3.1.5 shows general velocity. There are very few differences in the velocity profiles of these two plots, the primary area of difference being underneath the cab, suggesting that flow in this area is very turbulent, and likely to be caused by the high degree of accelerated flow entering the area underneath the cab front. These plots suggest that at 0 yaw, because of the separation evident aft of the cab, that limited airflow enters the trailer under-body.

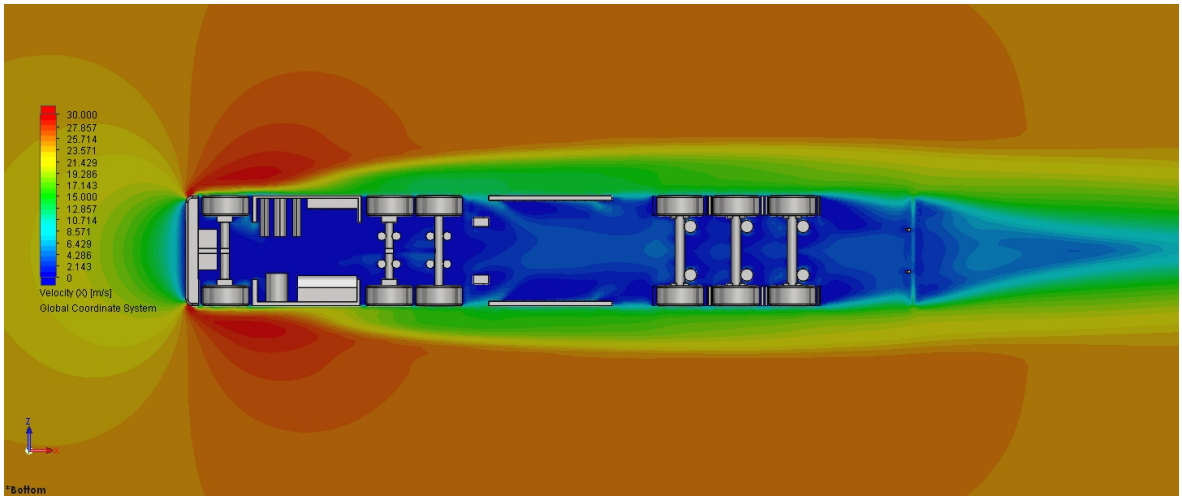

Figure 3.1.4: Under-body velocity in X 600mm height

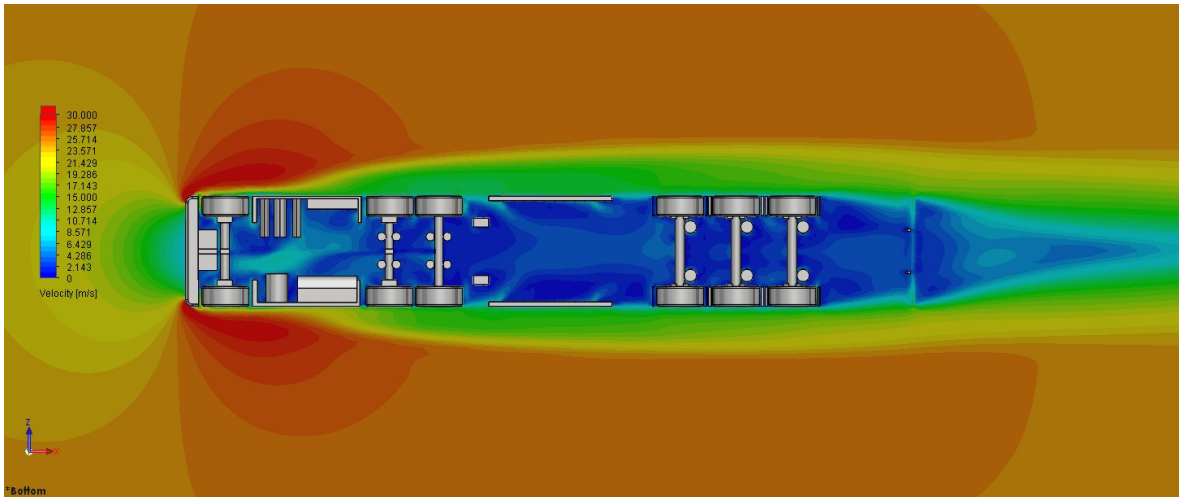

Figure 3.1.5: Under-body velocity 600mm height

Investigating the under-body region further, showing the pressure coefficient on the model surface, figure 3.1.6 shows the effects of the large degree of separation and the low velocity on the under-body region. This is most pronounced by the pressure difference between the tyre faces of the cab and trailer, with the former displaying significantly higher pressures on the forward faces due to exposure to higher velocity flow.

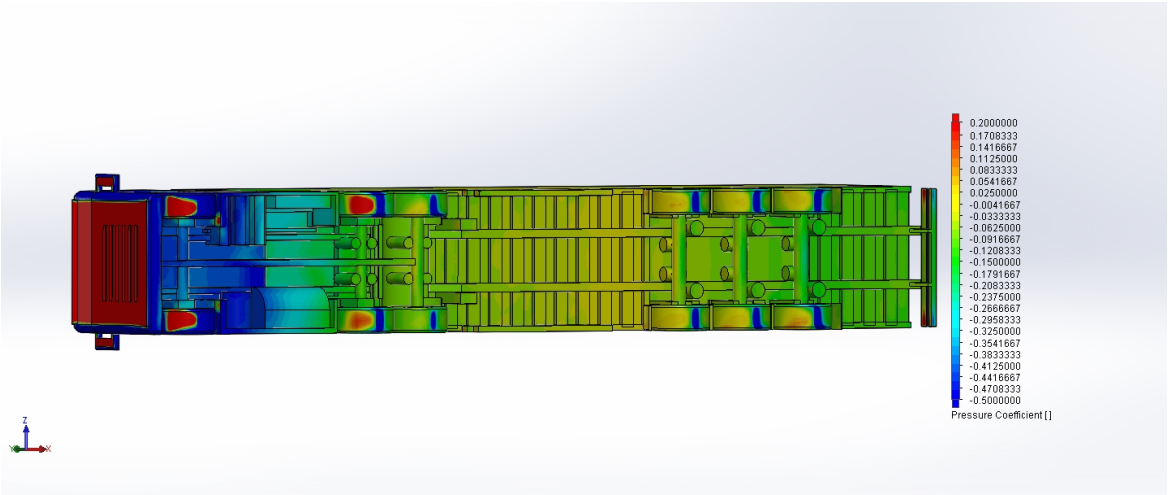

Figure 3.1.6: Under-body Cp

As has been identified, there is a large area of low pressure at the trailer rear, generating a sizeable low pressure wake. Figures 3.1.7, 3.1.8 and 3.1.9 show the trajectories of flow in contact with the trailer's rear face as it progresses through the computational domain.

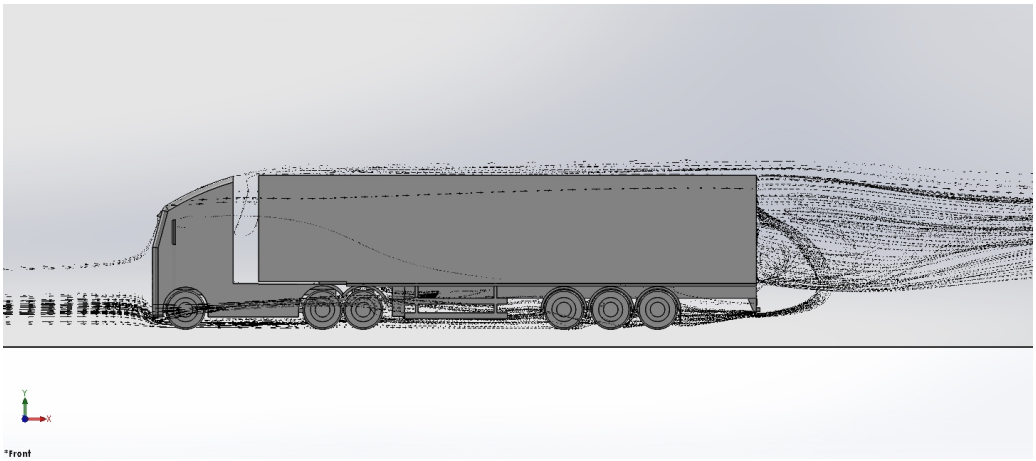

Figure 3.1.7: Flow trajectories of the rear face

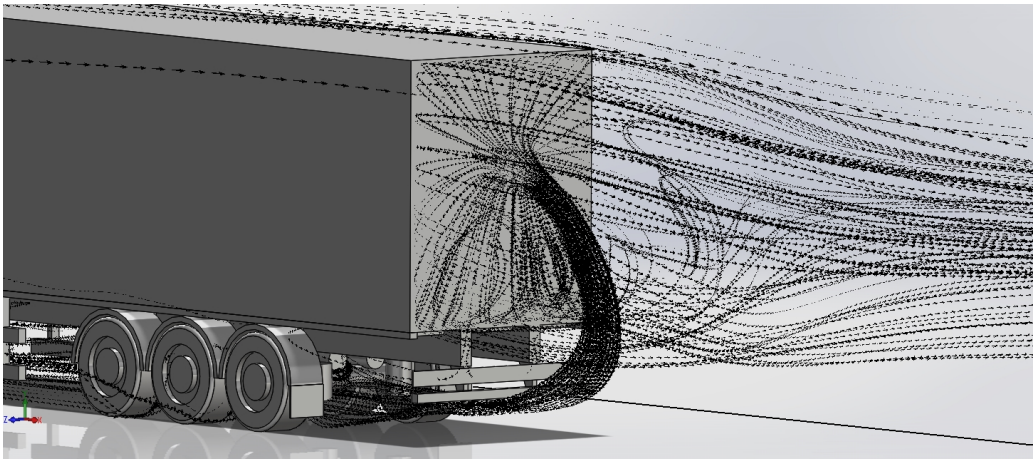

Figure 3.1.8: Flow trajectories of the rear face

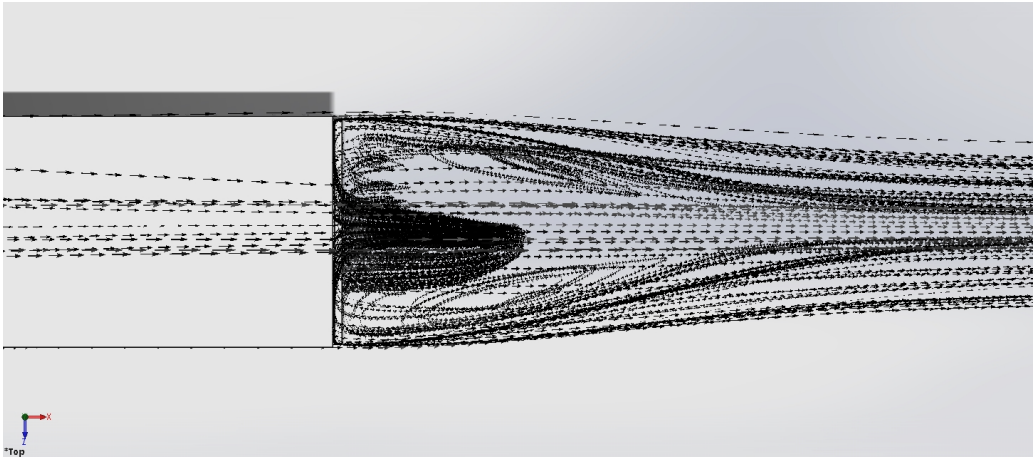

Figure 3.1.9: Flow trajectories of the rear face

These trajectories show the recirculation of air into the low pressure area, identifying how this area is occupied by flow. Flow is drawn into the low pressure area from the trailer under-body as the low velocity flow in this area reaches the trailer rear. It is drawn up to a point marginally above the centre of the rear face before filling out the low pressure area and rejoining the flow at the point of separation at the sides and roof line. Figure 3.1.25 shows the distribution of pressure on the rear face, identifying the point of recirculation contact after it has traversed the trailer under-body.

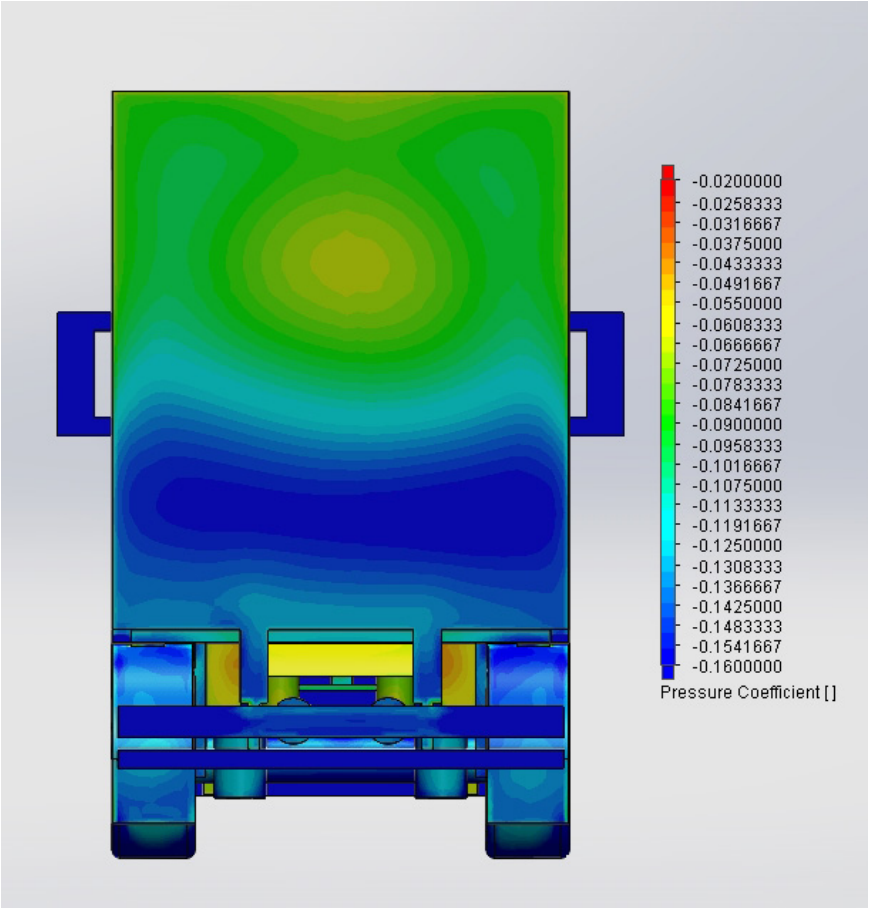

Figure 3.1.10: Pressure distribution on rear face

In addition, figure 3.1.10 also identifies low pressure and flow separation inherent with the cab side-mirrors. On this point, figure 3.1.11 shows an iso-suface representation of pressure equal to zero. This shows in greater detail the critical regions of separated flow, primarily the wake at the trailer's rear, the cab-sides including the mirrors and the entirety of the trailer under-body.

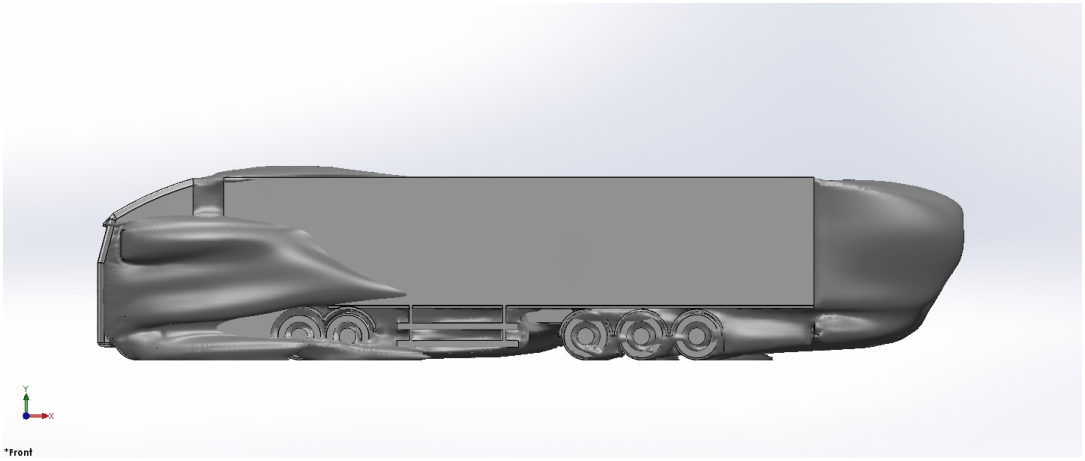

Figure 3.1.11: Pressure equal to zero

Figure 3.1.12 shows in greater detail the turbulent region of separation along the trailer roof line during the transition from cab to trailer.

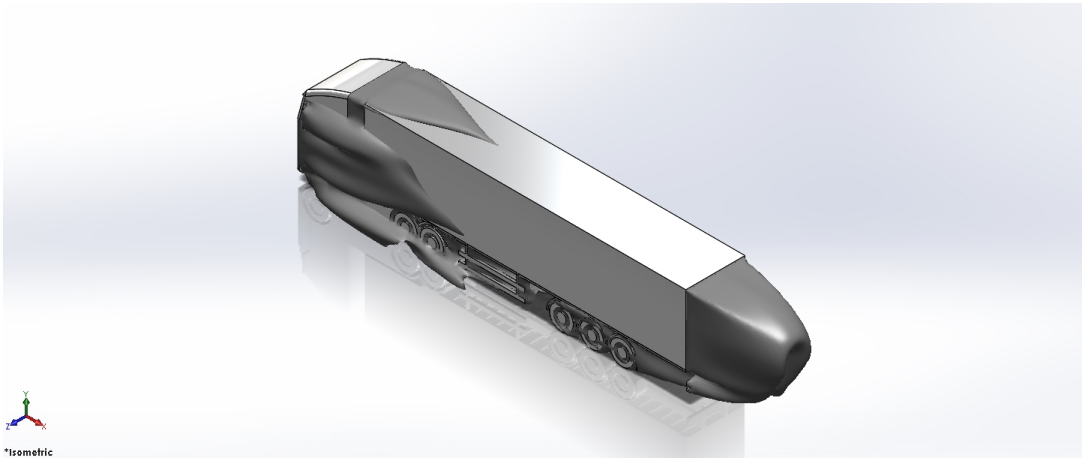

Figure 3.1.12: Pressure equal to zero

In addition to the roof line transition, cab separation, trailer wake and underbody, there is also identified from the iso-surface representation an enclosure of the cab-trailer gap. Investigating this area with velocity plots shows highly turbulent and chaotic behaviour. Figure 3.1.13 shows a cut through the centre of the cab-trailer gap, displaying flow velocity in the X direction. It displays reverse flow in the centre of the gap, as well as identifying reversed flow in the cavities of the underside of the cab model.

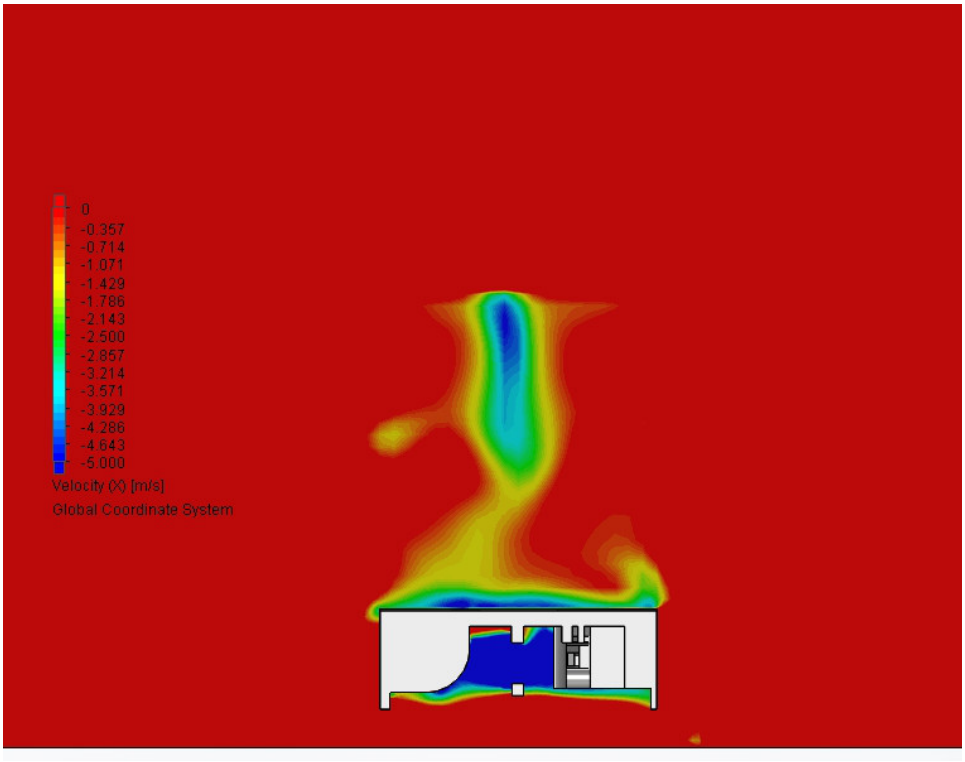

Figure 3.1.13: Cab-trailer gap Velocity in X

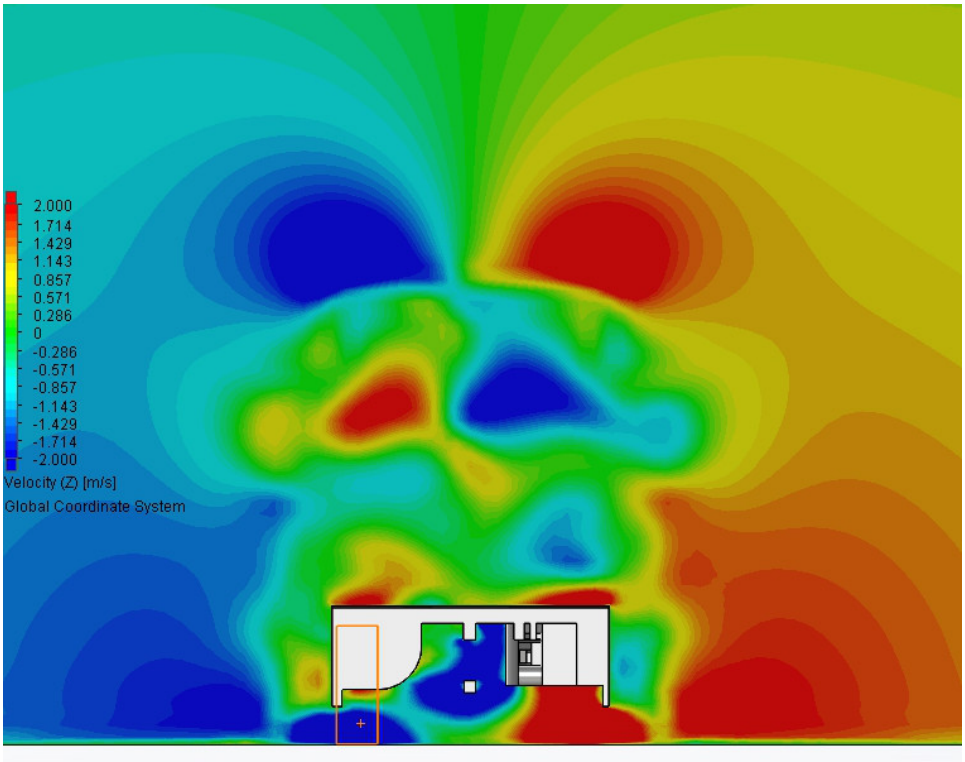

Figure 3.1.14: Cab-trailer gap Velocity in Z

Figure 3.1.14 shows the plot in the same position but displaying flow velocity in the Z direction to identify further the cause of the reverse flow. It shows that there are opposing flows in the region that meet in the centre of the gap thus creating two counter-rotating vortices that can be seen in greater detail in figure 3.1.15.

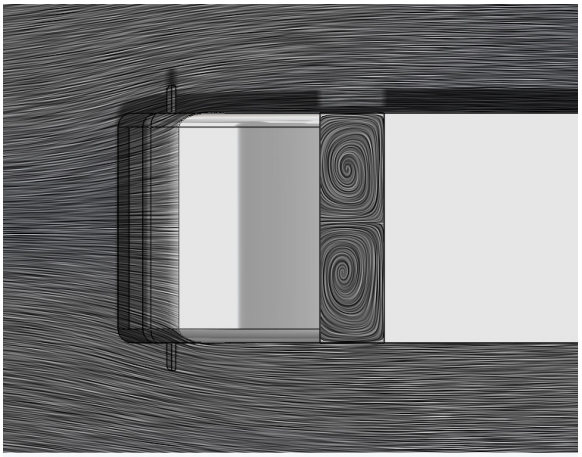

Figure 3.1.15: Cab-trailer gap vortices

Below a contour plot is shown of the central wake, displaying velocity in the X-direction. This shows the overall size of the area of reverse flow and indicates that reverse flow is in effect around 3.5 metres behind the trailer rear face.

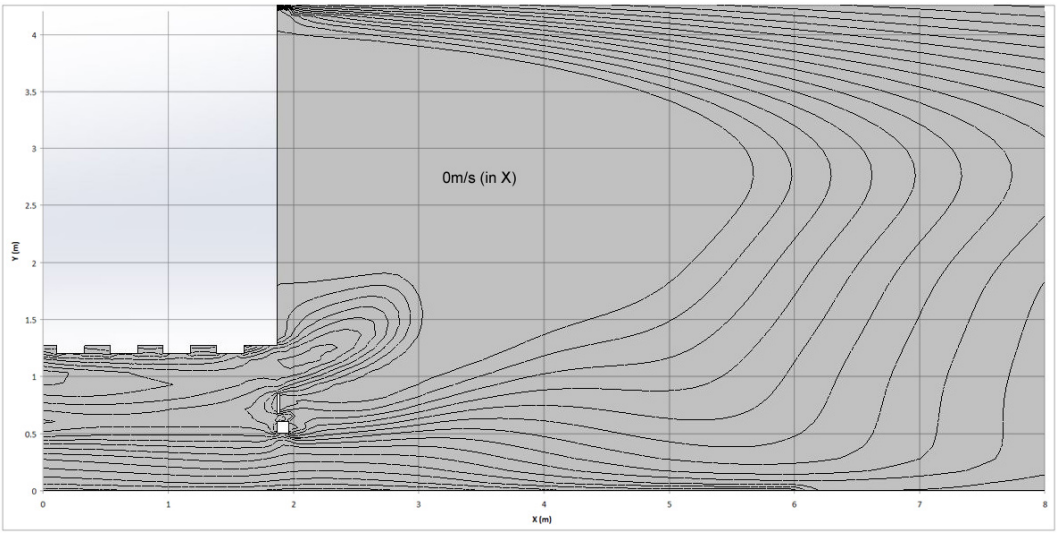

Figure 3.1.16: Contour plot of velocity in X showing the region of reverse flow.

3.1.2 10°yaw

The 10°yaw results represent flow structure around the model in a crosswind. Under these conditions, the Cd of the baseline model in the X direction (Fx) increases by 91.4% ($\Delta Cd\%$). The reason for this large increase is due to the additional exposure of the geometry to the free-stream flow, whereas at 0°yaw, much of the geometry was isolated from exposure due to the separation and resultant low velocity throughout the trailer under-body, as well as being geometrically matched to the flow direction.

Figures 3.1.17, 3.1.18 and 3.1.19 show iso-surface representations of zero pressure. the wake structures generated by points of flow separation and turbulence vary greatly to those captured from the 0°simulation. They show much larger wake structures, covering much of the geometry's length along the leeward side, unexposed to the oncoming flow. Figure 3.1.17 also shows a hole in the surface joining with the cab-trailer gap, indicating the flow is traversing the gap in the Z-direction at this point. This is unsurprising given the flow angle, but also indicates that the trailer face and general interactions in the cab-trailer gap during side-winds are potentially a large source of drag.

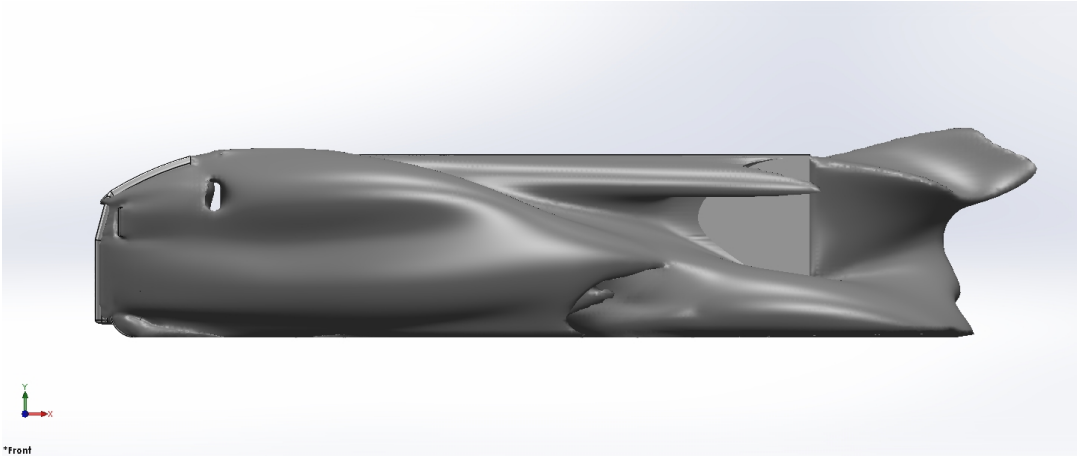

Figure 3.1.17: Pressure equal to zero

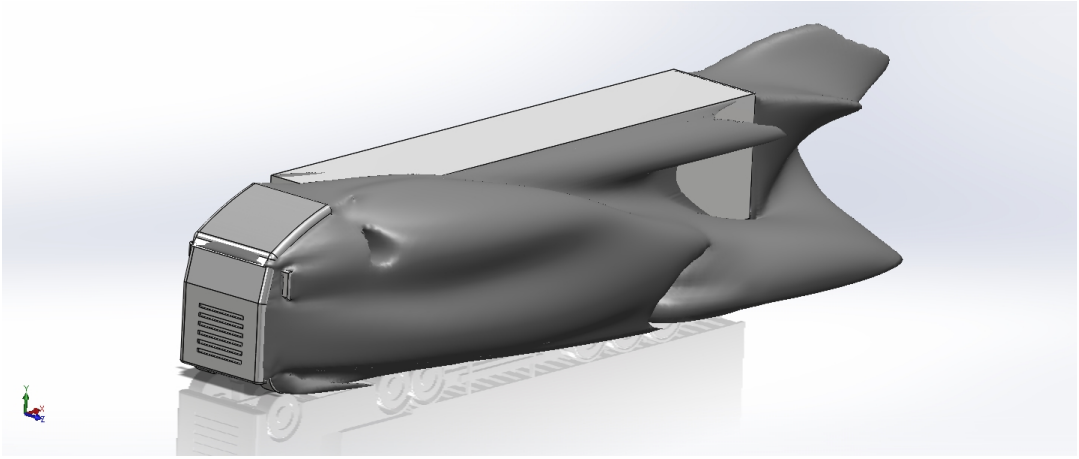

Figure 3.1.18: Pressure equal to zero

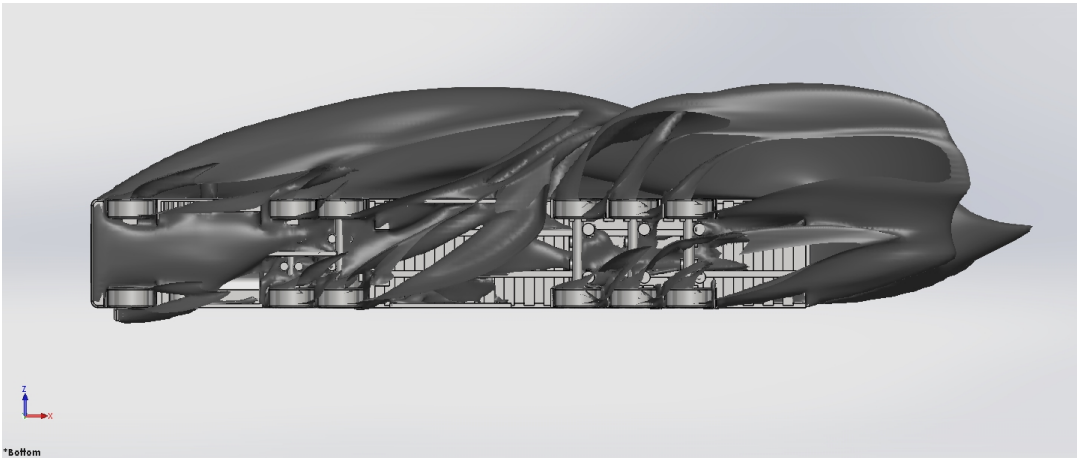

Figure 3.1.19: Pressure equal to zero

Figure 3.1.19 additionally shows the wake areas generated from the trailer under-body in crosswind conditions. It shows that interactions with areas of geometry such as the axles, side-guards and especially tyres, are turbulent and a source of drag. It can also be observed that the wake structure at the rear of the trailer is non-uniform, suggesting a highly chaotic wake in this region.

Investigating the flow through the under-body further, shows the extent of geometry in this area that is exposed to flow conditions and the resultant drag created. Figure 3.1.20 shows velocity at a height of 600mm.

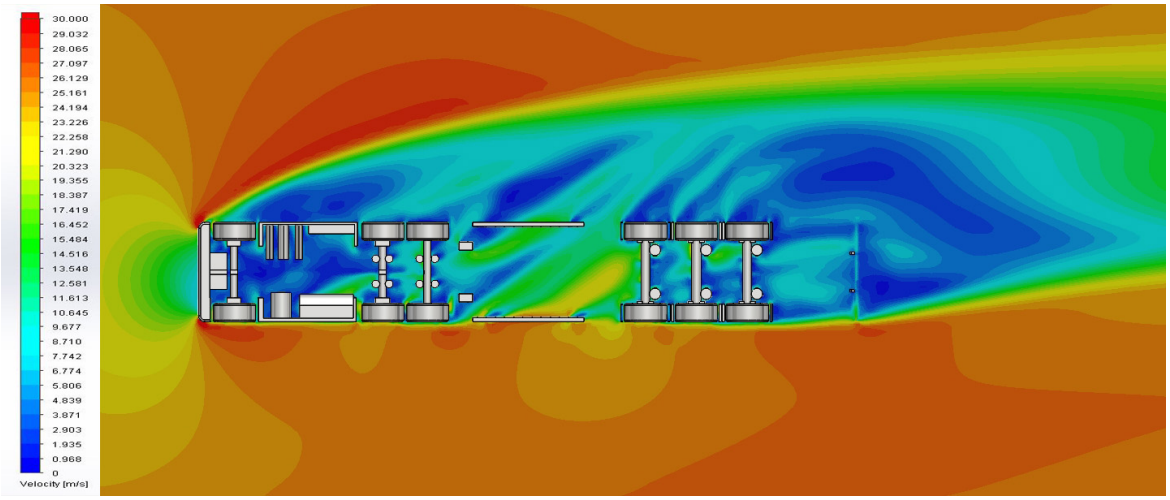

Figure 3.1.20: Velocity profile at 600mm height from the ground plane

The high degree of separation aft of the cab on the leeward side is most evident. Furthermore it can be seen that the geometric elements on the trailer under-body are directly interacting with the free-stream flow. The landing legs, side-guards, tyres, brake-chambers and axle geometry all contribute to the large and evident wake. With the rearmost two axles contributing directly to the largest wake formation at the leeward-rear of the trailer. Figure 3.1.21 shows a pressure coefficient plot of the trailer under-body, highlighting the largest contributing areas to overall drag and wake generation, in particular the inside tyre-faces, axles, support bearers and brake chambers.

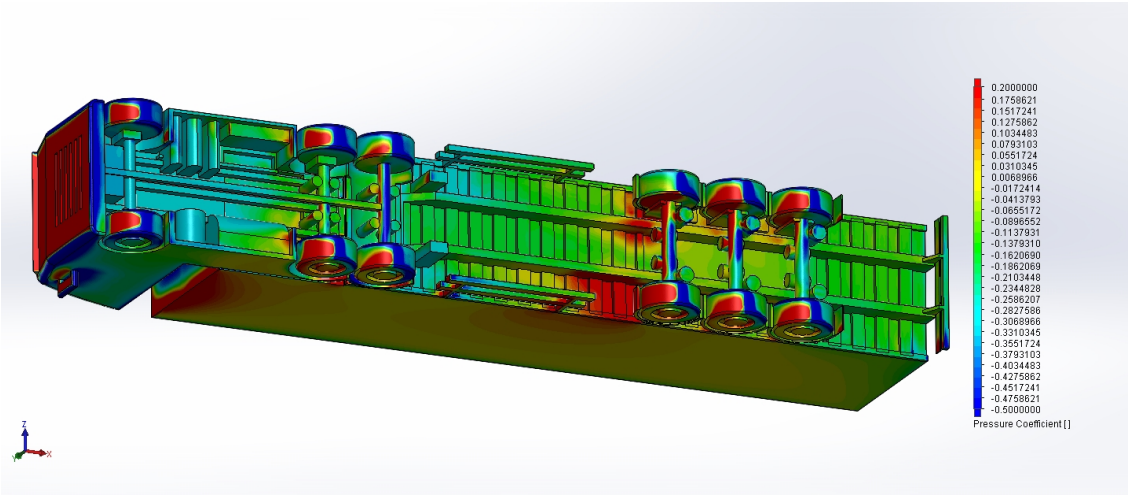

Figure 3.1.21: Pressure coefficient plot of the under-body surfaces

Partially visible above is the trailer front face with increased exposure to the flow due to the angle, a clearer view of the trailer bulkhead can be seen in figure 3.1.22 below. It shows a highly varied pressure profile across the width of the bulkhead, with the windward edge displaying high pressure before a low pressure core presents itself. To investigate the flow through the cab-trailer gap further, velocity plots show the profile of the flow through the centre of the gap in figures 3.1.23 and 3.1.24.

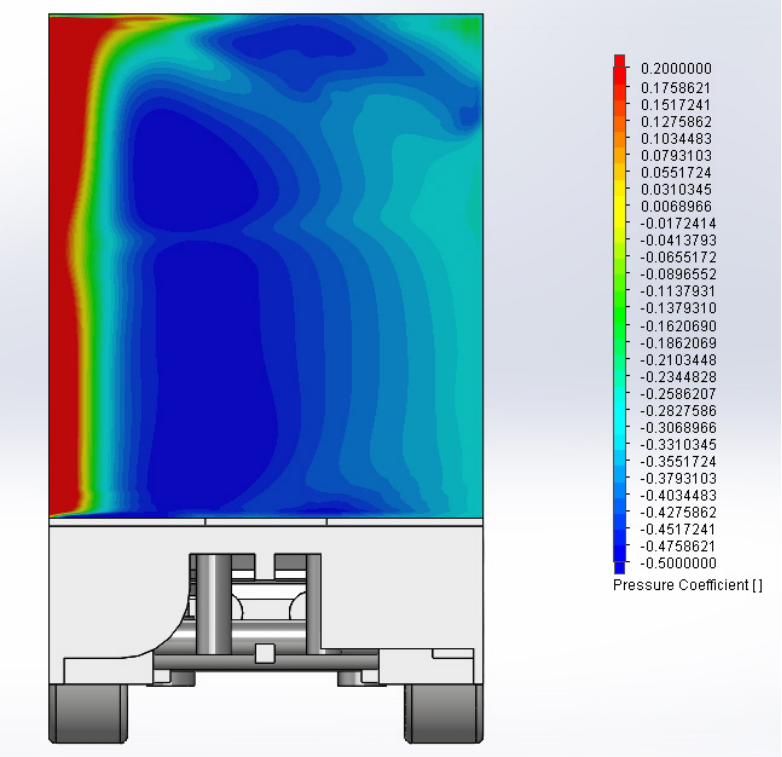

Figure 3.1.22: Trailer bulkhead pressure coefficient

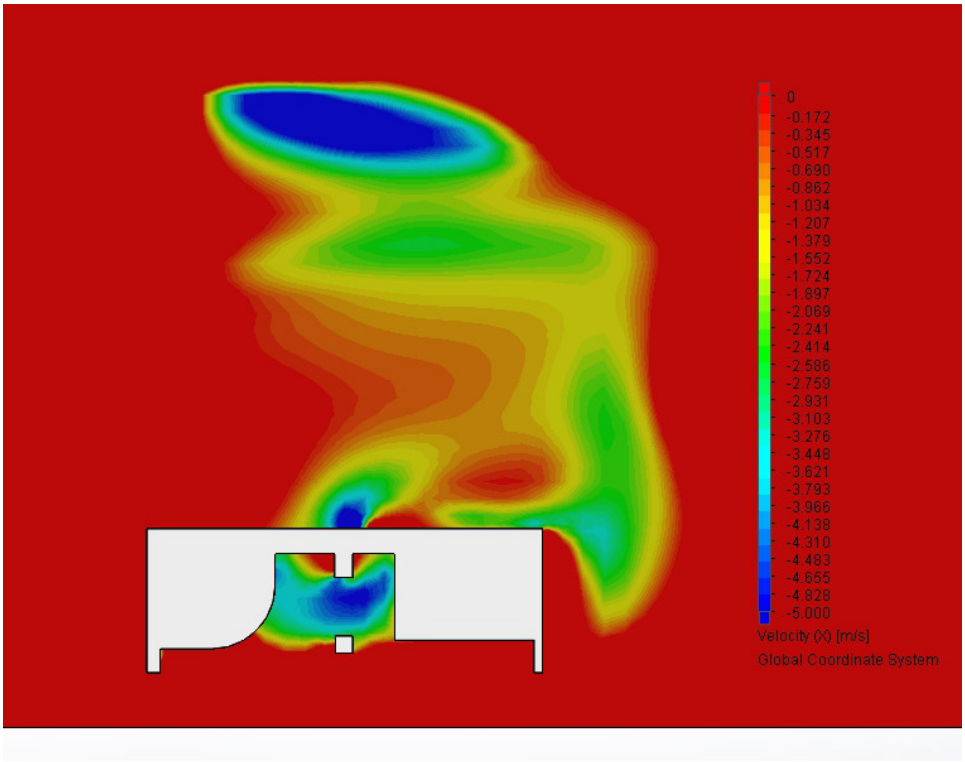

Figure 3.1.23: Velocity profile in X direction

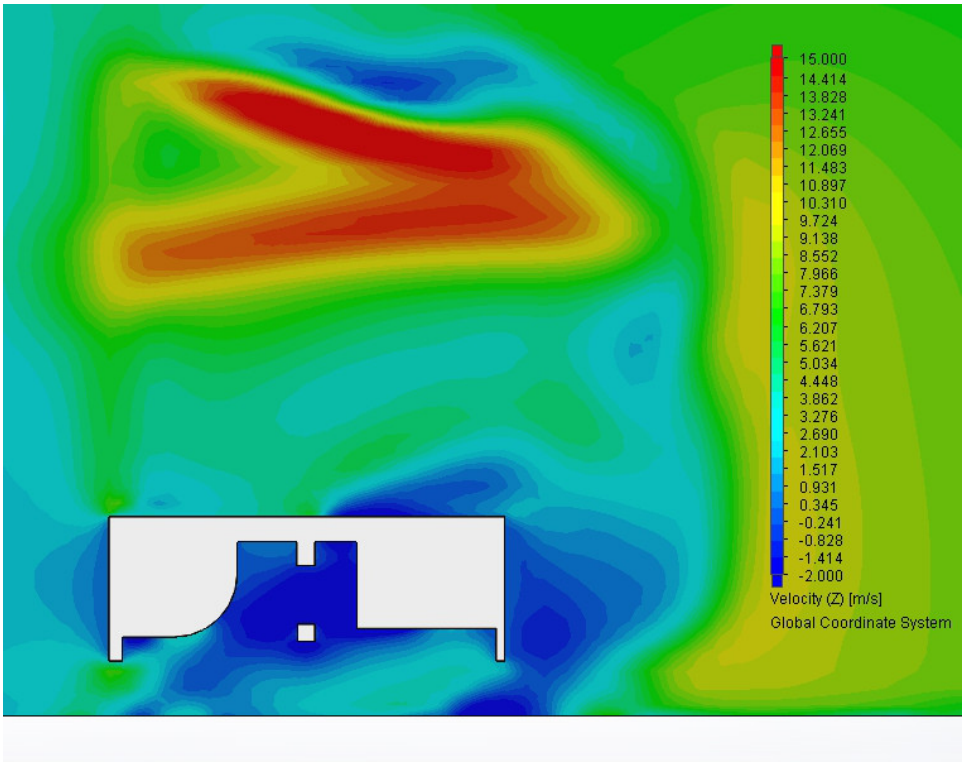

Figure 3.1.24: Velocity profile in Z direction

As with the 0°yaw simulation, flow in the gap displays recirculation vortices by means of reverse flow in the X-direction plot. The Z-direction plot shows high speed flow at the top portion of the trailer bulkhead, explaining the hole evident in the zero-pressure iso-surface of figure 3.1.17.

Reviewing the rear wake region of the crosswind conditions has displayed a much higher degree of turbulence than the 0°counterpart. Comparing the flow trajectories and pressure plots with that of the 0°simulation portrays in greater detail the differences in wake flow conditions.

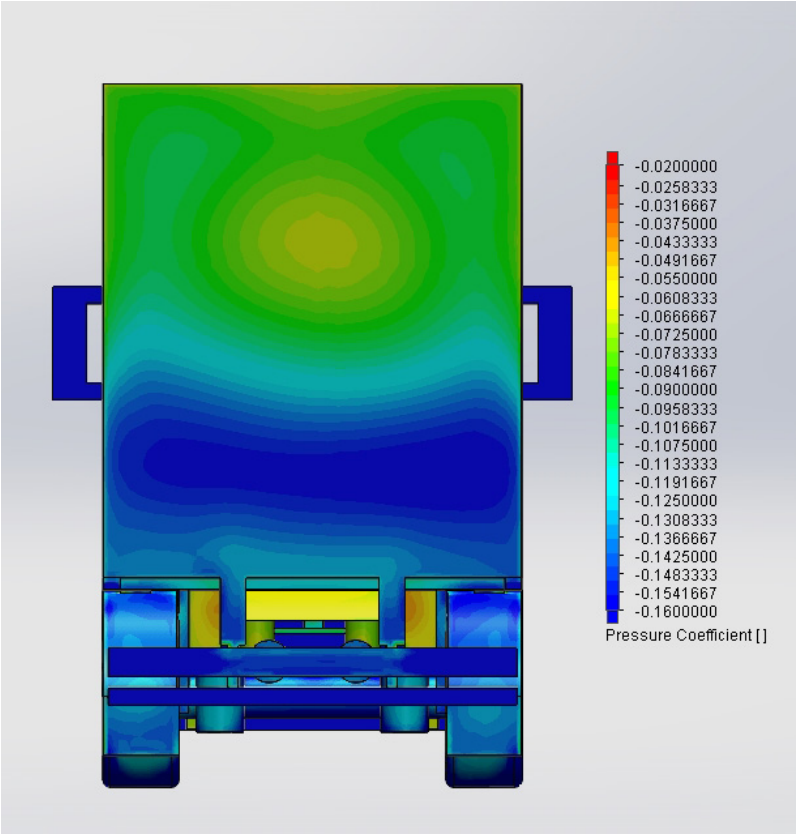

Figure 3.1.25: 0°yaw pressure distribution on rear face

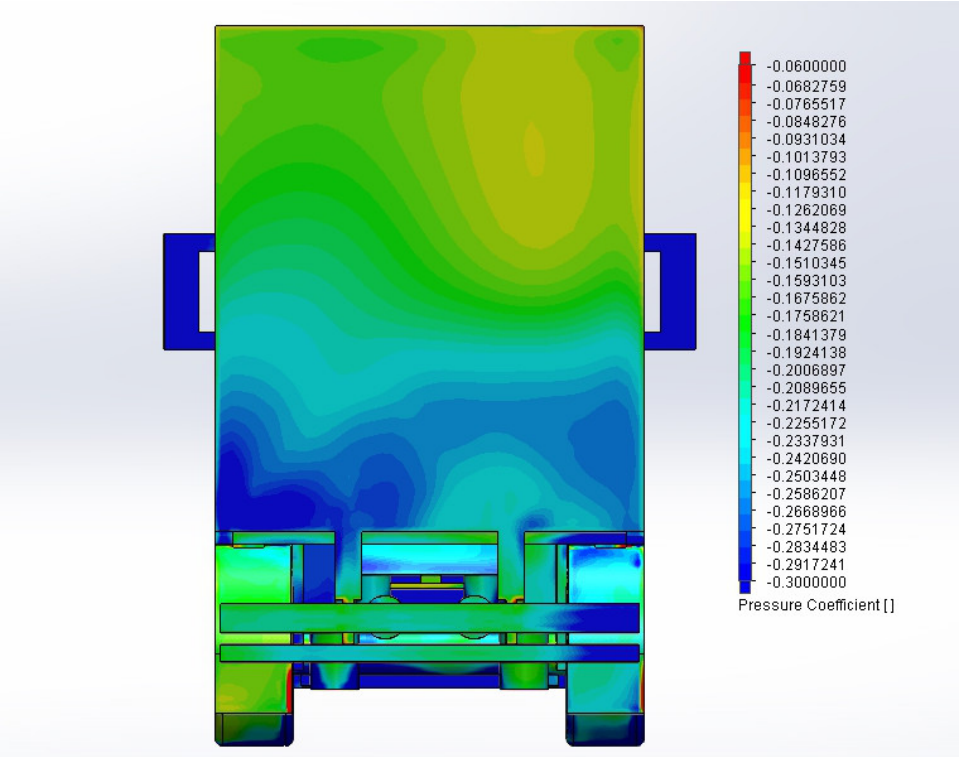

Figure 3.1.26: 10°yaw pressure distribution on rear face

The pressure distribution shows a shift off centre and an overall lower pressure in the 10°simulation. This further drop in pressure, caused by the increased wake size is evidenced further by increased drag in the X direction (Fx) of 75.6% on the rear face of the trailer over the 0°simulation.

3.2 Roof line modification

Two variations of modified roof line profile have been tested. The intention of the modifications is to reduce overall drag by attempting to influence the flow along the trailer roof line and the large low-pressure wake evident at the trailer rear.

In table 3.2 a summary of drag results reveals that both tested roof line modifications provided a modest reduction in overall drag of the geometry:

Table 3.2: Roof line Cd

Test Case	**ΔCdBase(%) 0-yaw**	**ΔCdBase(%) 10-yaw**
Full-curve roof line	-6.00	-2.13
Rear-curve roof line	-6.44	-2.91

3.2.1 Full-curve roof line

The model investigated here incorporates a curving roof line that gradually rises from the trailer bulkhead into a peak 0.3m higher than the bulkhead at the trailer centre, before falling again until the rear of the trailer. For directness of comparison, in the drag coefficient calculation the frontal area is kept identical to that of the baseline 4.2m trailer in order to avoid skewing the drag comparison. The roof line modification shows a good reduction in drag, investigating the flow in the area and its effects identifies reasons for this to be the case.

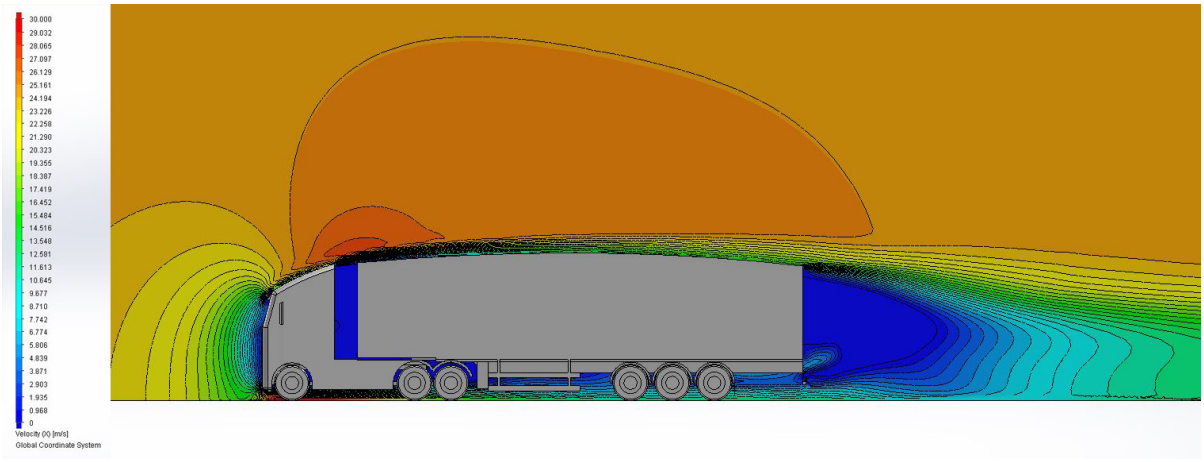

Figure 3.2.1: 0° Yaw velocity in the X direction

Figure 3.2.1 shows velocity through the central plane of the geometry. As the only variation against the baseline model is the curved roof line in this case, the primary area of study will be this area and the wake at the rear to determine how flow along the roof and at the point of detachment is affected. It can be seen that the wake at the rear of the trailer is reduced compared to that of the baseline case shown in figure 3.1.2, as the flow is directed downwards at the point of detachment thanks to the curved rear roof line section. The velocity profile also suggests that due to the sloping nature of the forward section of roof line, the area of detachment while transitioning from cab to trailer is also reduced. This can be seen further in figure 3.2.2 where the separation area along the trailer bulkhead is reduced over the baseline case. This is due to physical limitations of the recirculation area, now reduced by the upwards slope of the roof line. Further evidenced here is the reduced wake area once more, seen more clearly in 3.2.3. Further investigation of the wake region reveals that the pressure centre of the recirculating rear has also shifted slightly and increased in pressure as a consequence of the compacted area of detachment, as seen in figure 3.2.4 where additionally the small band beneath the centre, of lower pressure created by recirculation from the trailer under-body is of a higher pressure value due to the decreased wake size.

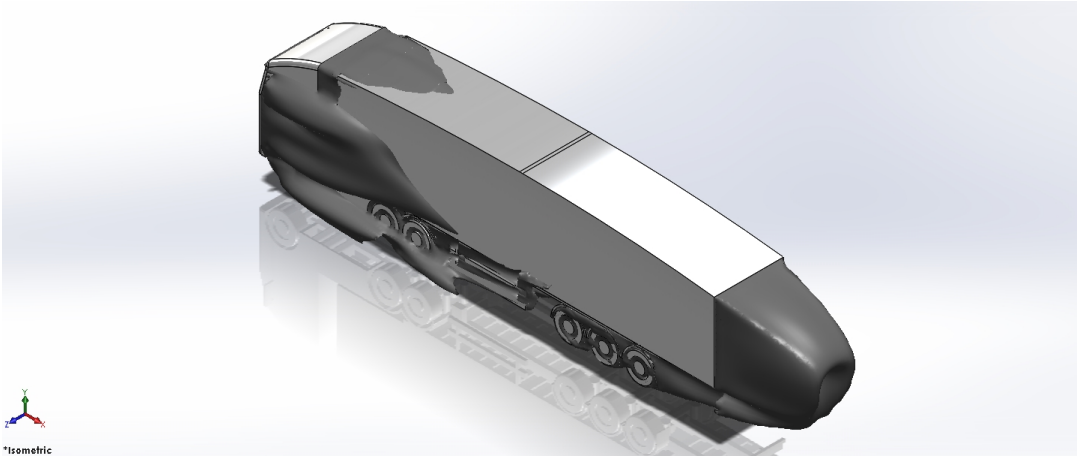

Figure 3.2.2: Zero pressure areas

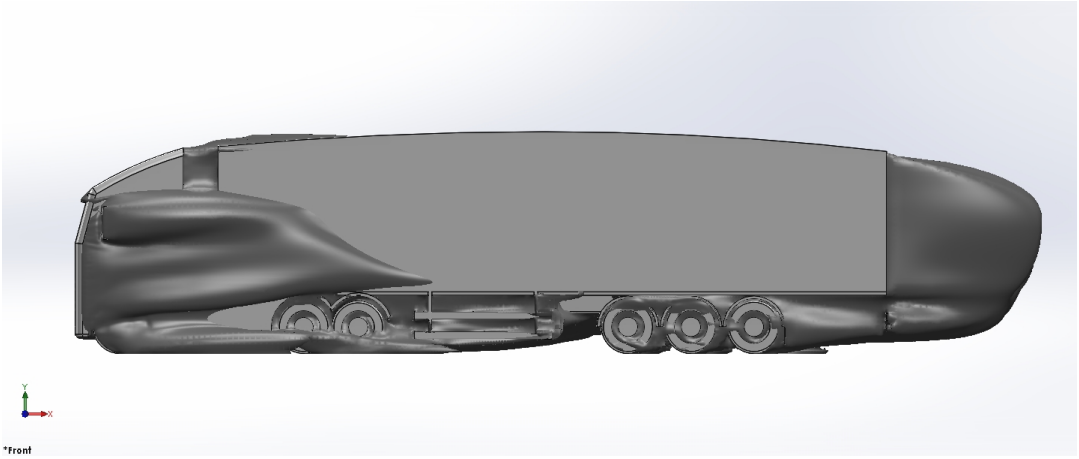

Figure 3.2.3: Zero pressure areas

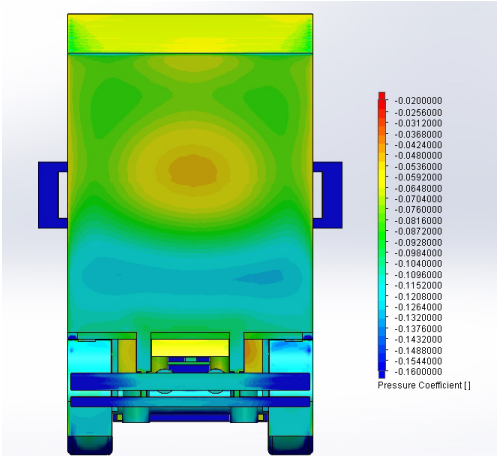

Figure 3.2.4: Pressure distribution on rear face

While the curved roof line shows evidence for good drag reduction in 0-yaw conditions, the 10-yaw case sees less of a drag reduction. This is likely to be as a result of the increase in surface area exposed to flow conditions due to the roof line curvature. Additionally, it may suggest differences between drag contribution proportions in the different conditions. Figure 3.2.5 shows the flow velocity through the under-body. As expected, it shows little variation to that of the baseline case in figure 3.1.20. One area of variation that is evident however is that of the extended rear wake area, which can be seen in the curved roof under-body profile to be of a larger significance than in the baseline case, most likely caused once more by the increased surface area.

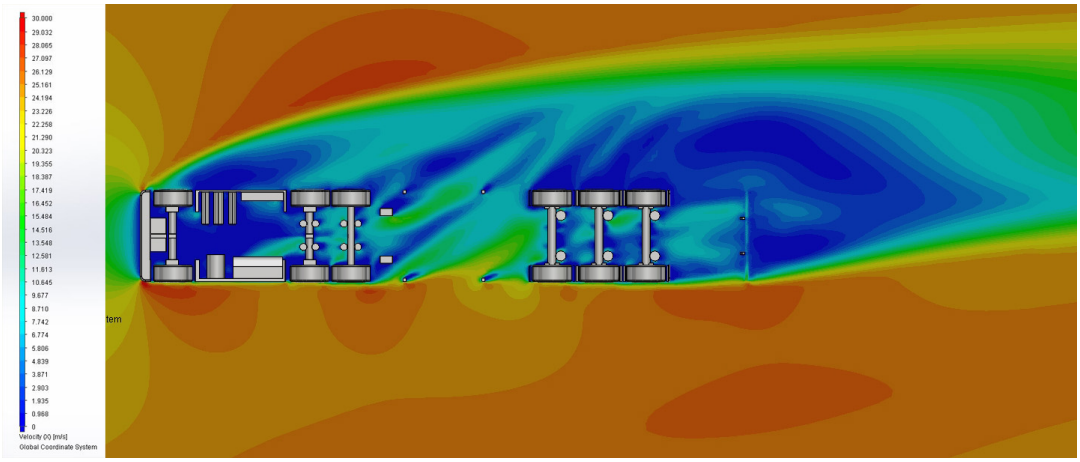

Figure 3.2.5: Velocity profile in the X direction 60mm above the ground plane

Investigating the enlarged wake structure further through a surface representing zero pressure reveals the extent of turbulent flow, as in 3.2.6 and with the baseline case, the under-body region is responsible for a large amount of turbulence. Furthermore, evidence of the large wake is once more visible despite the improved flow that the roof line displayed at 0°yaw.

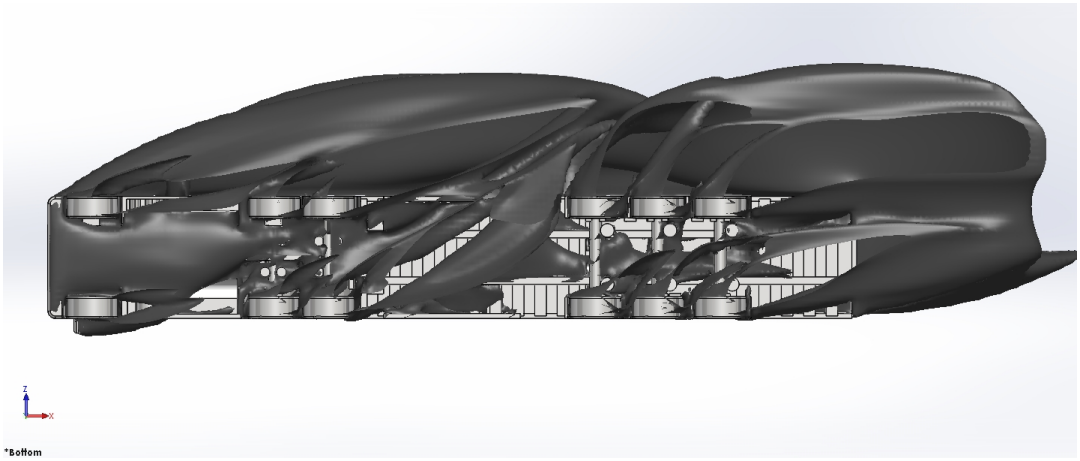

Figure 3.2.6: Zero pressure areas

Investigating the centre of pressure on the rear face shows correlation with the shift in pressure centre evident in the baseline case. Additionally, pressure distribution along the roof line shows a degree of separation along the trailer roof line edges in figure 3.2.7. The effect of this is exacerbated by the blunt edge of the model in this area, leading to the generation of a large trailing vortex that can be seen in greater detail via flow trajectories in contact with the rear portion of the roof line, in figure 3.2.8.

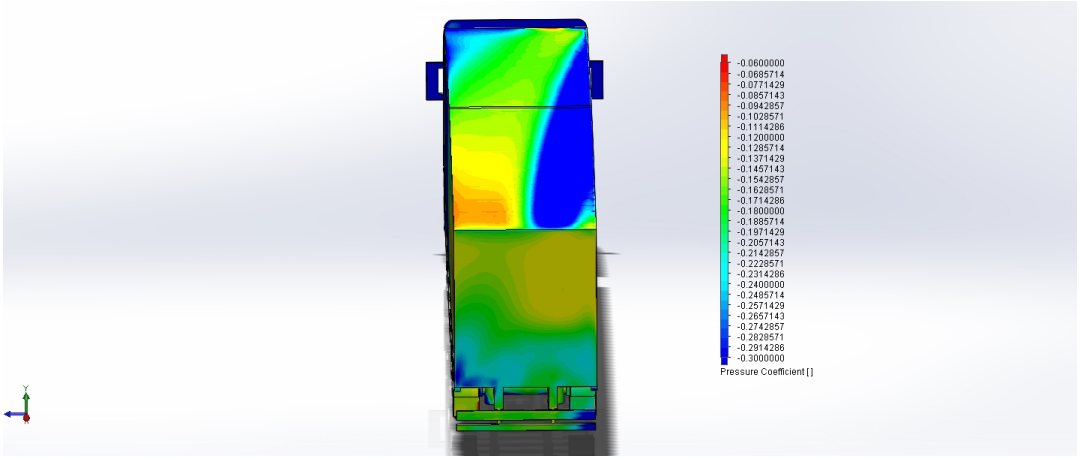

Figure 3.2.7: Roof line pressure distribution

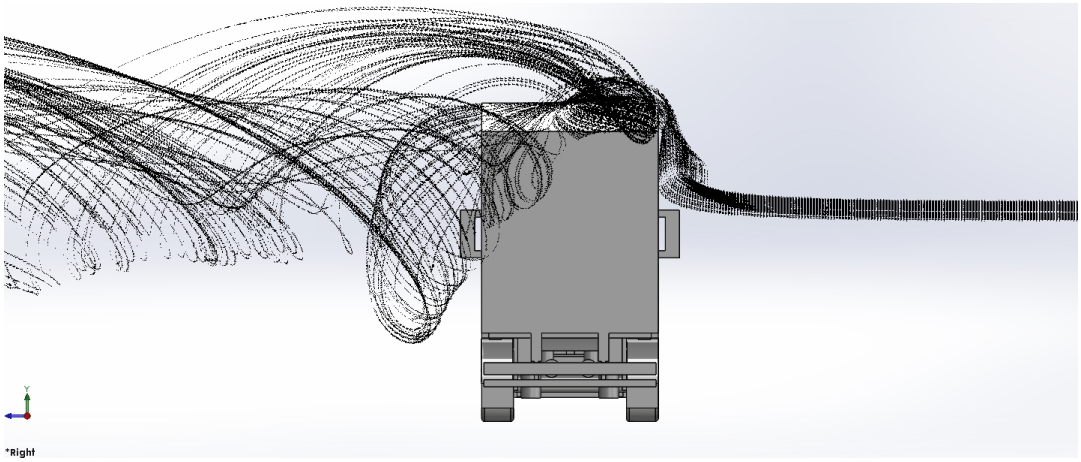

Figure 3.2.8: Roof line trailing vortex

3.2.2 Rear-curve roof line

Curving only the rear portion of the roof line results in higher rates of drag reduction than the full-curve geometry in both 0°yaw and 10°yaw cases. Although, as with the full-curve roof line, it's drag reduction is reduced in the crosswind study over the 0°yaw condition. The central plane velocity plot in figure 3.2.9 shows again, as with the full-curve, that the rear wake region has been reduced in size thanks to the effect of the angled roof line.

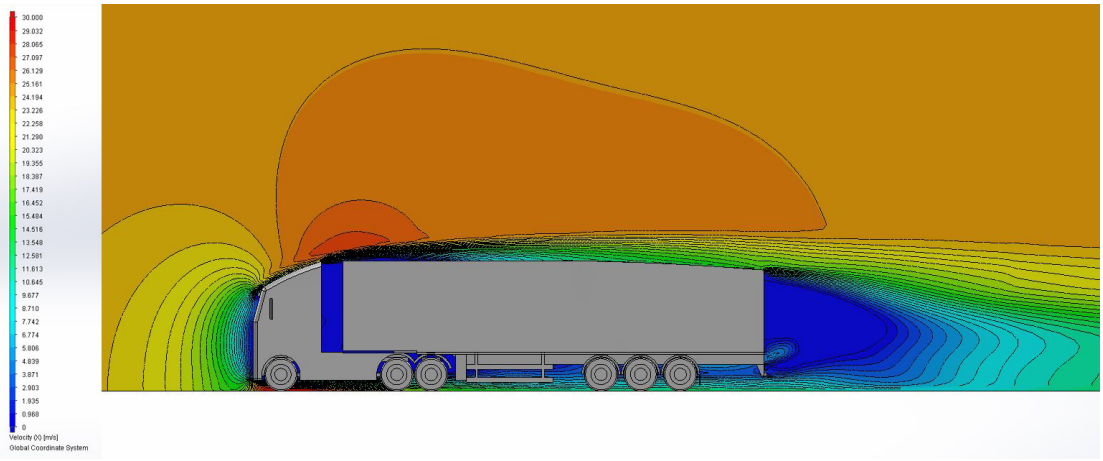

Figure 3.2.9: 0° Yaw velocity in X direction

As the front roof section is no longer inclined however, the larger area of separation during the cab-trailer transition that is evident on the baseline case returns,

though due to the overall greater reduction in drag of the rear-curve only it suggests that a reduction in the size of the rearmost section of the vehicle yields a greater drag reduction than a smoothing of the transitional area at the geometry-fore.

investigating the wake area shows that it is the smallest of the two roof line geometries in figure 3.2.10, and encourages downward flow aft of the rear edges into the negative pressure area. Figure 3.2.11 shows also that the converging area aft of the immediate negative pressure wake behind the trailer, has been brought forward accordingly with the reduction in wake size.

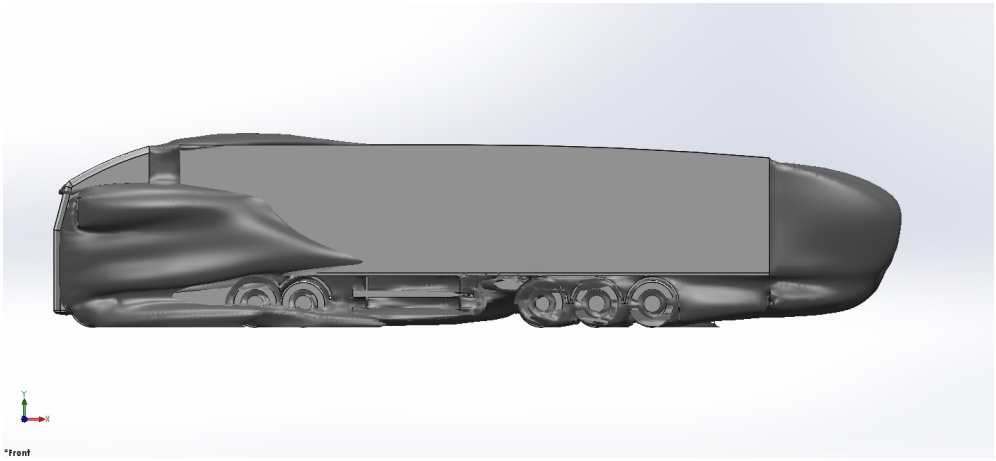

Figure 3.2.10: Zero pressure areas

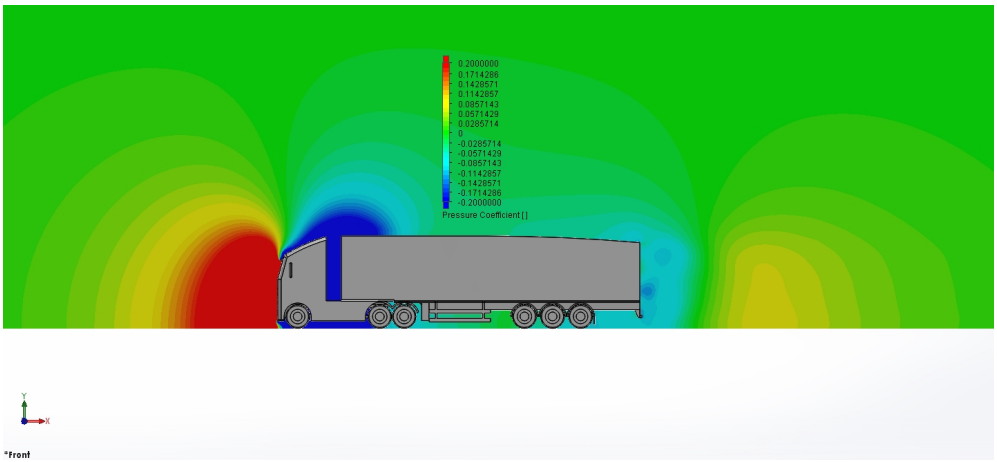

Figure 3.2.11: Pressure distribution in the central plane

As with the baseline case, figure 3.2.12 shows flow from the trailer under-body is

utilised to fill the negative pressure wake, the lower of two opposing vortex regions can also be seen clearly in this case.

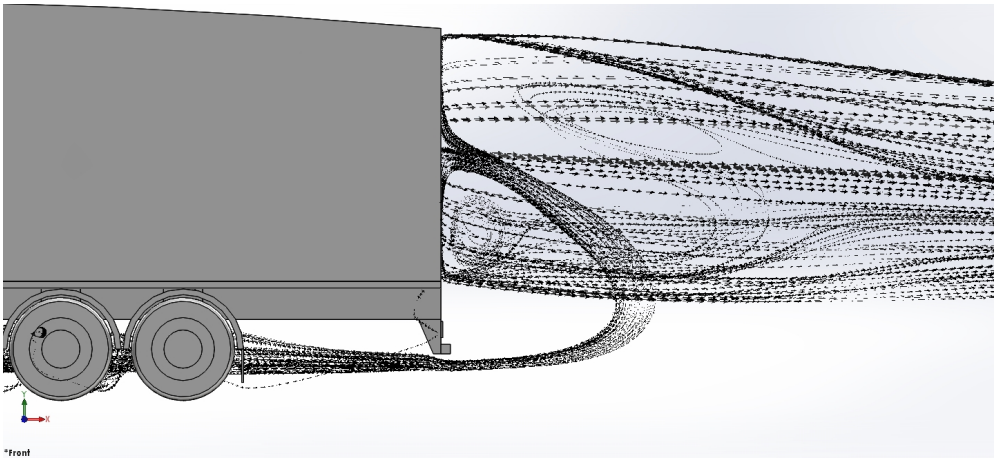

Figure 3.2.12: Flow trajectories in the rear wake

At 10°yaw, the drag reduction is lessened, but still exceeds that of the full-curve geometry. As discussed, this is likely due to the increased surface area generated by the roof incline. Flow behaviour appears similar in the rear-curve case to that of the full-curve, and zero pressure iso-surface representations show little difference between the two roof lines. The under-body velocity plot in figure 3.2.13 highlights a reduction in the extended wake once more however, indicating again that the increased side-aperture of the full-curve is generating larger areas of low velocity and pressure shown in 3.2.5. Also, as with the full-curve geometry, figure 3.2.14 shows a large trailing vortex generated over the trailer side-edge and along the roof line. It appears to initially settle as the rear recline begins, but regenerates over the trailer side-edge half way along the rear-curve.

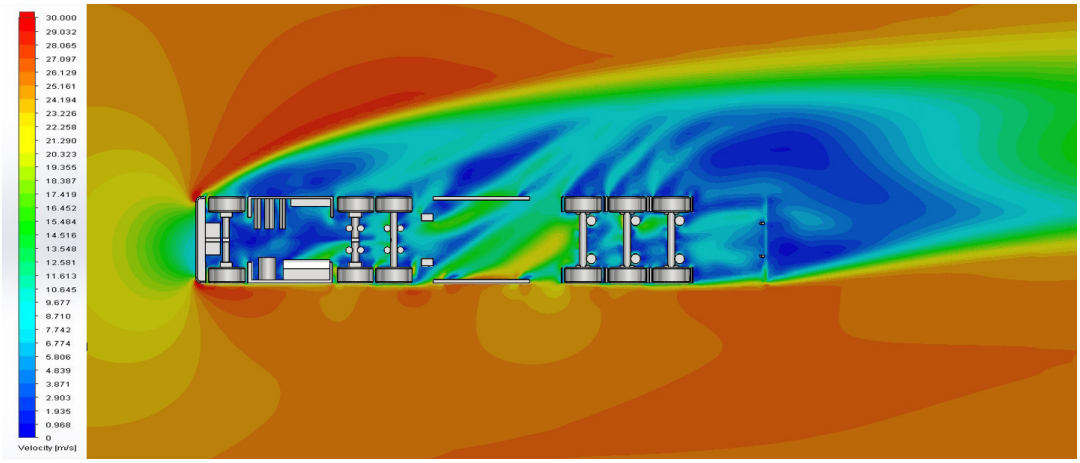

Figure 3.2.13: Flow velocity at 600mm

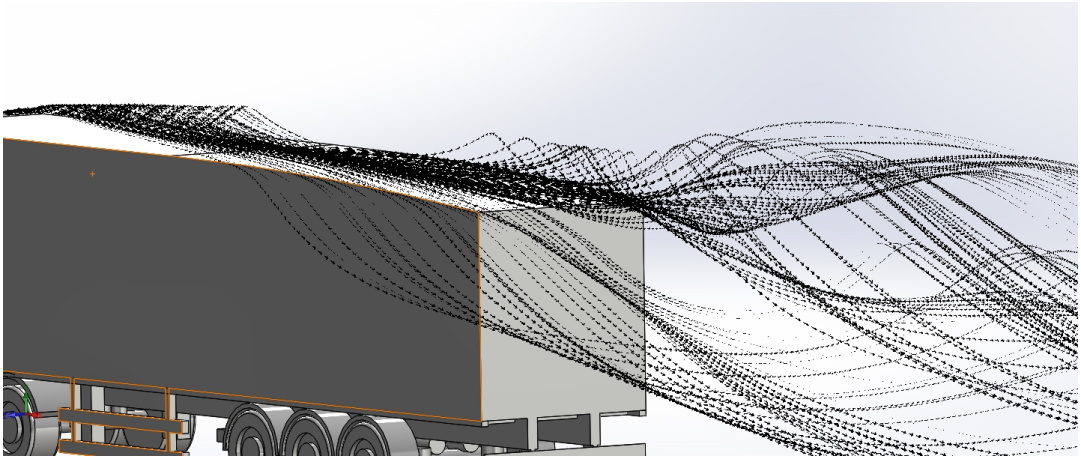

Figure 3.2.14: Flow Trajectories along the rear-curve

Based on analysis of the two different roof line geometries, it is shown that the drag reduction capabilities they display is likely to originate from improvement of the wake region, by means of its reduction. Table 3.3 shows the percentage reduction in drag on the rear face of each geometry, with both showing large reductions in the drag incurred on this area of the trailer. Additionally, it has been identified that although a full curve also reduces overall drag and smooths the transition between cab and trailer, the increased side aperture appears to create larger wake regions in crosswind scenarios. The table also shows the difference between force in the Z-direction of the roof line models and the baseline case, with the rear-curve reducing side-wind force while the full-curve, as predicted, showing an increase in

force imparted in the Z-direction.

Table 3.3: Rear face and Fz results

Test Case	**ΔFx(rear)%0-yaw**	**ΔFx(rear)% 10-yaw**	**ΔFz%**
Full-curve roof line	-26.36	-18.74	1.47
Rear-curve roof line	-36.3	-23.93	-9.38

The rear-curve only geometry shows that it is preferred over the full-curve geometry for general drag reduction, and owing to the continued reduction of force in the Z-direction also, it is likely to provide a more stable position on the road while in operation. The rear-curve geometry however also displays a reduction in rear aperture, which depending on operational requirements, may not be possible.

Contour plots overleaf highlight the differences in the two roof line configuration's rear wake structures.

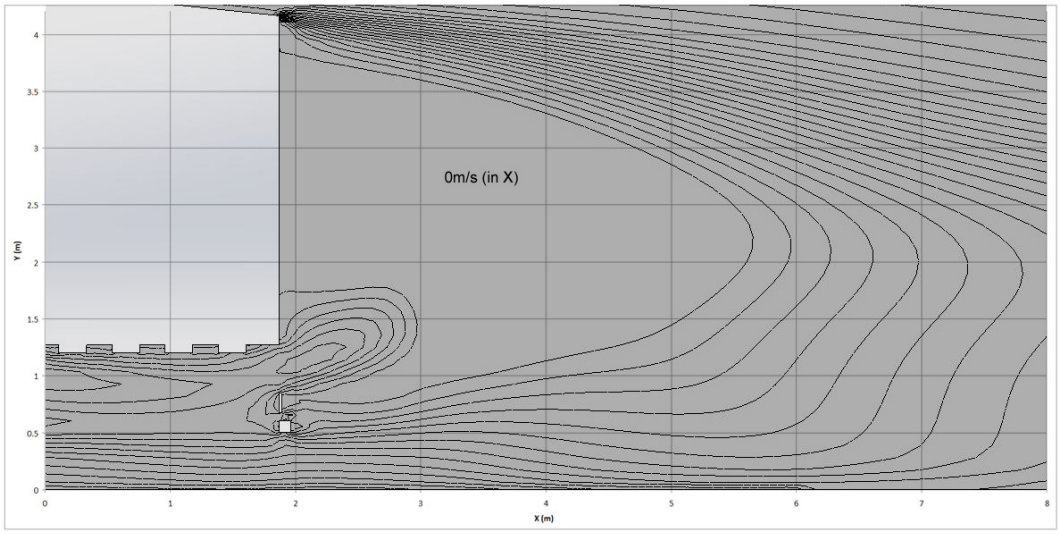

Figure 3.2.15: Plot of velocity in X showing the region of reverse flow in the full curve wake.

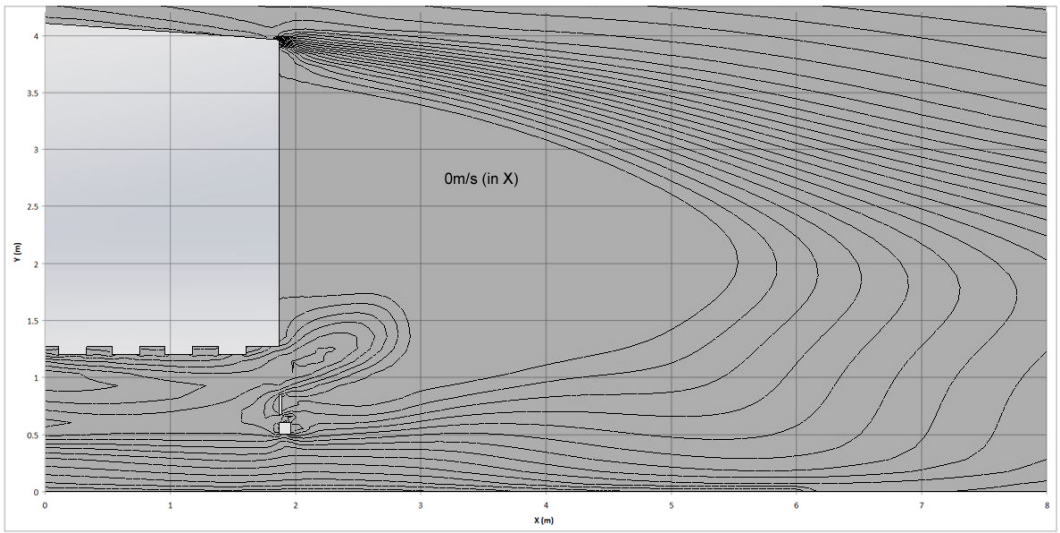

Figure 3.2.16: Plot of velocity in X showing the region of reverse flow in the rear curve wake.

3.3 Boat-tail devices

Initially, four alternatively angled boat-tail geometries have been tested and compared against the baseline case model, the general form of these three-sided models can be seen in figure 3.3.1. Their intention is to reduce the overall area of the detachment point at the trailer's rear, so as to reduce the overall size of the wake that is generated, while guiding flow at the point of detachment, inwards. The numerous angles exist to identify an optimum angle for the greatest drag reduction performance. Each of these angles is studied, with particular attention paid to the wake size and formation.

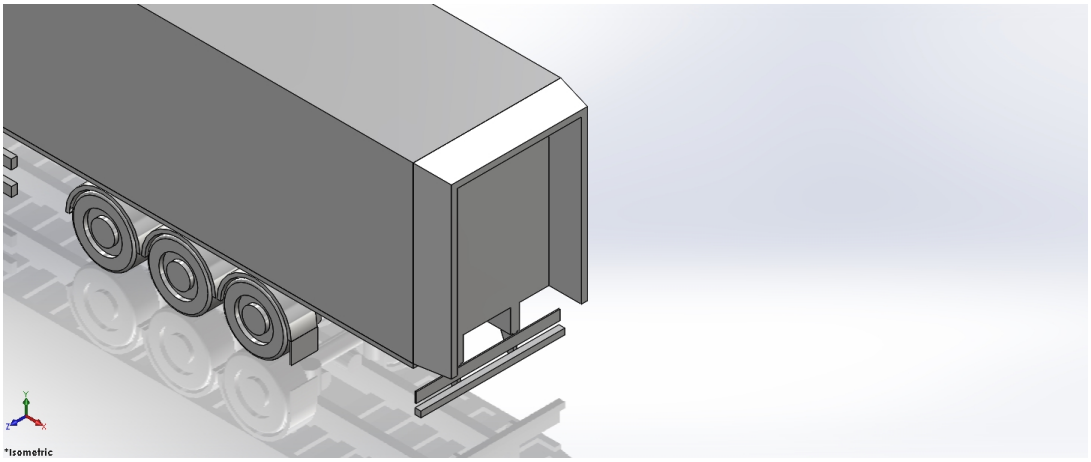

Figure 3.3.1: Boat-tail

In table 3.4 a summary of drag results shows that all of the boat-tails contribute to a good reduction in overall drag of the geometry, with the greatest reductions seen by the 12° and 14° variants.

Table 3.4: Boat-tails Cd

Test Case	**ΔCdBase(%) 0° yaw**	**ΔCdBase(%) 10° yaw**
10° Boat-tail (550mm)	-9.23	-5.82
12° Boat-tail (550mm)	-9.65	-6.39
14° Boat-tail (550mm)	-9.23	-6.61
16° Boat-tail (550mm)	-8.80	-6.50

As the boat-tail geometry only alters the rear of the vehicle, wake analysis highlights the effect the angled plates have on the flow aft of the trailer's rear face. Figure 3.3.2 shows a direct comparison between the boat-tail with plates angled at 10° and the wake of the baseline geometry.

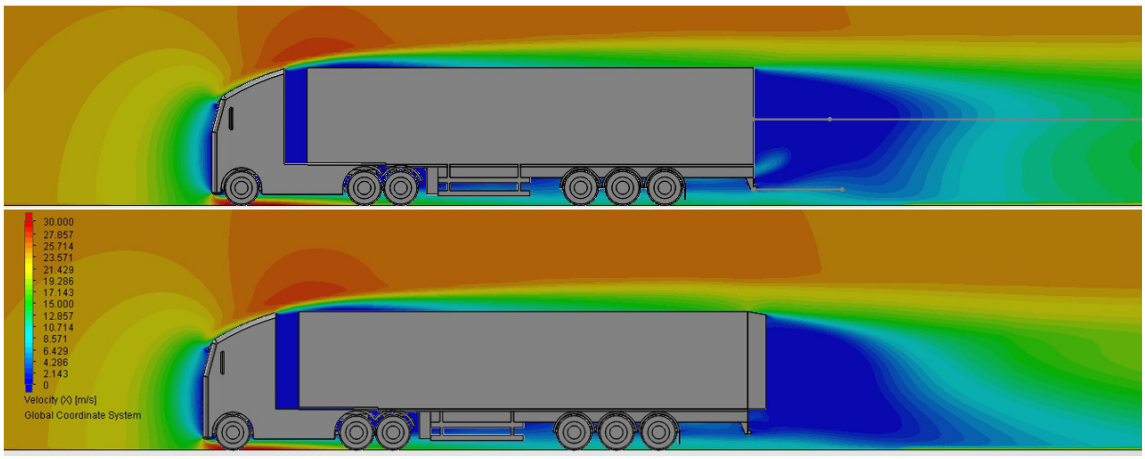

Figure 3.3.2: Baseline velocity comparison with 10° boat-tail

It can be seen that the wake profile is altered significantly. Rather than the linear elongation that the velocity plot shows for the baseline geometry, the velocity plot beyond the boat-tail shows significant downturn created by the vertical plate. Furthermore, the area of low-velocity flow that can be seen beneath the rear face of the baseline model and above the light and bumper-bars is no longer present in the boat-tail case, suggesting that the primary point of recirculation that fills the negative pressure at the rear may have shifted.

Area boundaries of the partial vacuum help define the difference in wake size that the angled plates, as shown in figure 3.3.3 exhibit. It shows a gradual reduction in overall wake size as the boat-tail plate angle increases, as well as a sharpening of the wake definition.

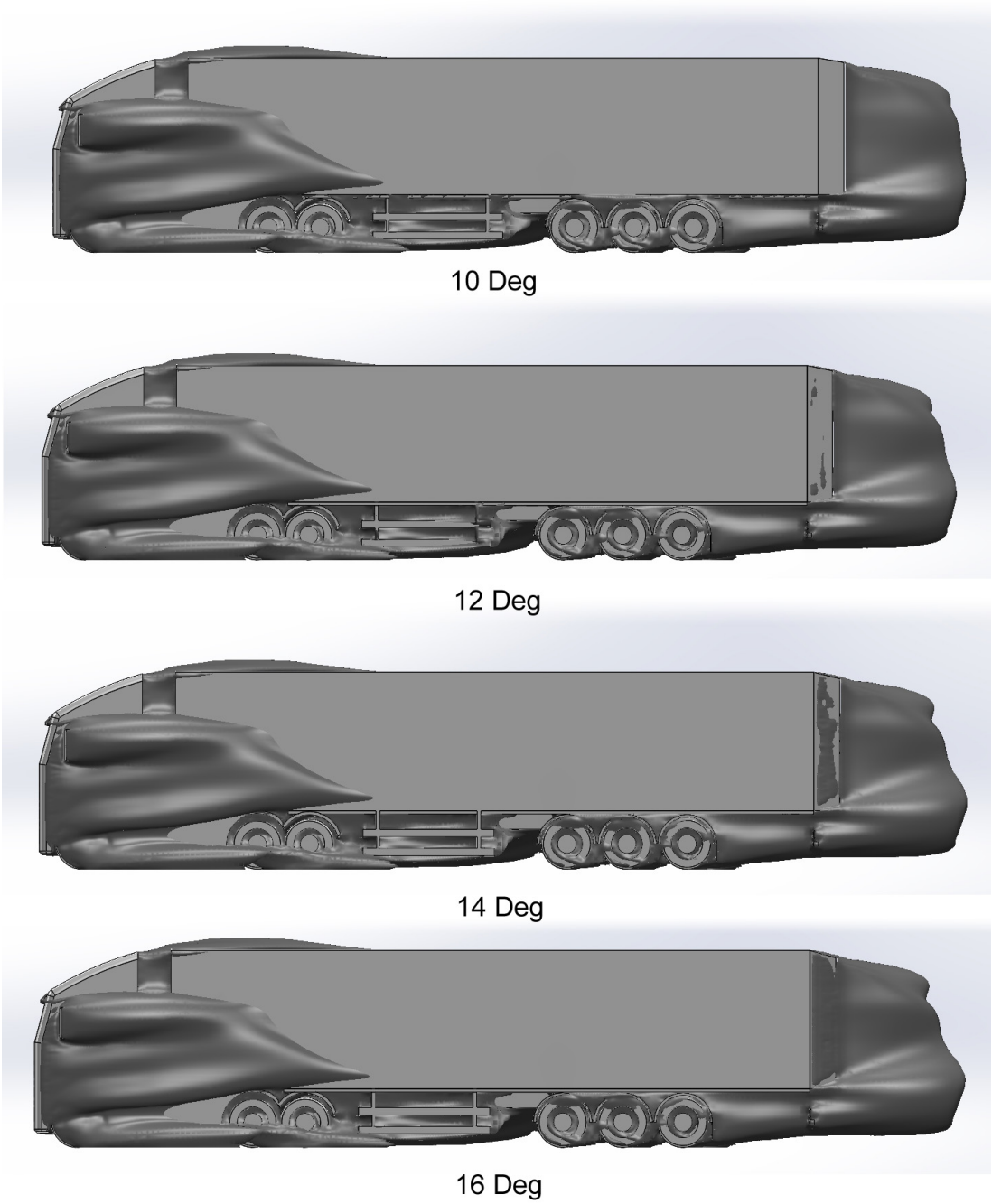

Figure 3.3.3: Pressure equal to zero for all angles (0° yaw)

This representation of the wake structure also begins to explain why it is that beyond the 12° and 14° angles there is a drop-off in the drag reduction created by the geometry: It can be seen that along the plates themselves there is no surface representing a zero-pressure boundary for the 10° case. However, as the angle increases, the plot displays increasing instances of zero-pressure boundaries over each

plate, with the 16° case having almost the entirety of the plate obscured. While a small degree of negative pressure along and aft of the plate surface is shown to not be obstructive of the overall drag reduction, beyond 14° the drag created in this area due to the small partial-vacuum begins to negate the drag reduction obtained by the narrowing of the wake.

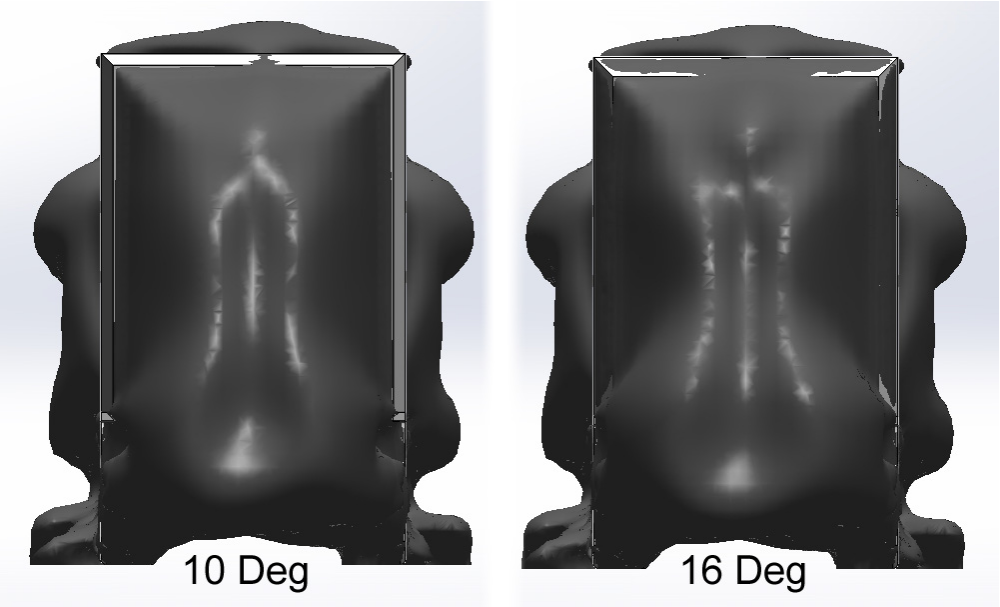

Figure 3.3.4: Pressure equal to zero at trailer rear

Figure 3.3.4 shows a clearer representation of the boat-tail plates and the negative pressure that appears as a result of separation at higher angles. On the left is the boat-tail angled at 10° and on the right the 16°. It is clearly seen that the 10° geometry shows no zero-pressure boundaries along its surfaces, while the 16° case is almost completely obscured. Beyond this most obvious differentiation, the only other variation is that of the tighter convergence points of the wake edge evident for the 16° geometry. Both also exhibit a narrower upper wake section than lower, below the bottom-most position of the side-plates.

investigating the wake structure and the influence of the plate angle further, Figure 3.3.5 shows surface pressure plots of each of the geometry variants.

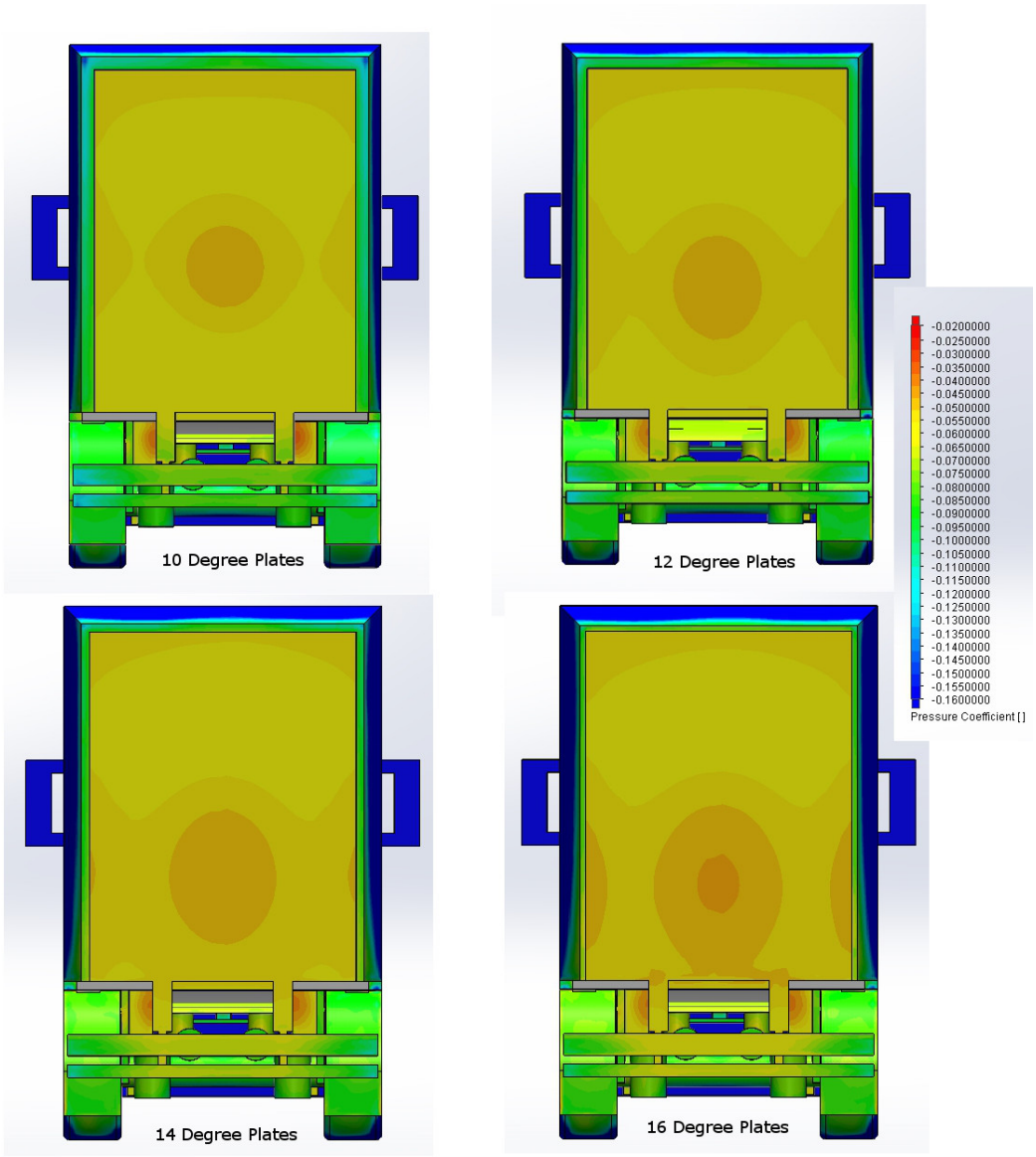

Figure 3.3.5: Pressure coefficient plots of the boat-tail rear faces

It can be seen that as the plate angle increases there is a downward shift in the centre of pressure on the trailer's rear face. This is due to the greater angle of the top-most plate, however it can also be seen that the pressure at the central point of recirculation is also increasing as the plate angle increases. Typically this coincides with a reduction in overall drag generated by the rear face, however the 16° geometry as previously discussed does not perform as well as lesser angles, the loss of efficiency due to separation over the higher-angled plates appears to outweigh the advantages gained by the higher pressure areas on the 16° geometry's rear face.

The lowering of the centre of pressure concurs with the earlier wake comparison in figure 3.3.2. A more obvious representation of this can be seen with the under-body velocity plot as shown in figure 3.3.6 where the velocity aft of the trailer rear-face in the boat-tail case at 600mm height is much lower than that of the baseline case due to the greater wake interaction at this height.

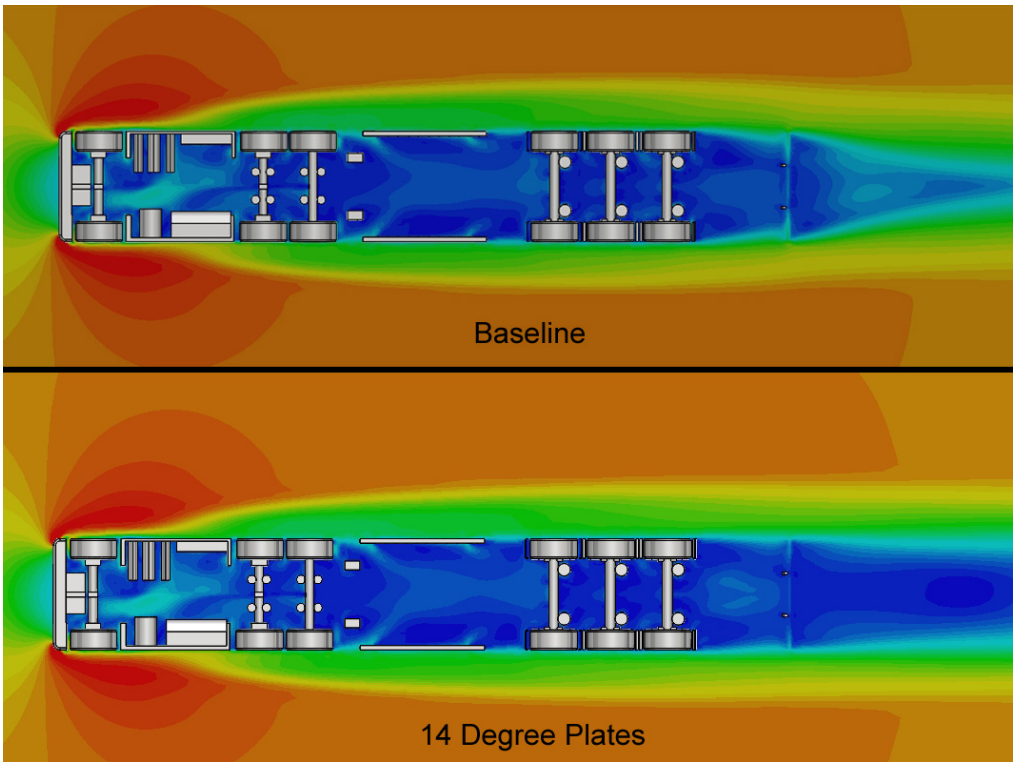

Figure 3.3.6: Flow velocity at 600mm

A final representation of the wake structures at 0° yaw can be seen in figures 3.3.7 and 3.3.8, where readings have been taken for velocity in the X-direction and the pressure coefficient respectively for 15 metres beyond the centre of the trailer's rear face.

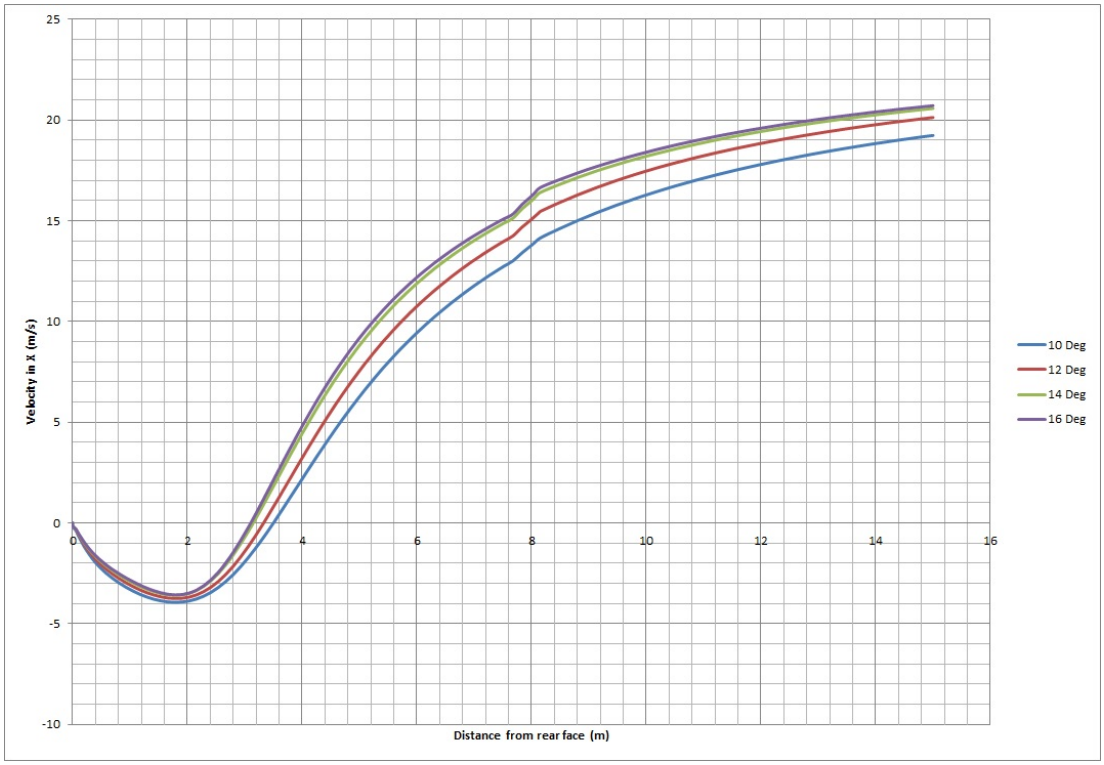

Figure 3.3.7: Velocity plot beyond the rear face

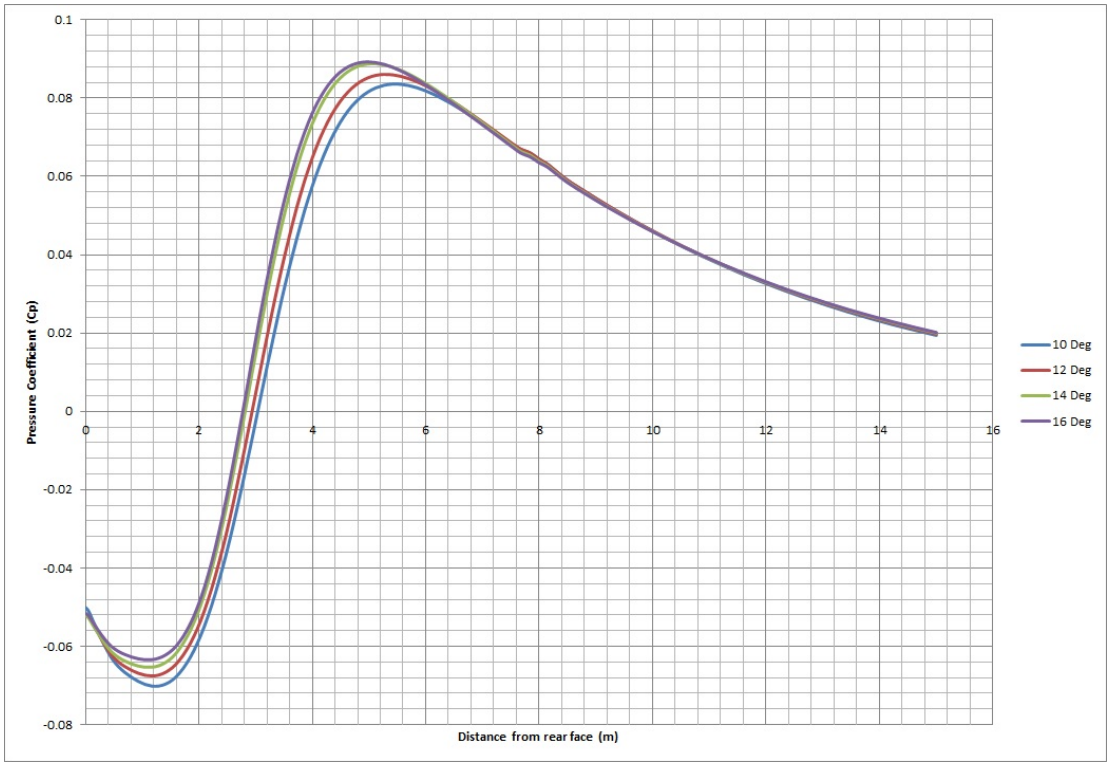

Figure 3.3.8: Pressure coefficient plot beyond the rear face

These plots show each of the angles paralleling one another with increased velocity and pressure overall with the increasing of plate angle. The least variation between plots can be seen between that of the 14° and the 16° plates, this once more suggests that the 16° boat-tail is of too great an angle as the improvement has ceased over that of the 14° characteristics. Each plot also shows a jitter in the values between 7.6m and 8m behind the rear face; this is the point of convergence for the opposing flows as they mix beyond the negative pressure wake.

At 10° yaw, once again there is a stifling of the drag reduction obtained over the baseline case, suggesting alongside the roof line comparisons that the overall contribution of the rear face drag in crosswind conditions to the overall Cd is less than at 0°. Examining the flow structure at the rear despite this, does show how it is affecting this region of flow compared to the baseline case. Figure 3.3.9 shows zero pressure boundaries for the 14° boat-tail compared to the baseline case.

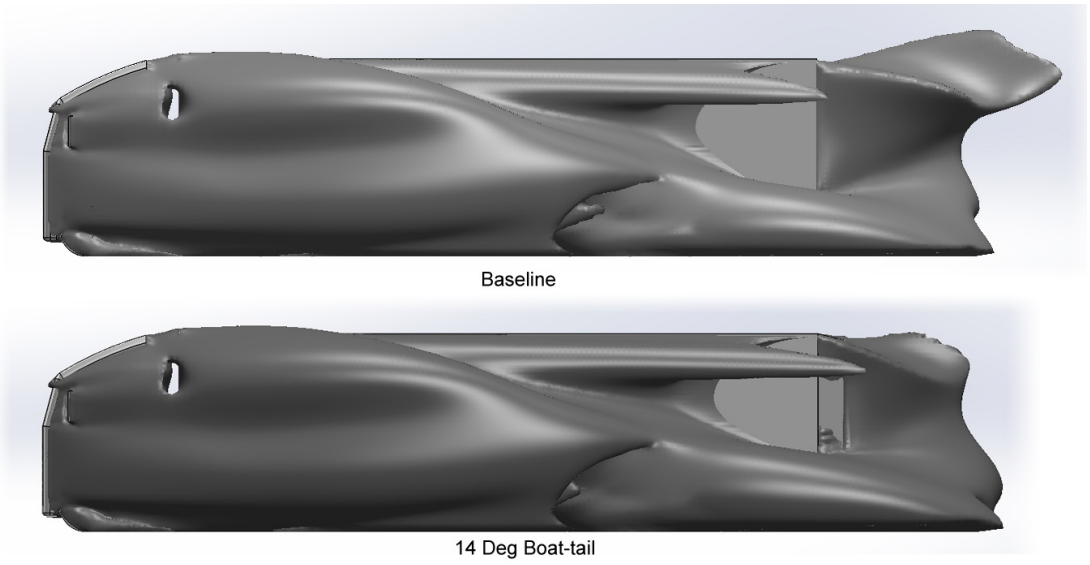

Figure 3.3.9: 10° yaw pressure equal to zero comparison

It is shown that once more the boat-tail does reduce the total size of the partial vacuum in the trailer wake, most evident in comparison to the baseline case where the wake structure generated by the large trailing vortices is reduced. While still evident along the roof line and aft of rear-most face the on the boat-tail geometries,

its overall pressure has been increased to the point where the elongated section at the topmost portion of the baseline case wake structure is no longer contributing to the negative pressure partial vacuum. Figure 3.3.10 compares the pressure distribution of the different boat-tail geometries.

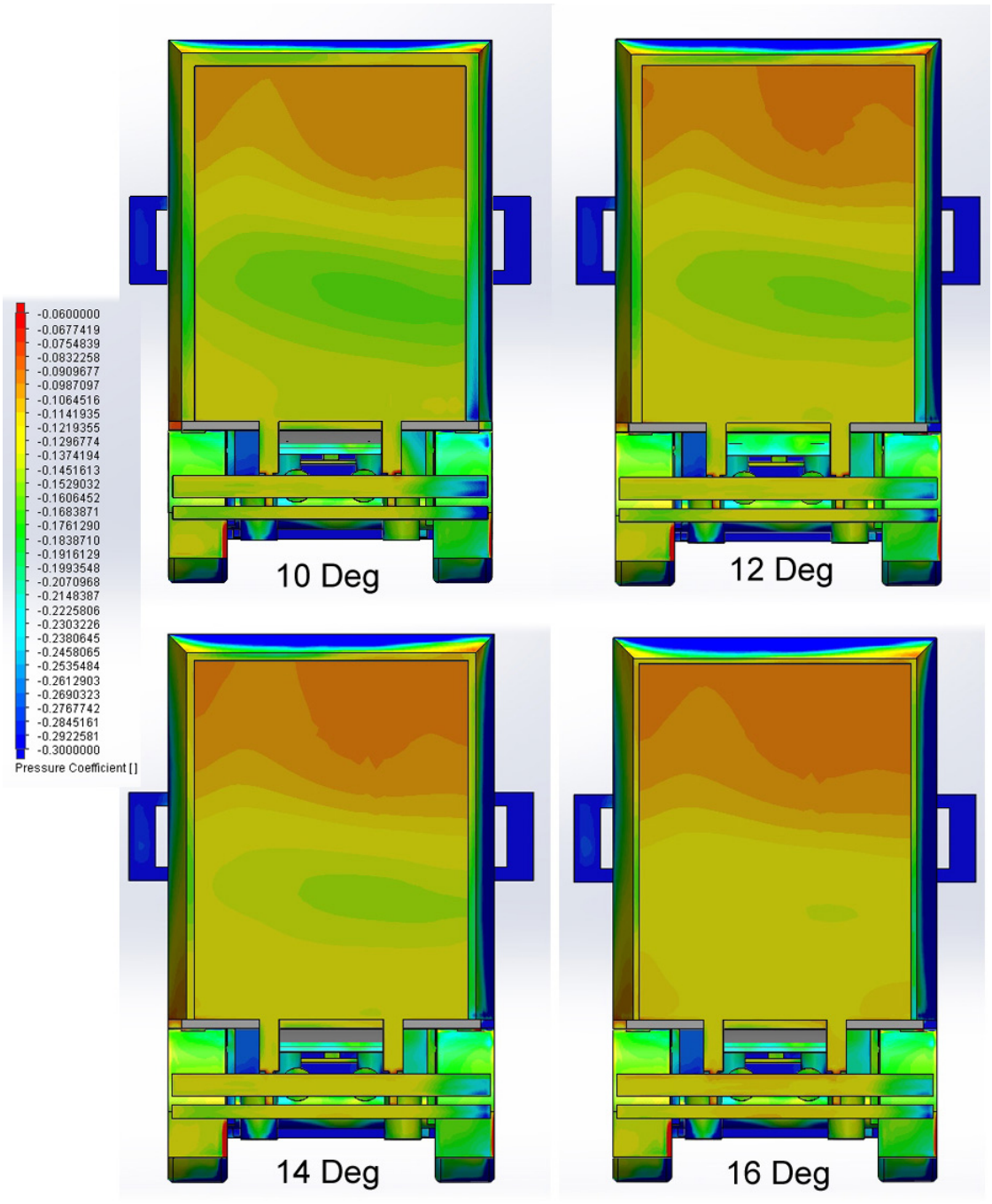

Figure 3.3.10: 10° yaw pressure distribution on the rear face

As with the 0° yaw cases, the overall pressure on the rear face increases along with the angle of the plates. Also in tandem with the 0° yaw case is the separation evident as the plate angle increases, with the right-most plate, the windward side, surface exhibiting an increasingly reduced surface pressure as the plate angles increase. Compared to the baseline pressure distribution seen in figure 3.1.26 earlier, for all boat-tail cases, the rear surface pressure is increased.

As seen, the boat-tail geometries show good wake reduction, and resultant overall drag reduction. Four further simulations have been conducted to identify the performance of the side and top plates in isolation. The drag reduction results of these can be seen in table 3.5.

Table 3.5: Side and Top-plate Cd

Test Case	**ΔCdBase(%) 0° yaw**	**ΔCdBase(%) 10° yaw**
14° Side-plates (550mm)	-5.58	-3.92
14° Top-plate (550mm)	-3.86	-2.13

As expected, greater reductions are once more seen for the 0° yaw cases than the 10°. From this however it can be seen that in isolation, the side-plates provide a greater drag reduction than the top-plate can. This is to be expected as the additional geometry influencing the flow is doubled for the side-plates. However, the side-plates do not provide double the reduction of the top-plate case, in fact the top-plate case alone provides 69% of the total drag reduction produced by the side-plates at 0° and 54% at 10° yaw. This reduction of comparative performance when in crosswinds is not surprising due to the additional influence the side-plates will have in yaw conditions on the flow, due to greater exposure of the windward side. Figure 3.3.11 compares the side-plates only case to that of the baseline.

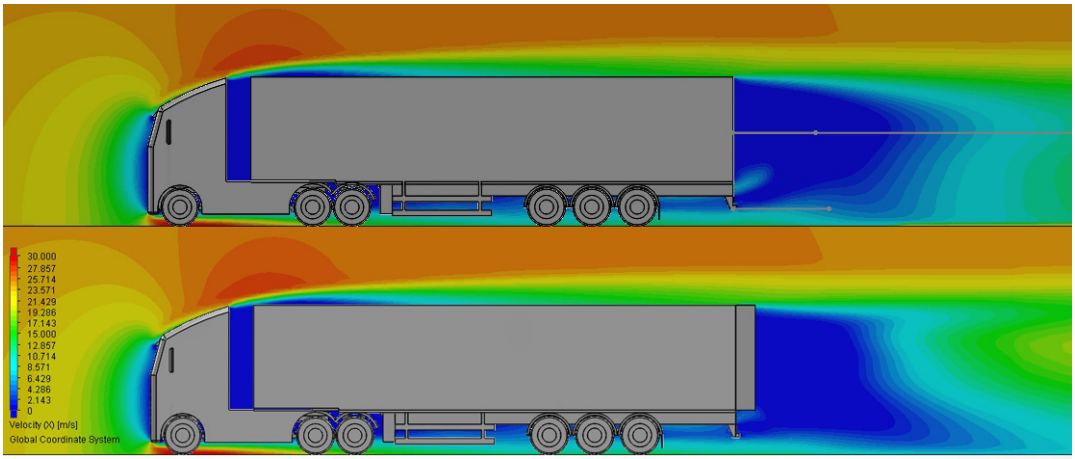

Figure 3.3.11: Baseline velocity comparison with side plates only

The alteration to the wake profile can be clearly seen, as with the full boat-tail testing prior. Due to the lack of the top-plate however, there is no downward direction of the immediate wake, instead its length at the upper section is reduced, while the lower section above the ground-surface is extended slightly due to the lack of uniformity as the flow separates at the rear. Unlike the full boat-tail cases also, the small region of higher velocity above the light and bumper-bars is still evident, due to the lack of vertical compression of the wake, once again from the top-plate.

The top-plate only case in contrast, as seen in Figure 3.3.12 shows a similar wake to that of the baseline case, albeit with vertical compression evident from the flow being guided downwards as it separates from the trailer roof line. The top plate exhibits good drag reduction from a relatively small change in overall geometry, while it cannot match the reductions obtained from total roof line modifications discussed previously at 0° yaw, it attains similar reductions at 10° yaw. Further, there is greater scope for adoption of this geometry due to flexibility within the roof line dimensions for manufacturers, which is rarely the case for trailer width, as it would need to be for the side-plates. It is possible for the top plate to be incorporated into the roof itself as oppose to being fitted to the rear face as a roof line extension. It is reasonable to assume that the benefit would be similar if not identical to the roof line extension method incorporated here.

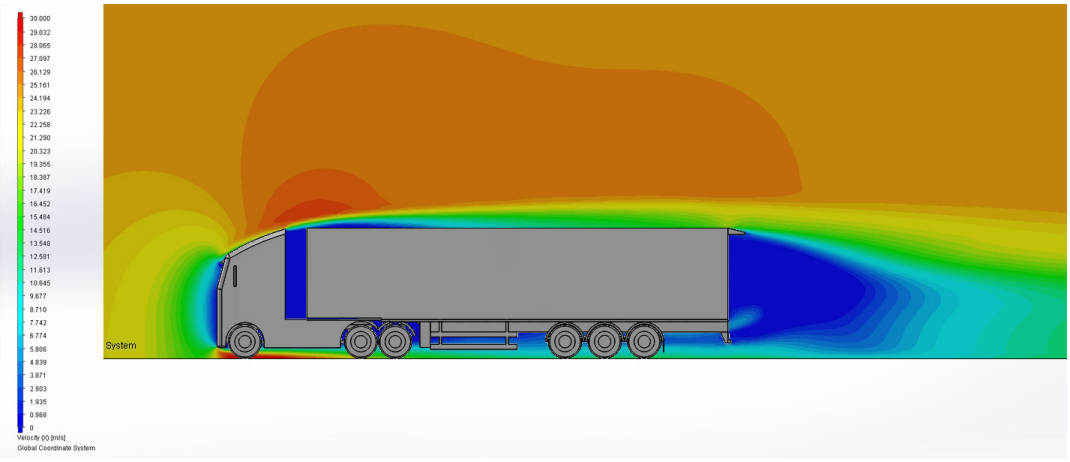

Figure 3.3.12: Velocity in X through the central plane for top-plate only

Boat-tail geometry shows excellent drag reduction potential. Even in isolation, the top-plate section testing shows that angling the rear roof section at the point of flow detachment can have a good influence on overall drag, for a conceivably small design modification. The full, combined side and top plate boat-tail geometry however displays excellent reductions over a range of plate angles, suggesting that even relatively crude geometry, if it is positioned correctly, can narrow the trailer's wake and reduce drag significantly.

Supporting the evidence seen over the increasing boat-tail angles are velocity contour plots in the X direction at the trailer rear. It can be seen that the reverse flow region in the wake is compressed as the plate angle increases.

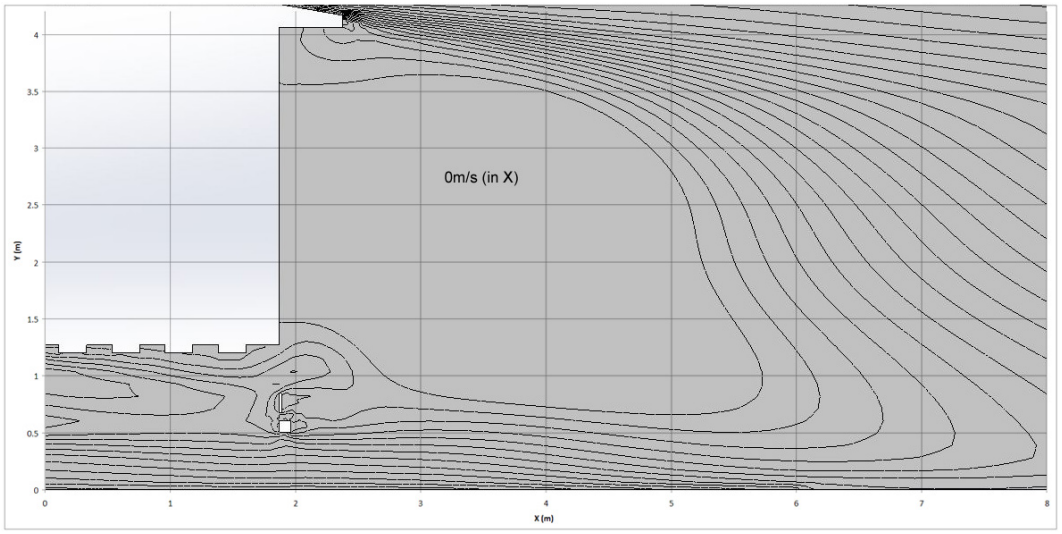

Figure 3.3.13: Plot of velocity in X showing the region of reverse flow in the 10 deg wake.

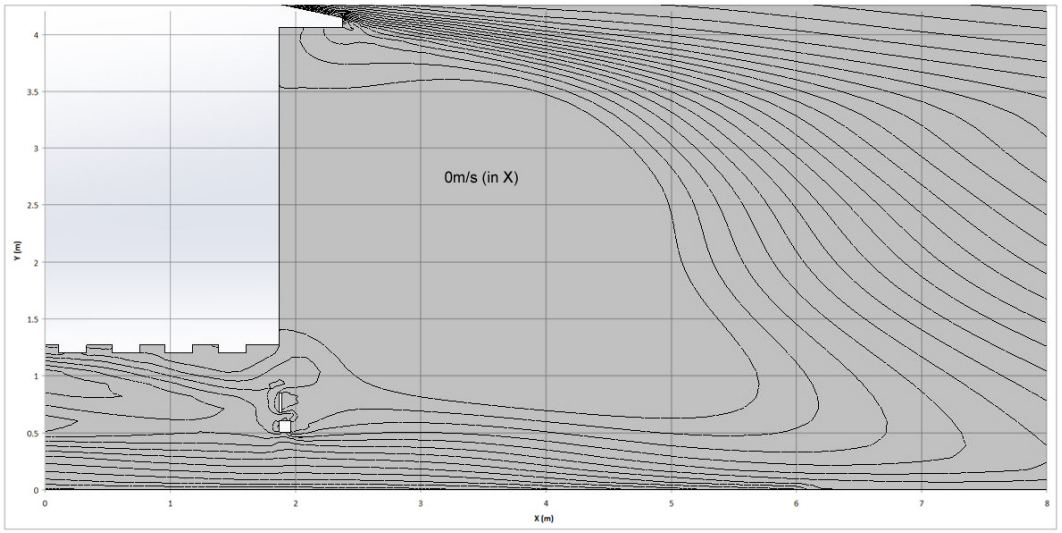

Figure 3.3.14: Plot of velocity in X showing the region of reverse flow in the 12 deg wake.

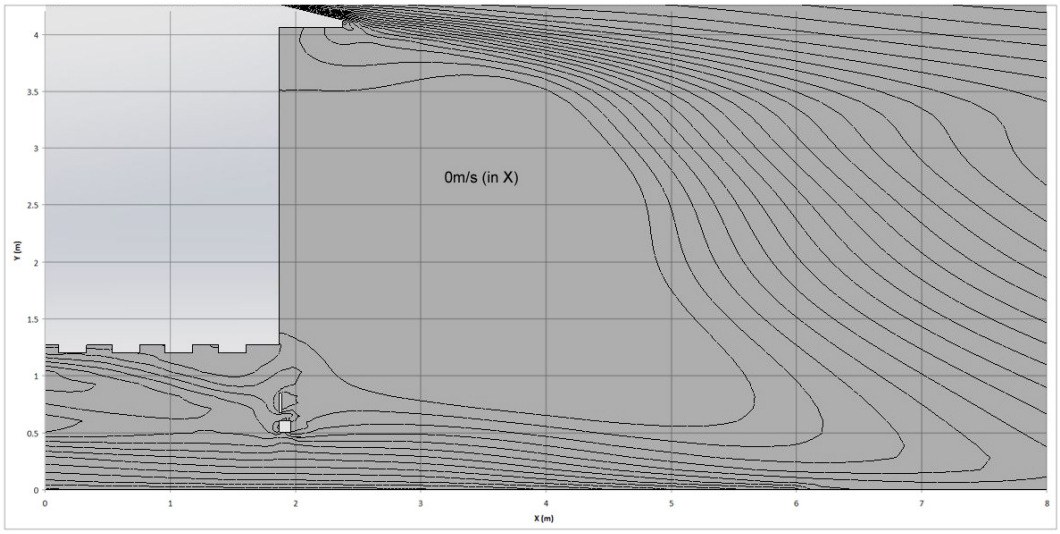

Figure 3.3.15: Plot of velocity in X showing the region of reverse flow in the 14 deg wake.

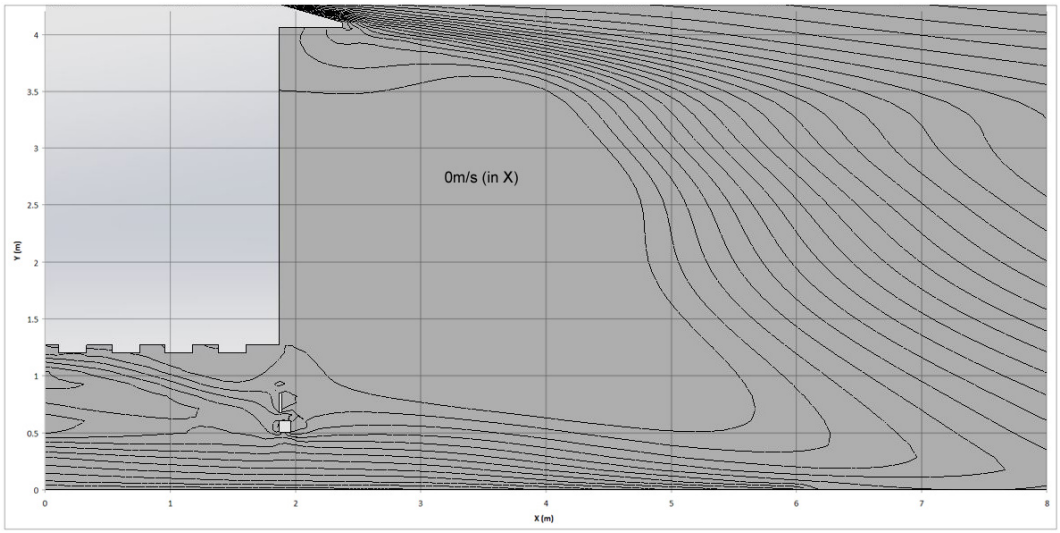

Figure 3.3.16: Plot of velocity in X showing the region of reverse flow in the 16 deg wake.

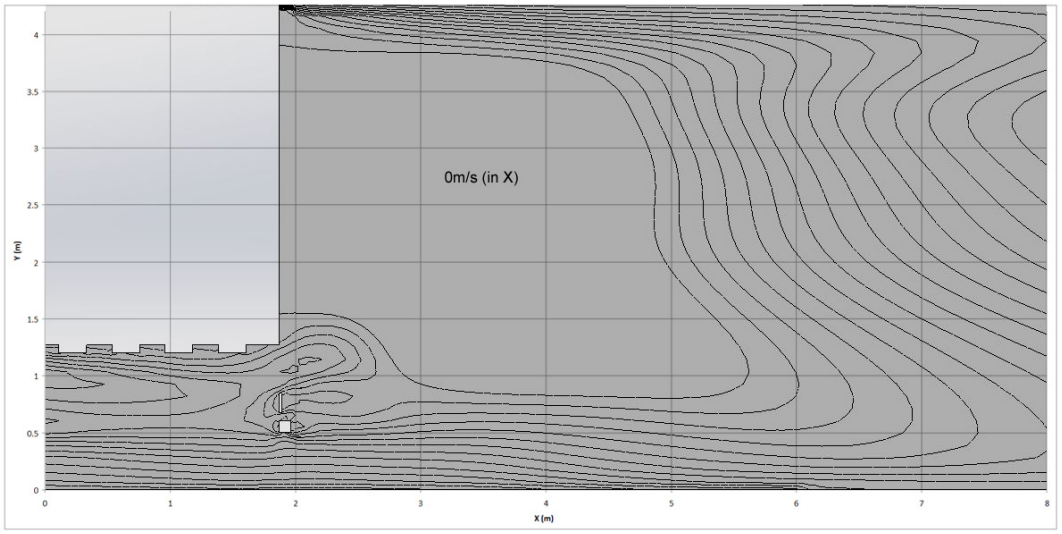

Figure 3.3.17: Plot of velocity in X showing the region of reverse flow in the side plate wake.

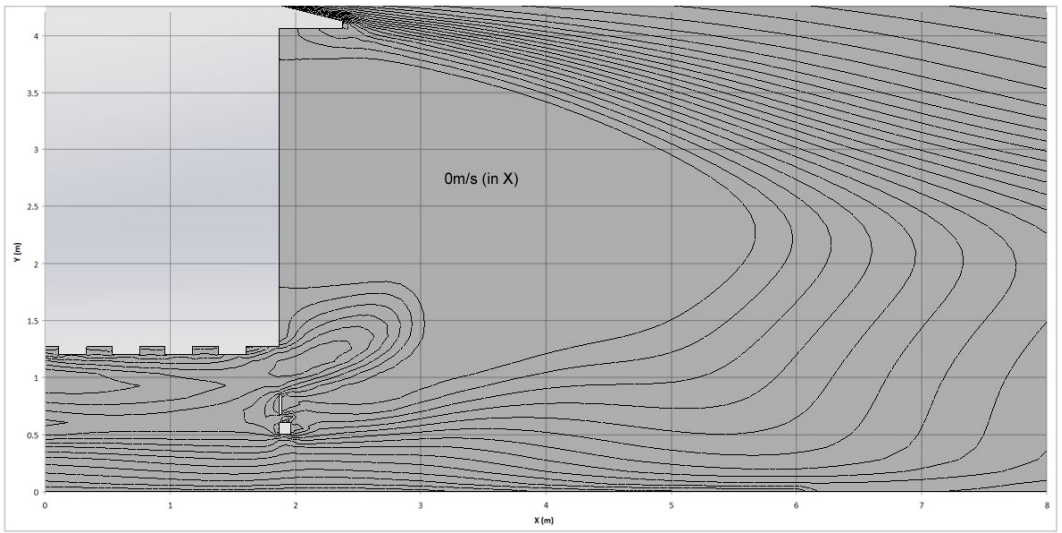

Figure 3.3.18: Plot of velocity in X showing the region of reverse flow in the top plate wake.

3.4 Side-guards, skirts and under-body

Side-guards and trailer skirts have long been a source of drag reduction for trailer manufacturers and operators. Their inclusion on British trailers combines well with safety legislation regarding protective guards flush with trailer sides, and therefore they have been included in designs for decades. There are still many trailers that do not incorporate drag reducing iterations of the side-guard. This section studies the premise of drag reduction via trailer skirts/side-guards and where reductions are possibly obtained, with particular attention paid to the flow through and around the under-body region of the trailer.

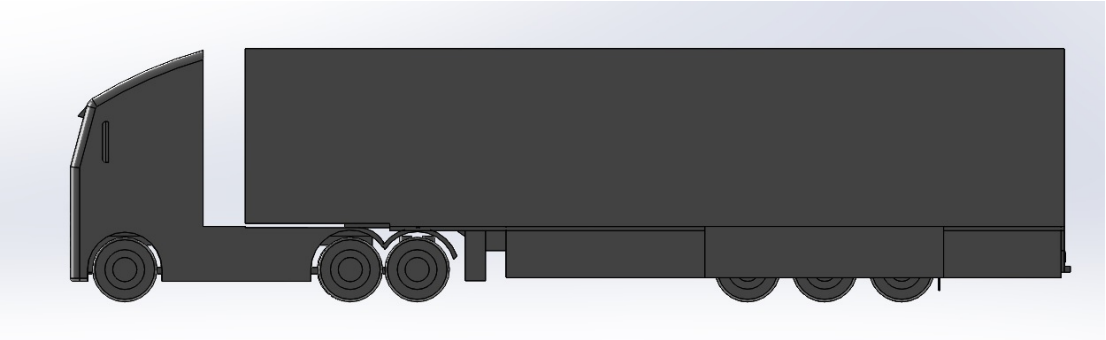

Figure 3.4.1: Basic Skirts with Wheels covered

Table 3.6 shows a summary of the results obtained for the skirt and under-body cases. It can be seen that for the first time in this study, there is a greater benefit from the geometry in side-wind conditions than there is at 0° yaw.

Table 3.6: Side-Skirt Cd

Test Case	**ΔCdBase(%) 0° yaw**	**ΔCdBase(%) 10° yaw**
Basic Skirts	-1.72	-4.26
Basic Skirts with Wheels Covered	-1.93	-5.94
Fuller Skirts with Under-plating	-1.93	-7.62

In general, it appears that side-skirts are not providing a large reduction in drag at 0°, perhaps because of limited exposure that is greatly increased in side-winds.

Studying the three cases in detail provides insight as to the beneficial properties of skirt design.

3.4.1 Basic Skirts

This geometry modification simply adds four plates to the baseline model, two at the forefront of the tyres and two at the rear, each is flush with the side face of the trailer. While basic, their function is to limit the amount of airflow that enters the under body region of the trailer, to prevent high energy interaction with the exposed geometry in this area, such as the axle regions. They provide little drag reduction at 0° yaw, as expected due to the high amount of separation aft of the cab, but there is still a reduction evident. Figure 3.4.2 shows a comparison with the baseline geometry.

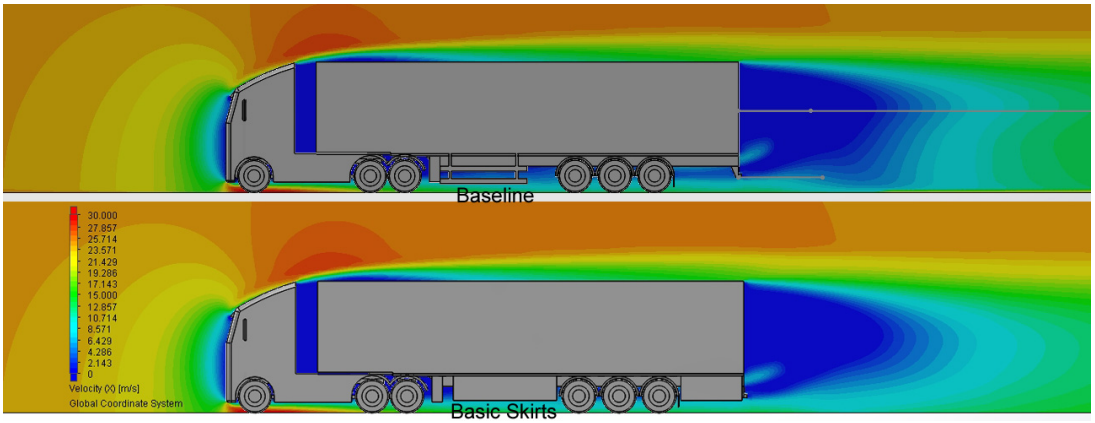

Figure 3.4.2: Skirt Comparison with Baseline Centre Velocity in X

This shows very little variation between the two, except for the wake region which appears to be influenced by the flow exiting the under side of the trailer on the skirt model. It shows a higher velocity of flow at the point above the light-bar where under body flow is pulled into the partial vacuum region, indicating that more energy is maintained through the under body region as it progresses, this in turn alters the wake to become more uniform vertically, dampening the downwards tendency of the rear flow.

Figure 3.4.3 plots flow through the under body region compared to the baseline.

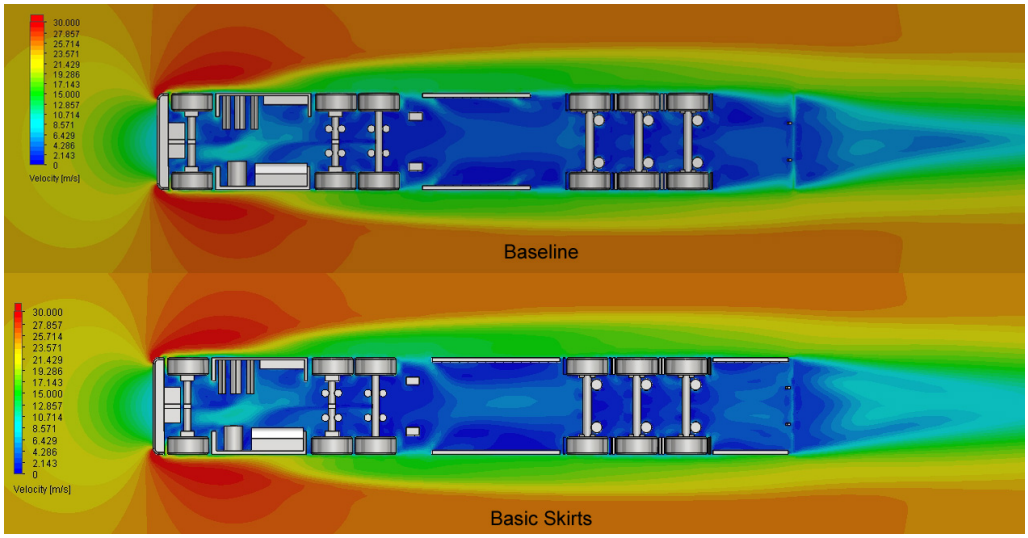

Figure 3.4.3: Skirt Comparison with Baseline Under Body Flow

Despite the high degree of detachment and energy loss due to the cab, flow is still entering the under body region at 0° flow. It can be seen that the skirt geometry does prevent this, although not very effectively due to their limited size. The flow they do allow to enter however appears to maintain more of its energy as indicated in figure 3.4.2 previously. The flow that is entering the under body despite the skirts is doing so in the gap not covered by the frontal skirt area, level with the trailer landing-legs. Extending the skirt to occupy this area should prevent flow entering the gap and improve the skirt's performance overall. The zero pressure boundary representation highlights the limited effect of the skirts at 0° yaw. Showing no real discernible difference between the baseline case and the basic-skirts. This suggests, alongside the limited drag reduction, that either the skirt geometry is not extensive enough, or that the cab geometry simply has too much of a negative effect on the flow in the first instance to be able to significantly affect the wake regions from forming in the trailer under body area. This in itself is of note, if the entire area is engulfed in a partial vacuum then the under body geometry is not necessarily contributing to drag generated at 0° yaw in any significant manner anyway, hence the small reduction in drag at this angle, however it is also possible that the under body is contributing to overall drag in the same manner that the rear face does,

within the wake.

Studying the flow characteristics at 10° yaw show the benefits of limiting under body flow however.

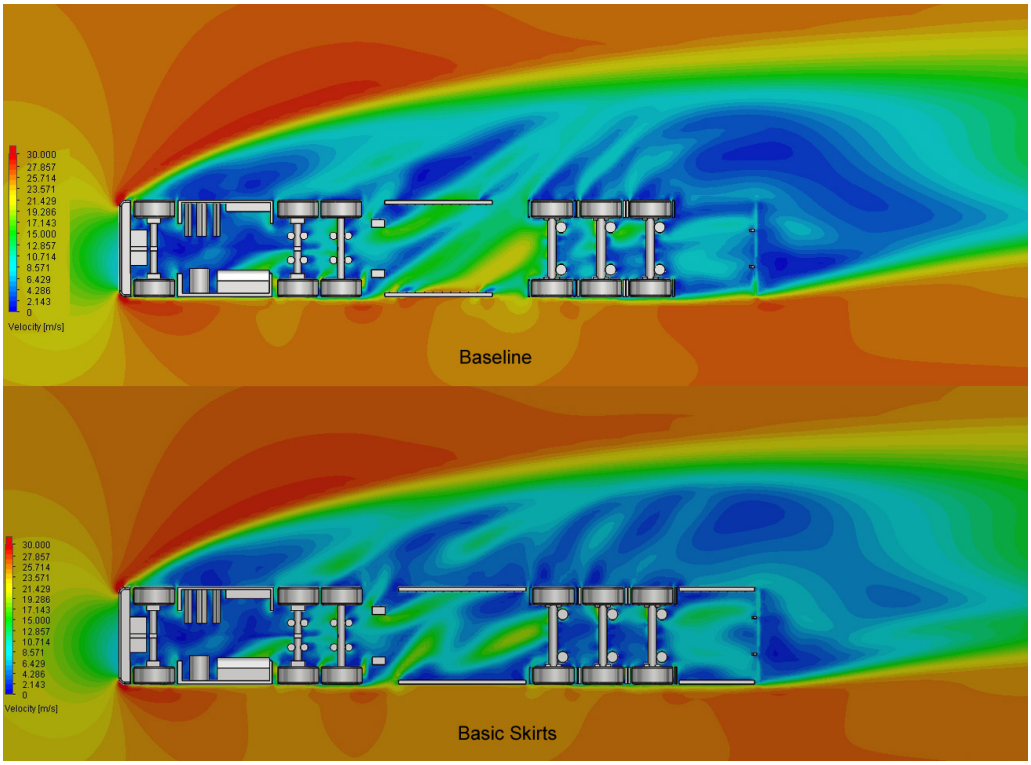

Figure 3.4.4: 10° Yaw Skirt Comparison with Baseline Under Body Flow

This shows the alterations in velocity at 600mm height. The Baseline geometry displayed relatively high velocity passing through the guard rails and consequently exposing the inside faces of geometry such as the axles and wheels to high-energy flow. The basic skirt geometry limits this, and shows reduced velocity in these areas. consequently there is also reduced velocity in the leeward wake region, however this serves to limit the chaotic nature of this area and displays less velocity variation than that of the baseline case, displaying a higher minimum velocity in the area than that of the baseline. The higher energy flow of the baseline case not only imparts a greater force on the under body area but also creates larger areas of partial vacuum as a result, and the rear wake region of the baseline case can be seen to be larger than that of the basic skirts case.

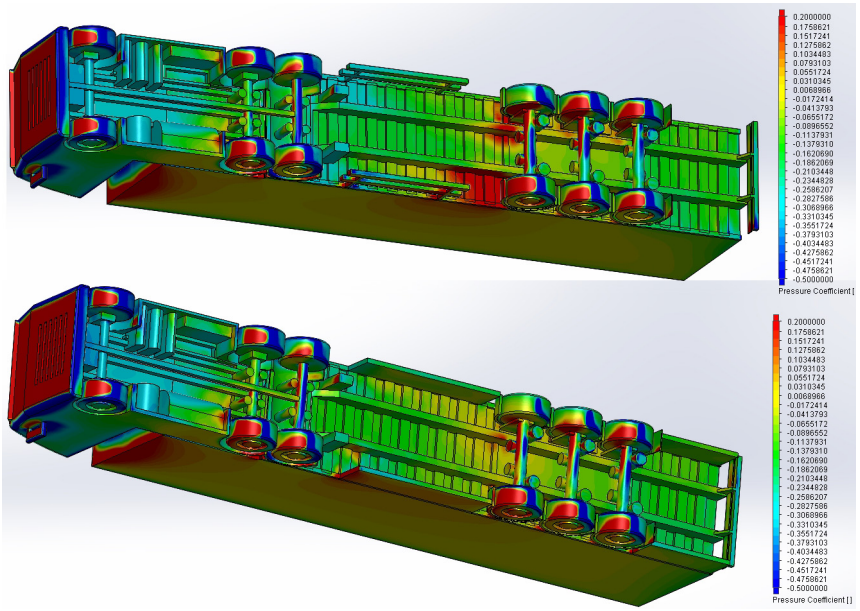

Figure 3.4.5: 10° Yaw Pressure Distribution Comparison

The pressure distribution shown in figure 3.4.5 shows further the areas of improvement on the under body through the inclusion of skirt geometry. There is a large area of higher pressure in front of the windward frontal trailer tyre that is reduced and the areas of pressure on the inside faces of the leeward side tyres is also limited by the skirt geometry. A flow trajectory plot of the windward side frontal skirt face however shows that flow immediately enters the gap created by the exposure of the wheels. A further case studies the effects of covering the wheel faces.

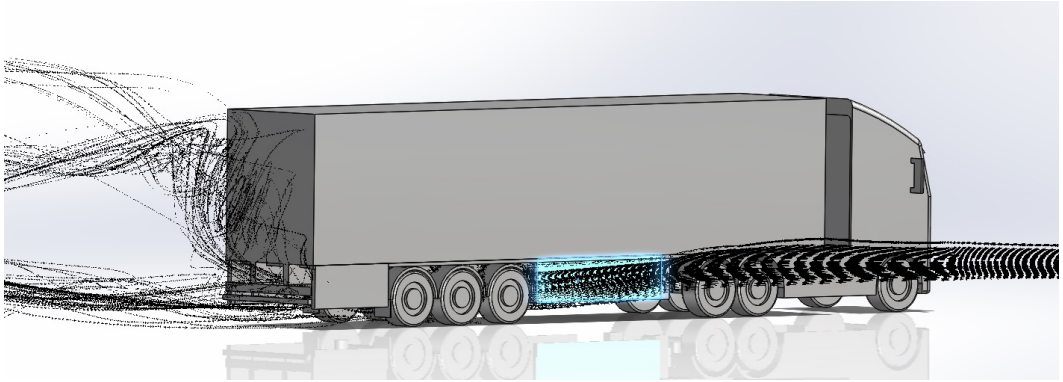

Figure 3.4.6: 10° Yaw Skirt Face Trajectories

3.4.2 Covered Wheels

This case adds geometry to the basic skirts that covers the wheel geometry, removing the outer exposure of their geometry and rotation from the flow field.

Table 3.7: Skirts with Covered Wheels Cd

Test Case	**ΔCdBase(%) 0° yaw**	**ΔCdBase(%) 10° yaw**
Basic Skirts with Wheels Covered	-1.93	-5.94

The table shows that there is only a slight improvement over that of the basic skirts for 0° yaw and a larger improvement for 10° yaw. As figure 3.4.7 shows, there is no real difference between the under body flow characteristics with or without the wheels covered. Therefore it is assumed that the slight drag reduction stems from the removal of the outer faces of the rotating wheels due to the additional geometry.

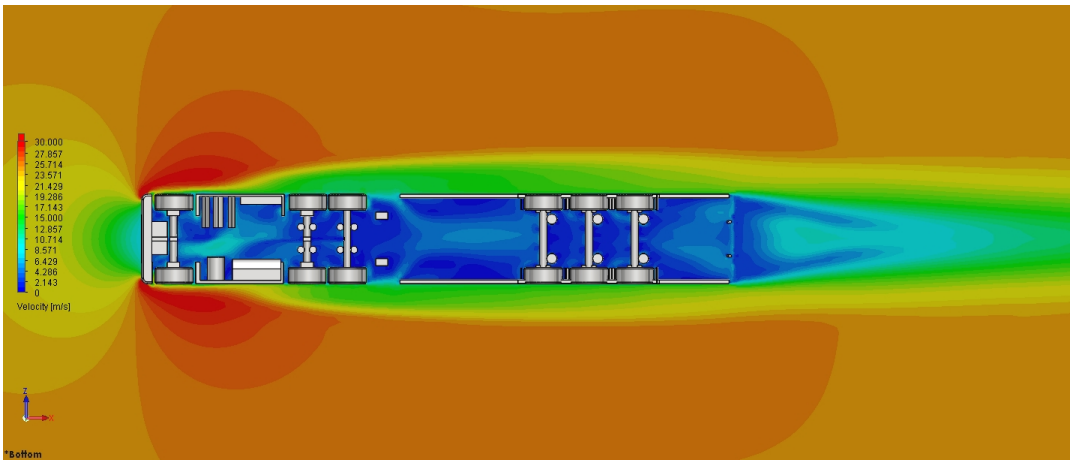

Figure 3.4.7: 0° Under Body Velocity with Wheels Covered

Once more it is hypothesised from this that the cab geometry is affecting flow downstream of it too much for the skirt geometry to have any great effect in these areas. As there is so little deviation between the basic skirts geometry and with the wheels covered at 0° yaw, further analysis of this is not covered as flow visualisation is largely unchanged at this angle. Investigations of 10° yaw however show greater drag reduction and further flow differentiation.

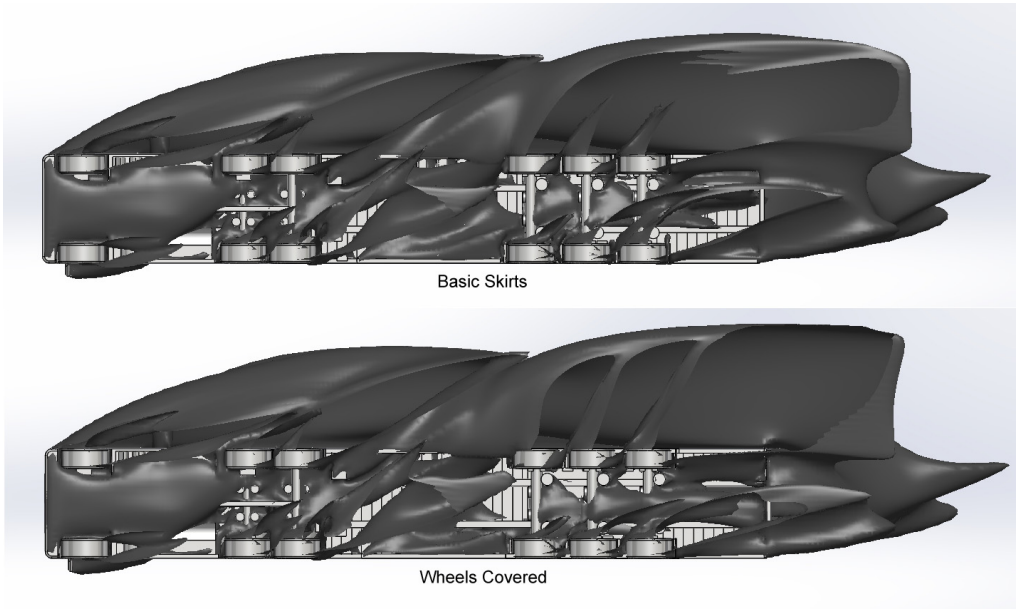

Figure 3.4.8: 10° Zero Pressure Boundaries

The zero pressure boundaries shown above show less partial wake regions in the under body due to reduced flow through the wheel areas. Consequently, it also shows an increased leeward wake region due again to the lack of access through and around the wheel areas. Despite the increased leeward wake however the drag is still reduced due to the reduced turbulence on the under body and even the more controlled flow in the enlarged wake area as shown below due to the lack of mixed velocity aft of the wheels, which are instead a singular large area of low velocity.

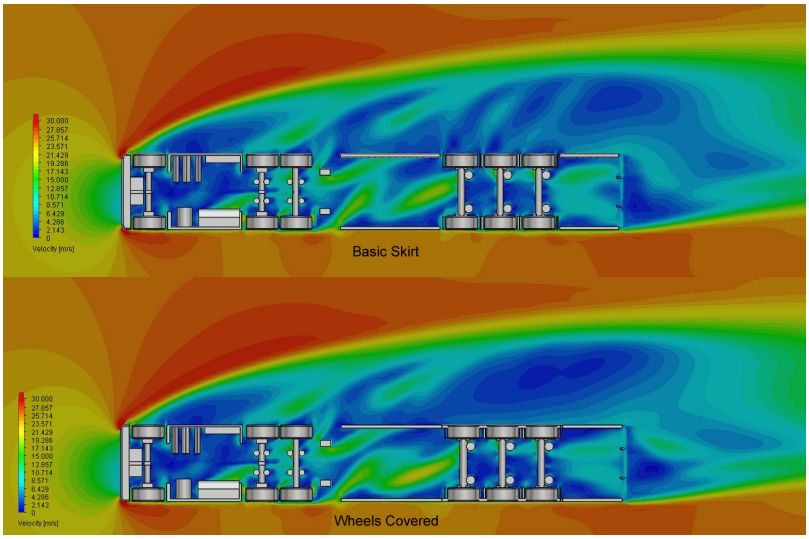

Figure 3.4.9: 10° Under Body Velocity Comparison

As intended, flow no can no longer enter the gaps around the wheel structures, as shown below. It shows flow trajectories that meet the skirts well and remain attached along the entirety of the structure. It also shows that flow circulates underneath the skirt geometry, this is undesirable as this can only contribute to the remaining turbulence in the trailer under body.

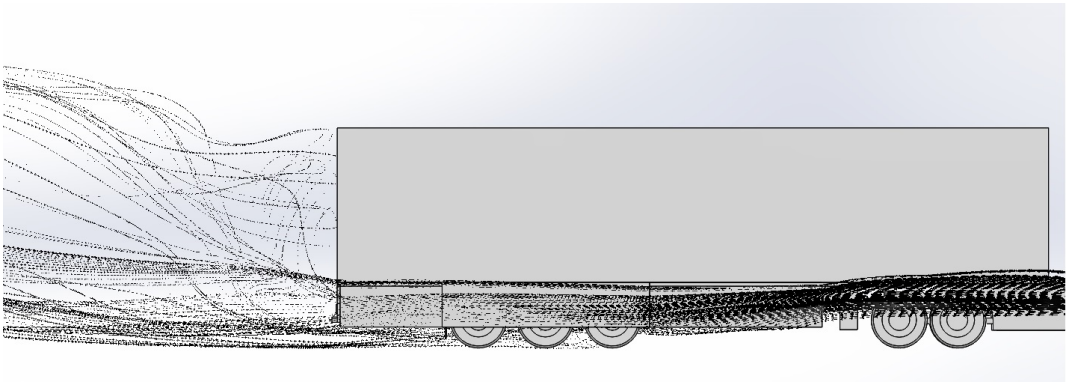

Figure 3.4.10: 10° Skirt Flow Trajectories

A further geometry extends the forward length of the skirt and increases the vertical size, leaving a reduced area above the ground plane to reduce further the flow that enters the under body region.

3.4.3 Fully-plated Skirts

As described, this geometry increases the size of the skirts in X so that they are more flush with the rear of the cab, alongside the trailer landing legs, and in Y so that they extend closer to the ground plane, leaving less room for flow to circulate underneath. Furthermore, the skirts are joined together by plating which covers the entire underside of the trailer, the intention being to completely remove the axle and wheel areas from exposure to flow and direct the flow either rearwards or out to the leeward side with minimal interaction with geometry. For this test the wheels have also been uncovered so as to compare the two methods and assess their relative improvements. The fully plated geometry can be seen in figure 3.4.11.

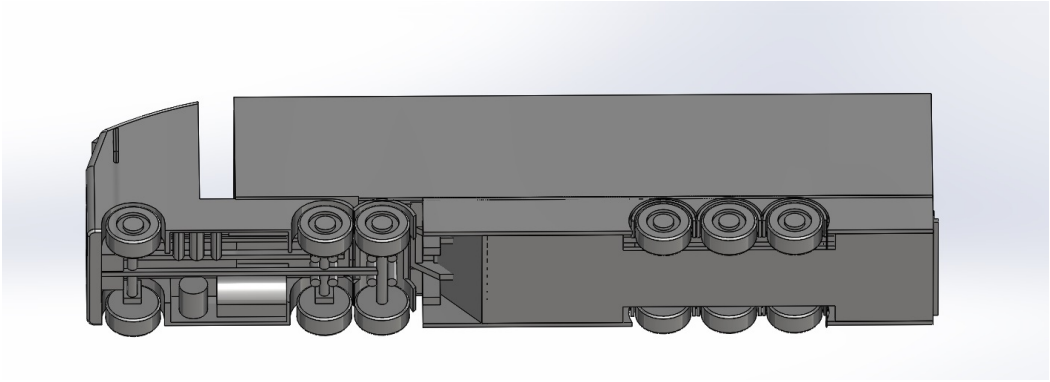

Figure 3.4.11: Fully-plated Skirts Geometry

The frontal skirt is now level with the landing legs, which are followed by an angled section preventing flow from entering above the lower plate which sits 250mm above the ground plane. This lower plate covers the entirety of the trailer under side, the only gaps are in place to allow exposure of the wheels.

Table 3.8: Full-plating Cd

Test Case	**ΔCdBase(%) 0° yaw**	**ΔCdBase(%) 10° yaw**
Fuller Skirts with Under-plating	-1.93	-7.62

The drag reduction of the under-plating geometry is equal to that of the covered wheels at 0° yaw, but exceeds it at 10°. Equalling the covered wheels at 0° suggests that the interaction between the axles at this angle is equal to the drag incurred by the rotating surface and exposure of the tyres. Due to little variation of the drag reduction at 0° there is expected to be little variation of the flow characteristics. Figure 3.4.12 shows flow for the fully-plated geometry at 0° in the X direction.

The flow appears as expected, interestingly however, there still appears to be a degree of velocity as flow exits the area above the light bar, as has been the case for all other flows under this analysis. This was not expected to be the case for the full-plated skirts however, because access to the area should have been completely prevented. Figure 3.4.13 shows the plot with the geometry removed, showing only the plot and exposing the flow between the trailer floor and the plated skirts.

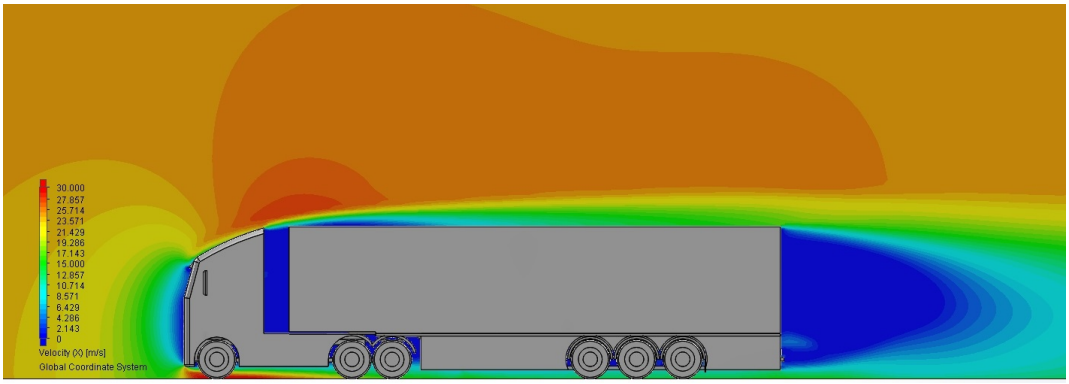

Figure 3.4.12: Fully-plated Skirts Velocity in X

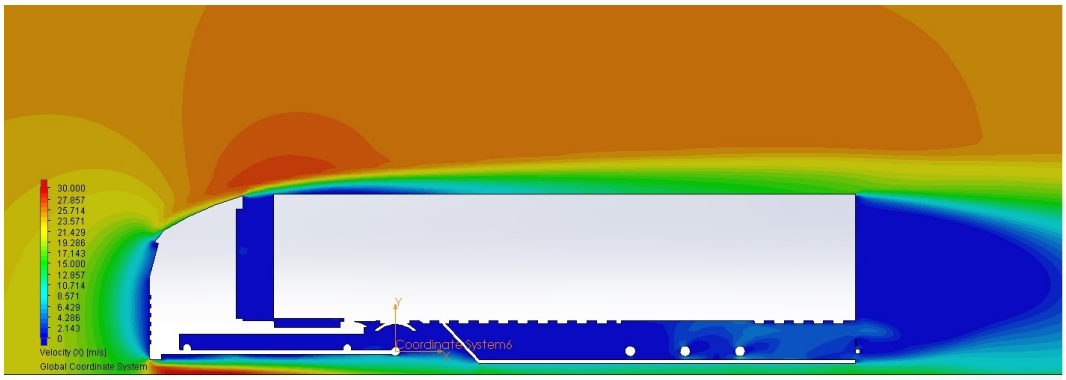

Figure 3.4.13: Fully-plated Skirts Velocity in X with Geometry Removed

It can be seen with the geometry removed that there is still interaction taking place in the plated region aft of the axle geometry. While there was space left open around the wheel structures for their movement, this space was not deemed to be excessive. Plotting flow around the surface of the forward axle however shows that flow is indeed entering the gap that was left around the wheels.

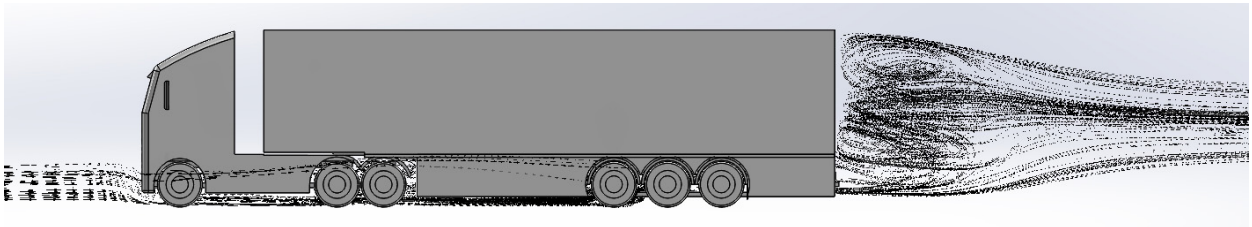

Figure 3.4.14: Flow Trajectories Plotted From the Forward Axle

This could be improved by further reducing the gaps surrounding the wheel structures, but regardless, it does not seem to have much of a negative effect on

the overall drag contribution. A test case that studied the plating with the wheels covered also would be interesting in this regard.

At 10° yaw the drag reduction obtained is the highest of the three skirt geometries tested. As discussed this is likely to be because the aim of the under-plating is to reduce or remove the interaction between the flow and exposed geometry features such as the axles, brake chambers and wheel structures. Firstly, figure 3.4.15 studies the flow velocity underneath the skirt geometries.

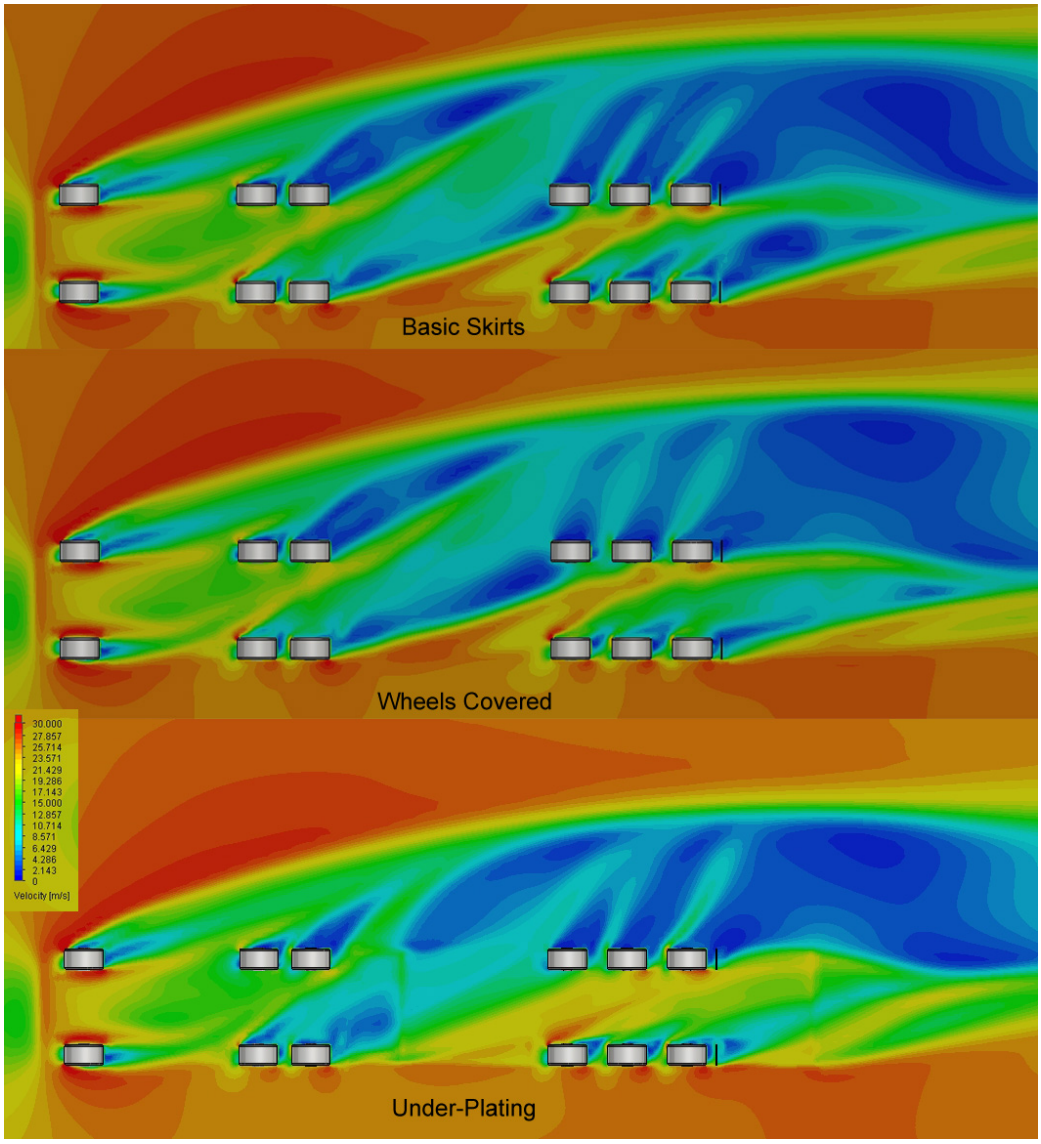

Figure 3.4.15: Under Body Flow at 200mm for Skirt Geometries

The height studied is 200mm so that the flow beneath the under-plating can

be captured and compared. It can be seen that because of the under-plating that a higher velocity is maintained at this height than for the other skirt geometries. Another area of difference is aft of the cab's rear wheel section, where the landing legs and sloping front of the under-plated area begins. Both of the previous skirt models show a large separation aft of the cab rear wheels. This is significantly reduced on the under-plated model due to the additional geometry, which gathers the side-wind flow due to the angles section, which then exits at the leeward side. Instead of lengthy areas of low velocity because of the cab rear wheels, there is a singular point of detachment aft of the angled plate on the leeward side. Additionally, there is reduced velocity at the front of the skirt section on the under-plated model, and increased velocity at the rear section compared to the previous models. This shows less variance over the course of the region, which is desirable as it indicates less energy loss, which is echoed in the improved drag reduction of the plated model.

Figure 3.4.16 shows the flow trajectories of the rear face. This highlights again that the gaps left in the plating to accommodate the wheels are influencing the flow.

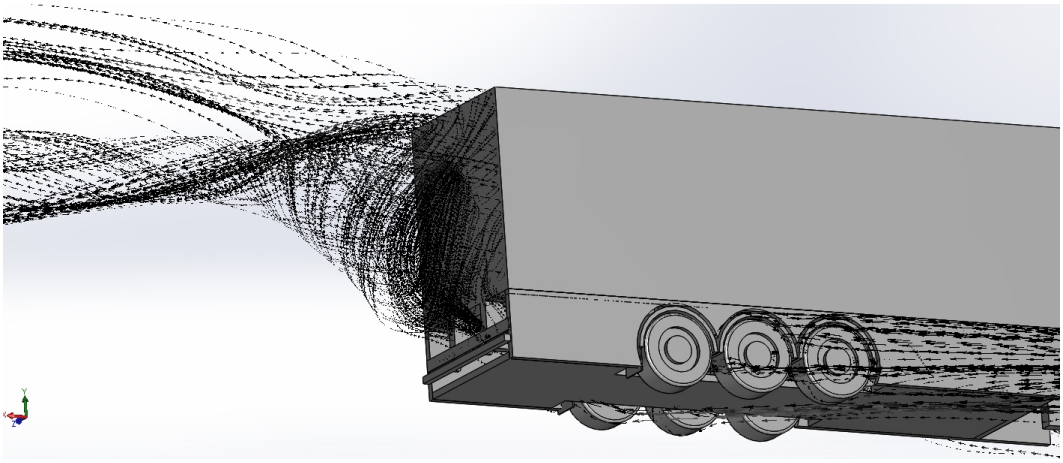

Figure 3.4.16: Rear Face Flow Trajectories

It can be seen that reducing the under-body interactions with flow can provide good drag reduction, despite the complications with the geometry required to achieve this.

Finally, investigating the rear faces of each of the skirt cases revealed the effect

that limiting the flow in the under body region has on the pressure distribution on the rear face and the formulation of the wake structure.

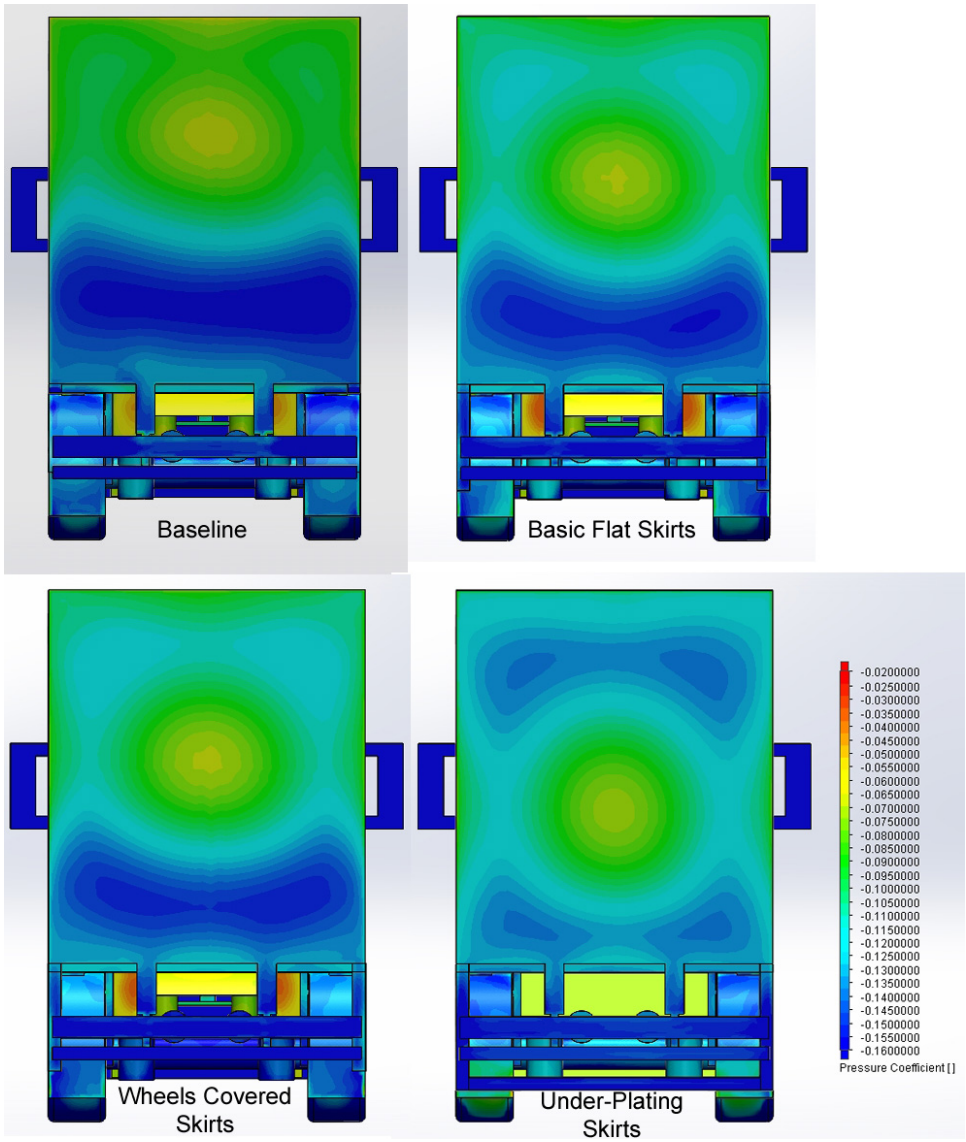

Figure 3.4.17: Rear Face Pressure Distribution

Figure 3.4.17 shows that as flow through the under body region decreases the pressure on the rear face shows less variation, with lower troughs of pressure as there is less flow to pull up from the under body to fill the partial vacuum created at the rear, more is pulled from the sides and roof of the trailer geometry, creating a more even wake structure at the rear.

3.5 Standalone Cases

Beyond the case categories, a number of configurations have been studied that do not easily fall into a larger category of study. These cases have been identified based on analysis of the baseline case for investigation either due to their likelihood of providing a drag reduction, or to provide information regarding a particular scenario that is likely to occur during operation.

Table 3.9 displays a summary of the standalone cases and their effects on the overall drag compared to the baseline case.

Table 3.9: Standalone Cases Cd

Test Case	**ΔCdBase(%) 0° yaw**	**ΔCdBase(%) 10° yaw**
Cab-trailer gap treatment	-3.65	-10.31
Rounded Edges	-6.87	-4.71
Under-aligned cab	+3.65	-2.13

There are some excellent drag reduction possibilities exposed, and also some unexpected and curious results to be studied, namely the under-aligned cab case which displays an overall drag reduction at 10° yaw, when conventional thinking would expect a drag increase, as was the case with the 0° yaw scenario.

3.5.1 Cab-Trailer Gap Treatment

This case considers the gap between the rear of the cab and the bulkhead of the trailer. This area is typically open due to the nature of cab-trailer articulation, firstly with the gap providing the simplest method of allowing articulation for manoeuvrability, and secondly, it allows easy access for the connecting of control and power cables, coupling the two structures. This gap provides a potential area for chaotic flow and turbulence, potentially having an insidious effect on the flow downstream of the gap itself. This chaotic potential was identified during the baseline

analysis, where it was observed that at 0° yaw there were large counter-rotating vortices present across the gap width, and at 10° yaw this area was seen to create large amounts of turbulence as flow cascades through the gap, creating vortices and affecting the leeward wake of the trailer and cab as it interacts with the bulkhead and cab-rear.

To investigate the full effects of the gap and the influence on drag, a case has been studied with the gap completely filled, with additional geometry connecting the cab to the trailer bulkhead, as can be seen in figure 3.5.1, with the observed drag reduction seen again in table 3.12.

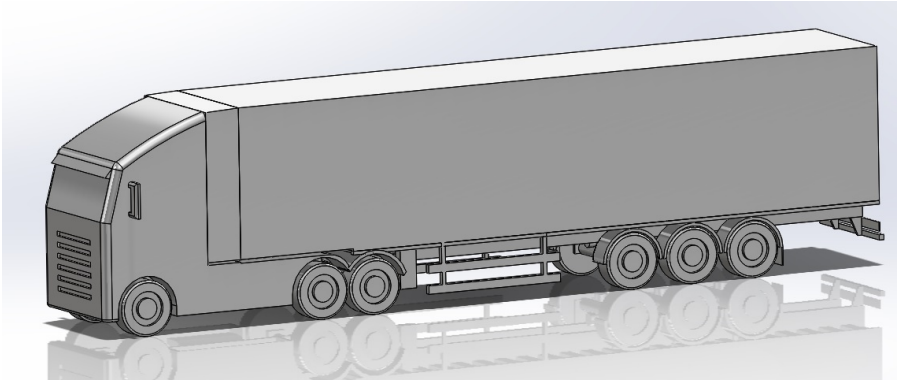

Figure 3.5.1: Cab-Trailer Gap Treatment Geometry

Table 3.10: Gap Treatment Cd

Test Case	**ΔCdBase(%) 0° yaw**	**ΔCdBase(%) 10° yaw**
Cab-trailer gap treatment	-3.65	-10.31

The drag reduction shown is impressive, and indicates what a large influence on overall drag the gap area is for the baseline case during side-wind conditions. This comes as little surprise based on the turbulent flow through the gap area as analysed on the baseline case. There is however still a good drag reduction evident at 0° yaw, investigating this initially, figure 3.5.2 shows the central velocity plot in the X-direction.

Figure 3.5.2: Centre plane velocity in X at 0° yaw

This shows excellent maintenance of attachment over the gap region, it is in stark contrast to the baseline and other cases where typically separation has been observed and evidenced by a recirculating vortex region along the roof line trailing the bulkhead. This can be seen further with a zero pressure plot, which also lacks evidence of separation along the roof line. This is shown alongside the separation present on the baseline case in figure 3.5.3.

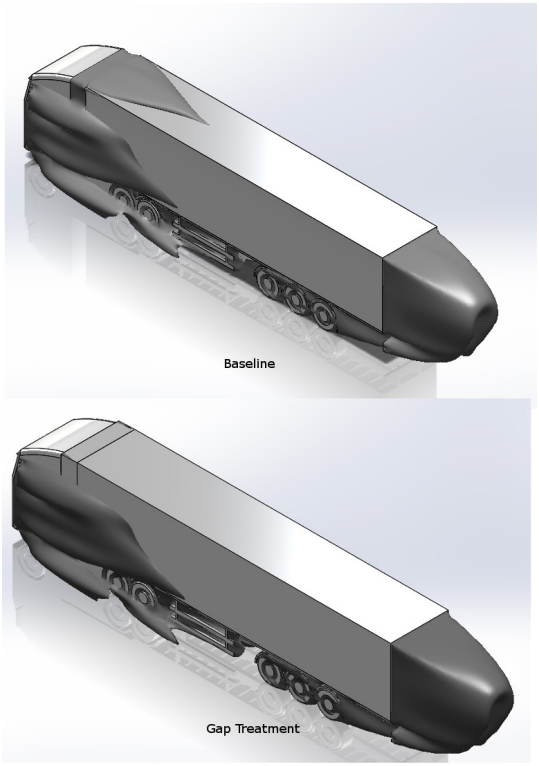

Figure 3.5.3: Pressure equal to Zero

This shows the zero pressure region which previously filled the gap to be removed, as well as the region of recirculation aft of the bulkhead, along the roof line. There are however, small areas of separation incurred by the sharp corners of the gap treatment geometry, that exist as it does not perfectly match the cab deflector profile with filleted edges, despite this, the negative influence is small. This is the only evident area of differentiation, as expected for this modification, and is responsible for the drag reduction at 0° yaw.

At 10° yaw, the reduction observed is much greater, highlighting the importance of this area on overall drag. It can be seen from figure 3.5.4 that the hole through the zero pressure boundaries generated by flow through the gap has been eliminated.

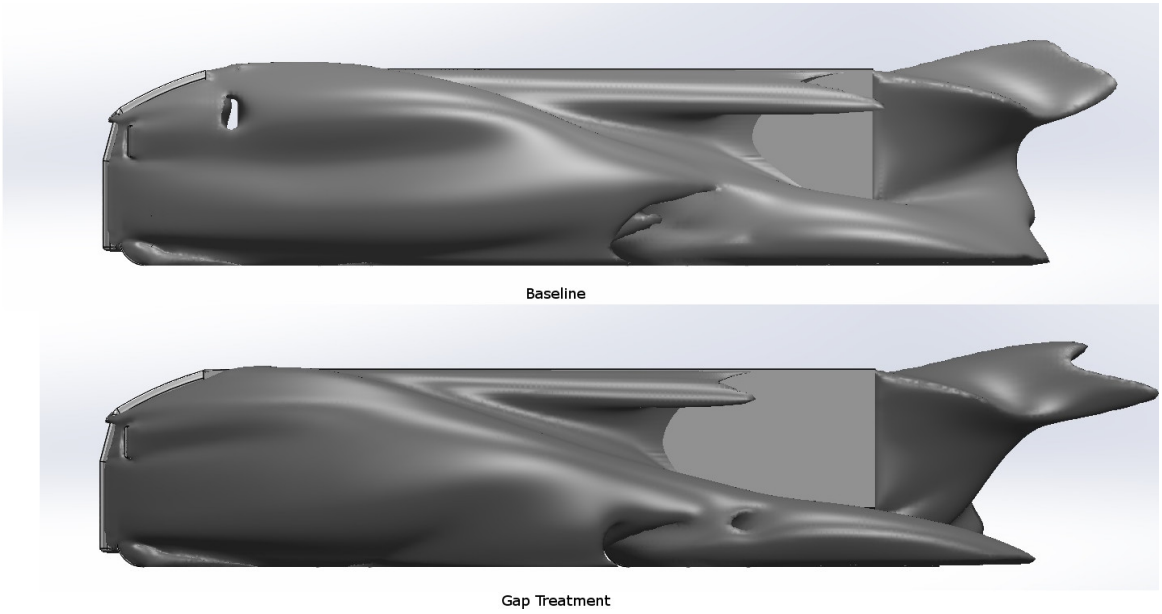

Figure 3.5.4: Pressure equal to Zero

As a consequence of the removal of turbulent flow through the gap, the overall size of the wake on the leeward side of the geometry has been reduced also, as is evidenced by a reduction in overall size and form at the extreme rear of the trailer and the overall length of the wake section that follows the leeward roof line edge. A more progressive reduction in leeward wake height is also observed, evidencing that the removal of turbulent flow through the gap region reduces the severity of the

partial wake and the turbulence occupying the region therein. The topmost point of the rear wake however is larger than that of the baseline counterpart, this is due to additional energy carried through the trailing vortex in this area created by flow separating over the roof line at the windward edge. The additional energy is as a result of increased flow on the windward side that no longer passes through the cab-trailer gap, and instead progresses flow along the windward side. An aspect of this can be seen in figure 3.5.5 where trajectories are calculated from the windward side of the gap treatment geometry.

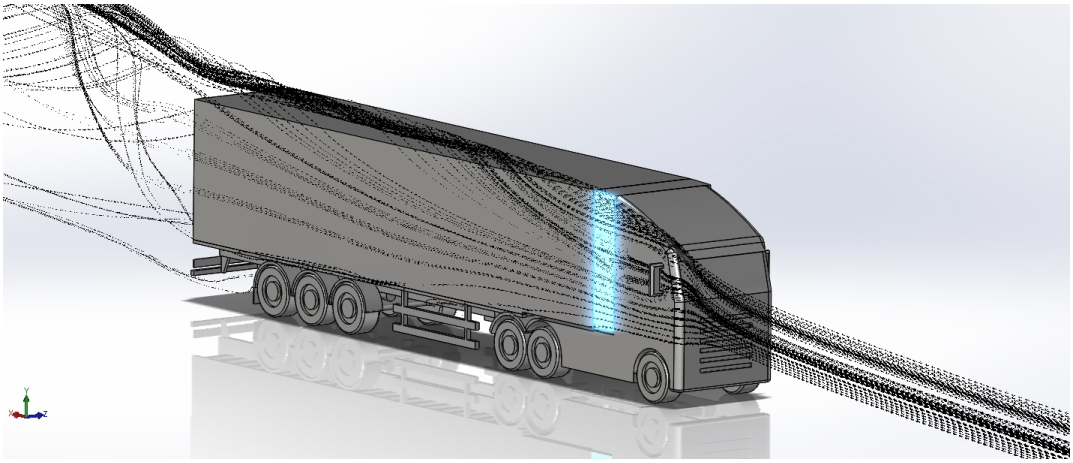

Figure 3.5.5: Trajectories from the Gap Treatment

As expected, this shows a large proportion of the flow that is interacting directly with the gap treatment windward face progresses on to become part of the trailing vortex separating over the roof line edge. As a consequence of the additional energy, and higher speeds of flow at the point of detachment, analysis on the rear face of the gap treatment geometry shows drag greater than that of the rear face of the baseline case, in the case of 10° this is a significant increase and can be seen in table 3.11. Despite this, the advantages to flow in the gap region outweigh the negatives incurred at the rear.

Table 3.11: Gap Treatment Rear Face Fx

Test Case	**ΔFxrear(%)0-yaw**	**ΔFxrear(%) 10-yaw**
Gap Treatment	3.08	9.9

3.5.2 Under-aligned Cab

This case considers the effect of a misaligned cab deflector with a trailer of 4200mm height. The purpose of this case is to investigate the effects of this misalignment, as it is a scenario that is likely to occur during operation. Similar to the mismatching of the double-deck case, operator's cabs can be used to pull many different trailers, and while many are equipped with adjustable deflectors so as to be able to match a variety of trailers, it can often be the case that these are either set incorrectly, or not set at all.

The double-deck case that considered a mismatched cab alignment highlighted the drastic effect this can have on drag incurred by the trailer. While a misalignment of 200mm in this case results in a much less severe drag increase, it still has an influence and is a likely scenario to occur during operation.

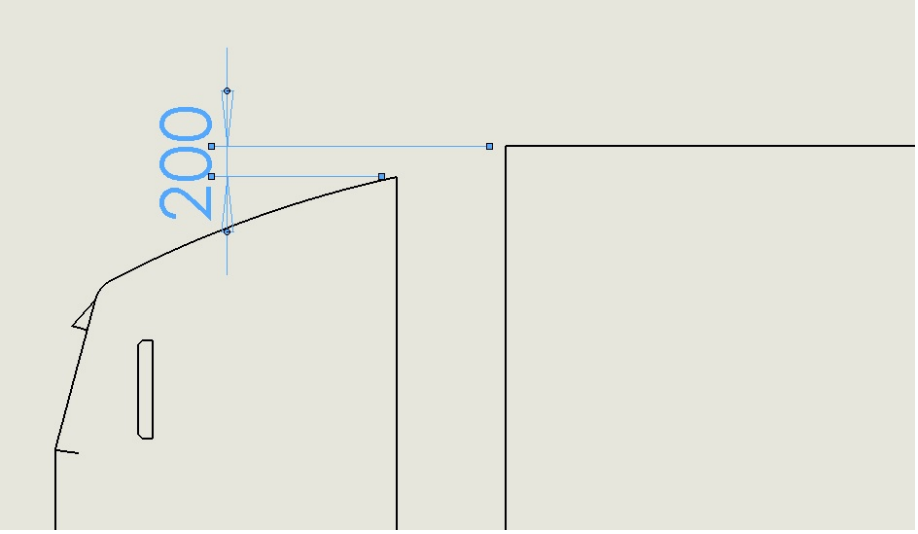

Figure 3.5.6: Cab Misalignment

Table 3.12: Cab Misalignment Cd

Test Case	**ΔCdBase(%) 0° yaw**	**ΔCdBase(%) 10° yaw**
Cab Misalignment (200mm)	+3.65	-2.13

The results show an expected increase in drag, but only at 0° yaw, unexpectedly

a reduction in drag is seen at 10° yaw. The reasons for this are not immediately clear, however analysis of the flow characteristics suggest reasons for this to be the case. Firstly however, analysis of the 0° case shows the reasons for the increase.

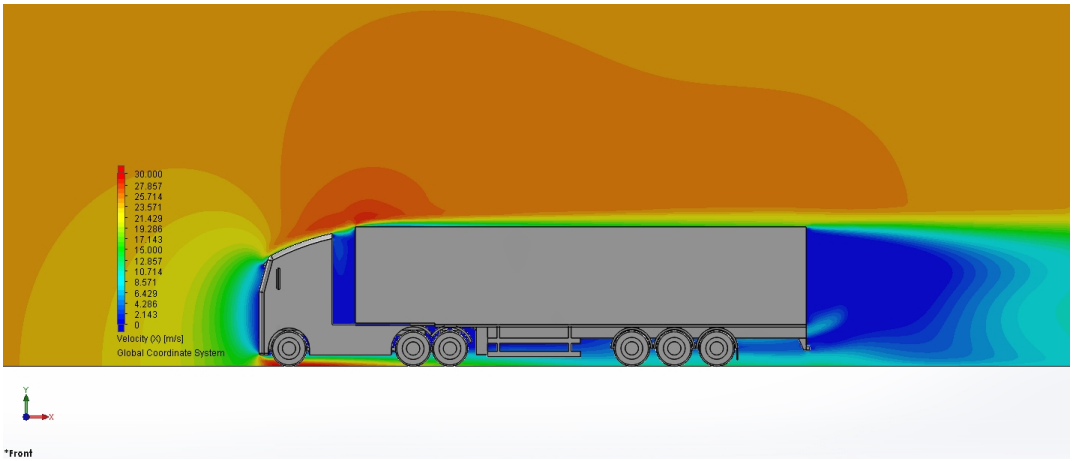

Figure 3.5.7: Velocity in X Over a Misaligned Cab

Figure 3.5.7 shows the centre plane velocity in X. It also shows a characteristic almost as unexpected as that of the 10° yaw results; it shows reduced separation and recirculation aft of the bulkhead leading-edge. It is expected that increased separation would be apparent here due to the additional exposure of the bulkhead to free-stream flow, however it appears that the angle of the cab deflector and the difference in height as the flow detaches from the deflector is having an effect on the degree of recirculation on the trailer roof line. This is not unexpected either, though the visual improvement in flow to this extent is unexpected. Figure 3.5.8 shows that there is still however a degree of separation that is not apparent from the velocity plot. It shows the expected separation extending along the roof line, this is however smaller than is evident on the other cases with a correctly matched cab deflector. This does however begin to show show the effects of the misalignment despite seemingly lacking a negative separation. Unlike the baseline case, the zero pressure boundaries extended aft of the cab deflector, engulfing the bulkhead and extending along the roof line. While this case shows reduced extension along the roof line, it also shows much smaller boundaries of zero pressure aft of the cab deflector, with the bulkhead exposed to view. This shows that this area is of a high pressure,

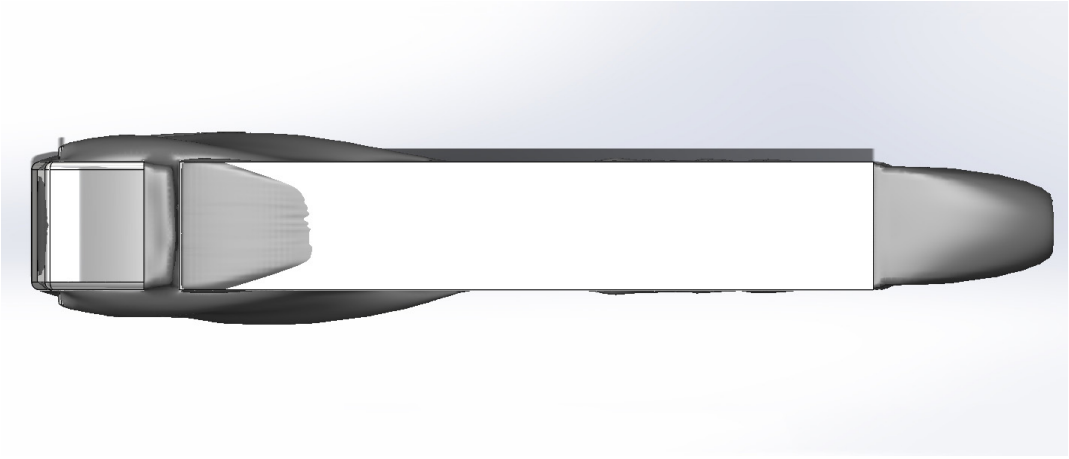

Figure 3.5.8: Pressure equal to Zero on the Bulkhead

indicating that there is a resultant force being exerted on the face of the bulkhead that is not evident in the baseline case. Figure 3.5.9 shows the results of this on the pressure distribution on the bulkhead.

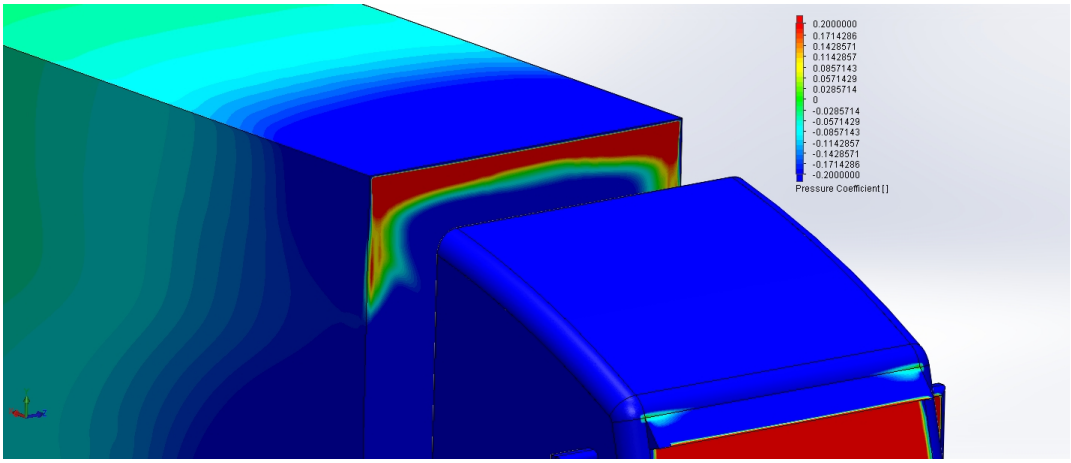

Figure 3.5.9: Bulkhead Pressure Distribution

As it shows, there is increased pressure along the leading edge of the bulkhead, corresponding to the height misalignment of the cab deflector. Despite the apparent improvement in the flow characteristics due to decreased separation, this is the area where the overall drag has increased nonetheless.

Investigating the flow at 10° yaw is much more curious, due to the unexpected reduction in drag. It would be expected that a similar increase would be seen to

that of the 0° case due to the same exposure of the bulkhead that increases the force imparted on its face. Figure 3.5.10 shows the zero pressure boundaries of the misaligned cab compared to that of the baseline case.

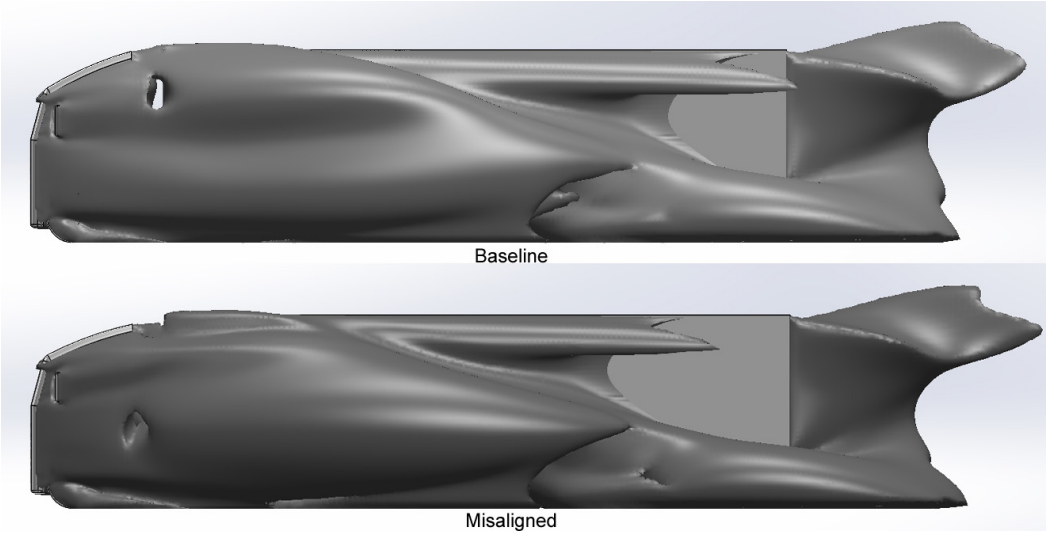

Figure 3.5.10: Zero Pressure Boundaries at 10° yaw

It shows an alteration in the positioning of the high pressure hole punched through the boundary due to turbulent flow resulting from vortices being formed during interactions between the cab and trailer inside the transition gap. The height of the point that the higher pressure region exits the gap has been reduced, which also results in the top most wake region that extends along the roof line edge to the rear of the trailer being shortened. It appears as though, in this 10° case the misaligned cab is causing an overall reduction in the total area consumed by the partial vacuum wake.

Investigating the cab-trailer gap region to expose the characteristics and reasoning for the lowering of the height of high pressure, reveals similar characteristics to that of the baseline case, that also showed highly turbulent flow in this area. However, as the velocity in the X direction (figure 3.5.11) and the Z direction (figure 3.5.12) show, the turbulent areas are forced further down the gap due to the additional high pressure at the top of the bulkhead face.

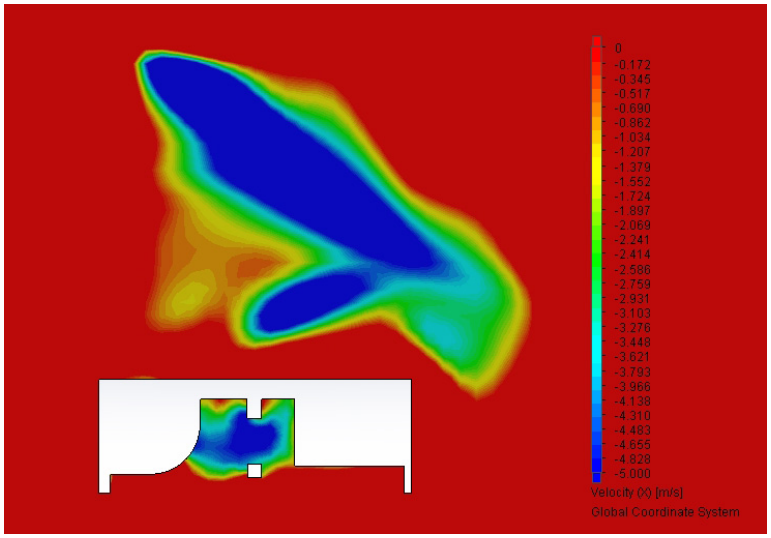

Figure 3.5.11: Velocity in X in the cab-trailer gap

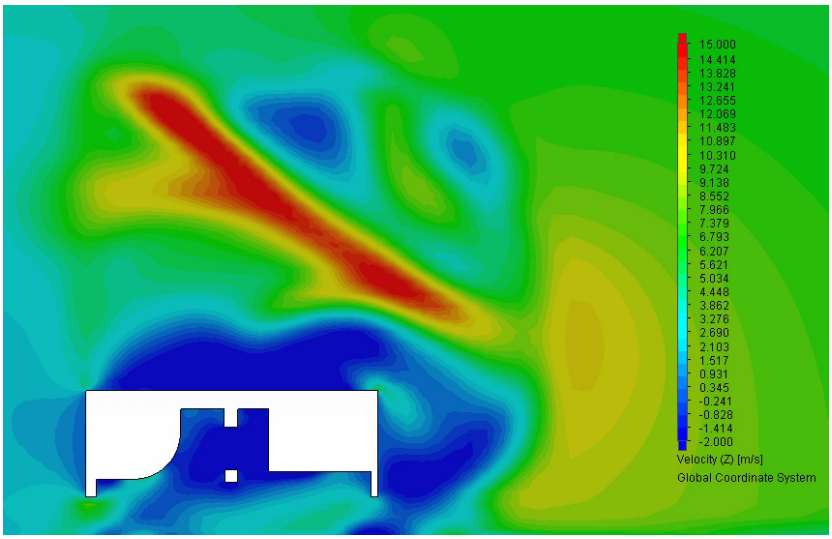

Figure 3.5.12: Velocity in Z in the cab-trailer gap

This is the cause of the lower exit point for the high pressure region, and is highlighted by area at the lower right of the trailer gap, the exit point, which shows higher velocity in the Z direction. This shows the high energy that is carried through the gap region, rather then being lost in it. This is likely to be the reason for the overall decrease in wake size on the leeward side of the trailer, despite the discrepancy in cab deflector and overall trailer height, the positive consequences of this outweigh the negative influence of the height differentiation on the overall drag.

A final illustration of this can be seen in figure 3.5.13 where the drastic difference in pressure is evident. As seen in the velocity plots, this is due to the additional pressure at the top of the bulkhead, which is not evident in the baseline case. Because of this, much higher pressures are carried through the gap rather than being lost, despite still being highly turbulent, the effects of this serve to have a positive effect on the overall drag of the geometry.

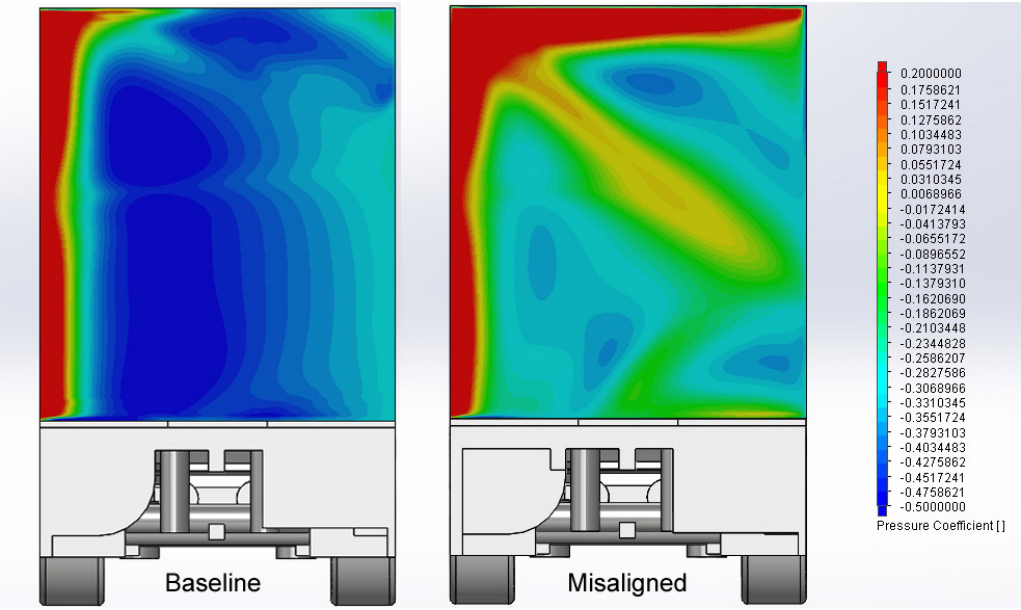

Figure 3.5.13: Pressure Distribution on the Bulkhead Face

This case more than any other highlights the unpredictable nature of the effects of differing angled flows. All other cases do alter with the differing free-stream flow angle, however they either dampen or enhance the effect seen at 0°. This is the only case where the outcomes are opposing dependent on the angle, due to an unpredictable characteristic of flow through the gap region.

3.5.3 Rounded Edges

This case compares the influence of sharp edges on the trailer superstructure against rounded edges with a radius of 150mm. All other cases including the baseline consider the trailer geometry to be sharp. This is not unlike many trailers that are manufactured, especially curtain-sider designs, due to the nature of the mechanism requirements to house the curtain rollers. There are however many trailers that are manufactured that round the edges of the cant-rail for both aesthetic and aerodynamic purposes. This case considers what benefit rounding the bulkhead, roof line and rear face edges of the trailer can achieve.

Figure 3.5.14 shows the rounded edges of the trailer considered in this case.

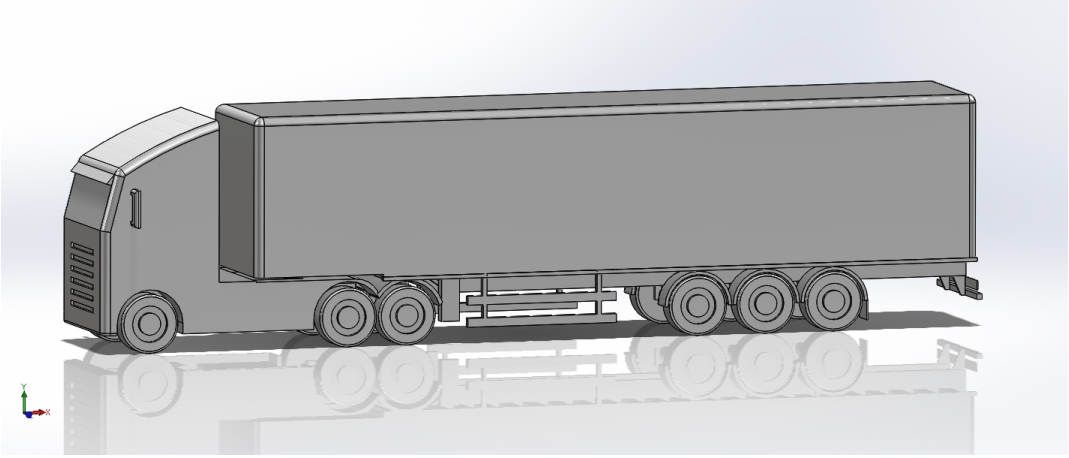

Figure 3.5.14: Trailer with Rounded Edges

The drag reduction obtained can be seen in table 3.13.

Table 3.13: Rounded Edges Cd

Test Case	**ΔCdBase(%) 0° yaw**	**ΔCdBase(%) 10° yaw**
Rounded Edges	-6.87	-4.71

It can be seen that for both yaw angles, the rounding of trailer edges provides an excellent drag reduction considering the relatively small change in the overall form

of the geometry.

Figure 3.5.15 shows the central velocity plot, which shows very little deviation from the profile of the baseline case. There is a small alteration to the rear wake structure where it appears that it is directed downwards slightly, a very small influence akin to that of the boat-tail cases.

Figure 3.5.15: Centre Velocity in X-direction

The small influence is likely to be due to the rounding of the rear edges. While it is nowhere near the effect of the boat-tail geometry, it is not unexpected that there should be a degree of increased attachment over the rounded surfaces due to the Coanda effect, whereas with the sharp edges, where only a sudden detachment of flow was possible.

Figure 3.5.16 compares the pressure distribution of the baseline case against that of the rounded edges and the 12° boat-tail case. It shows that the pressure distribution on the rear face of the rounded edges geometry does indeed show similar characteristics to that of the boat-tail cases. While not altering the distribution to the extent of the 12° boat-tail case, the lower area of low recirculating pressure is similarly removed from the baseline case and a completely central point of recirculation is established, suggesting that the rounded edges are indeed guiding the flow in a similar manner to the boat-tail, to the point of influencing the pressure of the

entire lower rear section of the trailer, as far back as the rear wheel-guard section.

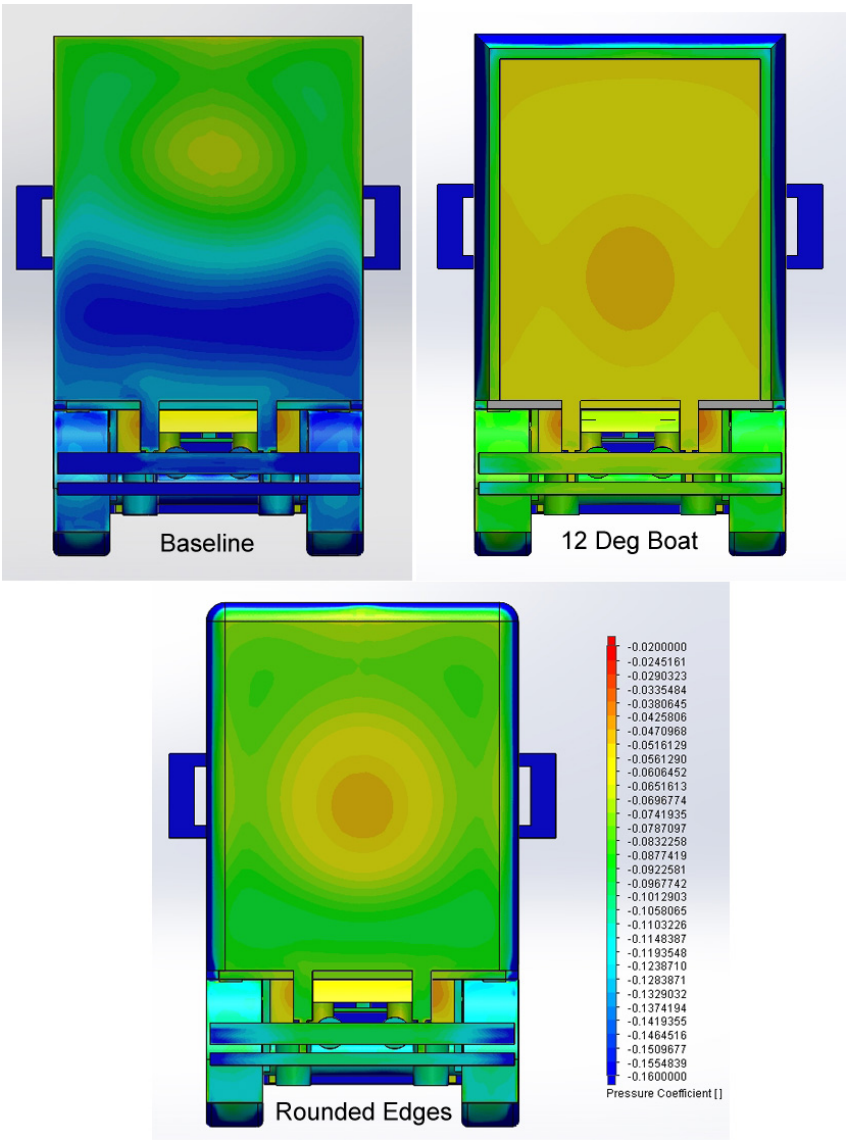

Figure 3.5.16: Pressure Distribution Comparison

The effects of rounding the rear edges and the increased and more uniform pressure on the rear face are evidenced by the force data taken from the rear face itself, shown in table 3.14

Table 3.14: Rounded Edges Rear Face Fx

Test Case	**ΔFxrear(%)0-yaw**	**ΔFxrear(%) 10-yaw**
Rounded Edges	-22.53	-6.36

There is a significant reduction in the force incurred by the rear face at 0° yaw, demonstrating that the rounding at the rear is indeed having a similar effect to that of the boat-tail geometry. This is reduced significantly at the 10° case, however this does not directly correlate to the difference in drag reduction between the two angles. This suggests that the rounded edges forward of the rear have greater importance at 10° yaw than at 0°, which is unsurprising given the additional exposure to the free-stream at greater yaw angles.

Investigating this, figure 3.5.17 shows the pressure distribution along the roof line of the geometry. On the sharp geometry of the baseline case there was a large area of low pressure where the flow separated over the side edge and onto the trailer roof before extending along the roof line as a large trailing vortex. In the case of the rounded edge, this large area of low pressure due to separation is greatly reduced, indicating that flow, particularly in the boundary layer is no longer exhibiting as large a scale detachment as with the baseline geometry.

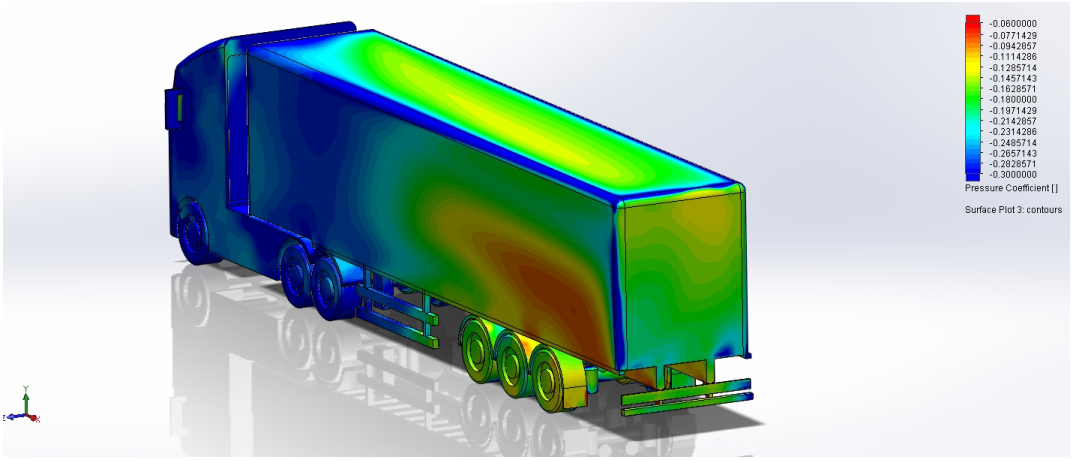

Figure 3.5.17: Pressure Distribution of the Roof Line

Further investigation into flow influenced by the windward rounded edge can be seen in the flow trajectories of the fillet itself in figure 3.5.18. These trajectories do not exhibit the large scale detachment and vortex that is shown over the baseline and other cases in cross-wind analysis, nor is it shown in the zero pressure boundary analysis in figure 3.5.19, which shows elongation of the wake aft of the rear roof

line, but without the increase in verticality evidenced by the baseline case where the trailing vortex was evident even in the immediate wake structure aft of the roof line.

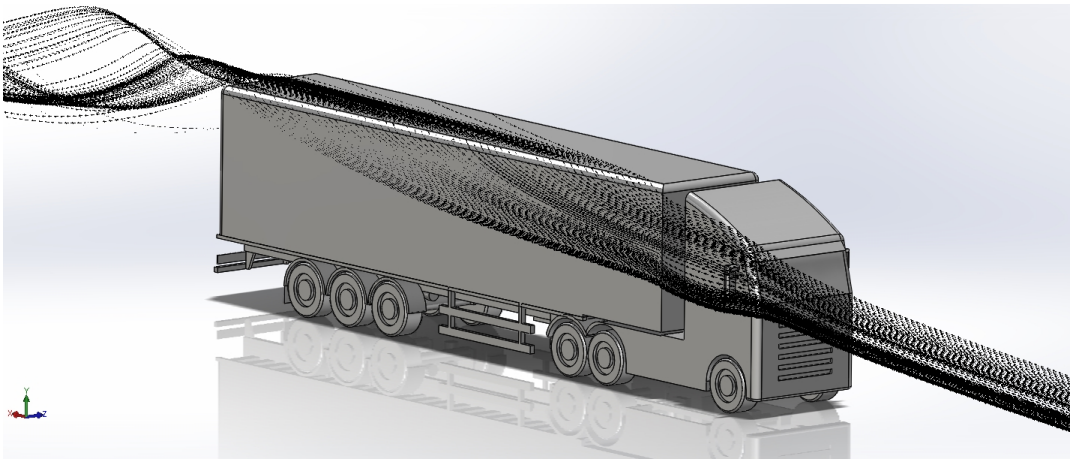

Figure 3.5.18: Flow Trajectories over the Windward Edge

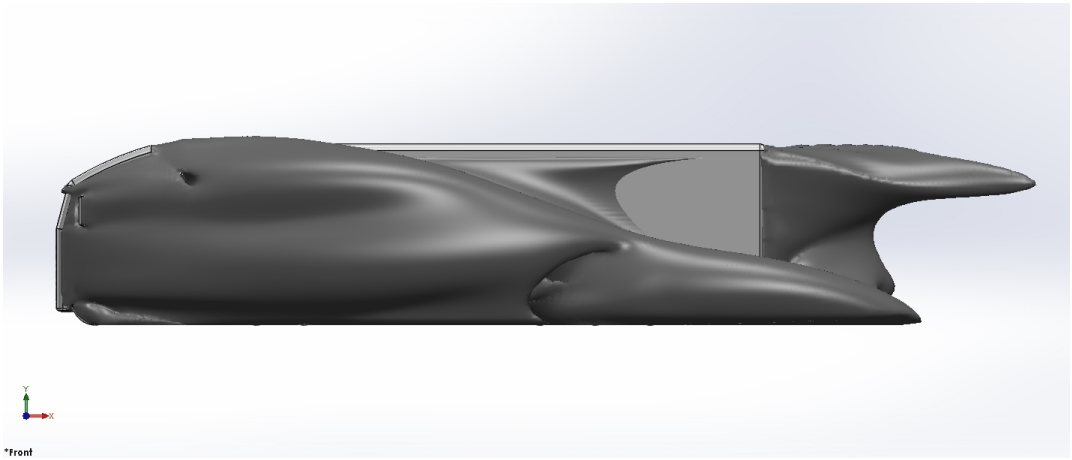

Figure 3.5.19: Zero Pressure Boundaries

This indicates the unexpectedly large impact of rounding the sharp edges of a trailer a the point of manufacture.

3.6 Double Deck Larger Trailers

This section studies briefly the consequences of larger trailer bodies over the baseline case. Unlike the rest of the EU, the UK does not have a limit on the overall height of a vehicle. Whereas the EU is limited to a 4m overall height limit, UK manufacturers often build trailers up to and exceeding 4880mm in height. These cases examine the effect of a trailer of this size coupled with the baseline cab used at 4200mm, and the effects of modifications to mitigate some of the additional drag created as a consequence. For many operators, the larger overall height provides room for an additional stowage deck within the trailer, meaning up to twice the amount of goods can be transported in the same journey. The additional efficiency of fewer trips required to transport the same amount is highly attractive, however there are additional costs due to weight and additional aerodynamic drag. Comparing the efficiency gained with that which is lost is difficult and dependent on the operational specifics, but if the drag incurred can be mitigated, this goes some of the way towards making the larger trailers as efficient as possible. The standard geometry used with increased height can be seen in figure 3.6.1.

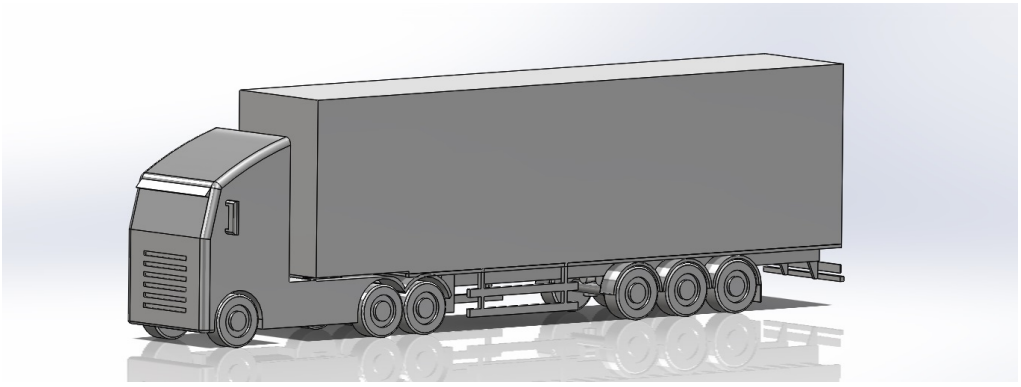

Figure 3.6.1: Double Deck Increased Height Geometry

Table 3.15 displays a summary of the double deck cases and their effects on the overall drag compared to the baseline case, and table 3.16 displays the difference of the deflector and sloping front geometry Cd against that of the untreated 4800mm geometry shown in figure 3.6.1.

Table 3.15: Double Deck Cd

Test Case	**ΔCdBase(%) 0° yaw**	**ΔCdBase(%) 10° yaw**
4880mm Trailer	+49.79	+16.59
4880mm Trailer with Deflector	+19.96	+7.29
4880mm Trailer with Sloping Front	+7.73	+2.91

All three test cases show an increase in drag over the 4200mm height baseline test, as expected. Though the sloping front geometry, with its roof line section curved downward shows relatively little consequence to the overall height increase over the majority of its length, indicating that good compromises of efficiency are certainly possible dependent on the operational requirements in place. The basic modified geometry with only the height increased and no mitigating geometry in place displays a very large increase in drag as a consequence of the height increase and additional exposed geometry to the free-stream flow.

Table 3.16: Double Deck Baseline Comparison

Test Case	**ΔCdDD(%) 0° yaw**	**ΔCdDD(%) 10° yaw**
4880mm Trailer with Deflector	-19.91	-7.98
4880mm Trailer with Sloping Front	-28.08	-11.73

The table above compares the modified double deck geometry with that of the unmodified double deck geometry to clarify the improvements over an inefficient cab and double deck pairing seen in figure 3.6.1. It shows that merely adding deflection geometry to the bulkhead can reduce the drag incurred by the bluff bulkhead significantly, and fully modifying the forward roof line to meet the cab height reduces drag incurred by over 28% at 0° yaw. Investigating the flow characteristics of each case identifies the effects of the height increase.

3.6.1 Baseline 4880mm Double Deck

This case studies geometry 680mm taller than that of the standard baseline model, with all other aspects identical, including cab height. It is expected that the increase in bluff frontal area without any flow mitigation will result in a large increase in overall drag incurred by the geometry. Velocity in X in the central plane can be seen in 3.6.2.

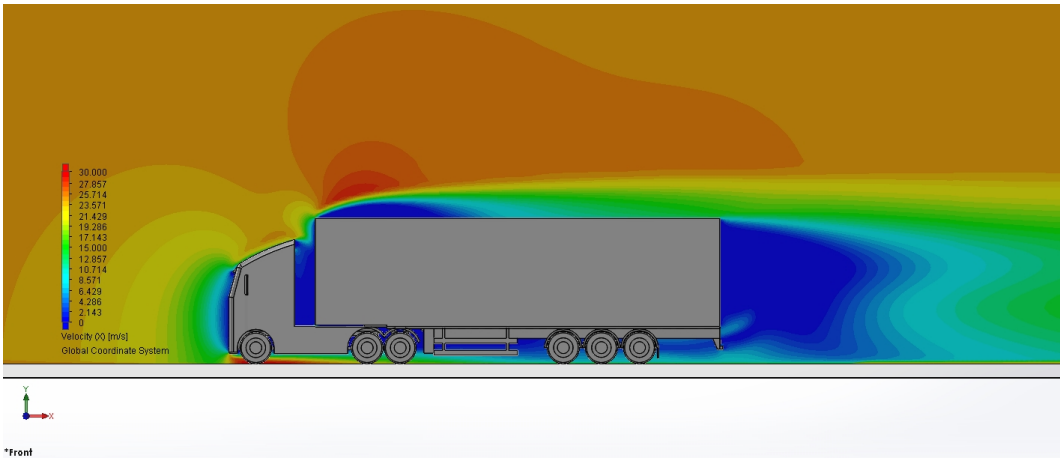

Figure 3.6.2: Double Deck Central Velocity in X

As expected, flow is directly impacting the newly exposed 680mm additional geometry of the trailer bulkhead, the resultant separation over the frontal roof line can clearly be seen in the low velocity recirculation vortex evident aft of the bulkhead leading edge. This further results in a large section of reduced velocity that continues on along the trailer roof line and beyond the rear face.

The exposure of the additional bulkhead area can be seen clearly in figure 3.6.3 which shows the pressure coefficient plot through the central plane. It can be seen that a large area of pressure is formed against the exposed area. This is the cause for the drastic increase in drag over the 4200mm baseline model.

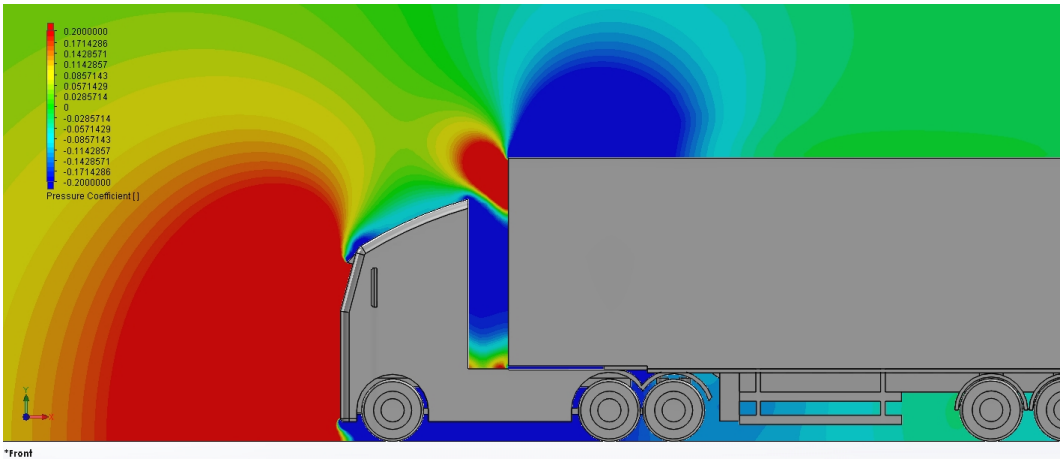

Figure 3.6.3: Double Deck Central Pressure Coefficient

Looking at the bulkhead in more detail shows the clearly defined high pressure region that is exposed to the flow.

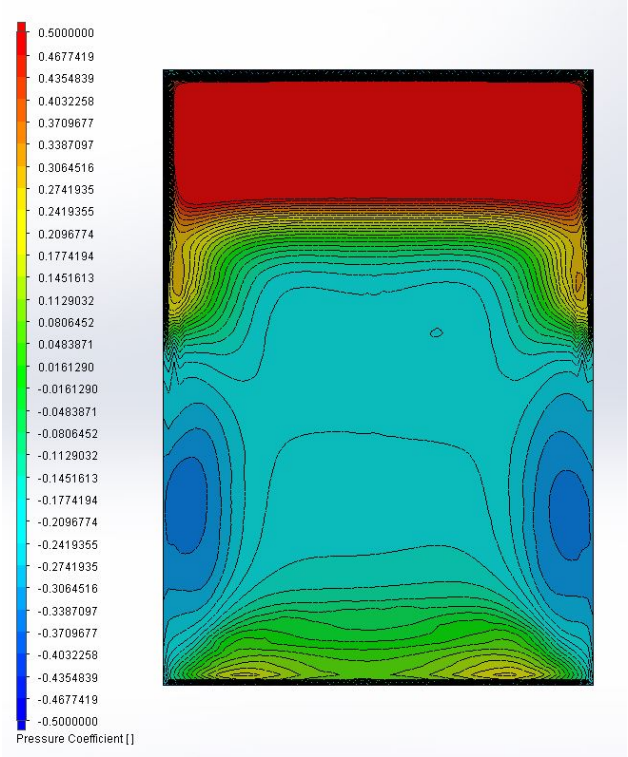

Figure 3.6.4: Double Deck Bulkhead Surfacel Pressure Coefficient Plot

Investigating this level of misalignment between cab and trailer shows the extent to which correct alignment or drag mitigating geometry are essential. Figure 3.6.5 shows the zero pressure contours, which once more highlights the extent of the

separation caused as a result of the bulkhead exposure.

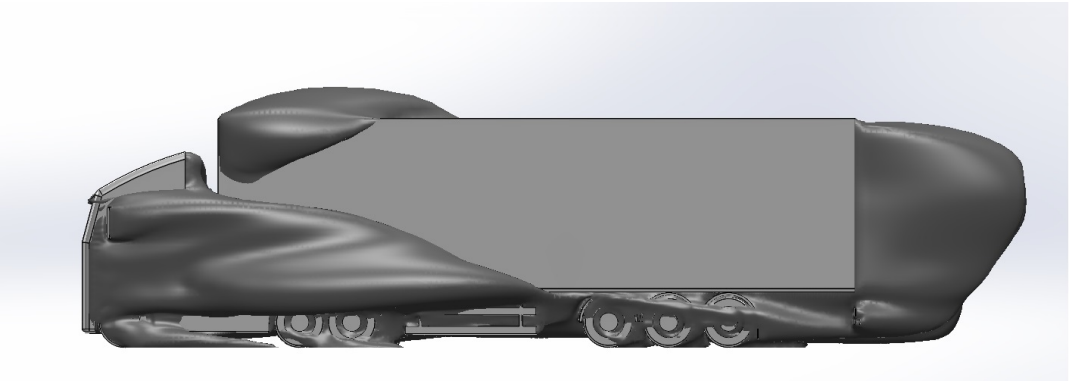

Figure 3.6.5: Pressure equal to Zero

As seen in the 200mm cab misalignment case, the zero pressure boundaries no longer engulf the entire cab-trailer gap, as a result of the high pressure on the bulkhead surface.

At 10° yaw the flow characteristics are similar, however the drag increase is reduced due to the proportional contribution of drag that the under-body region provides when in side-wind conditions. It still remains a significant increase, however.
Figure 3.6.6 shows the pressure distribution over the double deck body on the windward side and bulkhead. It shows the continued high pressure and drag region of the bulkhead exposed, but also displays a reduced degree of separation over the roof line edge. On the 4200mm geometry the low pressure line along the roof's surface is larger. This is due to energy loss of the flow separating over the windward edge due to the increased height.

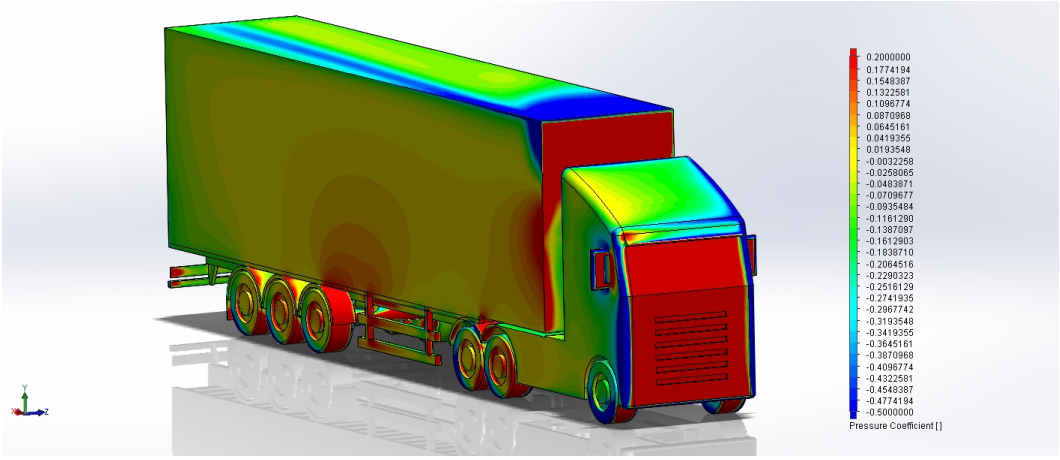

Figure 3.6.6: Pressure Distribution on the Windward Side

Investigating partial vacuum regions in the 10°case shows correlation with the effect of the previous misaligned cab case, where the additional pressure at the top edge of the bulkhead altered the flow through the cab-trailer gap significantly, and influenced the leeward side wake regions. Figure 3.6.7 shows the lower pressure point punched through the zero pressure boundary, lower still than of the previous misaligned cab case. As expected the flow in this area appears highly turbulent, though its overall size is not as large as expected given the additional height of the trailer. This is as a consequence of high energy flow passing through the cab-trailer gap limiting the total volume of the partial vacuum that is formed.

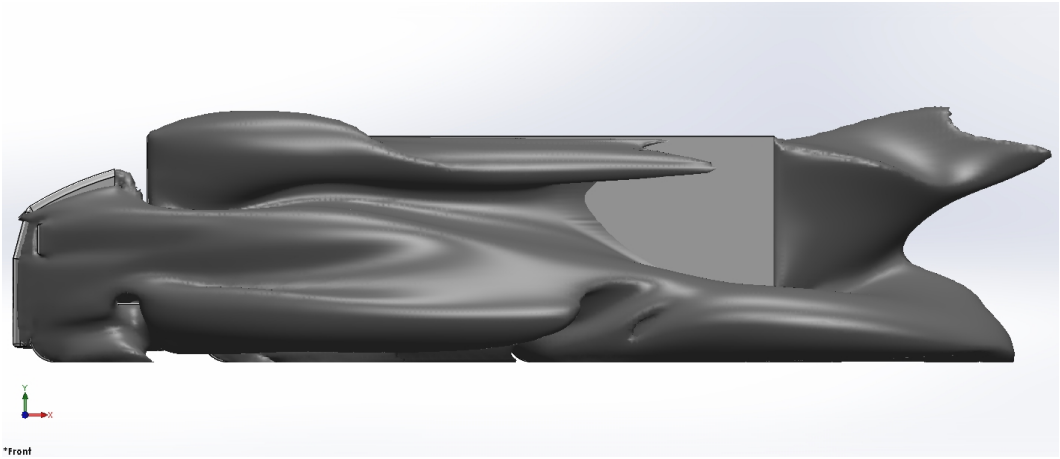

Figure 3.6.7: Pressure Equal to Zero on the Leeward Side

Looking again at the pressure plot of the bulkhead in these side wind conditions,

the high pressure area can clearly be seen to have an effect on overall flow through the cab-trailer gap region.

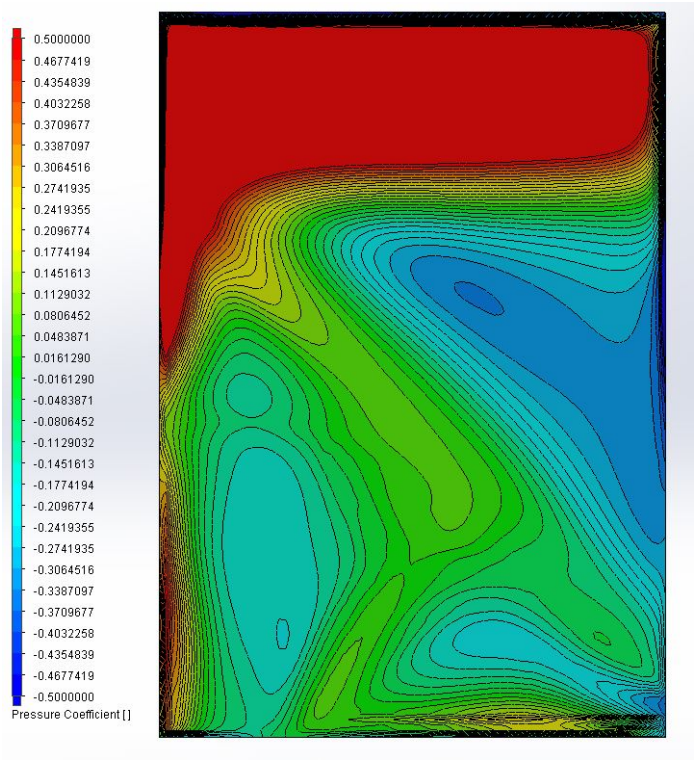

Figure 3.6.8: Pressure on the double deck bulkhead in side wind conditions

3.6.2 Bulkhead Deflector

In order to reduce the drag incurred on the exposed bulkhead, if the height is to remain at 4880mm, either the cab needs to accommodate this height, or changes to the bulkhead profile of the trailer need to be made. One such method of altering this profile is with a deflector applied to the region of exposed free-stream flow. The geometry tested as seen from the front and side in this case is found in 3.6.9.

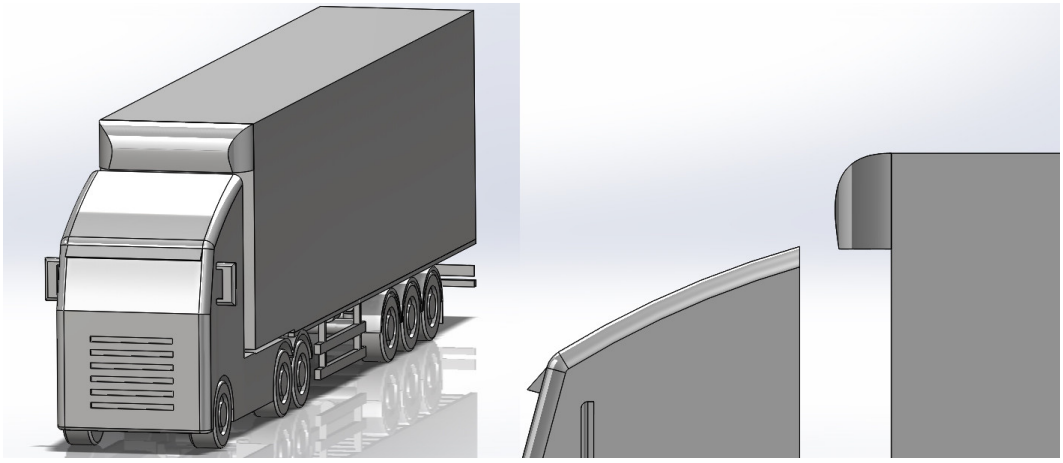

Figure 3.6.9: Double Deck Bulkhead Deflector

This type of geometry would typically be manufactured by either vacuum-forming or GRP modelling, and be used in the circumstances of this case, where a bulkhead is likely to be exposed in this manner. The purpose is to prevent flow separation and remove the bluff fronting of the bulkhead. Table 3.17 shows the drag reduction compared to the bluff-fronted 4800mm double deck geometry.

Table 3.17: Double Deck Deflector Cd Reduction

Test Case	**ΔCdDD(%) 0° yaw**	**ΔCdDD(%) 10° yaw**
4880mm Trailer with Deflector	-19.91	-7.98

This shows that the relatively simple geometry has a large impact on the overall drag of the vehicle, and successfully mitigates the high drag incurred by the blunt face to a good degree. Once more though, the influence of the upper and rear areas of the geometry are shown to be reduced in side-wind conditions as the reduction obtained by the deflector at 10° yaw is significantly affected, regardless, a good reduction is still evidenced.

Investigating the flow at 0° shows visual evidence of the drag reduction clearly. The central plot of velocity in X shows drastic differences in flow over the exposed bulkhead region.

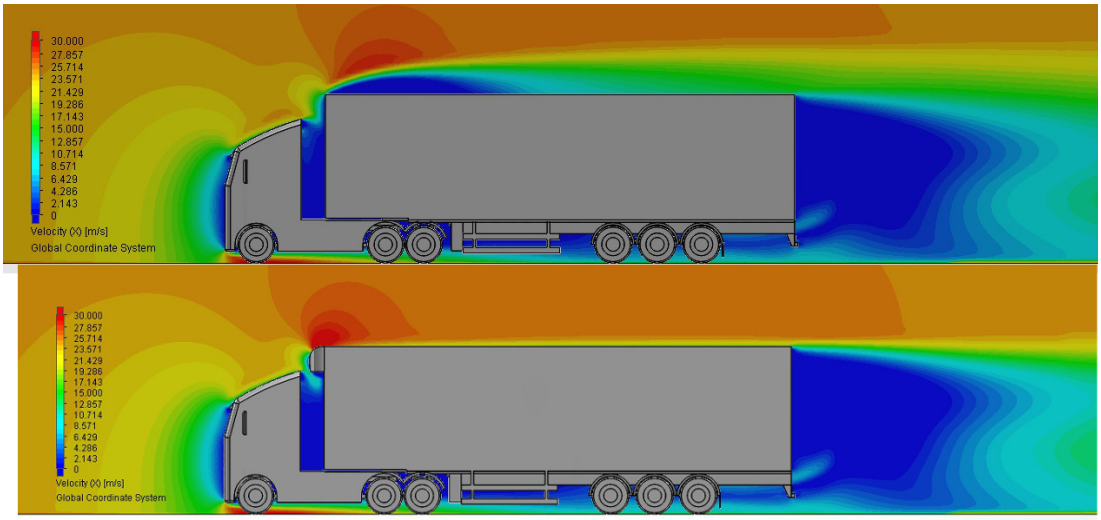

Figure 3.6.10: Central Plane Velocity in X

The huge separation caused by the blunt face of the unmodified bulkhead is removed and replaced with little to no separation that is evident along the roof line for the deflector case. Evident instead however is a degree of inefficient flow that enters the underside of the deflector geometry rather than being guided over it and on to the roof line as desired. This can be seen more clearly in figure 3.6.11 which shows the small area of pressure below the deflector, but also shows the pressure incurred on the deflector face itself. While the small pressure increase below the deflector is of very little magnitude, it does display the inefficiencies of this particular design, that could be improved by an increase in size to not only cover the 680mm discrepancy but also extend below this to prevent flow over the cab deflector from entering the cab-trailer gap below the deflector.

Figure 3.6.11: Central Plane Pressure Coefficient

The flow trajectories in contact with the faces also show evidence of this. As figure 3.6.12 shows both the 10° and 0° case trajectories over the deflector geometry. In both cases, while the majority of flow is directed over the roof line, a small amount is directed downwards into the gap, undesirably. Further, figure 3.6.13 shows that the negative pressure caused by the bluff bulkhead has largely been eliminated. There is a small degree of exchange wherein there are additional wake structures along the trailer side due to the bluff nature of the underside of the deflector, and flow being directed into this area, which then causes the partial vacuum regions. These could be removed if the deflector were larger, as stated.

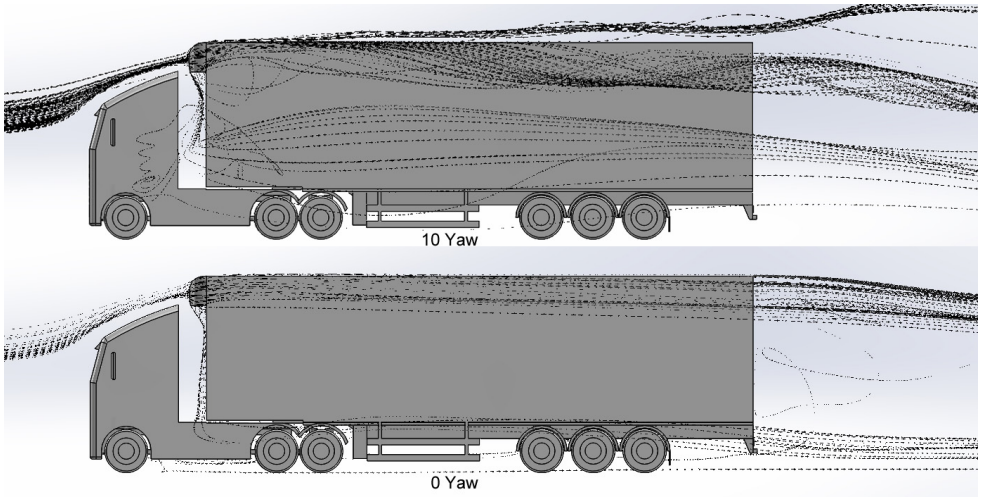

Figure 3.6.12: Flow Trajectories over the Deflector

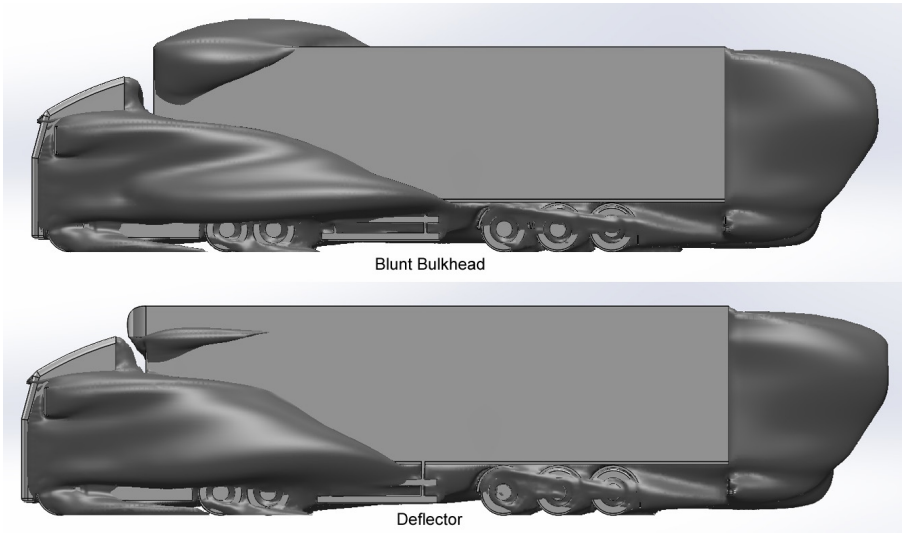

Figure 3.6.13: Pressure Equal to Zero Comparison

3.6.3 Sloping Front

A more integrated method of remedying the issue of the blunt bulkhead is to remove it altogether while still maintaining the ability to have increased internal and overall height for additional transportation capacity. This involves sloping the front section of the roof line to lower down to a height of 4200mm, matching the cab height. This provides the greatest drag reduction, and doesn't increase drag by an unacceptable level over that of the baseline 4200mm, single-deck trailer overall. However, this does remove some internal space, around 1/3 of the total upper deck, that is maintained with the deflector method.

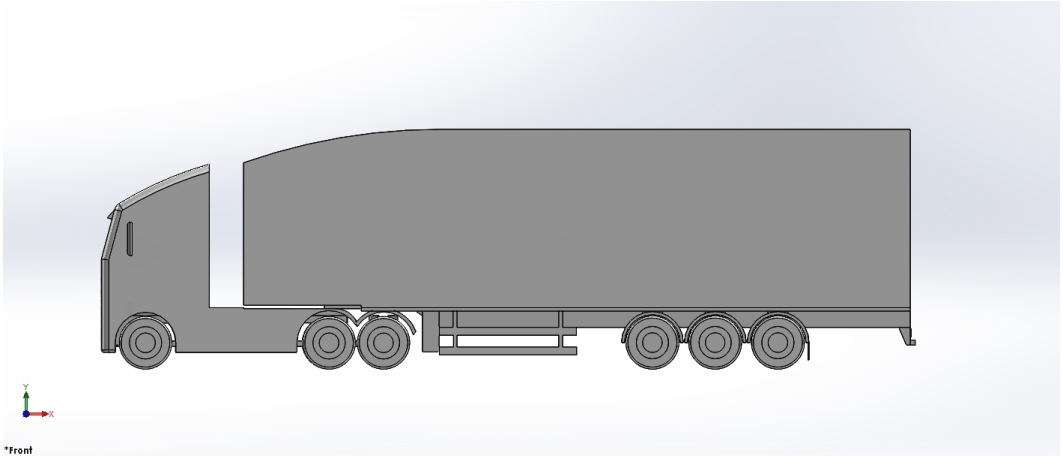

Figure 3.6.14: Double Deck Trailer with Sloping Front

Table 3.18 shows the drag reduction obtained with the sloping front geometry over that of the standard 4880mm double deck.

Table 3.18: Double Deck Sloping Front Cd Reduction

Test Case	**ΔCdDD(%) 0° yaw**	**ΔCdDD(%) 10° yaw**
4880mm Trailer with Sloping Front	-28.08	-11.73

An excellent reduction over the untreated double deck is achieved, and the drag increase over the 4200mm baseline, as seen in table 3.19 is not excessive either, especially in side-wind conditions, which is surprising given the additional surface area exposed by the additional height, despite the sloping front section.

Table 3.19: Double Deck Sloping Front Cd

Test Case	**ΔCdBase(%) 0° yaw**	**ΔCdBase(%) 10° yaw**
4880mm Trailer with Sloping Front	+7.73	+2.91

The flow characteristics over the geometry appear similar to that of the fully-curved roof line previously discussed, due to the similarities between the front roof line sections and the transition of flow from the cab to the trailer with reduced recirculation regions as a result.

Figure 3.6.15: Sloping Front Velocity in X

Due to the correctly matched bulkhead, other aspects of the flow are highly similar to that of the 4200mm baseline case. There are no unexpected areas of

differentiation in flow through the under body region, and studying the pressure plots and zero pressure boundaries show a similar wake structure, albeit larger, accounting for the increase in drag that is evident from the baseline case.

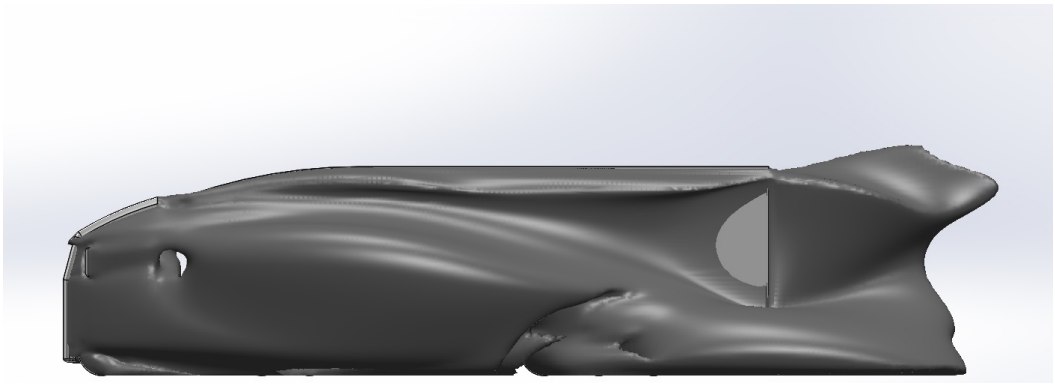

Figure 3.6.16: Zero Pressure at 10° yaw

The sloping front shows that it is possible to achieve a greater internal capacity while only incurring a small amount of additional drag in the process. A final comparison of the double deck geometries studies the drag difference in the cab-trailer gap region, including the entirety of the bulkhead faces to that of the unmodified and fully exposed bulkhead.

Table 3.20: Double Deck Bulkhead Fx comparison

Test Case	**ΔBulkFx**(%) **0° yaw**	**ΔBulkFx**(%) **10° yaw**
4880mm Trailer with Deflector	-83.34	-54.33
4880mm Trailer with Sloping Front	-90.74	-55.39

This shows in starker terms the degree to which both geometry modifications improve the drag caused by the exposure of the bulkhead. It is also interesting to note the difference in drag values for the rear face of each double deck geometry:

Table 3.21: Double Deck Rear Face Fx comparison

Test Case	**ΔRearFx(%) 0° yaw**	**ΔRearFx(%) 10° yaw**
4880mm Trailer with Deflector	+10.34	+2.05
4880mm Trailer with Sloping Front	+16.35	-5.52

In all cases with the exception of the 10° yaw sloping front case, the drag is greater on the rear face than for the unmodified double deck case. This provides evidence for the rear incurring greater drag if the flow upstream is less disturbed, and therefore retains more energy at the point of detachment at the rear, as was also seen in the previously studied case of the gap treatment of the 4200mm baseline model, which showed increased rear face drag as a result of higher energy retention of the flow.

3.7 Optimum Combinations

After assessing the capabilities and characteristics of the prior geometries and their various application points on the trailer geometry, two final geometries are studied. These incorporate the best performing option from each area of improvement to test their combined potential for drag reduction.

The first case incorporates every top performing geometry characteristic, this is the Optimised Complete case and incorporates the following:

- Rear-curve roof line
- 12° boat-tail
- Full skirts with under-plating
- Cab-trailer gap treatment
- Rounded Edges

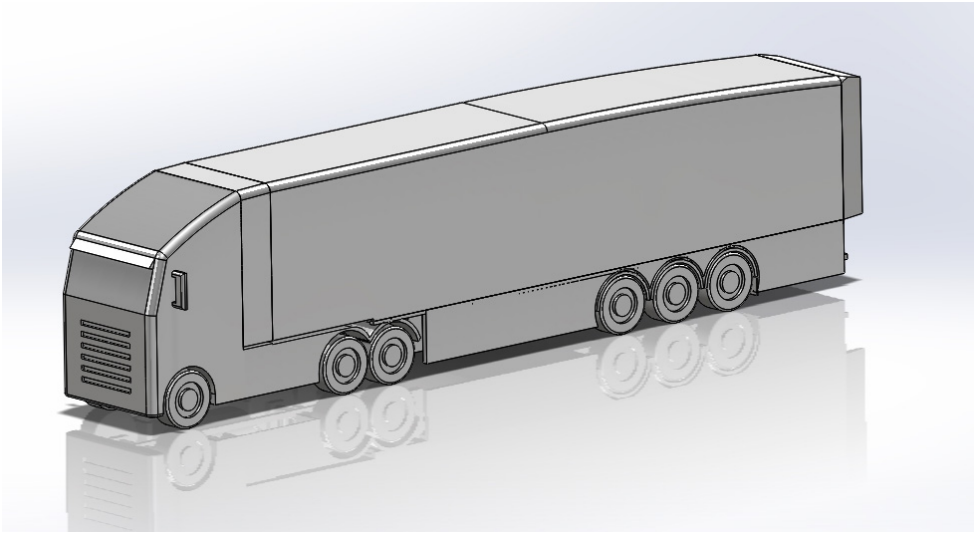

Figure 3.7.1: Optimised Complete Geometry

A second optimum case is also studied. This is the Optimum Limited case, and removes some of the features that are in place on the Optimum Complete case.

The reason for this is that certain elements such as the full cab-trailer gap treatment and skirt under-plating, despite being highly effective, are unlikely to be realistically implemented on a full-scale trailer in operation. While not impossible, the cab-trailer gap treatment firstly must accommodate the articulation nature of the geometry, and also the coupling mechanism between the cab and trailer would require modification as it currently relies on complete access in the gap. The under-plating method, while also not impossible is unlikely to be adopted by an operator without careful design due to issues regarding maintenance access to the under body area. While these options can be implemented, only testing an optimum configuration that incorporates them is not realistic. Furthermore, neither case incorporates covered wheels due to an open resistance in the UK market to this option based on long standing maintenance and safety issues that arise from this design.

The Optimum Limited case includes the following features:

- Rear-curve roof line
- 12° boat-tail
- Full skirts
- Rounded Edges

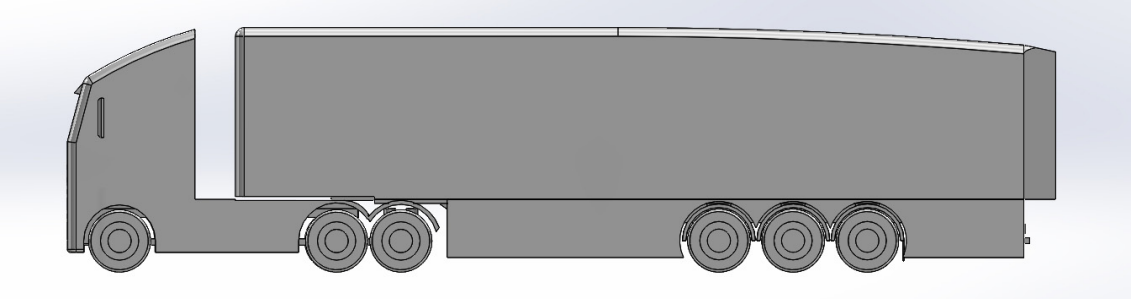

Figure 3.7.2: Optimised Limited Geometry

Table 3.22 shows the overall drag reduction obtained with both optimum designs.

Table 3.22: Optimised Cases Cd

Test Case	**ΔCdBase(%) 0° yaw**	**ΔCdBase(%) 10° yaw**
Optimised Complete	-16.52	-26.12
Optimised Limited	-12.66	-16.48

Both cases show excellent drag reduction capability overall. However the Optimum Complete case shows exceptional capabilities over that of the Limited case at 10° yaw, highlighting the potential of the gap treatment and under-plating methods. These results also show that the drag reduction benefits that each design feature has shown are not cumulative when combined.

3.7.1 Optimum Complete 0° yaw

This geometry shows the largest drag reduction of any geometry tested, as expected due to the combination of the highest performing design elements.

Figure 3.7.3: Optimised Complete Cental Plane Velocity in X

As expected, excellent attachment is shown over the trailer roof line at 0° yaw, as was displayed in the cab-trailer gap treatment test, it is due to this element once more that there is very little detachment along the roof line. This is extended along the curved rear section also and onto the angled boat-tail plate where the wake region is then compressed impressively into a very small area of low velocity. The

only negative impact along the roof line that is evident is due to the build up of the boundary layer, a natural consequence of refined attachment such as this.

The exceptionally small wake is a consequence of the combination of exceptional attachment along the rear curve of the roof line and the narrowing effects of the boat-tail.

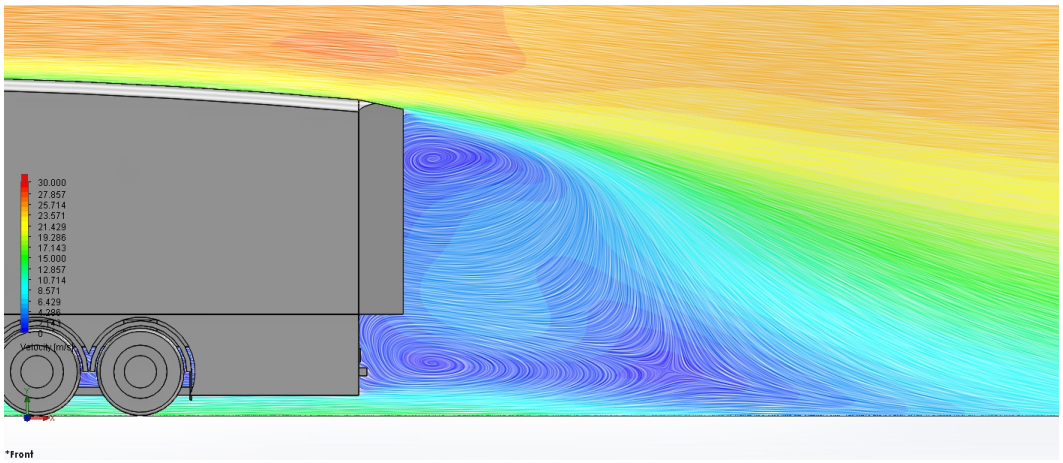

Figure 3.7.4: Optimised Complete Wake Streamlines

Looking more closely at the wake in the centre plane, and highlighting the streamlines reveals the two areas of counter-rotating flow that constitute the centre of the wake. The vortex originating from the roof line dominates the rear wake, compressing the lower vortex that emerges from the trailer under body and lowering the centre of recirculation. This is due to the high energy that is carried along the roof line and maintained due to the lack of detachment from the cab onwards, allowing for an impressively small rear wake region. Flow trajectories plotted from the rear curve highlight this impressive compression.

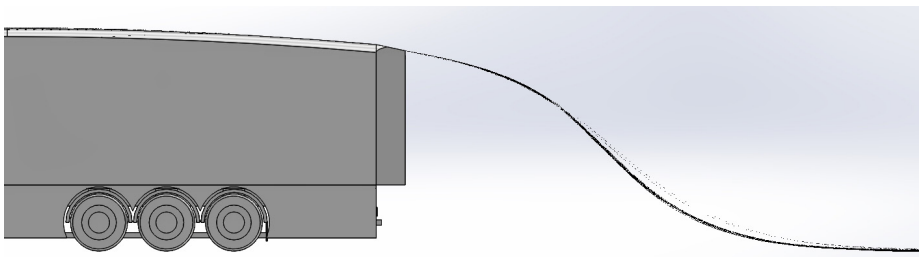

Figure 3.7.5: Optimised Complete Rear Curve Trajectories

Investigating the wake further, flow trajectories show that almost none of the flow that constitutes the counter-rotating vortices of the rear wake originates from the trailer sides or roof line. Due to the high discrepancy between the flow energy of the roof line, sides and under body, all the rear wake area is filled with flow that is sourced from the under body. Despite the under-plating, the flow velocity is still low enough for the partial vacuum to be filled with energy from this area alone.

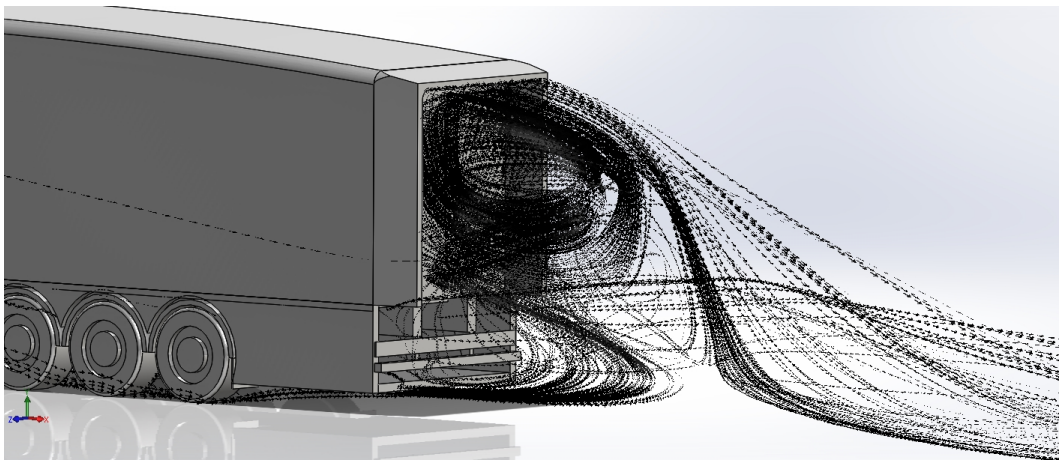

Figure 3.7.6: Optimised Complete Rear Face Trajectories

Flow trajectories of the boat-tail plate faces confirm this to be the case.

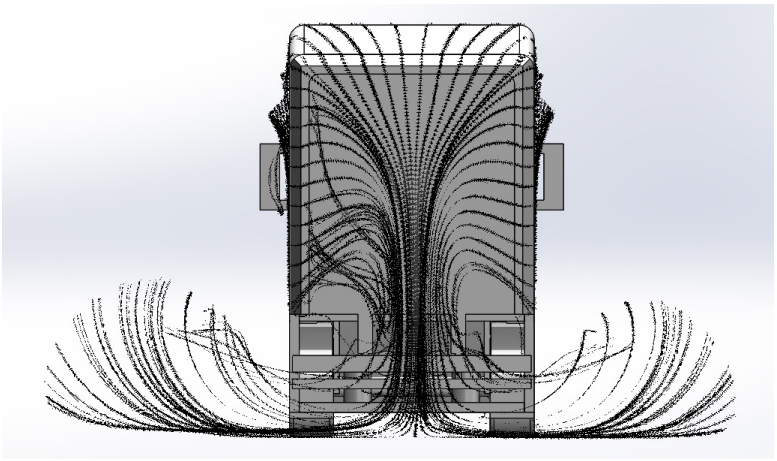

Figure 3.7.7: Optimised Complete Plate Face Trajectories

No flow that passes over the boat-tail plates is recirculated into the rear wake, as seen in figure 3.7.6, the wake is occupied by flow that originates from the trailer under body, the upper vortex created by the energy carried over the roof line.

Underneath the trailer, the flow conditions are as expected, with the under body plating preventing flow from interacting with complex areas of geometry around the wheel structures.

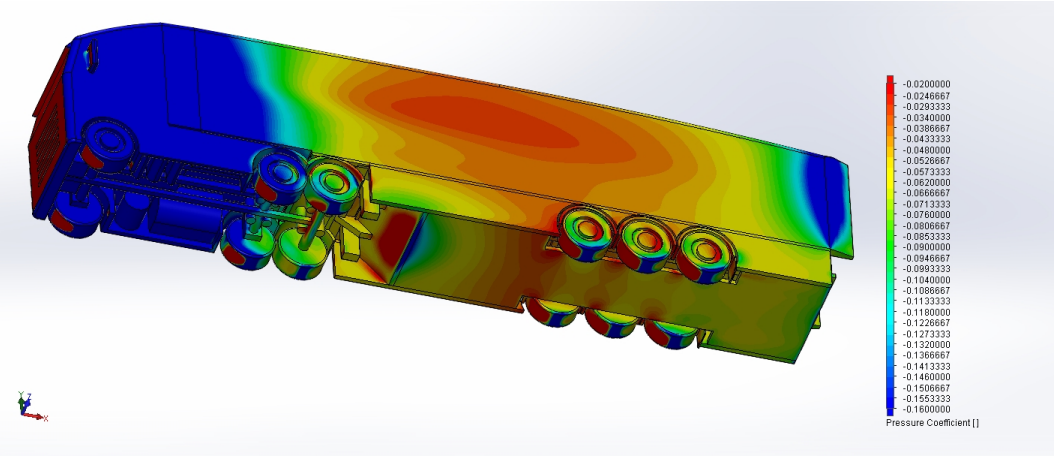

Figure 3.7.8: Optimised Complete Under Body Cp

The forward angled face is seen to be unoptimised, with an area of higher pressure followed by a small area of lower pressure, indicating a degree of detachment may be evident here. Besides this, flow on the under body is as expected. Once more the degree of detachment aft of the cab shows the limitations of modifying the trailer design while so much force is being imparted and energy lost in this area.

3.7.2 Optimum Complete 10° yaw

At 10° the drag reduction is the highest seen for any geometry in this study. This is to be expected due to the relative drag improvements seen in side-winds that elements such as the gap treatment and side-skirts exhibited. It is highly probable that the drag reduction would have been amplified further should the wheel covering geometry also be incorporated into the optimum designs, however as explained this element would be unlikely to find a place in operation in the UK.

Visualising the zero pressure boundaries shows the expected wake regions on the leeward side, however they appear much more controlled, with less turbulence at their core due to the inclusion of the gap treatment and side-skirts. Reducing the

leeward side wake further is very difficult due to the dimensional and shape requirements of the trailer itself.

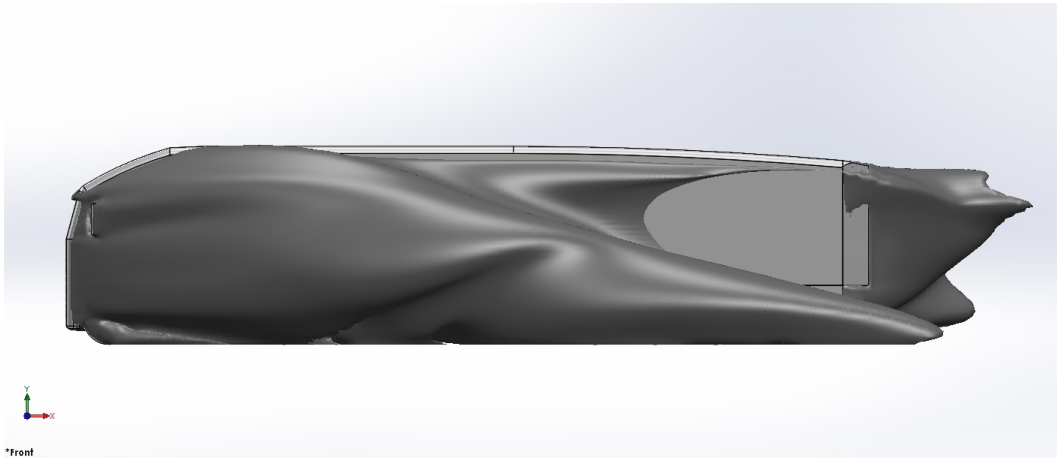

Figure 3.7.9: Optimised Complete Zero Pressure Boundaries

The reduced upper portion of the rear wake shows that once again the rounded edges are limiting the flow detachment over the windward roof line edge and the resultant trailing vortices. Though they do still form aft of the boat-tail as seen in figure 3.7.10 due to the angled flow itself.

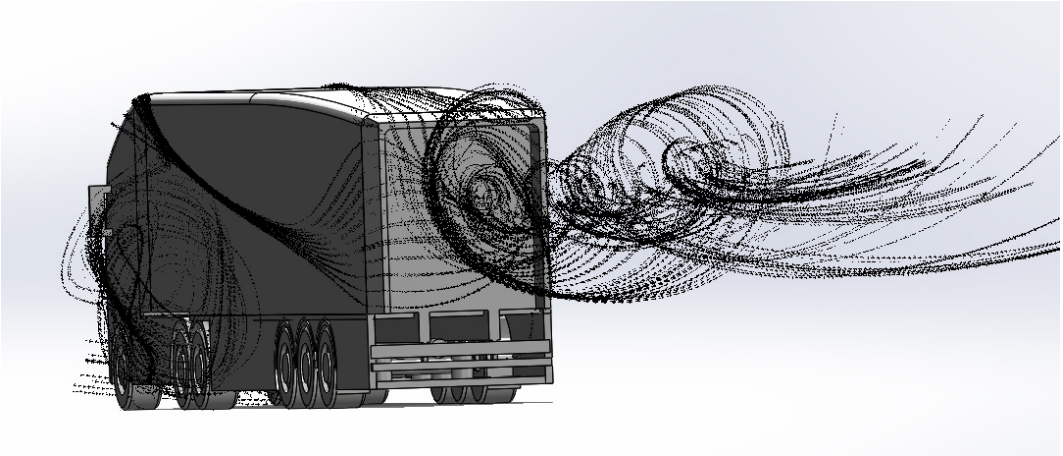

Figure 3.7.10: Optimised Complete Boat-Tail Trajectories

Flow through the under body region displays the same velocity increase as the standard under body plated case did, providing good maintenance of energy. While the plating does limit much of the interactions with complex geometry around the wheel structures, it also introduces interactions of its own that are not desirable.

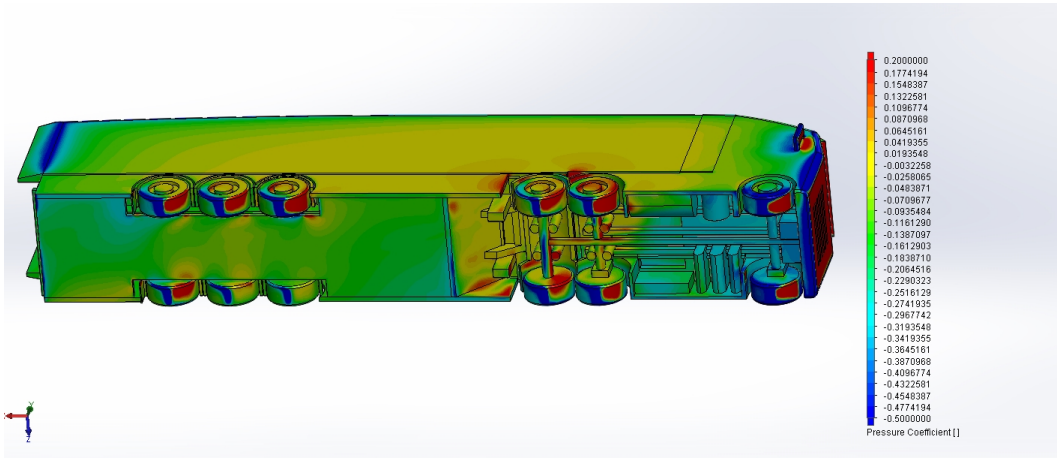

Figure 3.7.11: Optimised Complete under Body Cp

Figure 3.7.11 shows that where flow velocity is maintained due to the plating, there is direct contact with the rear leeward wheel as a result. Though this is largely reduced from the baseline case, it is not a perfect solution. Additionally, the angled geometry sealing entry to the inner area of the plated section behind the landing legs shows high pressure on its inside face that is exposed to the flow. This could be rectified with a less angular design approach to this section. Despite these small issues, as shown the under body plating shows good improvement to flow characteristics,a nd combines well with the other features.

3.7.3 Optimum Limited 0° yaw

The limited geometry removes the gap treatment and under-plating to represent a geometry more palatable with increased likelihood of being manufactured and used in operational conditions, with less issues that could negatively affect its adoption in industry.

The geometry represents a good reduction in overall drag at both 0° and 10° conditions, however the 10° case suffers from the removal of the gap treatment and under-plating quite heavily.

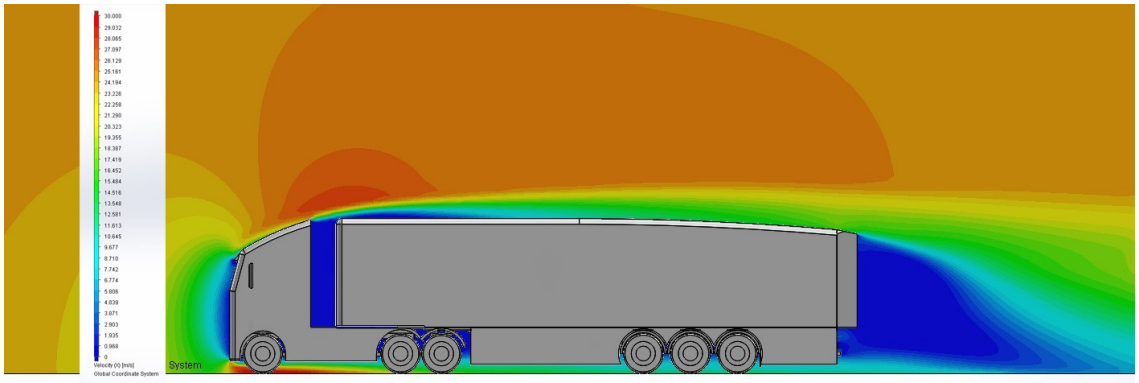

Figure 3.7.12: Optimised Limited Centre Velocity X

As expected, without the gap treatment, the detachment and recirculation is once again evident aft of the bulkhead as the flow detaches and attempts to reattach to the trailer roof line. This results in reduced velocity along the entire length of the roof. Despite this, the wake structure appears almost identical to that of the complete case, with the excellent compression of the rear wake still evident. Though the overall reduction in drag continues beyond the partial vacuum as a consequence of the detachment aft of the cab-trailer gap.

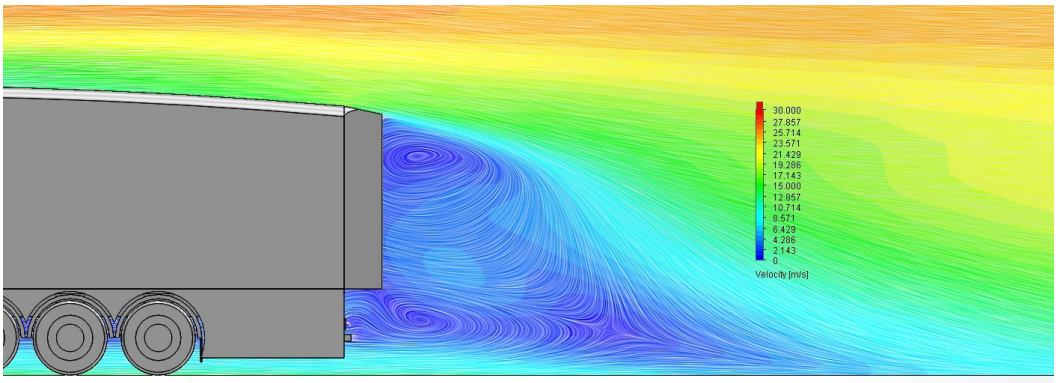

Figure 3.7.13: Optimised Limited Centre Wake Streamlines

The streamline representation of the wake appears similar to that of the complete case, and once again shows the partial vacuum being occupied by flow sourced from the trailer under body. This is no surprise as if there were to be a differentiator in this regard it is likely to be from the complete geometry due to the higher energy maintained by the under-plating.

Plotting streamlines of the surface flow onto the geometry allows identification of the detachment area aft of the cab-trailer gap.

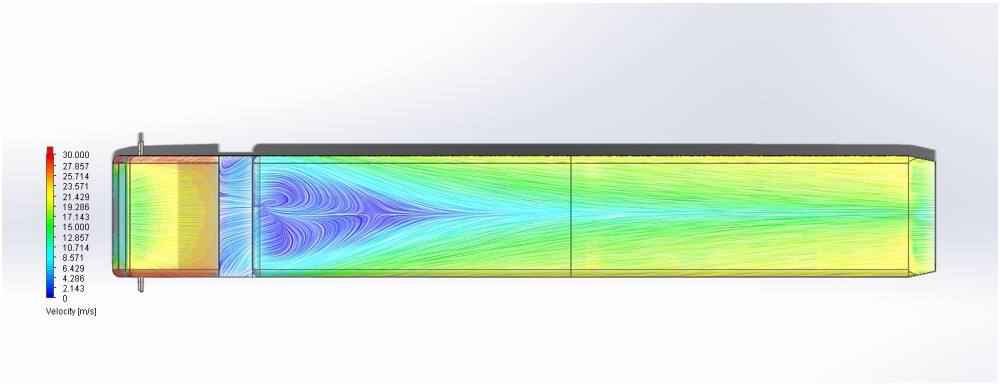

Figure 3.7.14: Optimised Limited Surface Streamlines

It shows clearly the detachment and resultant recirculation, previously displayed as a zero pressure boundary in this area. This is the main benefit of gap treatment at 0° yaw, the rectification of this loss of energy, which is then carried along the roof line and beyond the rear wake without being lost.

Flow through the under body region is as expected, as there is a high degree of detachment and resultant turbulence beyond the cab geometry, the skirt elements at 0° yaw have shown little variation and drag reduction characteristics. The Optimum Limited geometry is no exception to this as the same flow here is evident as with prior skirt geometries.

3.7.4 Optimum Limited 10° yaw

The discrepancy between the limited and complete geometry here is significant, with the complete geometry reducing drag by a further 10% over the baseline case than the limited geometry does. As shown in isolation, and confirmed here, this is likely to be as a consequence of the excellent side-wind performance of the gap-treatment geometry.

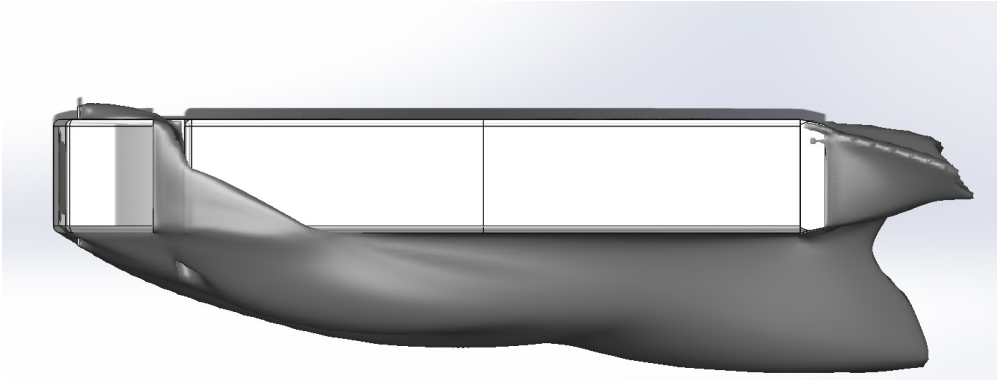

Figure 3.7.15: Optimised Limited 10° Zero Pressure

The enlarged leeward wake, once again extending into the rear wake shows evidence of the influence of the gap-treatment anf the under-plating. The high pressure puncture hole through the zero pressure boundaries is once again visible, as it has been in all geometry without the gap treatment, and the extension of the leeward wake is a consequence of the under-plating no longer in place.

There is largely nothing further of note to identify regarding the limited case in isolation, and would be better served in direct comparison with the complete case due to the previously identified flow characteristics of the individual elements corroborating here.

3.7.5 Complete and Limited Case Comparison

It has been noted that for both cases the wake is excellently compressed due to the combination of rear-curved roof line and the boat-tail. Studying the characteristics of the two side-by-side shows the smaller differences between the two geometries.

Looking firstly at the pressure distribution on the rear face of each case, both show small variation in the centre point of recirculation, with the complete case showing a lower centre than that of the limited case. This is likely due to the greater energy carried over the roof line edge of the complete case due to reduced separation over the cab-trailer gap region.

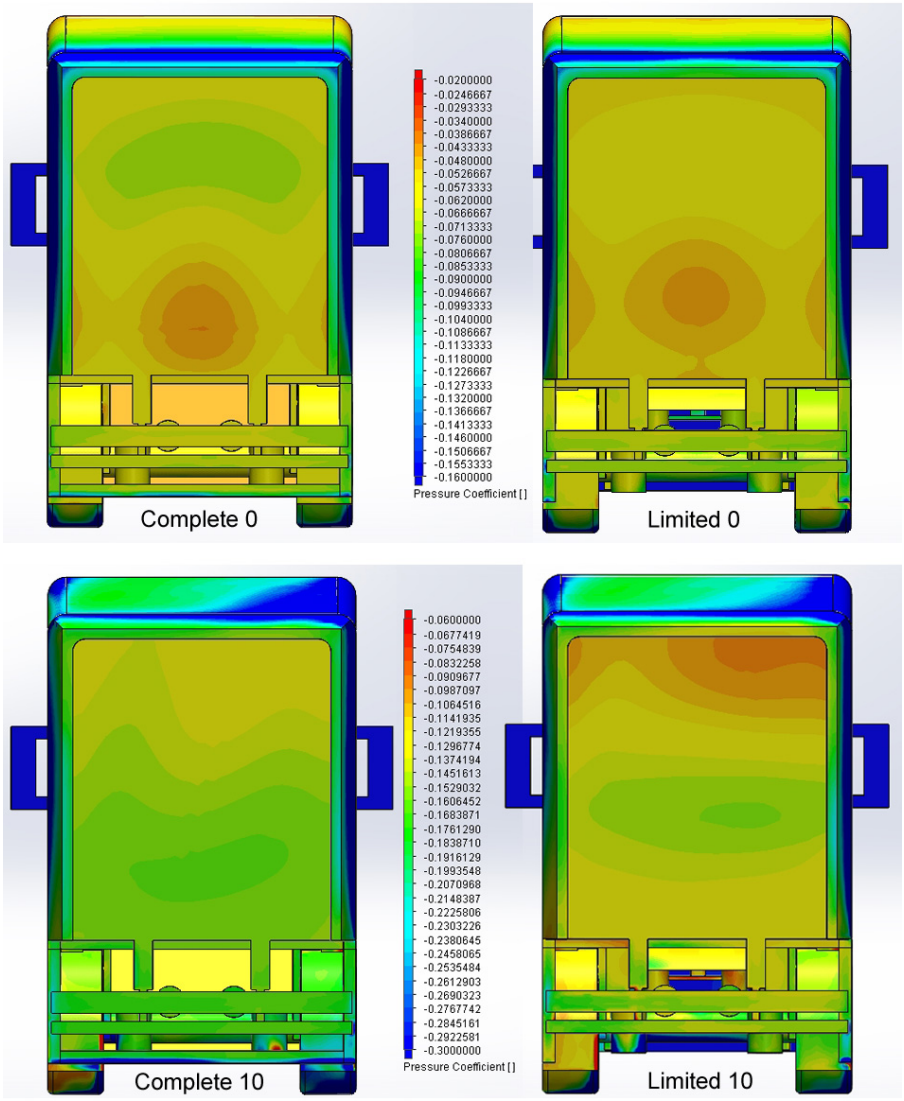

Figure 3.7.16: Optimised Rear Pressure Distribution

In addition to the variance in the central pressure point, pressure on the rear face overall is higher for the limited cases in both 0° and 10° yaw. This again is likely due to the additional energy that is carried over the point of detachment from the trailer. In this case for both the roof line and the under body region, as the under-plating of the complete case carries more energy through the under body due to higher velocity and reduced geometry interaction.

Investigating the impact of this pressure variation, table 3.23 shows the reduction in force on the rear face for both optimum cases against that of the baseline case.

Table 3.23: Optimum Rear Face Fx comparison

Test Case	**ΔRearFx(%) 0° yaw**	**ΔRearFx(%) 10° yaw**
Optimum Complete	-55.36	-40.73
Optimum Limited	-59.44	-47.96

In both cases, the additional pressure over the rear faces is shown to result in a greater reduction in Fx on the rear face compared to the baseline case for the limited case. Despite this, the benefits gained by the under-plating and gap treatment for the complete case outweigh the negative impact on the rear face.

The velocity and pressure coefficient beyond the trailer also corroborate the increased energy carried along the complete case. With the complete case exhibiting higher velocity properties beyond the wake, and peaking at a higher pressure four metres into the wake.

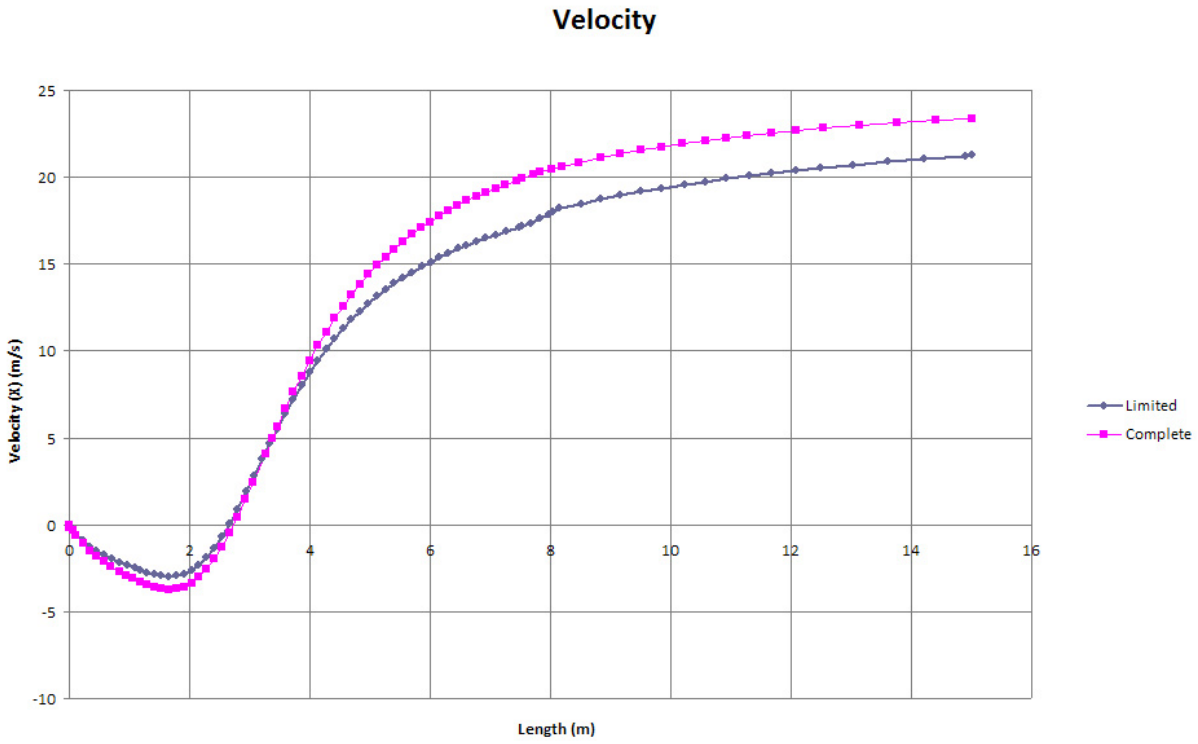

Figure 3.7.17: Velocity Plot at the Trailer Rear

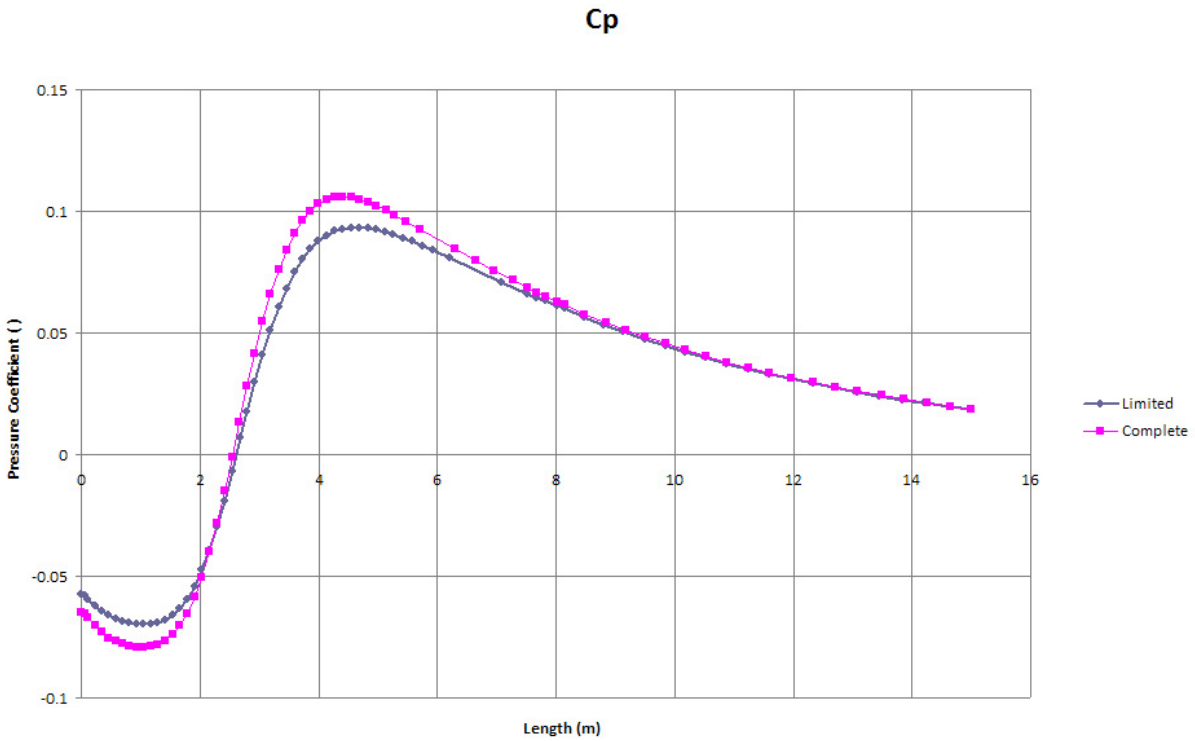

Figure 3.7.18: Cp Plot at the Trailer Rear

Another area of striking pressure difference is the windward edge and the effect of the gap-treatment on pressure along the entire length of the trailer. It can be seen in figure 3.7.19 that the limited case exhibits a much higher pressure along the side face of the trailer. In the complete case this is significantly different due to the additional flow allowed to continue along the trailer side because of the blocked gap entry point. This smooths flow overall down the edge, even affecting pressure along the roof line.

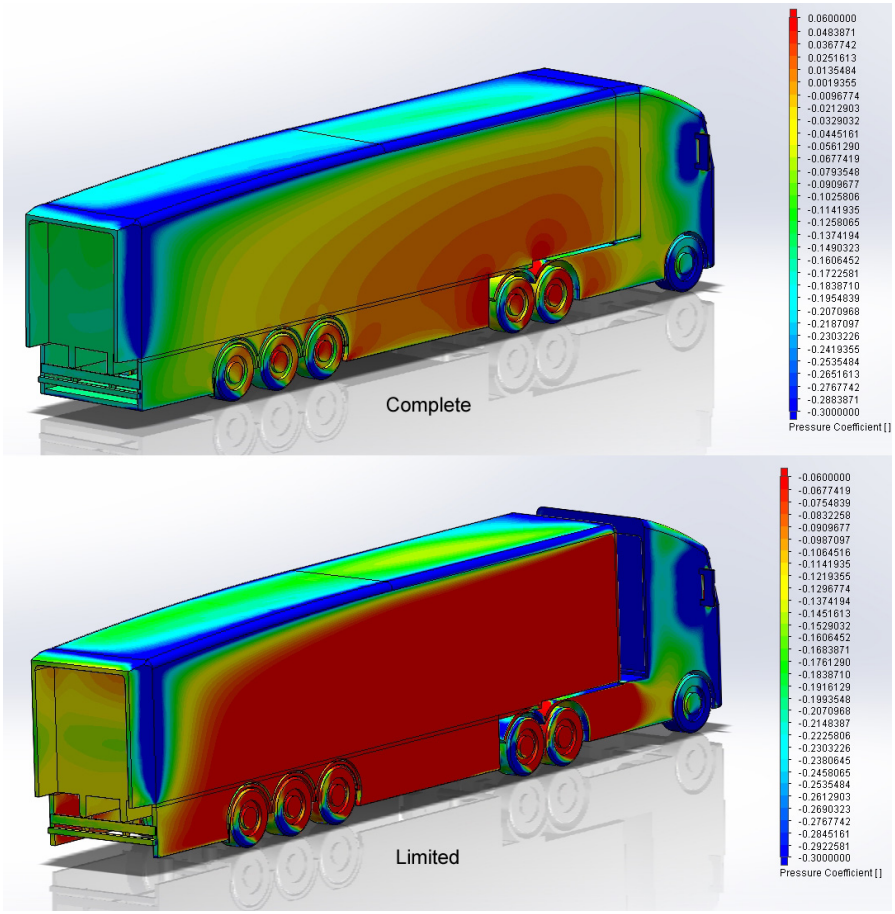

Figure 3.7.19: Cp Plot at the Windward Side

Looking at the leeward side, and how flow inside the wake is influenced by the gap-treatment and under-plating is shown by surface streamline representation.

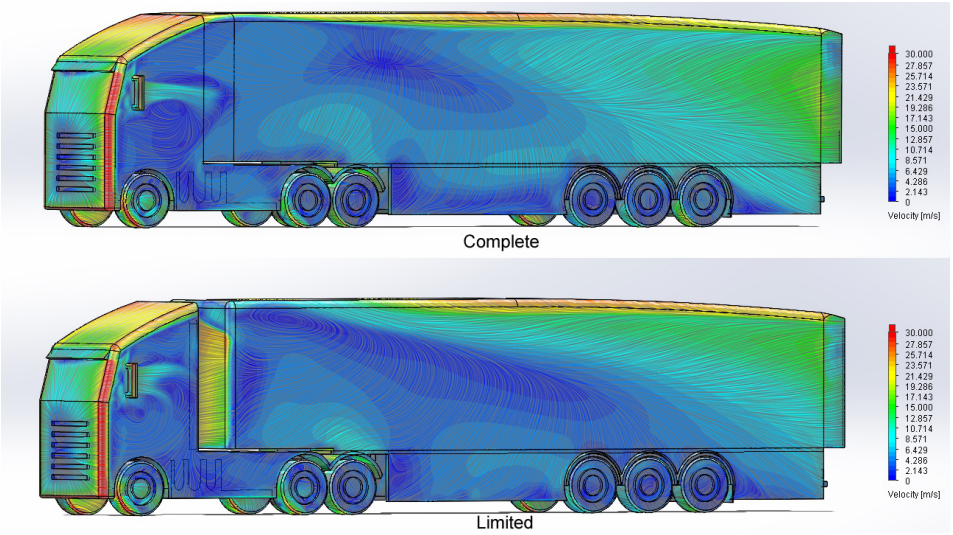

Figure 3.7.20: Cp Plot at the Leeward Side

The streamlines for the limited case show the chaotic influence that flow through the cab-trailer gap has on the leeward side flow. A central point of circulation can be seen high on the side face just beyond the bulkhead, whereas the complete case has a recirculation area much further along the side than this, and displays much less variance in velocity.

Contour plots show the differences in wake structure at 0° yaw between the two optimised designs, highlighting the increased compression of the Limited configuration.

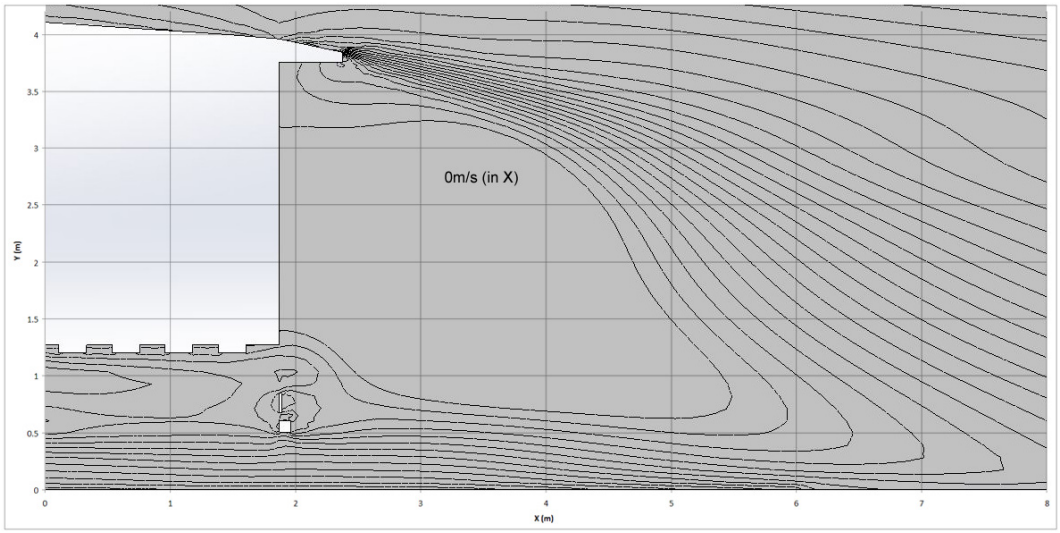

Figure 3.7.21: Plot of velocity in X showing the region of reverse flow in the Limited wake.

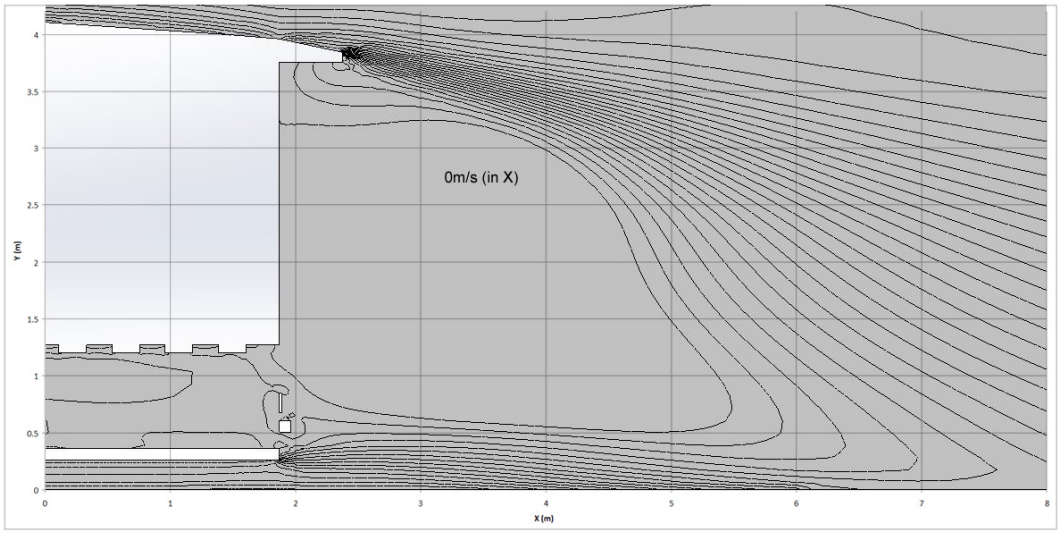

Figure 3.7.22: Plot of velocity in X showing the region of reverse flow in the Complete wake.

It cannot be avoided for these cases, despite the good reductions in both cases, that the gap-treatment in particular is responsible for exceptional drag reduction. Despite the difficulties in implementation, developing a method to incorporate this in a manufacturable trailer would be highly beneficial.

Chapter 4

Summary and Discussion

Twenty cases have been considered overall. Eighteen of these were defined initially, with a further two defined based on the best performing options as analysed from the initial eighteen. The first of these cases exists as the baseline case against which all others were built and compared against, in order to establish the relative differences in the resultant flow characteristics, and overall force values of the geometry.

The baseline case was designed to represent an average trailer that operates in the UK, and has a height beyond 4 metres to represent the UK sector specifically over that of a generalised European design, which would require a height of 4 metres or less. Through analysis of this case it was confirmed that much of the prior work that helped define contributory regions of drag and the fundamental methods of mitigating these effects are correct in their basis, and there are many correlating points between those of North-American articulated combinations and European/UK combinations. Base-drag, the cab-trailer gap and the under body all contribute to the overall aerodynamic performance of the geometry and can be improved with boat-tail methodology, gap treatment and skirts / under body design. The simulations conducted provide a basis for estimated improvements of each of the major areas of geometry modification on a UK-centric truck and trailer combination.

Beyond the testing of known methods, exploratory testing was undertaken to establish the impact of increased height in order to accommodate a second internal deck, as is possible within the UK due to a lack of legislation governing overall height of vehicles. This revealed both the extent to which this impacted the overall force imparted on the geometry if it was not correctly managed, but also the extent to which the effects of this can be reduced if steps are taken to manage the internal capacity increase while being mindful of the potential impact on overall drag and as a result the fuel consumption.

4.1 Observations

All of the geometry modifications exhibited drag reduction to some degree, illustrating the great potential there is for a wide breadth of improvements, from the very small to the very large. While large scale improvements will always be the most desired outcome, having the ability to incorporate small scale changes is important to both manufacturers and operators. It allows both to compromise on the additional cost, and enables small-scale testing without much financial consequence to be a possibility for operators with a desire to test the effectiveness of improved aerodynamics without a large commitment.

Roof line modification is one area that is specific to UK HGV trailer manufacturing, with a number of manufacturers incorporating curved or angled roof lines into designs. Testing on the full-curve and rear-curve only designs showed that while incorporating a full-sloping roof line did yield benefits through flow improvements over the trailer bulkhead, encouraging greater attachment over the length of the roof line, ultimately the design incorporating only a slope at the rear produced a greater drag reduction. This was not the only caveat of the fully curved roof line, as due to the increased height needed to facilitate the curvature, greater force was applied to the side faces in the side-wind testing over that of the baseline model. The consequence of the rear-curvature only however is that it results in a 300mm lower internal-aperture height at the rear, which both positively affects its aerodynamic performance and may negatively affect its operational capability. While it was not tested in this manner however, this can be rectified with the use of an angled chassis, a common attribute of some trailer designs in order to gain internal capacity.

Base-drag is identified in literature as one of the largest contributory areas of drag on the geometry, and this was seen to be the case on the baseline model when boat-tail geometry was introduced. Regardless of the plate angle, from 10° to 16° these modifications yielded the greatest drag reduction figures for a singular mod-

ification at 0° yaw. While their effectiveness did wane at 10° yaw, all plate angles displayed excellent drag reduction capabilities in both tested flow regimes. Out of the angles tested, the 12° plates showed the best reduction over both flows, with a 9.65% and 6.39% reduction respectively, however the 14° plates outperformed it at 10° yaw slightly. This correlates with the work done by Browand and Radovich (2005), where an angle of 13° was found to be optimum for boat-tail plates. The 14° angle was used to test the top and side plates separately to reveal their performance in isolation. Unlike typical combination testing where the drag reduction characteristics of individual devices combined provide diminishing returns, the top and side plates indicated good agreement to the overall drag of the complete 14° boat-tail geometry. From this it can be assumed that the contribution of drag reduction can be attributed as approximately 5/8 side plates and 3/8 top plate. This suggests that the top plate performs greater than its position as only 1/3 of the overall geometry, and greater still as the side plate geometry is greater in length than that of the top-plate. This indicates the relative importance of the treatment of roof line flow with regards base-drag and the rear wake, implying that treatment of flow detaching from the roof line has a greater affect on overall drag than that of the sides. The reason for this is likely to be that the flow along the side-structure shaped by the side-plates has a greater interaction with flows of lower velocity and areas of turbulence, such as flow exiting the under body that is shown to occupy the wake, as a result the side-plates produce less of an effect on the rear wake structure due to opposing forces being of a greater influence.

Under body testing using side-skirts showed opposing improvements to that of the roof line and base-drag improvements in that modifications in this area resulted in greater reduction potential during side-winds than at 0° yaw. This highlights the opposing characteristics of the flow structure around the geometries in the two flow conditions, showing very simply that the under body region is much less a contributor at 0° yaw than in side-wind conditions. It does not suggest that areas such as base drag is less of an influence in side-wind conditions, just that the contributory

amount has shifted due to a much greater influence offered by areas such as the under body.

In all three under body tests at 0° yaw the drag reduction was surprisingly small, varying from 1.72% to 1.93%. Given that the differences between each of these three geometries was significant, this suggests that the flow field at 0° is stagnated greatly with very low velocity in the area. This is seen to be as a result of flow around the cab, where the degree of detachment and recirculation is great and produces a wake region that extends throughout the trailer under body. As a result of this, there is a small overall drag contribution from the under-body at 0° yaw, meaning that geometry modifications will produce only a small improvement. With another cab geometry this may be greatly altered, however in this case the influence of the under body at 0° is seen to be very small. At 10° however the contribution of under body modification is seen to increase greatly, offering reductions of nearly 8% with full under body treatment, and lesser skirt geometry offering 4%. Covering of the wheels presents a middle-ground between basic skirt geometry and the full under body treatment, providing a 6% reduction and suggesting that the under body plating geometry could be improved further with the inclusion of a section that covers the wheels also. While the reduction capability at 0° is dampened significantly, skirting and under body treatment do show good drag reduction capability due to the reality of operation, where some degree of side-wind condition is likely to always be present when on the road.

Three test geometries were studied that were deemed to be 'standalone' due to the lack of other comparative geometries that addressed similar issues/areas of drag in this study. The gap treatment case sought to improve the flow field in the cab-trailer gap through its exclusion with additional geometry that joined the rear of the cab with the trailer bulkhead. This area was identified during analysis of the baseline case where it was seen that 0° yaw counter-rotating vortices occupied this region, and at 10° yaw there was high levels of chaotic, turbulent flow entering the

gap due to the angle, which then affected the leeward side wake along the length of the trailer due to turbulent flow entering the area, as was evidenced by the high pressure hole punched through the zero pressure boundary representations of the baseline case. The reduction to overall drag this geometry contributed was unexpectedly large, and was the single highest reduction for any single modification at 10° yaw, providing a reduction of over 10%. Additionally, a good reduction at 0° was also observed of over 3.5% reduction. In this study, the distance between the rearmost point of the cab deflector and the trailer bulkhead is 700mm, it is not uncommon for this to be 1000mm, and it is assumed from prior literature that greater gap distances generate greater drag, meaning that treatment of this area could produce even further reductions given the varied geometry combinations that are in operation.

The second 'standalone' case is that of the baseline case with the addition of rounded edges along the bulkhead, roof line and rear face. The sharp edges on the baseline model were in place to help better represent the geometry of curtain sided trailers due to the limitations of the required structures for securing and moving the curtain material. By rounding the edges as is the case for some box van trailers, an indication can be given as to the benefits of this. The drag reduction overall was seen to be large, offering over 6% and 4% in 0° and 10° yaw tests respectively. This is larger than expected, and indicates the impact that rounded edges can have, highlighting a negative area of curtain-sided design, which could encourage a renewed approach to incorporating the curtain slider mechanisms without the bluff edging as is typically used. An issue that may have provided this case with such good reduction values is that of the rounded rear-face edges. It is rare for these faces to be rounded due to the likelihood of damage occurring here, and that this area is usually manufactured in a standard manner which does not include a rounding of the edges, regardless of whether it is a box van or curtain-sided trailer. It would be useful to run this test once again, excluding the rounding of the rear face, in order to associate the contribution this unlikely inclusion provides to the overall reduction noted in this

case.

The final 'standalone' case does not study the effects of a potential improvement to overall drag of the baseline case, but instead studies the potential negative effects of a likely mismatching of cab and trailer that can often take place in UK operations due to the wide range of trailer heights available. This case studies the effects of a cab deflector matched 200mm below that of the bulkhead height of the trailer, exposing a portion of the bluff bulkhead directly to the flow. This case provided one of the most surprising and interesting results of the study. It was expected that there would be a drag increase, to what extent was unknown, but a drag decrease was not considered possible prior to running the case simulation. At 0° a drag increase was noted as expected, this was an increase of 3.65% and highlighted the importance of a correctly matched cab deflector. At 10° however, there was an overall reduction of 2.13%. Initially this result seemed as though it was likely to be erroneous, however upon studying the flow it was evident that the added pressure on the trailer bulkhead due to its additional exposure was influencing the turbulent flow through the cab-trailer gap. Analysing flow through this area gap showed that the added pressure on the bulkhead face forced flow entering the gap on the windward side downwards, and due to this guided influence the degree of turbulence inside the gap region was greatly reduced, instead, higher energy was carried though the gap and resulted in an overall reduction in the size of the leeward wake. This case highlights the inherent complexities and unpredictability of flow around geometries such as this. An introduction of additional form drag on the bulkhead face has an influencing effect on turbulent flow structures to the extent that its benefits outweigh its drawbacks, in this instance. This result should not be taken to assume that all misaligned cabs will perform better in side wind conditions, as the double deck cases show this is not the case. It does show the unpredictability of flow conditions, and that in this case, with this geometry, that a misaligned combination performs better in side-winds that a correctly aligned one.

A set of test cases was established as an expansion of the misaligned cab and to represent another set of circumstances that are specific to the UK industry but are also likely circumstances for a cab-trailer combination with likely consequences to overall drag. These tests concern the use of double-deck trailers, which involve a greater overall height to increase internal capacity. The standard double deck case expanded the 4200mm baseline case to give an overall height of 4880mm without modifying any other area of the geometry, this results in a heavily mismatched cab, a combination that is not unlikely given the UKs variety of trailer heights, meaning the chances of a cab mismatch are likely. The consequence of a mismatch to this degree is a drag increase of 50% at 0°, a large increase, though the effects of this are reduced in side-winds to only a 16% increase, once more attributed to the additional influence that the under body region gains at greater flow angles. The two modifications tested to mitigate this large drag increase without altering the cab geometry show that even with a simple modification, the consequences of higher overall height can be greatly reduced. A simple deflector is shown to improve drag by 20% and 8% in standard and yaw conditions respectively, while a roof line modification akin to that tested for the 4200mm baseline case improves the reduction further, to 28% and 12% over that of the unmodified double deck. These tests are perhaps the most stark in the study, with the degree to which they highlight the consequences of unmanaged height differentiation, and the relative ease with which it can be mitigated, raising the conclusion that there should be no mismatched double decks to this degree in operation when a simplistic bulkhead deflector can mitigate the height consequences to such effect.

Figure 4.1.1: Double Deck with Improper Cab

The optimised combinations showed excellent drag reduction capabilities over the baseline model, and represented the potential for these modifications should they be implemented together on a manufactured trailer. As described, two separate combination geometries were tested, as one defined a perfect combination of the modifications investigated in the study, and a further combination that removed particular elements that were unlikely to be able to be implemented on a manufactured trailer at this time.

The Optimised Complete case includes every item of the top performing modifications studied. The results of this combination was a drag reduction of 16.5% at 0°, and 26% at 10°. While this showed that the reductions from each modification in isolation are not additive when combined, it also showed the extent to which reductions are possible. The flow characteristics around this geometry exhibited the positive effects of each of the modifications included. The gap seal, under body modification, rounded edges, boat tail and rear-curving roof all contribute to an excellent maintenance of attachment and very small rear wake. As detailed regarding under body treatment, this test too did not include a wheel covering section due to the extent of the possibility of it being included on a trailer in the UK. If this were to be included, it is likely that the drag reduction could be improved further on this geometry.

The second combination test, the Optimised Limited case, removed the gap seal and under-plating evident on the Complete test case. The reasoning for this is the reduced plausibility of these elements being incorporated into a trailer in the UK that then works well in operational circumstances. The gap seal is very difficult to implement in reality because of implications regarding the vehicle articulation. The only way a method such as this would be possible is if a truck and trailer manufacturer worked in tandem to make this possible, even with this resolve issues such as control placement would be an issue for the manufacturing process. Similarly the under-plating geometry was removed because of maintenance issues regarding

the trailer and the additional work that would be required in order to access the axles, wheel structures or any other component on the trailer under body. This is in addition to elements such as the additional weight that would be incurred because of the plating structure and materials that would detract from the overall weight that could be carried as cargo, and also increase mechanical resistance, with a resultant negative effect on fuel efficiency. Despite the removal of these two large contributors to the overall drag reduction of the Complete case, the Limited combination still shows drag reduction of 12.5% and 16.5% at 0° and 10° yaw respectively.

4.2 Plausibility of Incorporation

The removal of geometry from the Optimised Complete case to create a more realistic representation of what elements would be possible on a trailer manufactured today, raises questions regarding all of the modifications discussed.

Classically, boat-tail geometry has not been adopted in North-America despite the research basis for their design having been established for decades, and in Europe legislation has made it impossible to incorporate such a design without removing valuable internal capacity. It is only recently that boat-tails have begun working in operation on a large scale in North-America due partially to improved design methodology and partially to specific legislation that was created to encourage their operation by allowing additional length at the rear, specifically for geometry to improve the aerodynamic performance of the vehicle. While their adoption in Europe is still limited by legislation, modifications are at present being made to the legislation governing the overall size and dimensions of HGVs which is due to be in effect at the end of 2014, which will make their use possible in the UK. Once the legal issue with their use is rectified, there is likely to be a period where very few are actually used in operation, while the long-term effects and operational and maintenance issues with their use are identified. In the United States,a period of years passed after the allowance was granted for geometry such as this to be used before

it began to become widely adopted.

The reality for haulage operations is that while drag reductions and potential fuel savings create great cost reductions, they must also account for any alteration in their operational capacity such as maintenance, vehicle downtime and repair costs. The consequential costs that can occur as a result of altering the design of their equipment must always be taken into account, and in many cases this is difficult for the operator to predict without first-hand experience of this. Because of this it is likely that operators will use an altered design on a trial basis, possibly only adding a single modification to the original design before testing it for a lengthy period of time and considering this for when their next batch of replacement trailers. These processes lengthen the adoption time required for modifications to take hold in the industry, and when a trailer has a typical lifespan in operation of 15 years this both adds to the adoption time-line but also exemplifies the potential benefits of drag reduction over the course of the trailer's lifespan due to drag at motorway speeds contributing 40-50% of the fuel consumption, depending on the configuration of cab and trailer that is used.

Other geometry such as that of trailer skirts has been through the periods of cautious adoption and is already used by many operators, though a conflict still occurs between the additional costs of including such geometry and not, with some opting to save in the short term as they replace their equipment by opting out of certain features. This can be as a consequence of personal experience in the business where skirting geometry has not worked well previously, or simply that the funds available are more suited to increased capacity at that point in time. Regardless, every operation is different, and in order to cater for these operations, as well as bespoke aspects of the trailer super-structure, the aerodynamic modifications should also provide the option for bespoke customisation.

As seen in the double deck testing, one area that clearly defines a low-cost, high ben-

efit aerodynamic solution that should not be avoided is that of the double deck. The drag incurred by an untreated bulkhead in this circumstance could be very costly in operation, and incorporating a deflector is the simplest way to mitigate this. As seen in figure 4.2.1 a deflector has been incorporated for exactly this purpose successfully.

Figure 4.2.1: Double Deck with Deflector Fitted

While UK manufacturers are capable of incorporating features into the design of their trailers, as evidenced by the roof line modifications that are operating within the UK, the plausibility of new designs hinges on their performance when tested by operators in their trials, and the willingness to operate said trials.

This work shows that there is good potential for the reduction of overall drag solely by altering the trailer geometry alone.

4.3 Further Recommendation

Areas that would benefit from further analysis have arisen as a result of this study. Firstly, additional work evaluating a range of different cab geometry effects would provide interesting insight as to the effects of particular areas of the cab on the overall flow characteristics along the trailer body, such as the effects on under body geometry at 0° yaw conditions, where in this study the flow had been impacted so heavily by geometry upstream of it that modifications in this area with zero side-wind provided little benefit. Furthermore, analysis of a range of different cab deflector configurations would be valuable to determine an optimum angle for de-

tachment, or overall height differentiation optimisation for optimising the travel over the cab-trailer gap.

Also, further evaluation of typical trailer geometry for the UK market would be beneficial, such as the effects of a tandem-axle trailer and a tri-axle or the influence of an angled chassis. There is more work that can be undertaken on skirt design, especially at the trailer rear. There is typically unused space behind the rear skirt section that could be used to angle the rear section of the skirts, creating a boat-tail like structure in this area, but testing needs to be done on this to find an optimum modification. There is a lot of additional testing that could be undertaken in order to create a more complete list of specific geometry modifications and their estimated drag reductions.

There is always a degree of uncertainty regarding computational simulation. To this end, the geometry used in this study all used identical settings when establishing the mesh that was used. As this is automated, the wall accuracy should be identical for all cases regardless of the geometry modification being studied. Additionally, the comparisons were made internally amongst one another in an isolated setting, meaning that the differences observed and the drag alterations noted are comparable. The good agreement with bluff body cases that have known values shows also that the mesh creation and solver used for this study has good agreement with observed drag values.

Work should be undertaken in tandem with operators and manufacturers to gain their input on potential methods of drag reduction. Considering this, the influence on operational capacity is difficult to comprehend without first-hand experience guiding developments.

Bibliography

Ahmed, S., Ramm, G. and Faltin, G. (1984), Some salient features of the time-averaged ground vehicle wake, Technical report, SAE Technical Paper.

Allan, J. (1981), 'Aerodynamic drag and pressure measurements on a simplified tractor-trailer model', *Journal of Wind Engineering and Industrial Aerodynamics* **9**(1), 125–136.

Andersson, J. and Karlsson, D. (2008), Improving rendering times of Autodesk Maya Fluids using the GPU Improving rendering times of Autodesk Maya Fluids using the GPU, PhD thesis.

Autodesk-Inc (2012), 'Maya - 3D Animation Software', `[online]http://usa.autodesk.com/maya/`. [Date Accessed May 2012].

Bachman, L., Erb, A. and Bynum, C. (2005), Effect of Single Wide Tires and Trailer Aerodynamics on Fuel Economy and NOx Emissions of Class 8 Line-Haul Tractor-Trailers, Technical Report 05CV-45.

Baker, H., Cornwell, R., Koehler, E., Patterson, J. and Powell, N. (2009), 'Review of low carbon technologies for heavy goods vehicles', *Ricardo RD* **9**(182601.7).

Baker, T. (1989), 'Developments and trends in three-dimensional mesh generation', *Applied Numerical Mathematics* **5**(4), 275 – 304.

Barzanooni, V. and Khoshnevis, A. (2011), Experimental investigation of the Near Wake of a Trailer, *in* '19th Annual Conference on Mechanical Engineering', Birjand, Iran, pp. 196–200.

Bearman, P. (2009), 'Bluff Body Flow Research with Application to Road Vehicles', *The Aerodynamics of Heavy Vehicles II: Trucks, Buses,* p. 11.

Bearman, P., Browand, F., McCallen, R. and Ross, J. (2009), *The Aerodynamics of Heavy Vehicles II: Trucks, Buses, and Trains*, Vol. 41 of *Lecture Notes in Applied and Computational Mechanics*, Springer Berlin Heidelberg, Berlin, Heidelberg.

Bettle, J. (2003), 'A computational study of the aerodynamic forces acting on a tractor-trailer vehicle on a bridge in cross-wind', *Journal of Wind Engineering and Industrial Aerodynamics* **91**(5), 573–592.

Bhatnagar, B. (2011), 'A Study of Reynolds Number Effects on Production Class 8 Tractor-Trailer Combinations', *Engineering Analysis* pp. 1–24.

Bongart, R. (2007), Efficient Simulation of Fluid Dynamics in a 3D Game Engine Efficient Simulation of Fluid Dynamics in a 3D Game Engine, Masters, Royal Institute of Technology, Stockholm, Sweden.

Browand, F. (2005), Reducing aerodynamic drag and fuel consumption, *in* 'workshop presentation, Global Climate and Energy Project Workshop on Advanced Transportation'.

Browand, F. and Radovich, C. (2005), Experimental measurement of the flow field of heavy trucks, Technical report, University of Southern California.

Browand, F., Radovich, C. and Boivin, M. (2005), Fuel savings by means of flaps attached to the base of a trailer: Field test results, *in* 'Transactions Journal of Passenger Cars: Mechanical Systems, SAE 2005 World Congress & Exhibition'.

Buckley, C. and Waltson, W. (1976), 'An evaluation of the aerodynamic drag reductions produced by various cab roof fairings and a gap seal on tractor-trailer trucks', *SAE Technical Paper 760105* .

Cheli, F., Corradi, R., Sabbioni, E. and Tomasini, G. (2011), 'Wind tunnel tests on heavy road vehicles: Cross wind induced loadsPart 1', *Journal of Wind Engineering and Industrial Aerodynamics* **99**(10), 1000–1010.

Cheli, F., Ripamonti, F., Sabbioni, E. and Tomasini, G. (2011), 'Wind tunnel tests on heavy road vehicles: Cross wind induced loadsPart 2', *Journal of Wind Engineering and Industrial Aerodynamics* **99**(10), 1011–1024.

Chen, J. X., da Vitoria Lobo, N., Hughes, C. E. and Moshell, J. M. (1997), 'Real-time fluid simulation in a dynamic virtual environment', *IEEE Computer Graphics and Applications* **17**(3), 52–61.

Clarke, R. M. (2006), Truck Manufacturers Program to Reduce Aerodynamic Drag, Technical report, Truck Manufacturers Association.

Coanda, H. (1938), 'Propelling device'. Patent 2157281.

Consano, L., Lucarelli, D. and Lupo, F. (2007), Fuel Reduction on a Tractor-Trailer Truck at IVECO, *in* '3rd European Automotive CFD Conference', Frankfurt, Germany., pp. 45–56.

Cooper, C., Kamakaté, F., Reinhart, T., Kromer, M. and Wilson, R. (2009), Reducing Heavy-Duty Long Haul Combination Truck Fuel Consumption and CO2 Emissions, Technical report, Northease States Center for a Clean Air Future, International Council on Clean Transportation, Southwest Research Institute.

Cooper, K. (1979), Sae wind tunnel test procedure for trucks and buses, Sae recommended practice j1252, Society Automotive Engineers.

Cooper, K. (2004), Commercial vehicle aerodynamic drag reduction: Historical perspective as a guide, *in* 'The Aerodynamics of Heavy Vehicles: Trucks, Buses, and Trains', Lecture Notes in Applied and Computational Mechanics, Springer.

Cooper, K., Leuschen, J. and Others (2005), 'Model and full-scale wind tunnel tests of second-generation aerodynamic fuel saving devices for tractor-trailers', *Configurations* .

Cooper, K. R. and Campbell, W. (1981), 'An examination of the effects of wind turbulence on the aerodynamic drag of vehicles', *Journal of Wind Engineering and Industrial Aerodynamics* **9**(1), 167–180.

Cowperthwaite, N. (1986), 'Scale model wind tunnel measurements on the leyland t45 and daf 3300 vehicles used for the t.r.r.l. spray dispersion programme', *Cranfield Institute of Technology* .

Croll, R., Gutierrez, W., Hassan, B., Suazo, J. and AJ, R. (1996), Experimental investigation of the ground transportation systems (gts) project for heavy vehicle drag reduction, Sae paper 960907.

Dassault Systemes SolidWorks Corp (2012), 'SolidWorks 3D CAD', [online]http://www.solidworks.com/sw/products/10141_ENU_HTML.htm. [Date Accessed May 2012].

Dassault Systemes SolidWorks Corp (2013), 'Flow Simulation Technical Reference'.

Davidson, L. (2011), An introduction to turbulence models, Technical paper, Chalmers University of Technology.

DECC (2009), 'Regional and local authority road transport consumption statistics: 2005, 2006, 2007, 2008 and 2009', [online]http://www.decc.gov.uk/en/content/cms/statistics/energy_stats/regional/road_transport/road_transport.aspx. [Date Accessed 2012].

Delaunay, B. (1911), 'Sur la sphere vide', *Izvestia Akademia Nauk SSSR, VII Seria, Otdelenie Matematicheskii I Estestvennyka Nauk* pp. 793–800.

Department of Energy and Climate Change (2013), Average wind speed and deviations from the long term mean, Report.

DFT (2010), 'The Streamlined Guide to Truck Aerodynamic Styling'.

Dings, J. (2010), The case for the exemption of aerodynamic devices in future type-approval legislation for heavy goods vehicles, Technical Report January, Transport and Environment, Brussels.

Don Bur Bodies and Trailers Ltd (2010), 'Aerodynamic Teardrop Trailer', [online]http://www.donbur.co.uk/gb/products/aerodynamic_teardrop_trailer.shtml. [Date Accessed May 2012].

Drollinger, R. A. (1987), Heavy duty truck aerodynamics, Technical report, SAE Technical Paper.

El-alti, M., Chernoray, V., Jahanmiri, M. and Davidson, L. (2011), 'Experimental and computational studies of active flow control on a model truck-trailer', *Experimental Fluid Mechanics 2011 Conference Proceedings* **2**, 600–615.

El-Alti, M., Chernoray, V., Kjellgren, P., Hjelm, L. and Davidson, L. (2010), 'Computations and full-scale tests of active flow control applied on a volvo truck-trailer', *Aerodynamics of Heavy Vehicles III: Trucks, Buses and Trains* .

Elankumaran, K. (1997), *Numerical Investigation of an Inflatable Aerodynamic Boattail for Tractor-trailers*, Texas Tech University.

Energy Efficiency Office (1992), Fuel savings using aerodynamic styling on articulated trucks, Report.

Englar, R. (2000), Development of Pneumatic Aerodynamic Devices to Improve the Performance, Economics, and Safety of Heavy Vehicles, Technical Report 724, Georgia Tech Research Institute, Atlanta, GA (US).

Favre, A. (1969), 'Statistical equations of turbulent gases', *Problems of hydrodynamics and continuum mechanics* pp. 231–266.

Ferrari, P. (2011), 'The dynamics of the competition between cars and trucks on motorways', *Transportation Research Part C: Emerging Technologies* **19**(4), 579–592.

Flynn, H. and Kyropoulos, P. (1962), 'Truck aerodynamics', *SAE transactions* **70**, 297.

Foster, N. and Metaxas, D. (1997), Modeling the motion of a hot, turbulent gas, *in* 'Proceedings of the 24th annual conference on Computer graphics and interactive techniques', SIGGRAPH '97, ACM Press/Addison-Wesley Publishing Co., New York, NY, USA, pp. 181–188.

Freight Best Practice (2006), Smoothing the Flow at TNT Express and Somerfield using Truck Aerodynamic Styling, Technical report, Department for Transport, St Helens, United Kingdom.

Freight-Wing-Inc (2012), 'Freight Wing Gap Fairing', [online]http://www.freightwing.com/gap_fairing.php. [Date Accessed 2012].

Frieght Best practice (2010), Quick Guide to Truck Aerodynamics, Technical report, Department for Transport.

Gamito, M. Lopes, P. G. M. (1995), Two-dimensional simulation of gaseous phenomena using vortex particles, *in* 'In Proceedings of the 6th Eurographics Workshop on Computer Animation and Simulation', Springer-Verlag, pp. 3–15.

Geropp, D. and Odenthal, H. (2000), 'Drag reduction of motor vehicles by active flow control using the Coanda effect', *Experiments in fluids* **28**(1), 74–85.

Ghosal, S. and Moin, P. (1995), 'The basic equations for the large eddy simulation of turbulent flows in complex geometry', *Journal of Computational Physics* **118**, 24–37.

Gilkeson, C., Thompson, H., Wilson, M., Gaskell, P. and Barnard, R. (2009), An experimental and computational study of the aerodynamic and passive ventilation characteristics of small livestock trailers, Technical Report 9-10.

Godderidge, B., Phillips, A. B., Lewis, S. G., Turnock, S. R., Hudson, D. A. and Tan, M. (2008), 'The simulation of free surface flows with Computational Fluid Dynamics', *2008 ANSYS UK User Conference Inspiring Engineering* **2025**, 1–13.

Gurlek, C., Sahin, B. and Ozkan, G. M. (2011), 'PIV studies around a bus model', *Experimental Thermal and Fluid Science* (November).

Gustavsson, T. (2006), 'Alternative approaches to rear end drag reduction Technical Report', *vortaflow.com* pp. 1–49.

Hakansson, C. and Lenngren, M. J. (2010), CFD Analysis of Aerodynamic Trailer Devices for Drag Reduction of Heavy Duty Trucks, Masters thesis, Chalmers University of Technology.

Hammache, M. and Michaelian, M. (2001), 'Aerodynamic Forces on Truck Models , Including Two Trucks in Tandem Aerodynamic Forces on Truck Models , Including Two Trucks in Tandem', *Mechanical Engineering* (October).

Hammache, M., Michaelian, M. and Browand, F. (2001), 'Aerodynamic forces on truck models, including two trucks in tandem', *Mechanical Engineering* .

Hammas, M. (2010), Large eddy simulations of the flow around an Ahmed body with active flow control Large eddy simulations of the flow around an Ahmed body with active flow control, Bachelors, Chalmers University of Technology.

Hardy, S. and James, J. (2008), Fuel Efficiency Trials Research, Technical report, Department for Transport.

Hemida, H. (2008), Numerical Simulations of Flows Around Trains and Buses in Cross Winds, Phd thesis, Chamlers University of Technology.

Henderson, M. (2010), 'The Impact of the Jaguar Super Computer on Large Truck Aerodynamic Design'.

Hess, J. and Smith, A. (1967), 'Calculation of potential flow about arbitrary bodies', *Progress in Aerospace Sciences* **8**(0), 1 – 138.

Hjelm, L. and Bergqvist, B. (2009), 'European Truck AerodynamicsA Comparison Between Conventional and CoE Truck Aerodynamics and a Look into Future Trends and Possibilities', *The Aerodynamics of Heavy Vehicles II: Trucks, Buses, and Trains* pp. 469–477.

Hoerner, S. F. (1965), *Fluid-dynamic drag: practical information on aerodynamic drag and hydrodynamic resistance*, Hoerner Fluid Dynamics Midland Park, NJ.

Hsu, T.-Y., Hammache, M. and Browand, F. (2004), Base flaps and oscillatory perturbations to decrease base drag, *in* 'The Aerodynamics of Heavy Vehicles: Trucks, Buses, and Trains', Springer, pp. 303–316.

Hyams, D. G., Sreenivas, K., Pankajakshan, R., Stephen Nichols, D., Roger Briley, W. and Whitfield, D. L. (2011), 'Computational simulation of model and full scale Class 8 trucks with drag reduction devices', *Computers & Fluids* **41**(1), 27–40.

Ihlein, K. and White, R. B. (2007), 'On Drag Coefficients of Tractor Trailer Trucks', pp. 1–17.

Johansson, M. (2010), The Effects of Oscillatory Boat-Tail Flaps on the Near Wake of a Prototypical Heavy Vehicle, Masters thesis, LuleåUniversity of Technology.

Jones, W. and Launder, B. (1972), 'The prediction of laminarization with a two-equation model of turbulence', *International Journal of Heat and Mass Transfer* **15**(2), 301 – 314.

Kiel, F. (2009), 'Damage control pushes change in trailer skirts', *Transport Topics* (3826).

Knight, I. (2010), Comparing the results of cost benefit analyses for the longer semi-trailer and previous lhv studies, Report, Transport Research Laboratory.

Koike, M., Nagayoshi, T. and Hamamoto, N. (2004), 'Research on aerodynamic drag reduction by vortex generators', *Mitsubishi Motors Technical Review* **16**(2), 11–16.

Ladjedel, O., Adjlout, L., Imine, O. and Yahiaoui, T. (2012), 'Experimental and numerical studies of turbulent flow in an in-line tube bundles', **010**.

Lam, C. and Bremhorst, K. (1981), 'A modified form of the k-ε model for predicting wall turbulence', *Journal of Fluids Engineering* **103**(3), 456–460.

Launder, B. E. and Spalding, D. (1974), 'The numerical computation of turbulent flows', *Computer methods in applied mechanics and engineering* **3**(2), 269–289.

Launder, B. E. and Spalding, D. B. (1972), 'Lectures in mathematical models of turbulence'.

Lav, C. (2013), Three dimensional cfd analysis on aerodynamic drag reduction of a bluff tractor trailer body using vortex generators, Technical report, SAE Technical Paper.

Laydon-Composites-Ltd (2012), 'laydon Composites Vortex Stabilizer', `[online]http://www.laydoncomp.com/nose-fairing-vortex-stabilizer.php`. [Date Accessed 2012].

Le, H., Moin, P. and Kim, J. (1997), 'Direct numerical simulation of turbulent flow over a backward-facing step', *Journal of Fluid Mechanics* **330**, 349–374.

Leuschen, J. and Cooper, K. (2006), 'Full-scale wind tunnel tests of production and prototype, second-generation aerodynamic drag-reducing devices for tractor-trailers', *SAE Technical Paper 06CV-222* .

Leuschen, J. and Cooper, K. (2009), Summary of full-scale wind tunnel tests of aerodynamic drag-reducing devices for tractor-trailers, *in* 'The Aerodynamics of Heavy Vehicles II: Trucks, Buses, and Trains', Vol. 41 of *Lecture Notes in Applied and Computational Mechanics*, Springer Berlin / Heidelberg, pp. 451–462.

Lin, J., Howard, F. and Selby, G. (1990), 'Small submerged vortex generators for turbulent flow separation control', *Journal of Spacecraft and Rockets* **27**, 503–507.

Lindhqvist, A. and Bengtsson, A. (2010), *Development concept for timber truck*, Machine Design, Department of Design Sciences, LTH.

Lutz, T. and Sayers, A. T. (1999), 'Wind tunnel boundary layer effects on the aerodynamic drag of model trucks', **2**(December 1995).

Malviya, V., Mishra, R. and Fieldhouse, J. (2009), 'CFD Investigation of a Novel Fuel-Saving Device for Articulated Tractor-Trailer Combinations', *Engineering Applications of Computational Fluid Mechanics* **3**(4), 587–607.

Malviya, V., Mishra, R. and Fieldhouse, J. D. (2008), 'Comparative computational analysis of drag-reducing devices for tractor-trailers'.

Martini, H., Bergqvist, B., Hjelm, L. and Lofdahl, L. (2012), Aerodynamic investigation of gap treatment-and chassis skirts strategies for a novel long-haul vehicle combination, Technical report, SAE Technical Paper.

Mason Jr, W. and Beebe, P. (1978), The drag related flow field characteristics of trucks and buses, *in* 'Aerodynamic Drag Mechanisms of Bluff Bodies and Road Vehicles', Springer, pp. 45–93.

McCallen, R. (2002), September 2002 Working Group Meeting on Heavy Vehicle Aerodynamic Drag: Presentations and Summary of Comments and Conclusions, Technical Report September, Lawrence Livermore National Lab., CA (US).

McCallen, R., Browand, F., Leonard, A. and Rutledge, W. (1997), Systematic approach to analyzing and reducing aerodynamic drag of heavy vehicles, Technical report, Lawrence Livermore National Lab., CA (United States).

McWherter-Payne, M. and Salari, K. (2003), Computational flow modeling of a simplified integrated tractor-trailer geometry., Technical Report September, Sandia National Laboratories.

Mentor Graphics (2011), 'Enhanced Turbulence Modeling in FloEFD'.

Miralbes, R. (2012), Analysis of some aerodynamic improvements for semi-trailer tankers, *in* 'Proceedings of the World Congress on Engineering', Vol. 3.

Mohamed-kassim, Z. Filippone, A. (2009), Realistic Fuel Saving on a Heavy Vehicle via Aerodynamic Drag Reduction, Technical report, The University of Manchester, The University of Manchester.

Mohamed-Kassim, Z. and Filippone, A. (2010), 'Fuel savings on a heavy vehicle via aerodynamic drag reduction', *Transportation Research Part D: Transport and Environment* **15**(5), 275–284.

Motor-Industry-Research-Association (2010*a*), Airtabs vortex generators technical trials articulated hgv tractor-trailer gap tests, Technical trials, Institute of Road Transport Engineers.

Motor Industry Research Association (2010*b*), Fuel Saving Semi-Trailers: An Independent Report, Technical report, Motor Industry Research Association, Nuneaton, United Kingdom.

Muirhead, V. (1978), 'An investigation of drag reduction for tractor trailer vehicles', *NASA* .

Muirhead, V. (1981), 'An investigation of drag reduction for tractor trailer vehicles with air deflector and boattail', *NASA* .

Munson, B. R., Rothmayer, A. P., Okiishi, T. H. and Huebsch, W. W. (2012), *Fundamentals of fluid mechanics*, Wiley.

Munson, B. R., Young, D. F. and Okiishi, T. H. (1990), *Fundamentals of fluid mechanics*, New York.

Mustofa, M. (2012), 'An experimental study of the aerodynamics forces acting on a truck', *MEKTEK* **11**(3).

Navier, C. (1823), 'Mémoire sur les lois du mouvement des fluides', *Mémoires de lAcadémie Royale des Sciences de lInstitut de France* **6**, 389–440.

Nayeri, C., Haff, J., Greenblatt, D., Loefdahl, L. and Paschereit, C. (2009), 'Drag Reduction on a Generic Tractor-Trailer using Active Flow Control in Combination with Solid Flaps', *The Aerodynamics of Heavy Vehicles II: Trucks, Buses, and Trains* pp. 179–191.

New, W. (2010), Technologies and Approaches to Reducing the Fuel Consumption of Medium and Heavy Duty vehicles, Technical report, Transportation Research Board, Washington.

News, O.-h., Dussault, B., Power, P. and Tips, D. (2005), 'Operating Caterpillar On-Highway Engines with ACERT Technology', pp. 1–13.

Olson, M. and Fry, P. (1988), Highway tractor-trailer splash and spray reduction through aerodynamic design, Technical report, SAE Technical Paper.

Ortega, J. and Salari, K. (2004), 'An Experimental Study of Drag Reduction Devices for a Trailer Underbody and Base', *AIAA Paper* **2252**.

Ortega, J., Salari, K., Brown, A. and Schoon, R. (2013), 'Aerodynamic drag reduction of class 8 heavy vehicles: a full-scale wind tunnel study', *Livermore, CA: Lawrence Livermore National Laboratory (LLNL)* .

Ortega, J., Salari, K. and Storms, B. (2009), 'Investigation of Tractor Base Bleeding for Heavy Vehicle Aerodynamic Drag Reduction', *The Aerodynamics of Heavy Vehicles II: Trucks, Buses, and Trains* pp. 161–178.

Östh, J. and Krajnović, S. (2012), 'The flow around a simplified tractor-trailer model studied by large eddy simulation', *Journal of Wind Engineering and Industrial Aerodynamics* **102**, 36–47.

Pankajakshan, R., Mitchell, B. and Whitfield, D. (2009), 'Full-Scale Simulations of Drag Reduction Devices for Class 8 Trucks', *The Aerodynamics of Heavy Vehicles II: Trucks, Buses, and Trains* pp. 339–348.

Pointer, D., Sofu, T., Chang, J. and Weber, D. (2009), 'Applicability of Commercial CFD Tools for Assessment of Heavy Vehicle Aerodynamic Characteristics', *The Aerodynamics of Heavy Vehicles II: Trucks, Buses, and Trains* pp. 349–361.

Poisson, S. D. (1831), *Mémoire sur les équations générales de l'équilibre et du mouvement des corps solides élastiques et de fluides*, L'imprimerie Royale.

Qi, X.-n., Liu, Y.-q. and Du, G.-s. (2011), 'Experimental and numerical studies of aerodynamic performance of trucks', *Journal of Hydrodynamics, Ser. B* **23**(6), 752–758.

Qi, X.-n. and Liu, Z.-y. (2008), 'Investigation on drag reduction of trucks', *Journal of Shanghai Jiaotong University (Science)* **13**(2), 201–205.

Raemdonck, G. v. (2006), Design of an aerodynamic aid for a tractor trailer combination, Masters thesis, Delft University of Technology.

Raemdonck, G. V. and Tooren, M. V. (2008), Time-Averaged Phenomenological Investigation of a Wake behind a Bluff Body, *in* 'BBAA VI international Colloquium on: Bluff Bodies Aerodynamics & Applications', Milan, Italy, p. 13.

Rajsinh, C. and Raj, T. K. (2012), 'Numerical investigation of external flow around the ahmed reference body using computational fluid dynamics', *Research journal of recent Sciences* **1**, 1–5.

Reynolds, O. (1883), 'An experimental investigation of the circumstances which determine whether the motion of water shall be direct or sinuous, and of the law of resistance in parallel channels.', *Proceedings of the royal society of London* **35**(224-226), 84–99.

Richardson, L. F. (1911), 'The approximate arithmetical solution by finite differences of physical problems involving differential equations, with an application to the stresses in a masonry dam', *Philosophical Transactions of the Royal Society of London. Series A, Containing Papers of a Mathematical or Physical Character* pp. 307–357.

Roscoe, L. et al. (1988), 'Stereolithography interface specification', *America-3D Systems Inc* .

Roy, C., Brown, J., DeChant, L. and Barone, M. (2004), 'Unsteady Turbulent Flow Simulations of the Base of a Generic Tractor/Trailer', *AIAA Paper* **2255**, 28–1.

Roy, C. and Ghuge, H. (2009), 'Detached eddy simulations of a simplified tractor/-trailer geometry', *The Aerodynamics of Heavy Vehicles II: Trucks, Buses, and Trains* pp. 363–381.

Roy, S. and Srinivasan, P. (2000), 'External flow analysis of a truck for drag reduction', *SAE transactions* **109**(2), 808–812.

SAE J1252 (1981), Sae wind tunnel test procedure for trucks and buses j1252, Sae recommended practice j1252.

Salari, K., Mccallen, R., Ortega, J., Paschkewitz, J., Castellucci, P., Leonard, A., Rubel, M., Ross, J., Storms, B., Cooper, C. K. and Leuschen, J. (2006), Heavy Vehicle Drag Reduction Devices : Computational Evaluation & Design Acknowledgment Goal : Reduce heavy vehicle drag by 25 %, Technical report, University of california, Lawrence Livermore National Laboratory.

Salari, K. and Ortega, J. (2010), Aerodynamic Design Criteria for Class 8 Heavy Vehicles Trailer Base Devices to Attain Optimum Performance, Technical report, Lawrence Livermore National Laboratory, Livermore, CA.

Saltzman, E. J. and Meyer Jr, R. R. (1999), 'A reassessment of heavy-duty truck aerodynamic design features and priorities'.

Saltzman, E. and Meyer, R. (1999), 'A Reassessment of Heavy-Duty Truck Aerodynamic Design Features and Priorities', (June).

Sandberg, T. (2001), 'Heavy truck modeling for fuel consumption simulations and measurements'.

Saunders, J. W., Watkins, S., Hoffmann, P. H. and Buckley, F. T. (1985), Comparison of on-road and wind-tunnel tests for tractor-trailer aerodynamic devices, and fuel savings predictions, Technical report, SAE Technical Paper.

Savkoor, A., Manders, S. and Riva, P. (2001), 'Design of actively controlled aerodynamic devices for reducing pitch and heave of truck cabins', *JSAE review* **22**(4), 421–434.

Schoon, R. E. (2007), On-road evaluation of devices to reduce heavy truck aerodynamic drag, Technical report, SAE Technical Paper.

Schroeder, W. J., Martin, K. M. and Lorensen, W. E. (1996), The design and implementation of an object-oriented toolkit for 3d graphics and visualization, *in* 'Proceedings of the 7th conference on Visualization '96', VIS '96, IEEE Computer Society Press, Los Alamitos, CA, USA, pp. 93–ff.

Seifert, A., Stalnov, O., Sperber, D., Arwatz, G., Palei, V., David, S., Dayan, I. and Fono, I. (2009), 'Large Trucks Drag Reduction using Active Flow Control', *The Aerodynamics of Heavy Vehicles II: Trucks, Buses, and Trains* pp. 115–133.

Sherwood, A. (1974), Wind tunnel test of trailmobile trailers, Technical report, University of Maryland Wind Tunnel Report 85.

Singh, S. N., Rai, L., Puri, P. and Bhatnagar, a. (2005), 'Effect of moving surface on the aerodynamic drag of road vehicles', *Proceedings of the Institution of Mechanical Engineers, Part D: Journal of Automobile Engineering* **219**(2), 127–134.

Slezak, L. (2005), Annual Progress Report Heavy Vehicle Systems Optimization Program, Technical report, US Department of Energy, Washington DC, USA.

Smagorinsky, J. (1963), 'General circulation experiments with the primitive equations', *Monthly Weather Review* **99**, 99–64.

Smith, C. and Kent, J. (2007), 'An assessment of factors affecting fleet fuel performance', *Journal of Transportation Management* .

Sreenivas, K., Mitchell, B., Nichols, S., Hyams, D. and Whitfield, D. (2009), 'Computational Simulation of the GCM Tractor-Trailer Configuration', *The Aerodynamics of Heavy Vehicles II: Trucks, Buses, and Trains* pp. 325–338.

Stam, J. (1999), Stable fluids, *in* 'SIGGRAPH 1999 Conference Proceedings', Autodesk Inc.

Steers, L. L. and Saltzman, E. J. (1977), 'Reduced truck fuel consumption through aerodynamic design', *Journal of Energy* **1**(5), 312–318.

Sterling, M., a.D. Quinn, Hargreaves, D., Cheli, F., Sabbioni, E., Tomasini, G., Delaunay, D., Baker, C. and Morvan, H. (2010), 'A comparison of different methods to evaluate the wind induced forces on a high sided lorry', *Journal of Wind Engineering and Industrial Aerodynamics* **98**(1), 10–20.

Stokes, G. G. (1846), 'Report on recent researches in hydrodynamics', *Brit. Ass. Rep* **1**, 1–20.

Storms, B., Satran, D., Heineck, J. and Walker, S. (2004), 'A study of reynolds number effects and drag-reduction concepts on a generic tractor-trailer', *AIAA paper* **2251**, 2004.

Tan, J., Chen, Z., Hu, Y., Parameswaran, S., Rahman, S., Gleason, M. and Sun, R. (2010), 'Effects of cross wind on sport utility vehicles (SUV): A computational study', *atdd.noaa.gov* (Fletcher 1991).

Taubert, L. and Wygnanski, I. (2009), 'Preliminary Experiments Applying Active Flow Control to a 1/24 th Scale Model of a Semi-Trailer Truck', *The Aerodynamics of Heavy Vehicles II: Trucks, Buses, and Trains* pp. 105–113.

Taylor, C. and Hood, P. (1973), 'A numerical solution of the navier-stokes equations using the finite element technique', *Computers & Fluids* **1**(1), 73–100.

The-Automobile-Association (2012), 'Fuel price report UK and overseas prices - May 2012', `[online]http://www.theaa.com/motoring\_advice/fuel/index.html`. [Date Accessed May 2012].

The Carbon Trust (2013), Conversion factors - energy and carbon conversions, Technical report.

The Cartwright Group (2010), 'Cheetah Fastback Aerodynamic Trailer', `[online]http://www.cartwright-group.co.uk/cheetah\_fastback.asp`. [Date Accessed May 2012].

Thibault, J. (2009), 'CUDA implementation of a Navier-Stokes solver on multi-GPU desktop platforms for incompressible flows', *Mechanical and Biomedical* (January), 1–15.

Truck Manufacturers Association and others (2007), 'Test, evaluation, and demonstration of practical devices/systems to reduce aerodynamic drag of tractor/semi-trailer combination unit trucks', *Final Report, April* .

United States Department of Energy (2010), 'Secretary Chu Announces $187 Million to Improve Vehicle Efficiency for Heavy-Duty Trucks and Passenger Vehicles', [online]http://energy.gov/articles/secretary-chu-announces-187-million-improve-vehicle-efficiency/-heavy-duty-trucks-and. [Date Accessed January 2012].

Using, R. and Flow, A. (2009), 'Computational Analysis of Base Drag Reduction Using Active Flow Control', *Technology* (November).

Van Driest, E. R. (1956), 'On turbulent flow near a wall', *Journal of the Aeronautical Sciences (Institute of the Aeronautical Sciences)* **23**(11).

Van Leeuwen, P. (2009), Computational Analysis of Base Drag Reduction Using Active Flow Control, Masters thesis, Delft university of Technology.

Van Raemdonck, G. and van Tooren, M. (1993), 'Design of an Aerodynamic Aid for the Underbody of a Trailer within a Tractor-Trailer Combination', *bbaa6.mecc.polimi.it* pp. 1–2.

Van Raemdonck, G. and van Tooren, M. (2008), 'Design of an Aerodynamic Aid for the Underbody of a Trailer within a Tractor-Trailer Combination', *bbaa6.mecc.polimi.it* pp. 20–24.

V.J. Modi, S. Hill, St.T. Yokomizo (1995), 'Drag reduction of trucks through boundary-layer control', *Journal of Wind Engineering and Industrial Aerodynamics* **55**, 583–594.

Wacker, T. (1985), 'A preliminary study of configuration effects on the drag of a tractor-trailer combination'.

Watkins, S. (1990), Windtunnel modelling of vehicle aerodynamics: with emphasis on turbulent wind effects on commercial vehicle drag, Phd, Victorian University of Technology.

Watkins, S., Saunders, J. and Hoffmann, P. (1995), 'Turbulence experienced by moving vehicles. Part I. Introduction and turbulence intensity', *Journal of wind engineering and industrial aerodynamics* **57**(1), 1–17.

White, M. (1999), *Fluid Mechanics*, fourth edn, WCB Mcgraw hill.

Williams, G. P. (1969), 'Numerical integration of the three-dimensional navier-stokes equations for incompressible flow', *Journal of Fluid Mechanics* **37**(04), 727–750.

Wilson, F. and Hildebrand, E. (2004), Lateral forces on heavy trucks contributions from wind, Technical Report 2, University of New Brunswick.

Wong, H., Cox, R. and Rajan, A. (1981), 'Drag reduction of trailer-tractor configuration by aerodynamic means', *Journal of Wind Engineering and Industrial Aerodynamics* **9**(1), 101–111.

Wood, R. and Bauer, S. (2003), 'Simple and low-cost aerodynamic drag reduction devices for tractor-trailer trucks', *SAE transactions* **112**(2), 143–160.

Yaeger, L., Upson, C. and Myers, R. (1986), 'Combining physical and visual simulationcreation of the planet jupiter for the film 2010', *SIGGRAPH Comput. Graph.* **20**(4), 85–93.

Appendices

.1 Geometry Dimensions

.1.1 Baseline Case

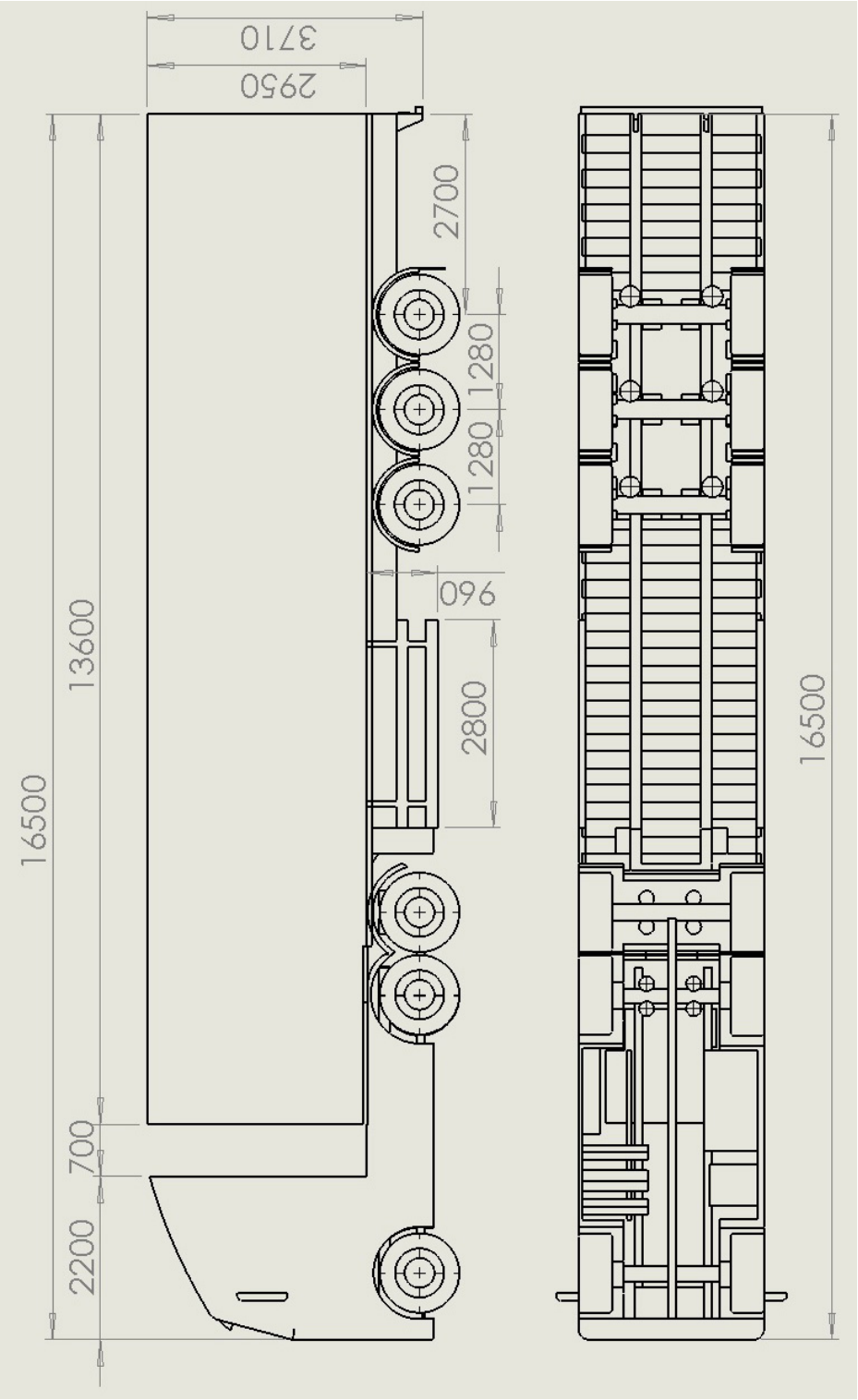

Figure .1.1: Baseline Dimensions

.1.2 Roof Line Modification

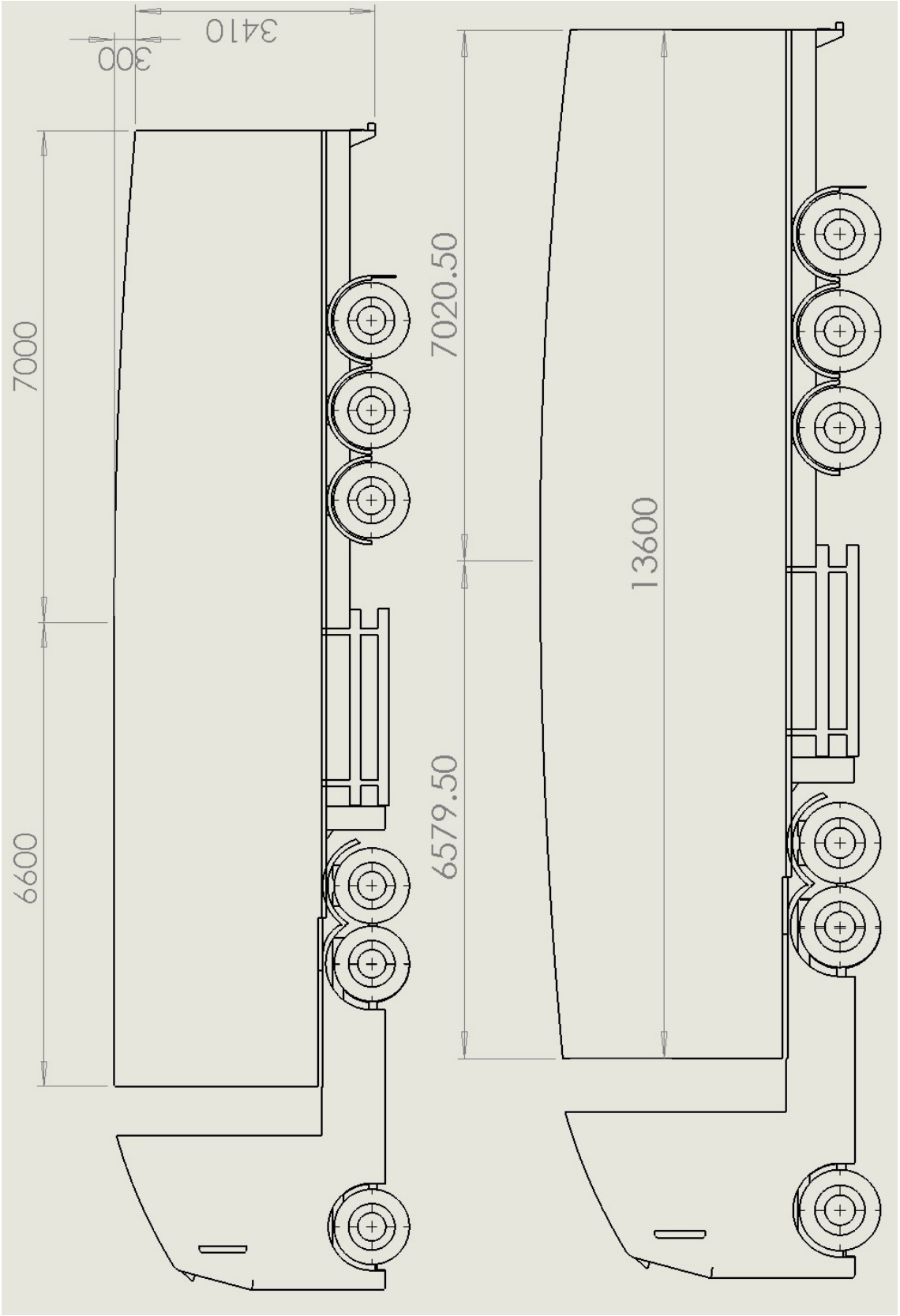

Figure .1.2: Roof Line Modification Dimensions

.1.3 Boat-Tail Dimensions

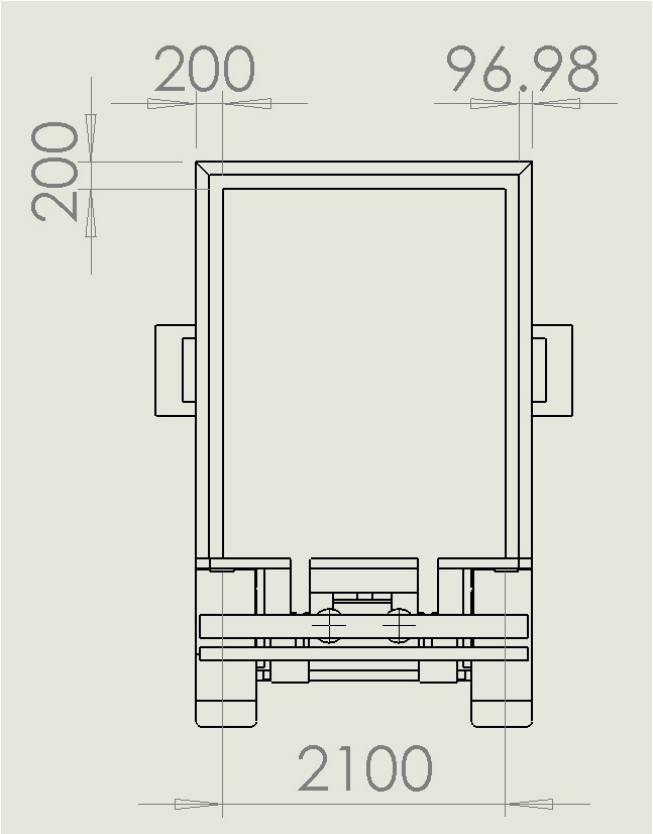

Figure .1.3: Boat-Tail Rear Dimensions

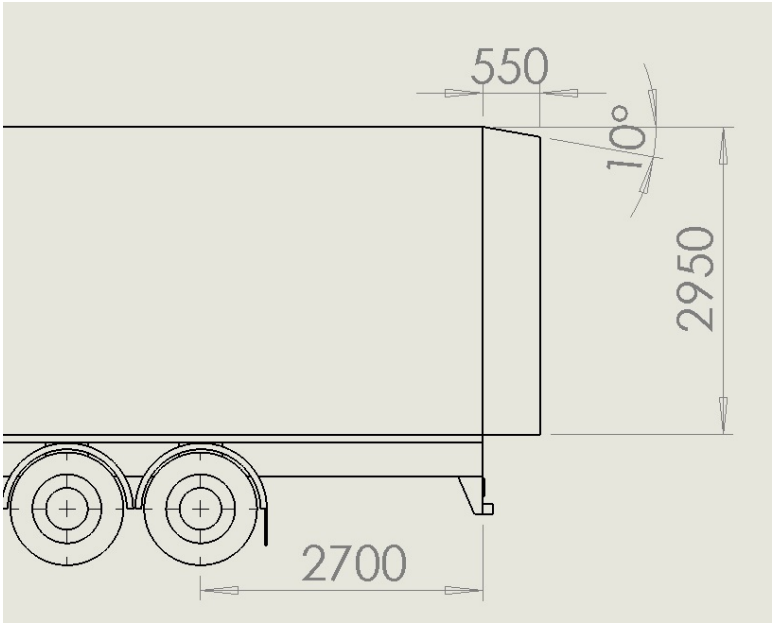

Figure .1.4: Boat-Tail 10° Dimensions

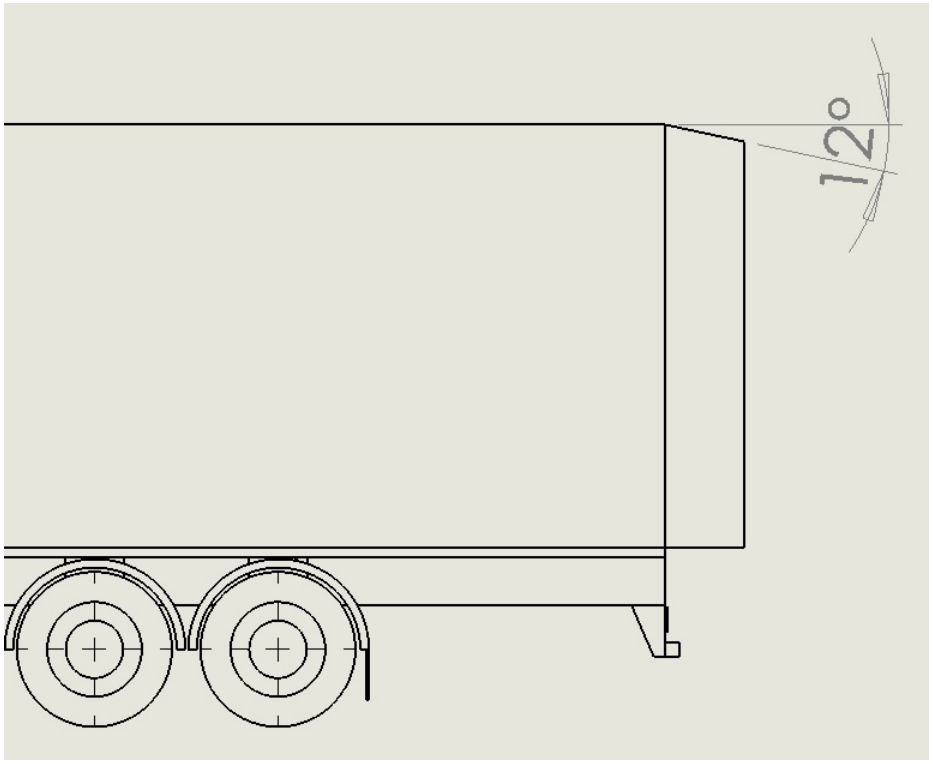

Figure .1.5: Boat-Tail 12° Dimensions

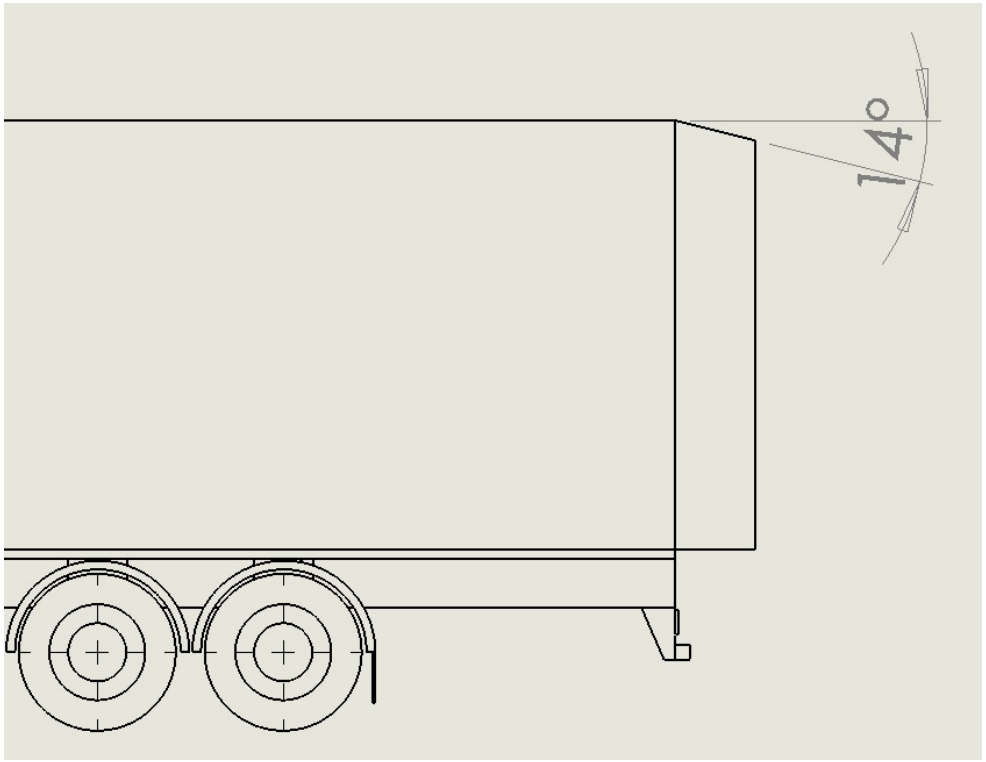

Figure .1.6: Boat-Tail 14° Dimensions

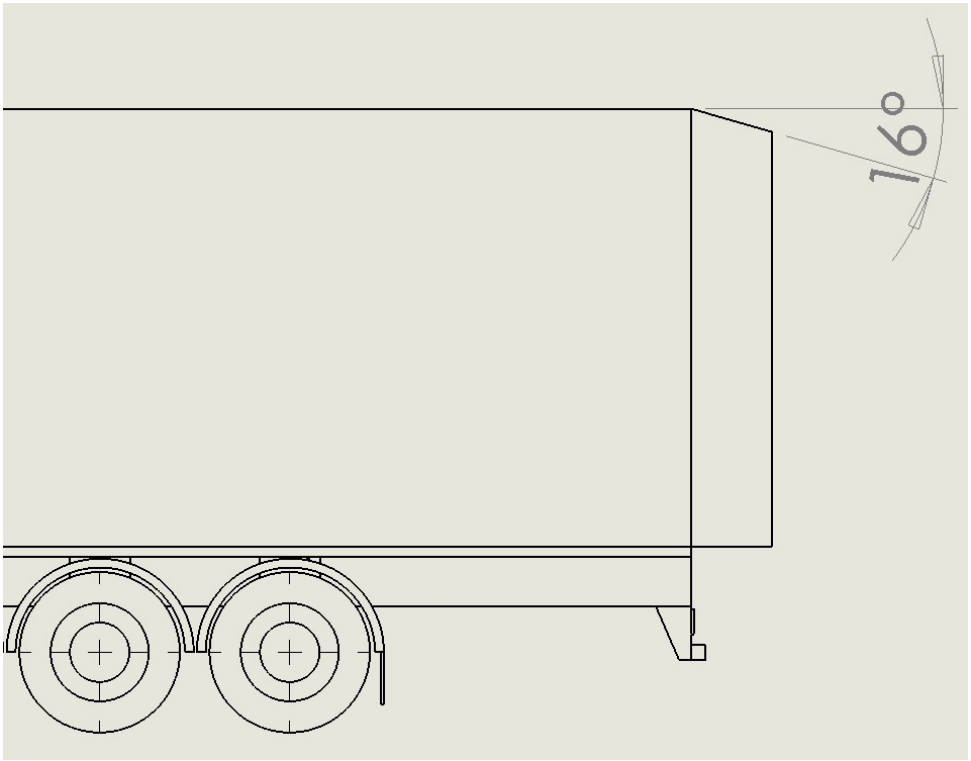

Figure .1.7: Boat-Tail 16° Dimensions

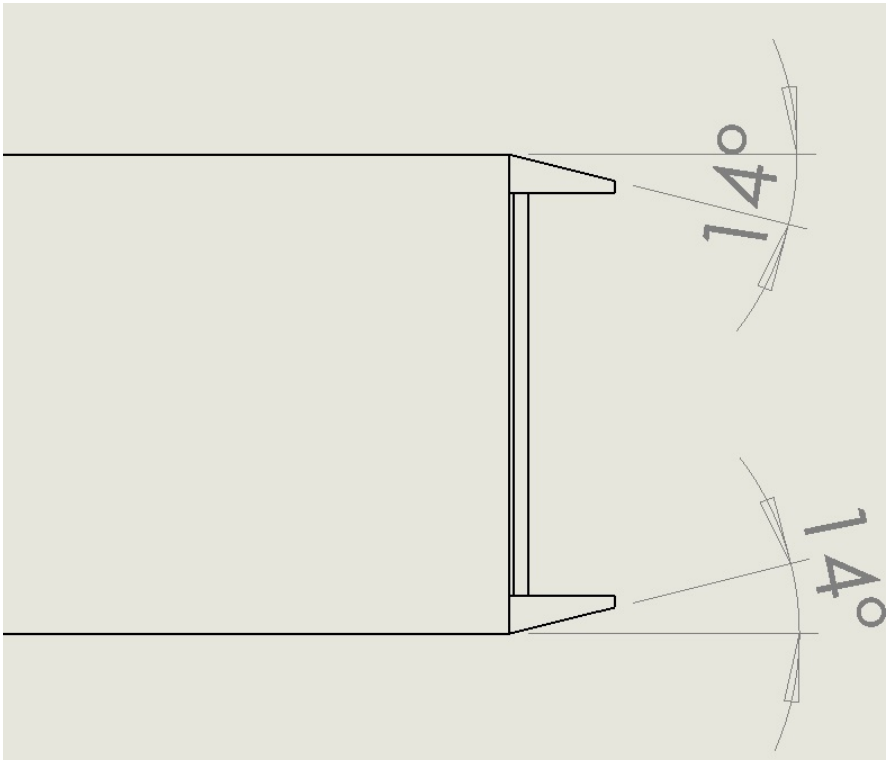

Figure .1.8: Side-Plates 14° Dimensions

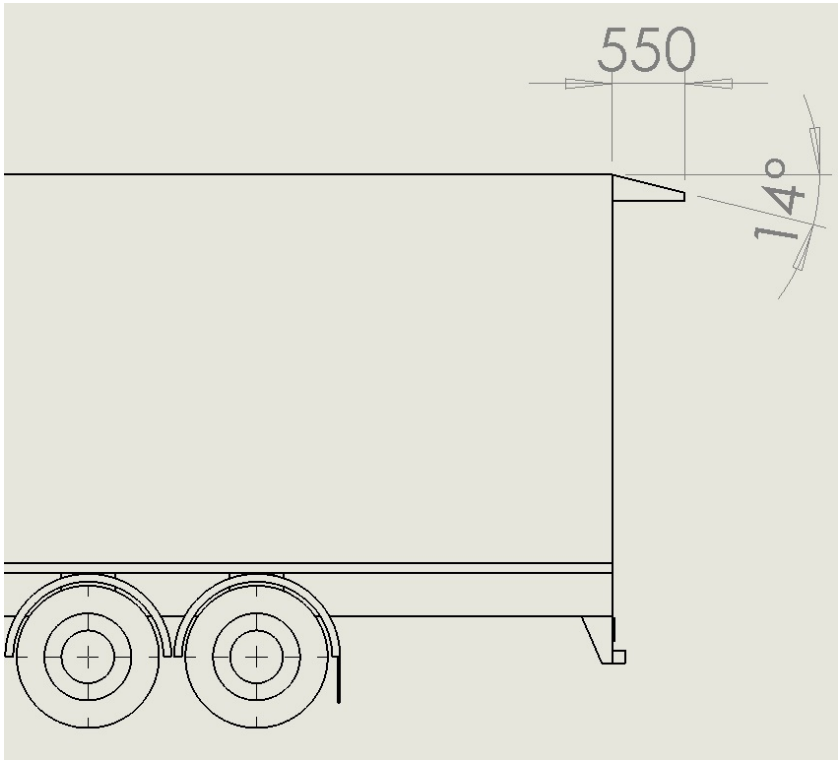

Figure .1.9: Top-Plate 14° Dimensions

.1.4 Side Guards and Under Body

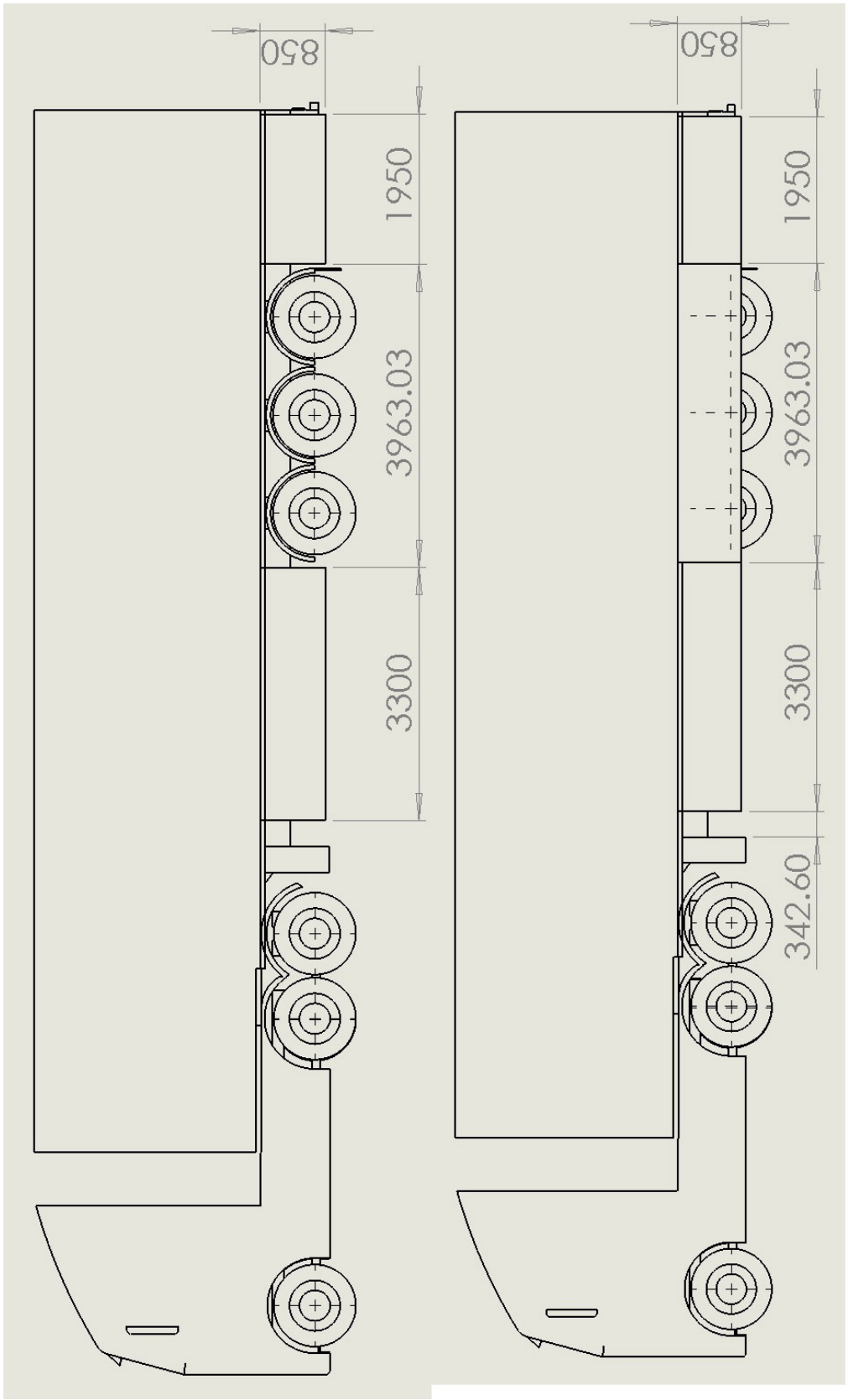

Figure .1.10: Basic Skirts and with Wheels Covered Dimensions

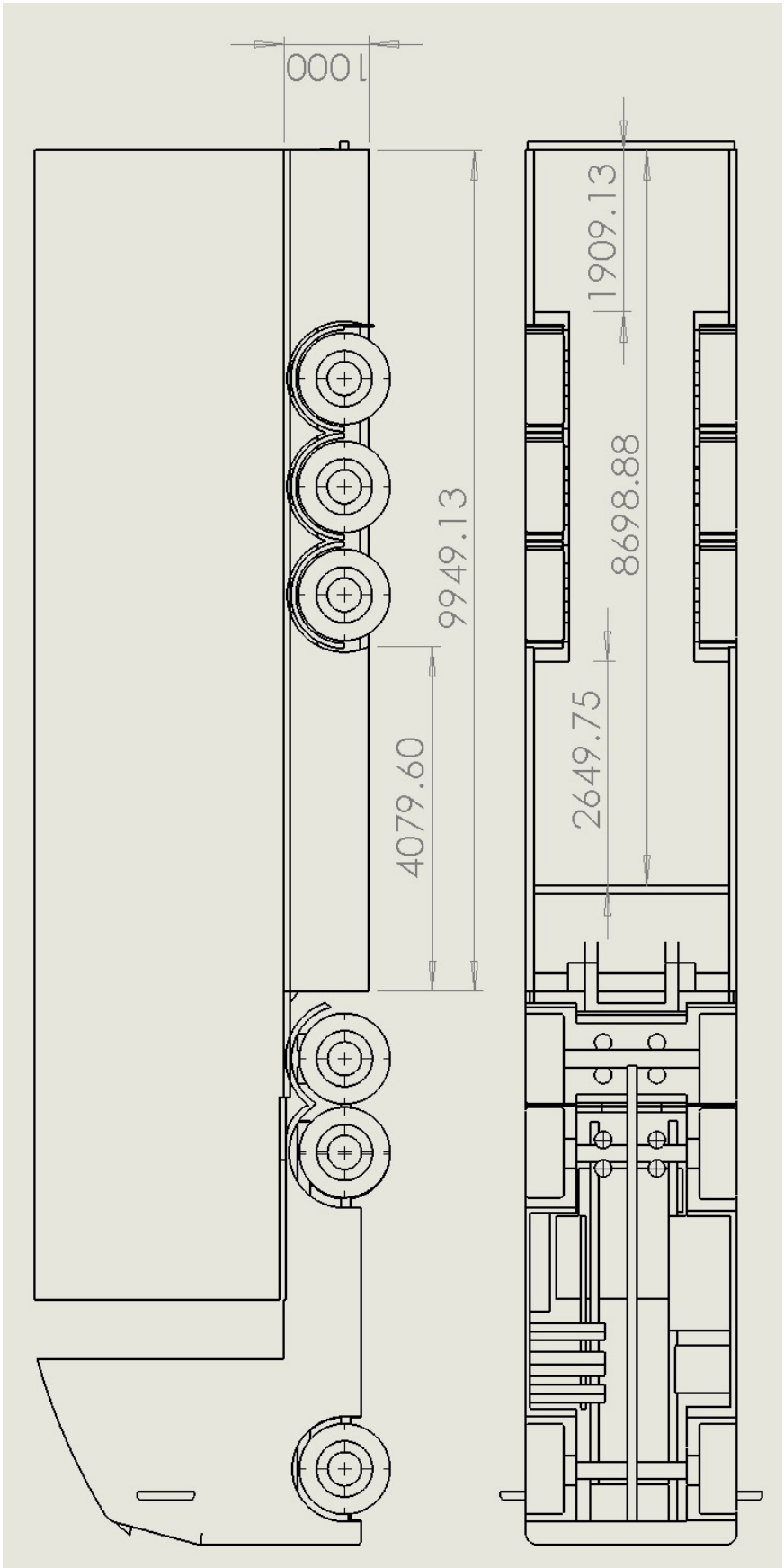

Figure .1.11: Full Skirt with Under-Plating Dimensions

.1.5 Standalone Cases

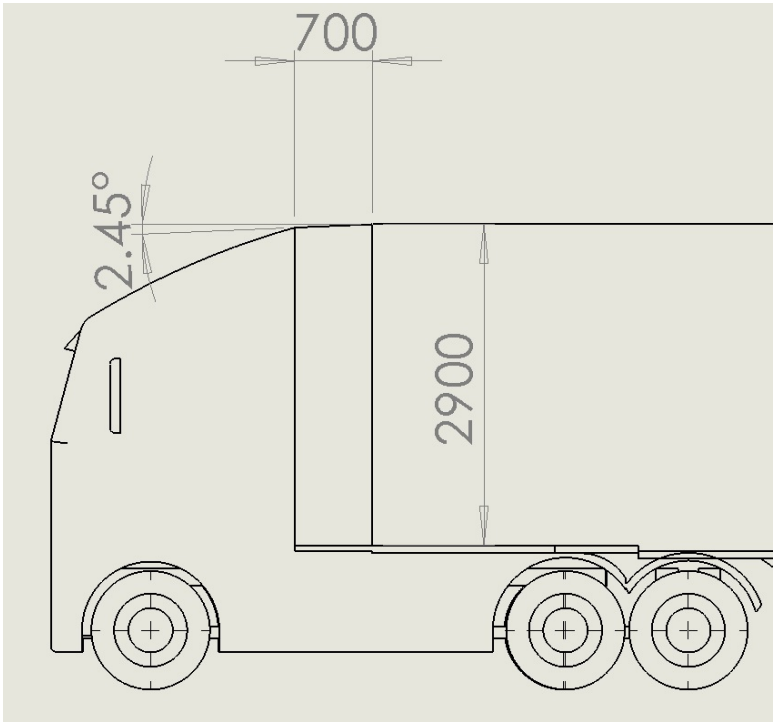

Figure .1.12: Cab-Trailer Gap Treatment Dimensions

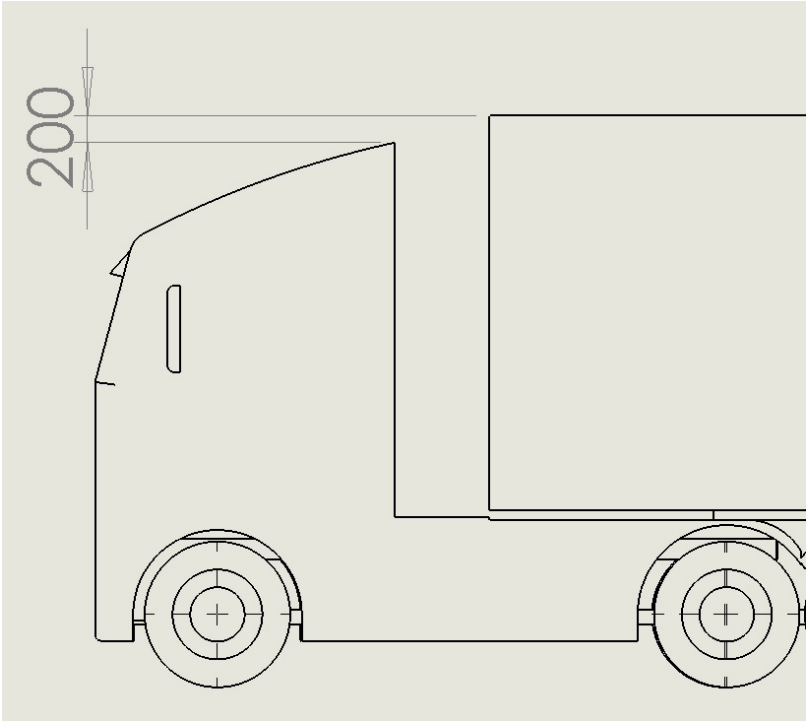

Figure .1.13: Misaligned Cab Deflector Dimensions

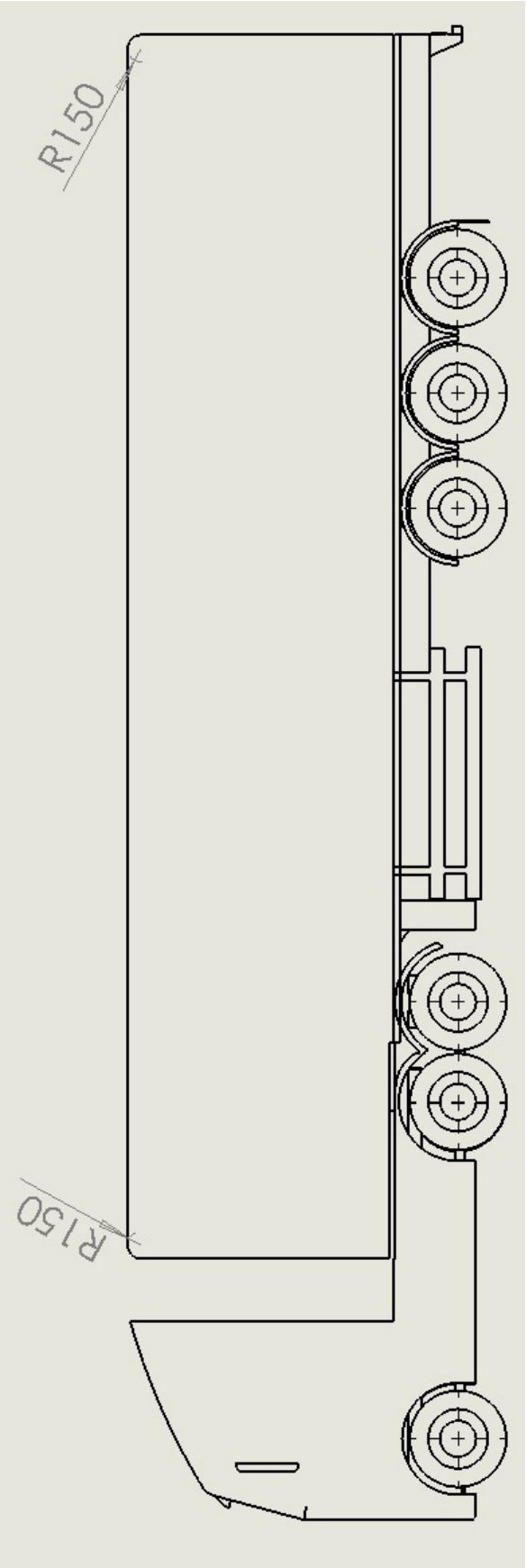

Figure .1.14: Rounded Edges Dimensions

.1.6 Double Deck Cases

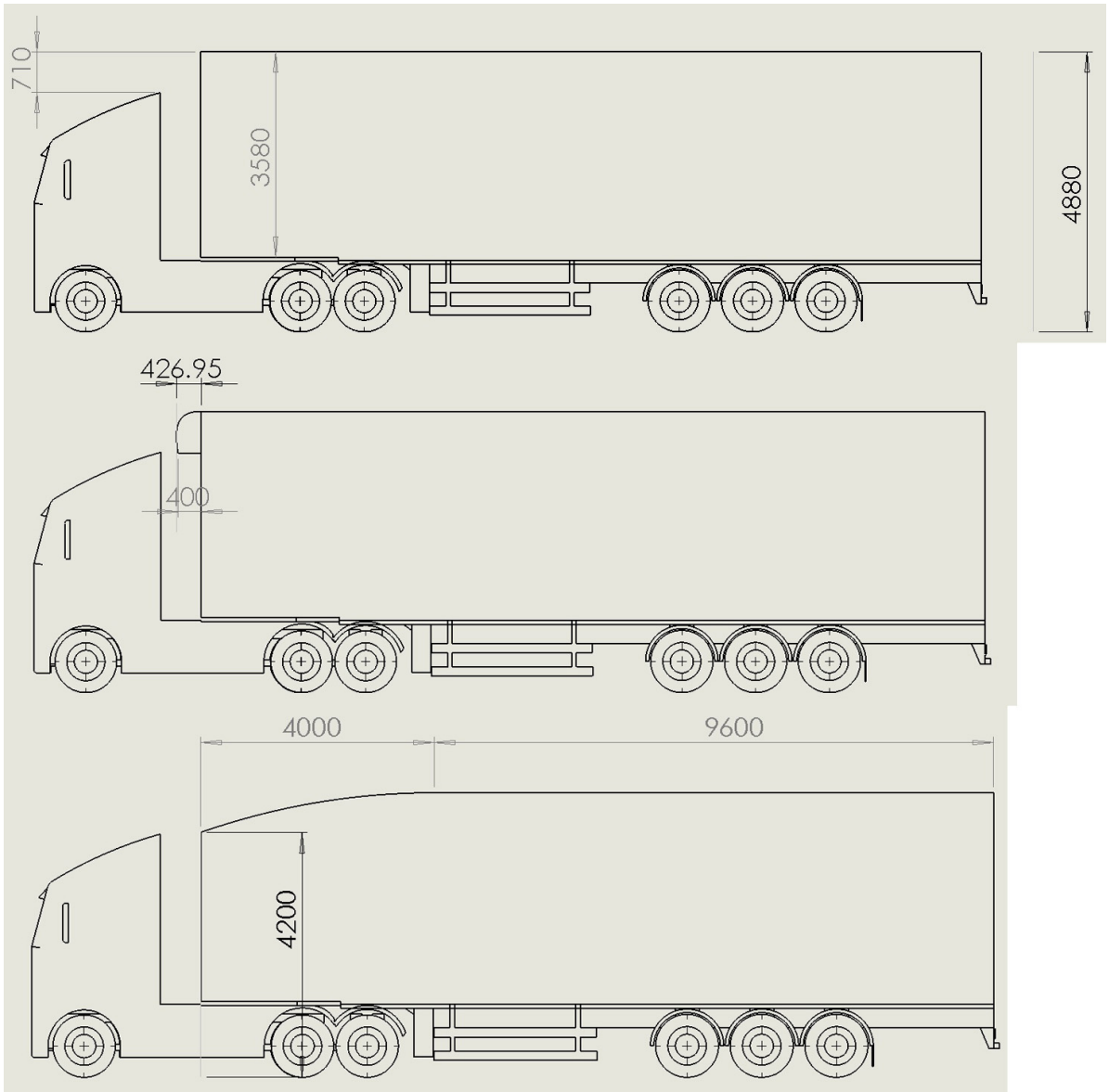

Figure .1.15: Double Deck Standard, Deflector and Sloping Roof Dimensions

.1.7 Optimised Combination Cases

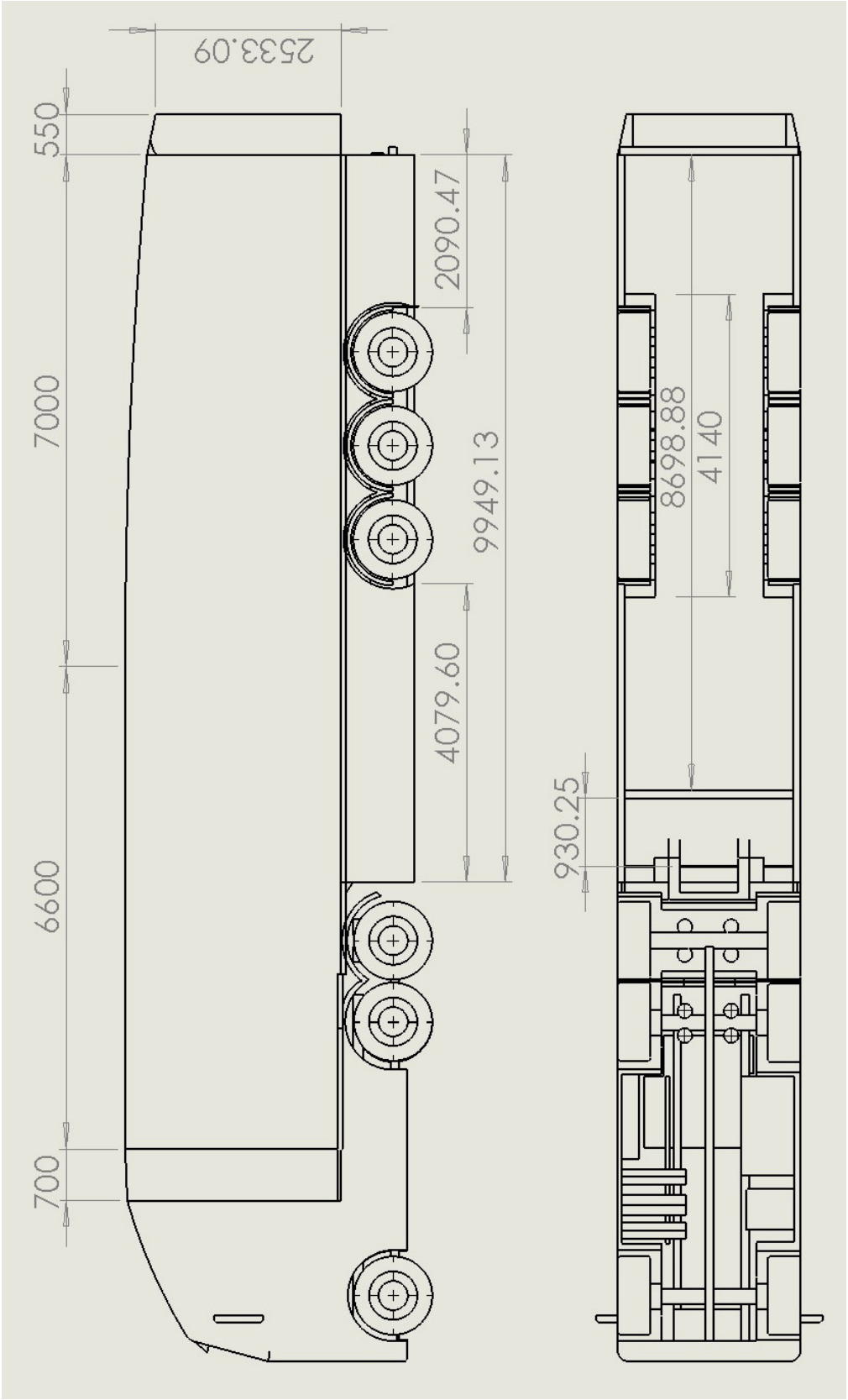

Figure .1.16: Optimised Complete Dimensions

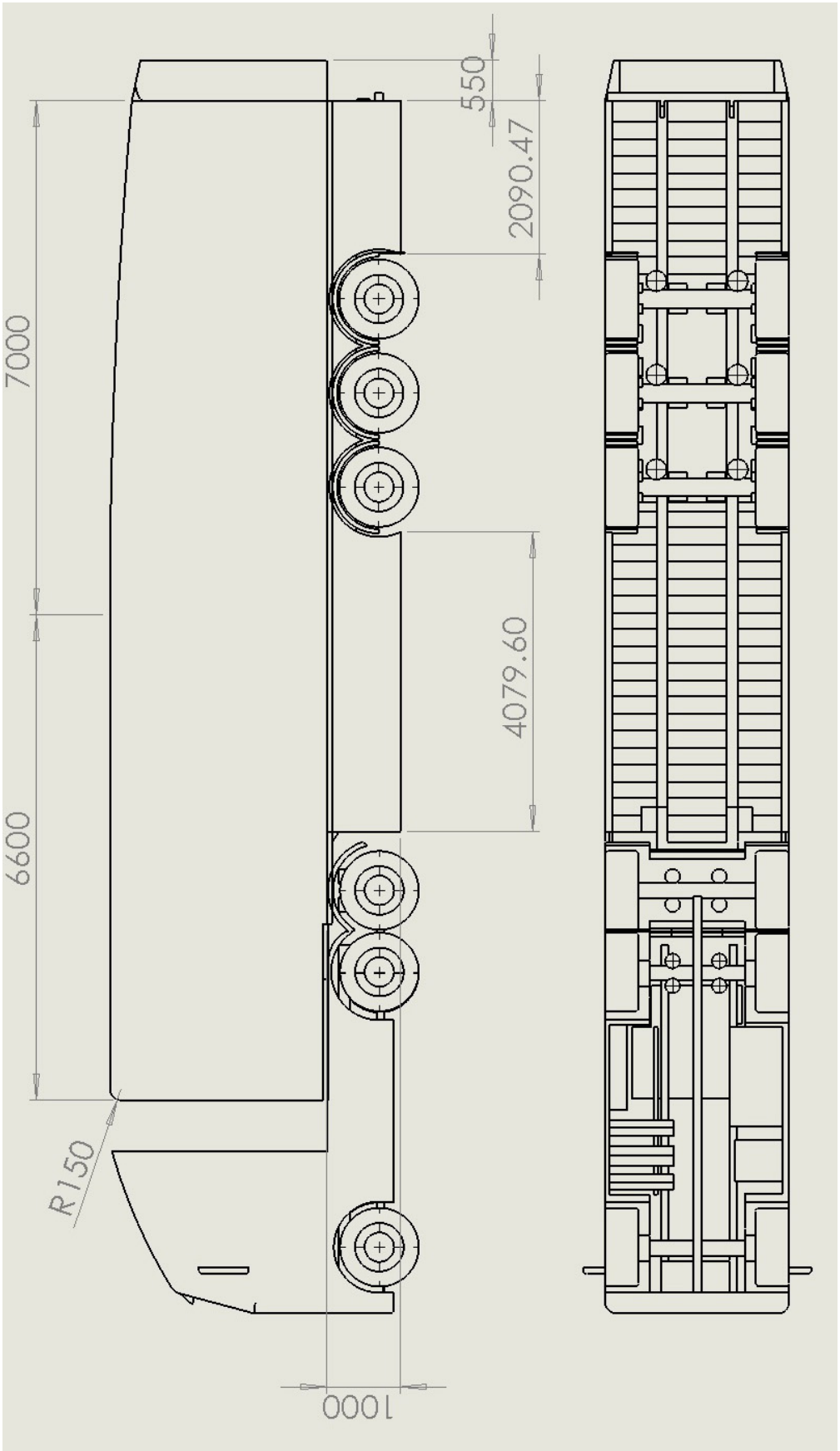

Figure .1.17: Optimised Limited Dimensions

.2 Summary Results

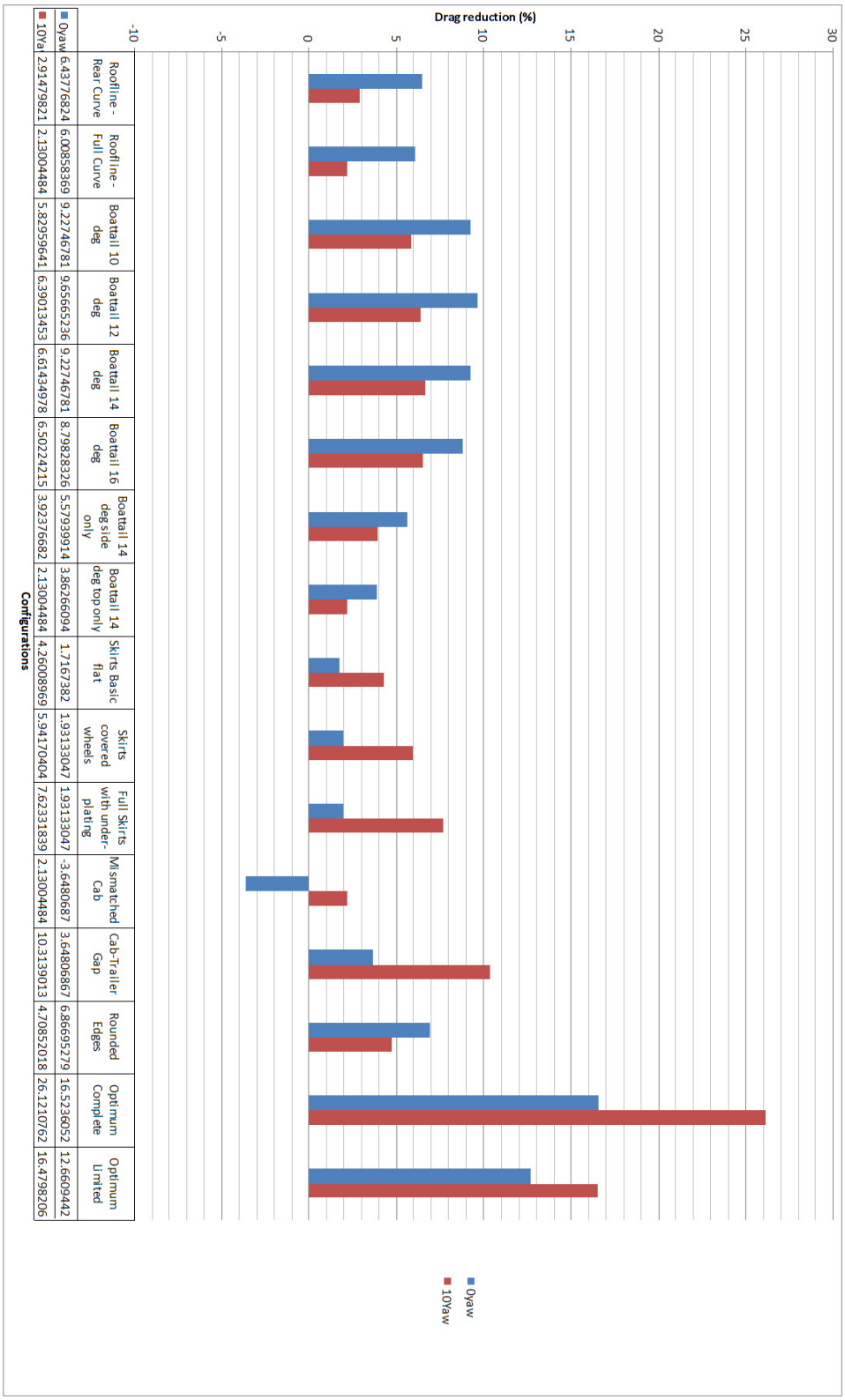

Figure .2.1: All configurations drag reduction in 0 and 10 yaw

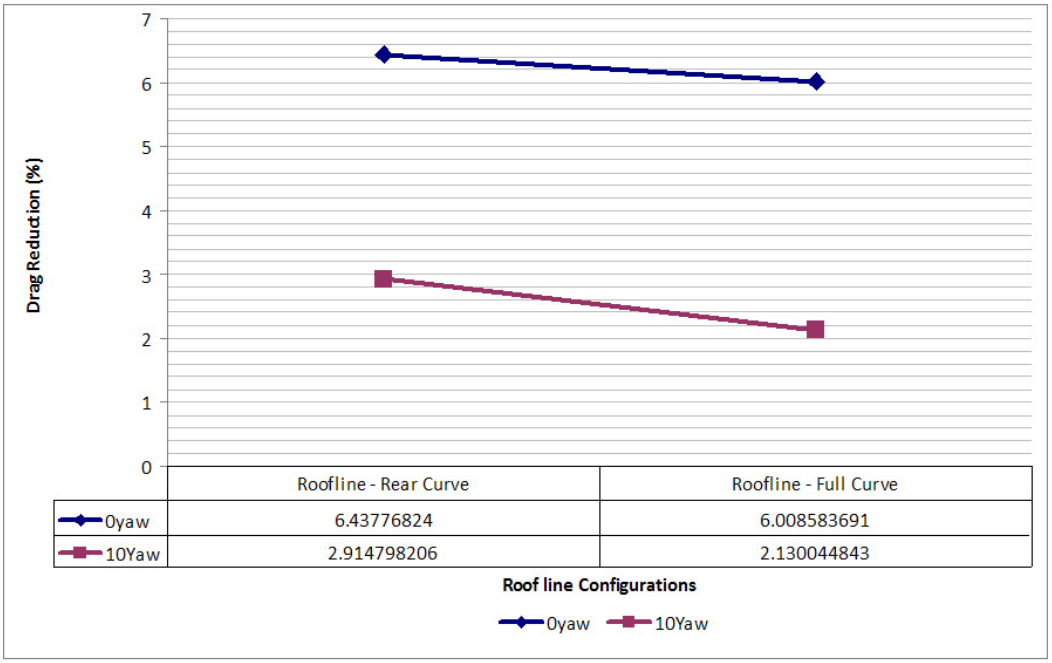

	Roofline - Rear Curve	Roofline - Full Curve
0yaw	6.43776824	6.008583691
10Yaw	2.914798206	2.130044843

Figure .2.2: Roofline drag reduction over the baseline case

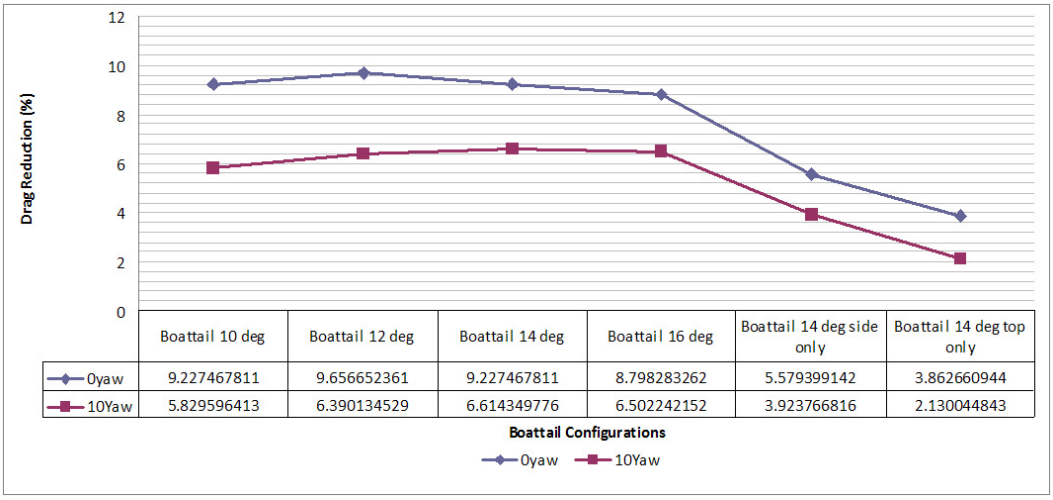

	Boattail 10 deg	Boattail 12 deg	Boattail 14 deg	Boattail 16 deg	Boattail 14 deg side only	Boattail 14 deg top only
0yaw	9.227467811	9.656652361	9.227467811	8.798283262	5.579399142	3.862660944
10Yaw	5.829596413	6.390134529	6.614349776	6.502242152	3.923766816	2.130044843

Figure .2.3: Boattail configurations drag reduction over the baseline case

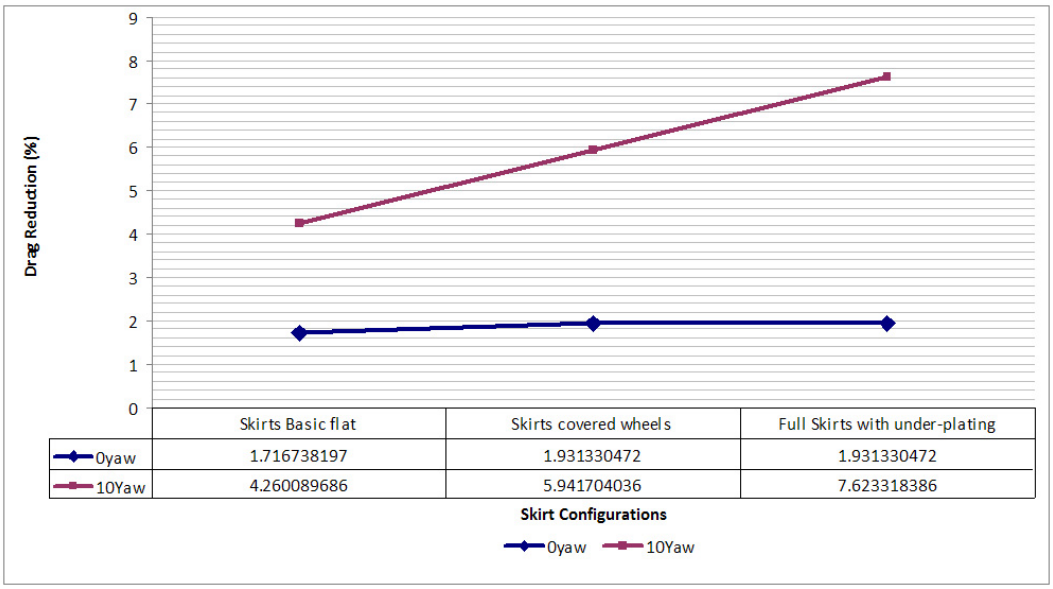

Figure .2.4: Skirt and underbody configurations drag reduction over the baseline case

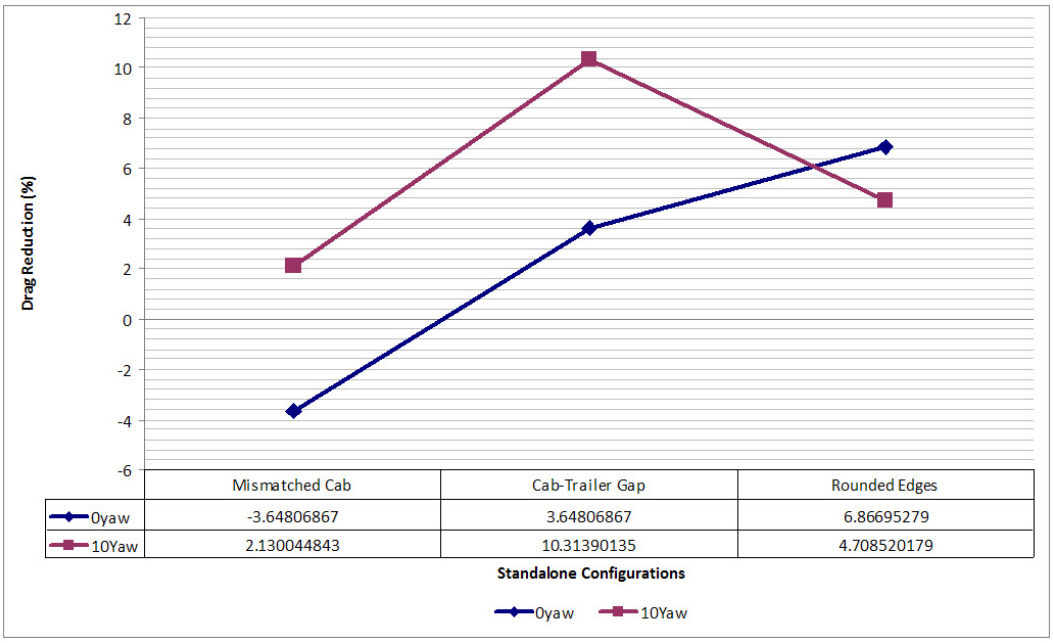

Figure .2.5: Standalone configurations drag difference over the baseline case

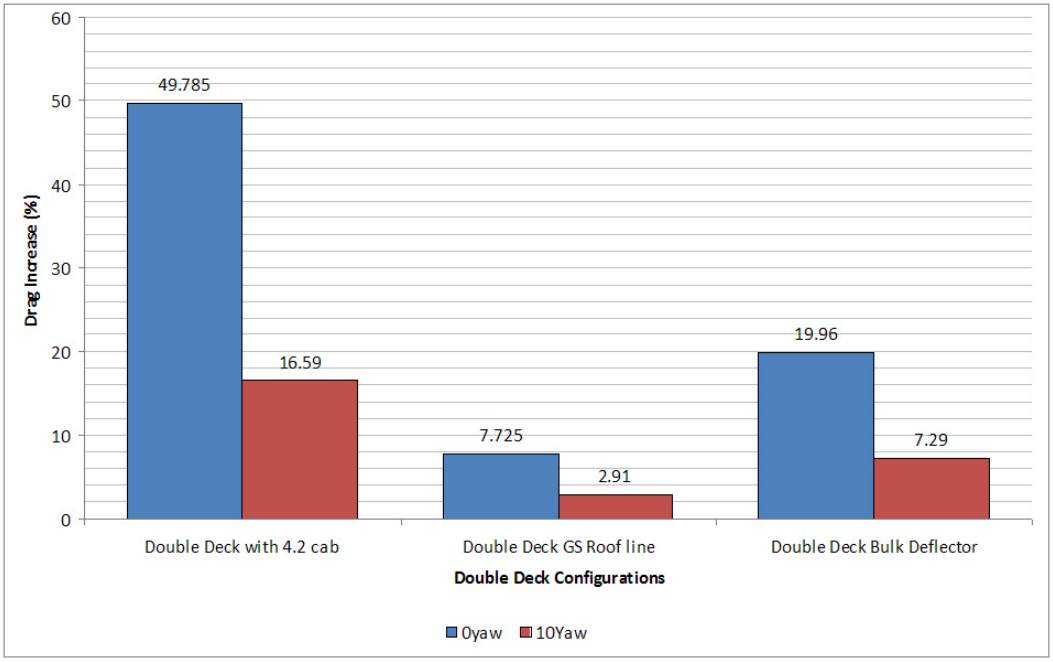

Figure .2.6: Double deck configurations drag increase over the baseline case

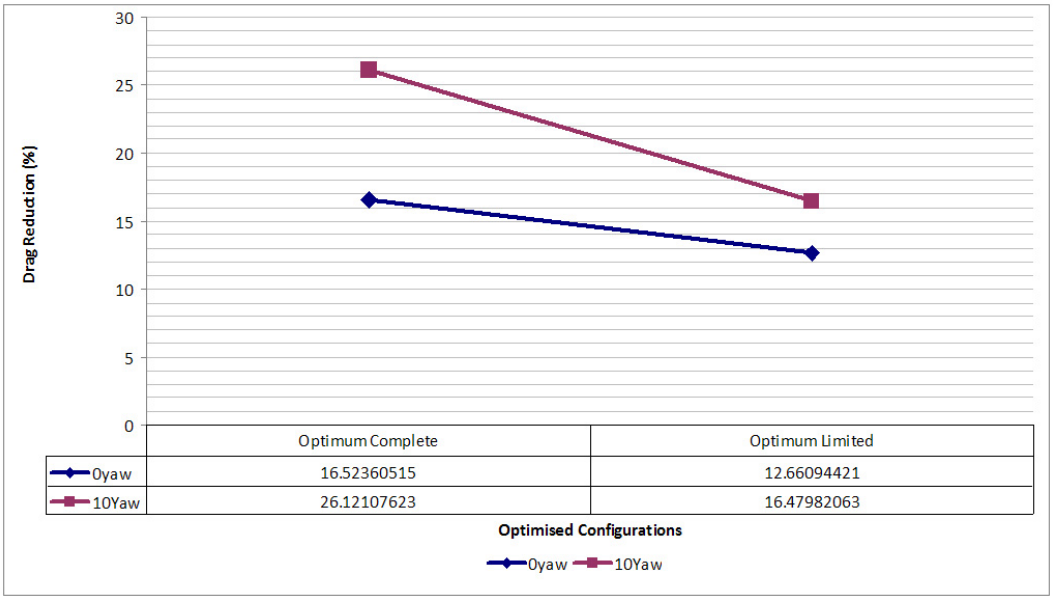

Figure .2.7: Optimised configurations drag reduction over the baseline case

.3 Additional Results Visualisation

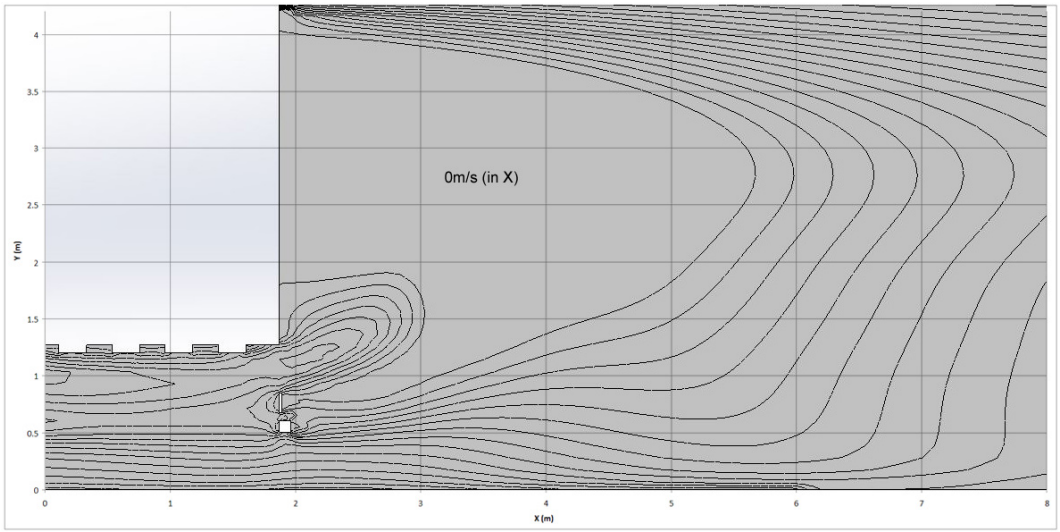

Figure .3.1: Baseline case rear wake contour plot of velocity in X

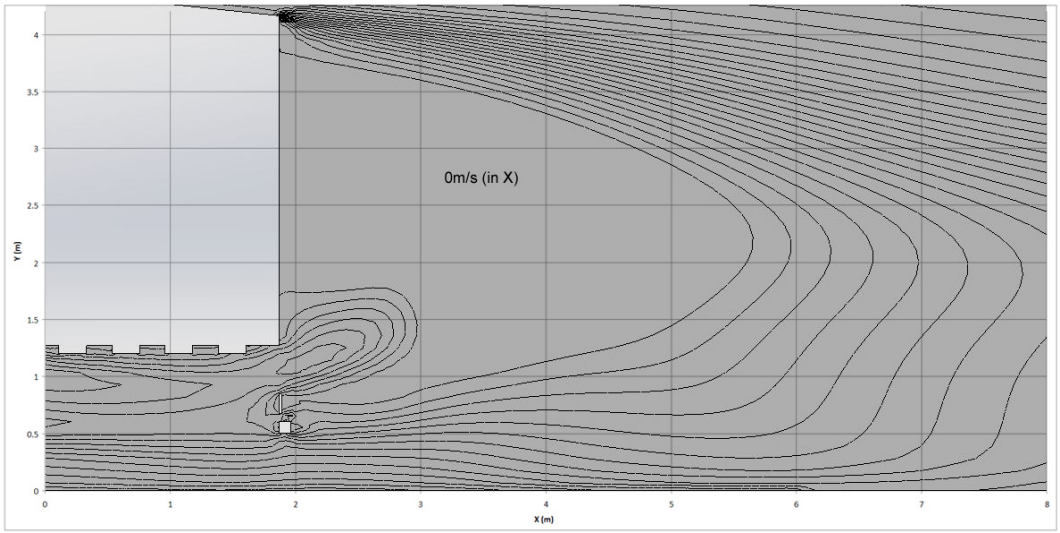

Figure .3.2: Full curve roof line case rear wake contour plot of velocity in X

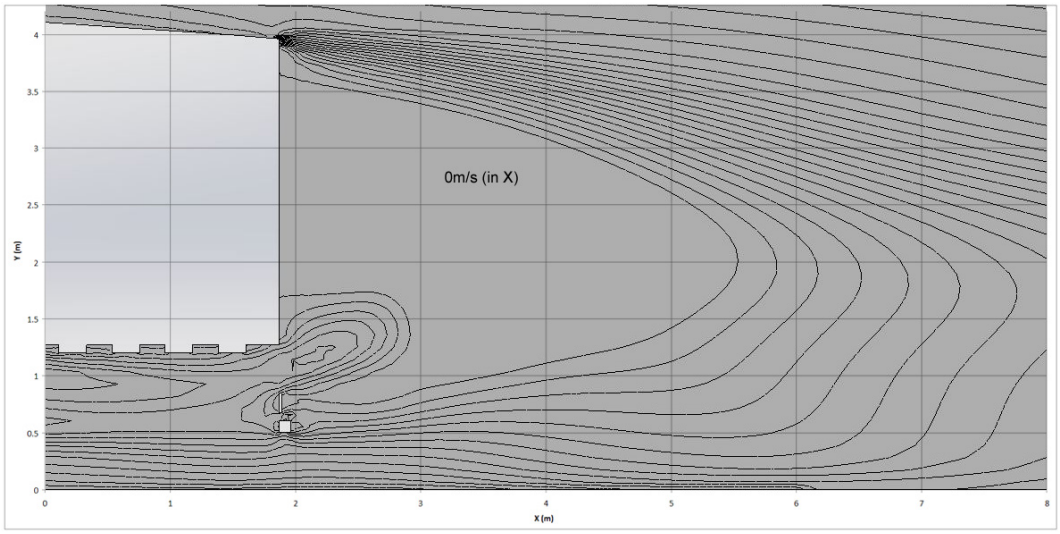

Figure .3.3: Rear curve roof line case rear wake contour plot of velocity in X

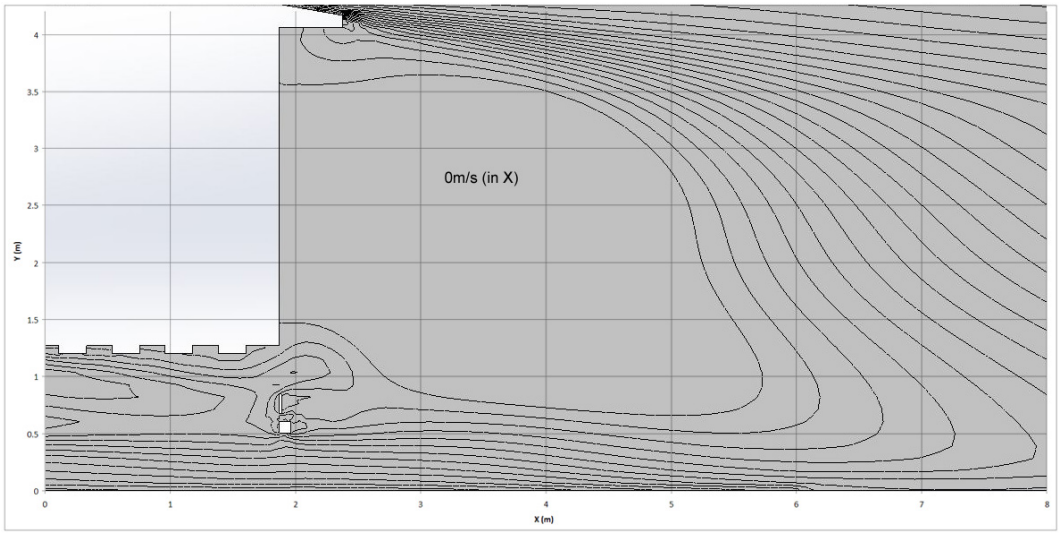

Figure .3.4: 10° boattail case rear wake contour plot of velocity in X

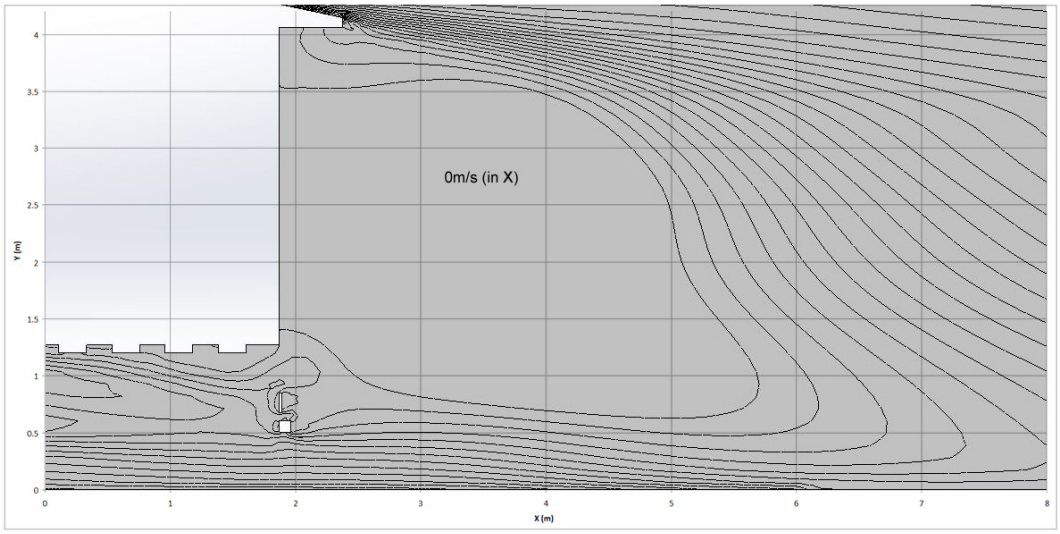

Figure .3.5: 12° boattail case rear wake contour plot of velocity in X

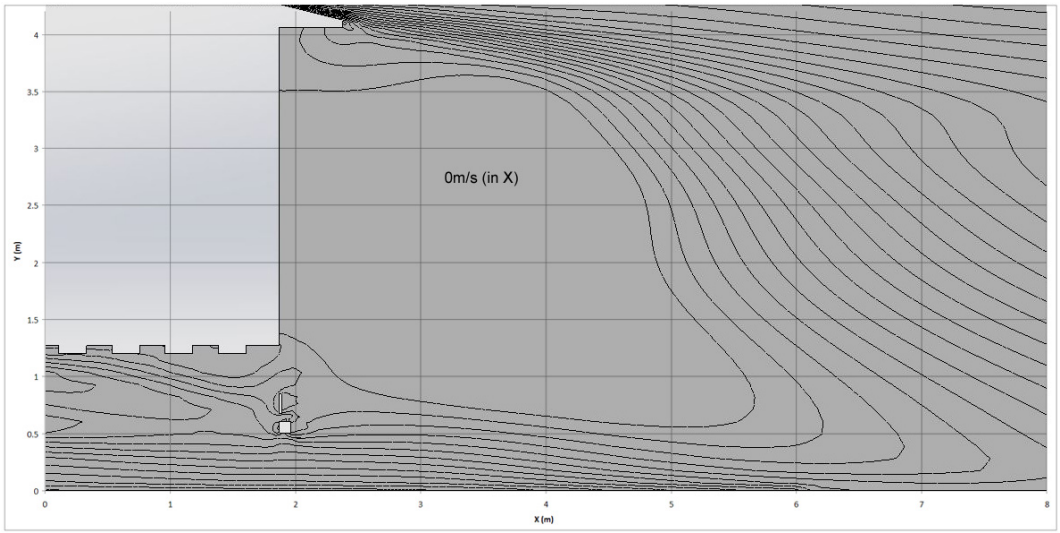

Figure .3.6: 14° boattail case rear wake contour plot of velocity in X

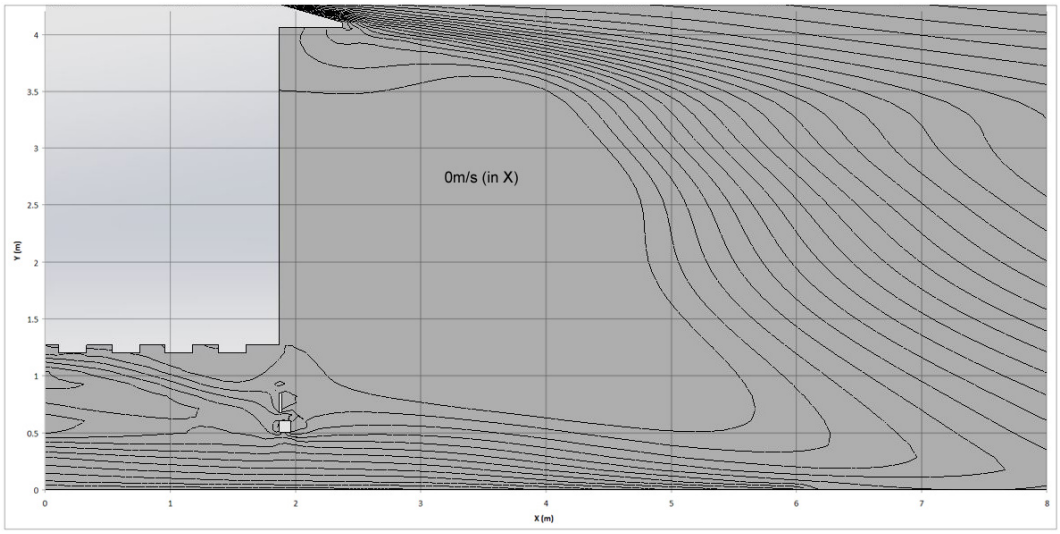

Figure .3.7: 16° boattail case rear wake contour plot of velocity in X

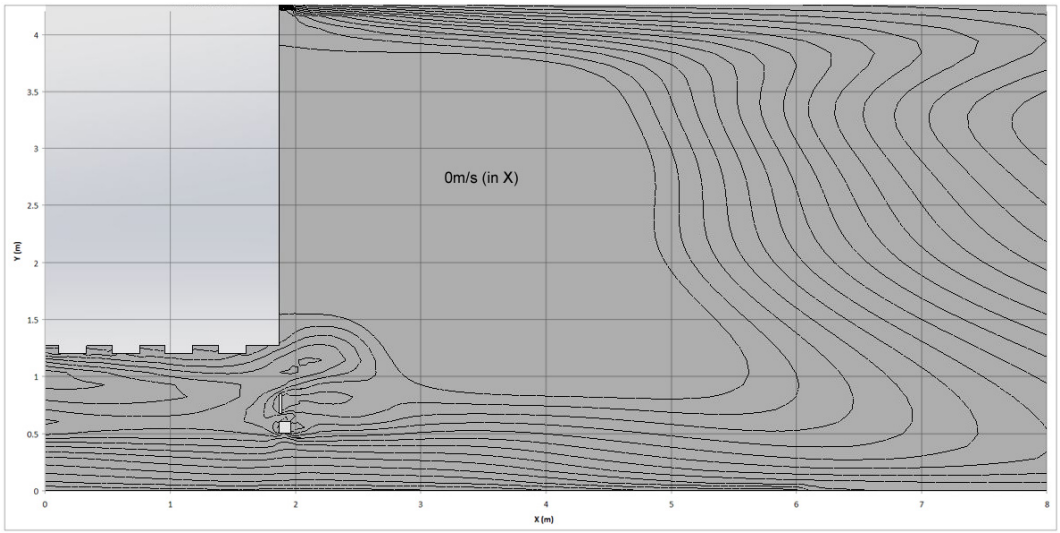

Figure .3.8: Side-only boattail case rear wake contour plot of velocity in X

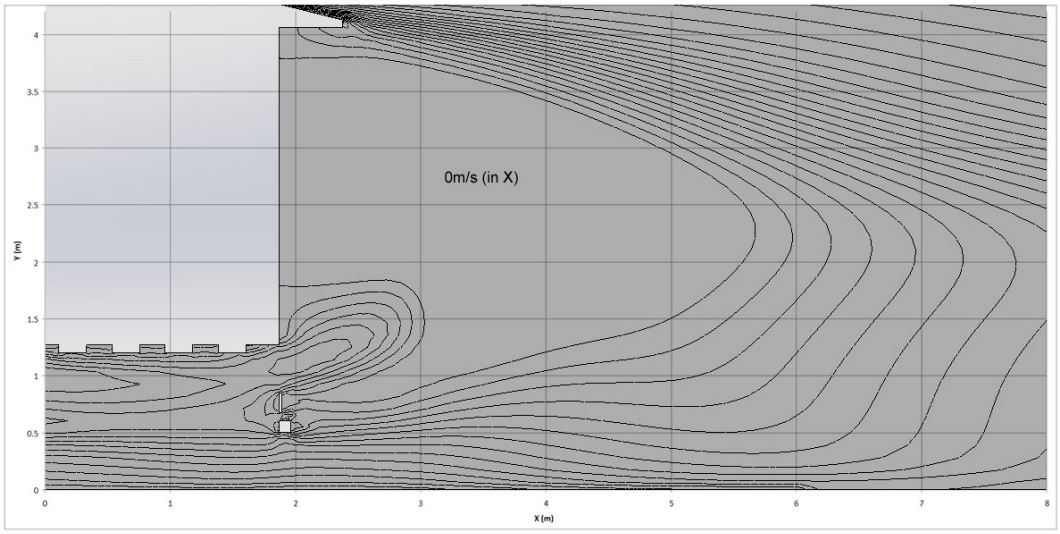

Figure .3.9: Top-only boattail case rear wake contour plot of velocity in X

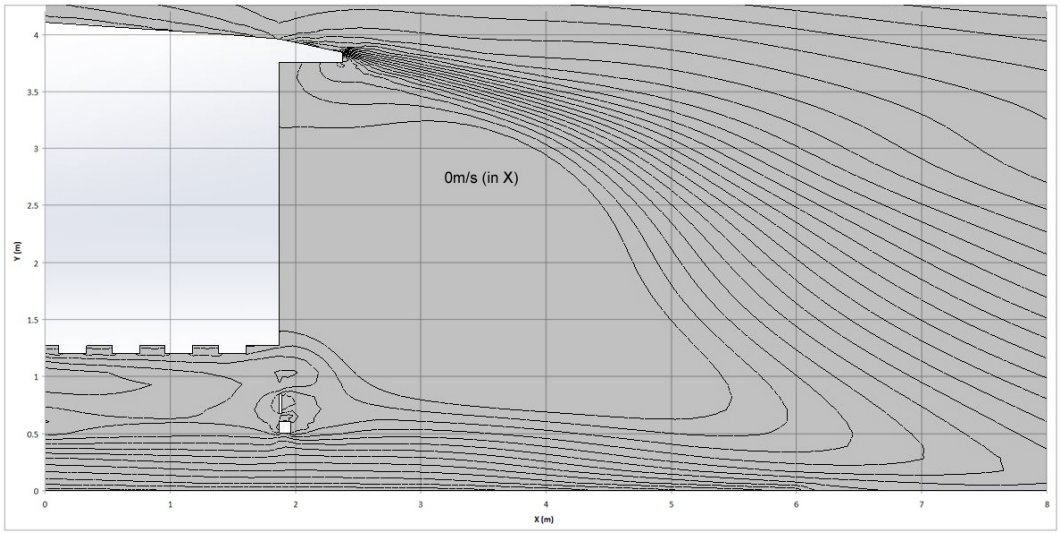

Figure .3.10: Optimised Limited case rear wake contour plot of velocity in X

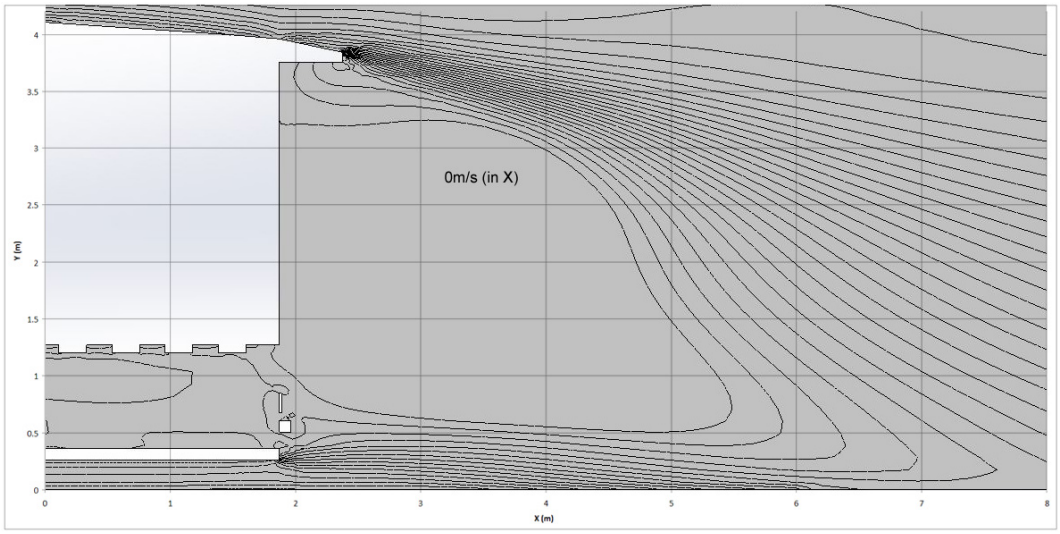

Figure .3.11: Optimised Complete case rear wake contour plot of velocity in X